NASA CR-114436
BAC Rept. No. 6272-933010

FINAL REPORT

STUDY OF AUTOMATIC FLARE AND DECRAB GUIDANCE AND CONTROL SYSTEM FOR THE SPACE SHUTTLE VEHICLE

by

William Cockayne and Walter Rusnak

Bell Aerospace Company Division of Textron
P.O. Box 1 Buffalo, N.Y. 14240

prepared for

NASA/Ames Research Center
Contract No. NAS 2-6077
July 1971

TABLE OF CONTENTS

		Page
I	SUMMARY	I-1
II	INTRODUCTION	II-1
	A. Background	II-1
	B. Objectives	II-1
	C. Approach	II-1
	D. Capsule History of the Study	II-4
	E. System Concept	II-6
III	SYMBOLS	III-1
IV	GUIDANCE CONCEPT	IV-1
	A. General Description of the Guidance System	IV-1
	1. Longitudinal Guidance	IV-1
	2. Lateral Guidance	IV-6
	B. Organization of the Guidance System	IV-7
	C. Problems and Requirements	IV-8
	1. Problems Due to Lack of Power	IV-8
	2. Problems Due to Vehicle Characteristics	IV-15
	3. Nominal Trajectory	IV-17
	4. Longitudinal Guidance Design Approach	IV-21
	5. Lateral Guidance Design Approach	IV-29
	D. Detailed Description	IV-36
	1. Flareout Predictor	IV-36
	2. Phase Selection Logic	IV-45
	3. Feedback Laws	IV-49
V	CONTROL	
	A. History and Description of the Flight Control	V-1
	B. Problems Due to Vehicle Characteristics	V-4
	C. FCS Design Philosophy	V-7
	D. Detailed Description of the Flight Control System	V-24
	1. Pitch Channel	V-24
	2. Roll Channel	V-26
	3. Yaw Channel	V-30
VI	NAVIGATION	VI-1
	A. Background	VI-1
	B. Ground Based Reference System Considerations	VI-3
	C. Blending Algorithm	VI-8
	D. Blending Algorithm, Discussion of Results	VI-11
VII	SIMULATION RESULTS	VII-1
	A. Task II	VII-1
	1. System Sensitivities to Initial Condition (I.C.) Errors	VII-1
	2. System Sensitivities to Vehicle Characteristics	VII-5
	3. System Sensitivity to Winds	VII-9
	4. Influence of Hardware Errors	VII-12

TABLE OF CONTENTS (CONTINUED)

		Page
	B. Task III - Monte Carlo Results	VII-20
	1. General	VII-20
	2. SC117 Scanning Beam System Results	VII-23
	3. SC117 Scanning Beam System - Analysis of Results	VII-33
VIII	MODIFIED SYSTEM	VIII-1
	A. Introduction	VIII-1
	B. Modifications to Guidance and Flight Control Systems	VIII-3
	C. Influence on Flareout Initiation Conditions	VIII-6
	D. Comparison of Performance	VIII-7
	E. True Monte Carlo Comparison of SC117 Scanning Beam	VIII-11
IX	CONCLUSIONS	IX-1
X	RECOMMENDATIONS FOR FUTURE STUDY	X-1
APPENDIX A	HISTOGRAMS FOR TASK III HIGH WIND AND HIGH GUST RUNS	A-1
APPENDIX B	HISTOGRAMS OF RESULTS FOR MODIFIED SYSTEM	B-1
APPENDIX C	DATA BASE, MODELS AND CRITERIA	C-1
APPENDIX D	DERIVATION OF PREDICTOR EQUATIONS	D-1

ILLUSTRATIONS

Figure		Page
II-1	Simplified Block Diagram - System Concept	II-7
IV-1	Methods of Compensation for Wind	VI-13
IV-2	Sink Rate Transient at End of Constant Acceleration Flare	IV-20
IV-3	Predictive Longitudinal Guidance	IV-23
IV-4	Flareout Predictor	IV-24
IV-5	Range - Height Control Technique	IV-26
IV-6	Predictive Guidance Trajectories for Nominal and Off Nominal Initial Conditions	IV-28
IV-7	Decrab and Deroll Maneuvers Prior to TD	IV-34
IV-8	Combined Decrab and Deroll Maneuver in 15 Knot Crosswind	IV-35
V-1	Pitch Control Channel	V-10
V-2	Aileron Channel - Roll	V-11
V-3	Rudder Channel - Yaw	V-12
V-4	Flight Control System Responses at Primary Flare Initiation	V-13
V-5	Flight Control System Responses at Final Flare Initiation	V-14
V-6	Influence of Direct Aileron Compensation on Responses at Final Flare	V-16
V-7	Influence of Direct Aileron Compensation on Decrab Respones	V-18
V-8	Roll Responses at Final Flare for FCS Using Lateral Acceleration Directly	V-20
V-9	Comparison of Roll Responses at Final Flare for FCS Using Either Sensed Sideslip or Compensated Lateral ACC	V-21
V-10	Comparison of Roll Responses at High Angle of Attack for FCS Using Either Sideslip or Compensated Lateral ACC	V-23
VII-1	Nominal Initial Conditions	VII-2
VII-2	Influence of I.C. Errors	VII-3
VII-3	Influence of Vehicle Characteristics	VII-6
VII-4	Influence of Lateral Control Power Variations with Mean Crosswind	VII-7
VII-5	Influence of Wind Shears (No Gusts)	VII-10
VII-6	Influence of Gusts	VII-11
VII-7	Radar	VII-14
VII-8	Scanning Beam System	VII-15
VII-9	ILS Systems	VII-16
VII-10	PRS System	VII-17
VII-11	Comparison of Hardware Systems	VII-19
VII-12	Monte Carlo Miss Distance Statistics for Scanning Beam System	VII-34
VII-13	Monte Carlo Airspeed Statistics for Scanning Beam System	VII-36
VII-14	Monte Carlo Sink Rate Statistics for Scanning Beam System	VII-38
VII-15	Monte Carlo Laterial Offset Statistics for Scanning Beam System	VII-40

ILLUSTRATIONS (CONTINUED)

Figure		Page
VII-16	Monte Carlo Lateral Velocity Statistics for Scanning Beam System	VII-41
VII-17	Monte Carlo Yaw Attitude Statistics for Scanning Beam System	VII-43
VII-18	Monte Carlo Roll Attitude Statistics for Scanning Beam System	VII-45

TABLES

Number		Page
VI-1	SBS Blending and Touchdown Errors (rms)	VI-12
VI-2	SC117 Blending and Touchdown Errors (rms)	VI-17
VII-1	Wind Magnitudes	VII-22
VII-2	Means and Standard Deviations of TD Variables	VII-25
VIII-1	Variation in Flareout Initiation Conditions with Wind for Modified System	VIII-8
VIII-2	Comparison of System Sensitivity to Deterministic Variations	VIII-10
VIII-3	Comparison of System Performance on Set No. 2 of Monte Carlo Runs	VIII-12
VIII-4	Comparison of True Monte Carlo Evaluation Statistics for SC117 Scanning Beam and Precision Tracking Radar Systems	VIII-16

I. SUMMARY.

A study was performed for the automatic landing of the unpowered Space Shuttle Vehicle. The study encompassed the design of the guidance and flight controls, selection of the ground reference component of the landing system (signals in space) and evaluation of the performance of the overall system. The study was carried out by means of an all-digital simulation which incorporated wind shears, gusts and error models for the hardware components. The performance of the landing system operating in winds and turbulence and with hardware errors was determined by Monte Carlo techniques.

It was found that the interactions of turbulence and vehicle characteristics were the limiting factors on system performance. The touchdown errors due to the measurement errors of the ground reference system were less significant.

The guidance designed was predictive in the longitudinal direction and fixed path in the lateral direction. It was determined that the prediction could be expressed in terms of closed form solutions to implicit equations. With an unpowered vehicle, the expected strong influence of winds on the touchdown area attainable was confirmed. The effectiveness of the predictive technique to adapt to unknown winds was demonstrated.

A relatively straight forward flight control system was designed. It was found that angle of attack and sideslip angle sensors were not required which is significant when the re-entry

heating and structural problems involved with mounting external hardware on the Space Shuttle Vehicle are considered.

The problem of combining the data from the ground reference system with data from an airborne inertial navigator was satisfactorily solved by a blending algorithm based on complementary filters . This finding is important in reducing the computer's work load.

II. INTRODUCTION.

A. Background.

A number of studies have been initiated to determine the problems involved with the guidance of the Space Shuttle Vehicle (SSV) from re-entry to touchdown. NASA/Ames Research Center recognized the need for an in-depth study of the critical terminal phase of the approach and landing. For this purpose, NASA/Ames awarded Contract No. NAS2-6077 for the Study of Automatic Flare and Decrab of the Space Shuttle Vehicle to Bell Aerospace Company. This report presents the design of the guidance, navigation and flight control system and the simulation evaluations which resulted from that study.

The terminal phase of the landing was studied beginning at the transition from the steep re-entry glide slope to the conventional approach glide slope and continuing to touchdown (termed: primary flare, glide and final flare). The vehicle studied was the unpowered North American Delta Wing Orbiter (NADWO). The aerodynamic data and actuator characteristics were supplied by NASA/Ames and were those available for the vehicle design as of July 1970.

B. Objectives.

The specific objectives of the study were to employ digital computer simulations:

(1) to develop the guidance and control (G&C) laws for automatic terminal approach and landing (primary flare, glide phase, final flare and decrab) of a candidate SSV configuration

(2) to investigate hardware configurations suitable for mechanizing the guidance system and to select a ground reference system for detailed evaluation.

(3) to evaluate the touchdown errors of the candidate SSV which would result from employment of the selected landing system hardware with the guidance and control laws developed.

C. Approach.

The study was divided into three task groups. These were:

Task I. System Definition & Development of the G&C Laws.

1. Definition of the specific SSV to be studied
2. Develop the 6 DOF digital model of the SSV
3. Incorporate the wind shear and gust models defined by NASA/Ames.
4. Define the flare and runway alignment maneuver
5. Formulate the flight control laws (FCS) for the selected SSV
6. Formulate the guidance laws.

Task II. Selection & Evaluation of Candidate Landing System Hardware.

1. Select the candidate landing systems hardware mechanizations; most importantly, the ground reference system.
2. Develop error models for the hardware
3. Define the window for the primary flare
4. Select the touchdown criteria
5. Define the state estimation errors at primary flare initiation
6. Evaluate G&C laws sensitivities to deterministic variations in key vehicle and aerodynamic parameters
7. Evaluate guidance system sensitivity to initial conditions
8. Evaluate G&C laws sensitivities to wind shears and wind gusts
9. Evaluate the candidate ground reference systems
10. Select one ground reference system for detailed evaluation with the G&C laws developed.

Task III. Monte Carlo Evaluation of Selected Landing System.

1. Define the Monte Carlo Test Plan
2. Perform Monte Carlo evaluation of the selected system
3. Determine performance limits of the selected system.

D. Capsule History of the Study.

The contract was awarded July, 1970. It was mutually agreed that the study would be most meaningful if the vehicle studied was a good candidate for selection as the actual vehicle. NASA/Ames agreed to define this vehicle and on August 13, aerodynamic data for the North American orbiter was obtained. This vehicle is identified as the NADWO (North American Delta Wing Orbiter) or the HCR (High Cross Range) vehicle in this report. The study concentrated on the unpowered vehicle.

It was jointly recognized by NASA/Ames and BAC that this data was not necessarily final and could, in fact, change even beyond the end date of the study. In order to proceed with the development of the concepts, it was decided that freezing the vehicle in the configuration as defined by the initial data was adequate for the study. Most notably missing at study initiation were specifications for the actuator dynamics, surface position and rate limits and the influence of ground effects. Assumptions were made and the G&C design proceeded. As these data were firmed up, the G&C laws were revised, a process that continued throughout the program.

It was also apparent at the beginning of the study that the selection of the primary flare as the start point of the study required dependency on other, earlier, studies to define the initial conditions of the vehicle states, to define the estimation of these states, and to define the window at flare initiate.

Various earlier and concurrent studies by NASA/Ames and BAC were used to determine these parameters.

These parameters, along with the vehicle's characteristics, wind models, the hardware error models, touchdown criteria and flight control system criteria were compiled and served as the data base for the study. The data base is presented in Appendix C.

The candidate ground reference systems were confined to "state-of-the-art" or "high potential" for coming into being systems. These were narrowed down to:

1. precision tracking radar
2. scanning beam systems
3. conventional ILS
4. conventional ILS with radar altimeter.

Later in the study it was decided to consider the possibility of systems utilizing range only measurements obtained by interrogation of appropriately placed DME's (ground beacons). Some idealized assumptions were made to avoid the problem of determining the DME numbers and locations necessary (or allowable) since this appeared to require an independent study.

It was decided at the outset that data from the candidate ground reference systems would be combined with the airborne inertial navigation system for improved vehicle state estimation. Prior studies at BAC had already shown the importance of precise velocity data, particularly sink rate, in guiding an unpowered vehicle. A preliminary three degree of freedom study was made with suitable error models and it was found that a simple complementary filter was adequate for blending the information from the two data sources.

Studies in Task I established that a predictive guidance technique in the longitudinal direction could best handle winds and wind shears. The unpowered vehicle, as expected from prior studies, required substantially different trajectories to attain the desired touchdown conditions for each wind condition. Fixed path guidance was found to be adequate in the lateral direction.

In Task II, the G&C system designed was found to be highly tolerant of deterministic variations in winds, initial conditions and key vehicle parameters. The precision tracking radar gave the least touchdown errors, but both the radar and the scanning beam system were determined to be suitable for the landing mission. Because of the planned widespread deployment of the scanning beam system proposed by the RTCA SC117 Committee, NASA/Ames selected this for detailed high wind and high gust evaluation in Task III.

After the final oral presentation, it was discovered that the sign convention for the ground effects data had been misinterpreted. The G&C laws were revised to account for the change and a limited Monte Carlo evaluation of both the scanning beam system and the precision radar was made. It was shown that the basic conclusions were not significantly altered.

E. System Concept

The system which emerged from the study is snown in the simplified block diagram of Figure II-1. It consists of three major subsystems which are discussed in detail in later sections of this report. These major subsystems are:

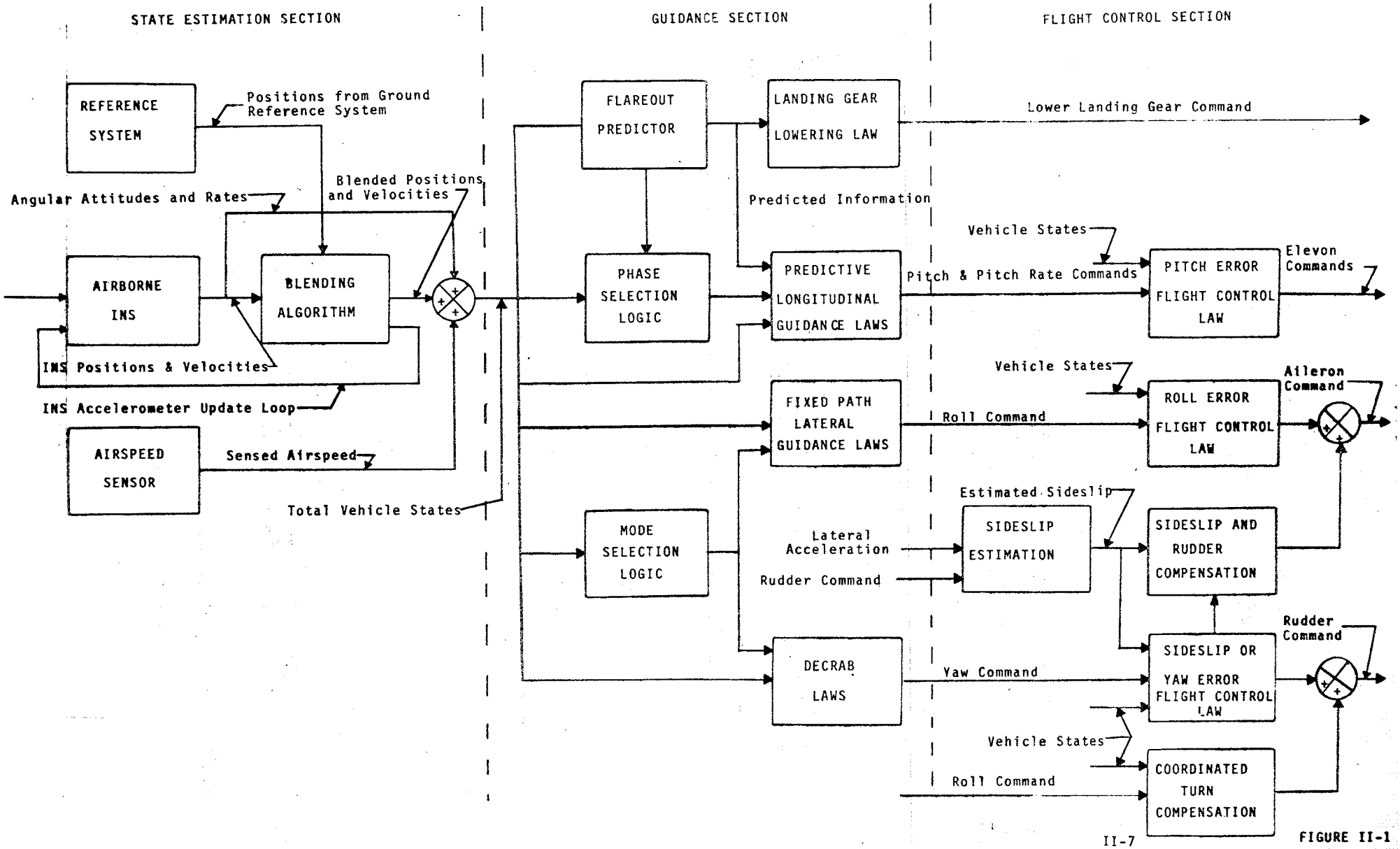
STATE ESTIMATION SECTION
GUIDANCE SECTION
FLIGHT CONTROL SECTION
REFERENCE SYSTEM
Positions from Ground Reference System
Angular Attitudes and Rates
Blended Positions and Velocities
AIRBORNE INS
BLENDING ALGORITHM
INS Positions & Velocities
INS Accelerometer Update Loop
AIRSPEED SENSOR
Sensed Airspeed
Total Vehicle States
FLAREOUT PREDICTOR
LANDING GEAR LOWERING LAW
Lower Landing Gear Command
Predicted Information
PHASE SELECTION LOGIC
PREDICTIVE LONGITUDINAL GUIDANCE LAWS
Vehicle States
Pitch & Pitch Rate Commands
PITCH ERROR FLIGHT CONTROL LAW
Elevon Commands
FIXED PATH LATERAL GUIDANCE LAWS
Vehicle States
Roll Command
ROLL ERROR FLIGHT CONTROL LAW
Aileron Command
Estimated Sideslip
MODE SELECTION LOGIC
Lateral Acceleration
Rudder Command
SIDESLIP ESTIMATION
SIDESLIP AND RUDDER COMPENSATION
DECRAB LAWS
Yaw Command
SIDESLIP OR YAW ERROR FLIGHT CONTROL LAW
Rudder Command
Vehicle States
Roll Command
COORDINATED TURN COMPENSATION

FIGURE II-1

1. the State Estimation Section which is described in Section VI.

2. the Guidance Section which is described in Section IV.

3. the Flight Control Section which is described in Section V.

The State Estimation Section includes the ground reference system and the airborne INS. The outputs of these are combined by the Blending Algorithm to obtain the estimate of vehicle position and velocities. These, along with sensed airspeed are utilized by the Guidance Section.

The Guidance Section includes a Flareout Predictor which determines the phase of flight (primary flare, glide, final flare) for selection of the appropriate guidance laws. These laws are mechanized as closed form equations in the Predictive Longitudinal Guidance subsection. The Flareout Predictor also determines the time of landing gear lowering to control the touchdown airspeed. The Guidance Section also includes the laws for fixed path lateral guidance. The Mode Selection Logic determines if the lateral laws are in the heading hold or coordinated turn modes. The Decrab Laws and Fixed Path Lateral Guidance Laws select the yaw and roll commands, respectively, to the lateral channel of the flight control system.

The Flight Control System Section accepts pitch, pitch rate, roll and yaw commands from the Guidance Section. The ailerons are commanded by a summation of roll commands and compensation

to account for the roll moments produced by sideslip and rudder. The rudder is commanded by the sideslip or yaw error depending on whether the mode is appropriate for coordinated turns or decrab. The elevon (functioning as an elevator) is commanded by pitch and pitch rate commands from the Guidance Section.

III. SYMBOLS

This section lists the symbols used in the body of the report. The appendices individually list the symbols used with the appendix.

For ease of reading the report, the symbols are identified in the text the first time they appear in addition to their listing in this section.

The coordinate system which is used, unless otherwise specified, has its origin at the nominal touchdown point. The X-axis lies in the horizontal plane along the runways centerline. The sign convention is such that the vehicle X coordinate is negative in the direction of approach to the touchdown point. The Z-axis is the local vertical and the sign convention is such that the Z coordinate of the vehicle is negative above the touchdown horizontal plane. The Y axis is orthogonal to the X and Z axes with the sign convention following the right hand rule.

A	a designation used for generalized angles
$\overline{b}$	lateral reference moment arm
$\overline{c}$	longitudinal reference moment arm
CW	crosswind
C_{L_α}	slope of lift due to α
$C_{L\delta_e}$	slope of lift due to δ_e
$C_{m\alpha}$	slope of pitch moment due to α

$C_{m\delta_e}$ slope of pitch moment due to δ_e

$C_{N\beta}$ slope of yaw moment due to β

$C_{Y\delta_r}$ slope of side force due to δ_r

$C'_{Y\delta_r}$ assumed value of $C_{Y\ \delta_r}$

$C_{Y\beta}$ slope of side force due to β

$C'_{Y\beta}$ assumed value of $C_{Y\beta}$

DME Distance Measuring Equipment

FCS Flight Control System

G&C Guidance and Control

$G_x(s)$ spectrum of horizontal gust along vehicle heading

$G_y(s)$ spectrum of horizontal gust orthogonal to vehicle heading

$G_z(s)$ spectrum of vertical gust

g gravity constant

HW headwind

h altitude (= -Z)

h_o initial altitude

ILS Instrument Landing System

INS Inertial Navigation System

K a gain constant

K_W ratio of magnitude of wind shear to mean wind shears ($\overline{K}_W$=1)

k_A gain on angle A, A being a general angle designation

k_{AI} integrator gain on general angle A

$k_{\dot{A}}$ rate gain on general angle A

k_I an integrator gain

k_p a gain on roll rate

k_q a gain on pitch rate

k_r a gain on yaw rate

k_x a gain on longitudinal error

k_{xi} value of k_x for flight phase i

k_{vg} variable gain (function of range)

k_y a gain on lateral offset

k_z a gain on vertical error

k_{zi} value of k_z for flight phase i

$k_{\dot{y}}$ a gain in crosstrack rate

$k_{\dot{z}}$ a gain on sink rate

$k_{\dot{z}i}$ value of $k_{\dot{z}}$ for flight phase i

k_ε a gain in an angular error, ε

k_β a gain on sideslip angle

$k_{\delta a \delta r}$ a gain on rudder into aileron commands

$k_{\delta r \delta a}$ a gain on aileron into rudder commands

k_θ a gain on pitch angle error

$k_{\theta i}$ an integrator gain on pitch angle error

$k_{\dot{\theta}}$ a gain on pitch rate

k_ϕ a gain on bank angle error

$k_{\phi i}$ an integrator gain on bank angle error

k_ψ a gain on heading angle error

(L/D) lift to drag ratio

$(L/D)_{f\ avg}$ average (L/D) during primary flare

$(L/D)_{ff\ avg}$ average (L/D) during final flare

$(L/D)^p_{ef}$ predicted (L/D) at end of primary flare, gear up

$(L/D)^p_{eg}$ predicted (L/D) at end of glide, gear down

$(L/D)^p_{gd}$ predicted (L/D) at gear lowering point, gear down

$(L/D)^p_{gd\ avg}$ predicted average (L/D) glide, gear down

$(L/D)^{p}_{gu}$	predicted (L/D) at gear lowering point, gear up
$(L/D)^{p}_{gu\ avg}$	predicted average (L/D) glide, gear up
L_{β}	roll moment due to β
$L_{\delta a}$	roll moment due to δ_a
$L_{\delta r}$	roll moment due to δ_r
NADWO	North American Delta Wing Orbiter
PRS	Precision Ranging System
PTR	Precision Tracking Radar
p	vehicle roll rate
Q	sensed dynamic pressure
Q_f	filtered dynamic pressure
q	vehicle pitch rate
q_c	commanded pitch rate
R	range
RMS	root mean square value of the variable
R_{θ}	range from elevation scanning antenna to vehicle
R_{ψ}	range from azimuth scanning antenna to vehicle
r	vehicle yaw rate
r_c	commanded yaw rate
SB, SBS	Scanning Beam System
SC117 System	SB proposed by RTCA Committee SC117
(S/m)	ratio of vehicle reference area to mass
(S/m)'	assumed value of (S/m)
s	LaPlace operator
TD	touchdown
TW	tailwind
t	current flignt time (sec)

TR	tracking radar
t_{sff}	time of start, final flare
t_{tdc}	time to decrab
t_{ttd}	time to touchdown
V	vehicle groundspeed
V_a	vehicle airspeed
$V_{a\ gd\ nom}$	airspeed at nominal gear lowering point
V_{atd}	desired touchdown airspeed
V_{MW}	mean wind shear magnitude
V_{td}	desired touchdown groundspeed
V^p_{aef}	predicted airspeed, end of primary flare
V^p_{aeg}	predicted airspeed, end of glide
V^p_{agd}	predicted airspeed, nominal gear lowering point
V^p_{ef}	predicted groundspeed, end of primary flare
V^p_{eg}	predicted groundspeed, end of glide
V^p_{gd}	predicted groundspeed, nominal gear lowering point
$\dot{v}_a$	sensed lateral acceleration, body axis system
X	X coordinate of vehicle
X_N	value of X measured by INS
X_o	X coordinate of location of ground reference system
X_r	value of X measured by ground reference system
$\dot{X}$	time derivative of X
$\dot{X}_N$	value of $\dot{X}$ measured by INS
$\hat{X}$	estimated value of X
$\overline{X}$	average value of X
$\overline{\dot{X}}$	average value of $\dot{X}$
$\hat{\dot{X}}$	estimated value of $\dot{X}$
$\ddot{X}_{NU}$	updated measured acceleration from INS

Y	Y coordinate of vehicle
Y_l	limited lateral offset for bank command computation
Y_{max}	maximum value of Y_l
$\overline{Y}$	average value of Y
$\dot{Y}$	time derivative of Y
$\overline{\dot{Y}}$	average value of $\dot{Y}$
Z	Z coordinate of vehicle (= -h)
$\dot{Z}$	time derivative of Z
Z_{ci}	height command, flight phase i
Z_{sff}	height at start of final flare
Z^p_{sf}	predicted height required, primary flare start
Z^p_{sff}	predicted height required, final flare start
$\overline{Z}$	average value of Z
$\dot{Z}$	time derivative of Z
$\dot{Z}_c$	commanded sink rate
$\dot{Z}_{ci}$	commanded sink rate, flight phase i
$\dot{Z}_{sff}$	sink rate, start of final flare
$\dot{Z}_{td}$	desired sink rate, touchdown
$\dot{Z}^p_{ef}$	predicted sink rate, end of primary flare
$\overline{\dot{Z}}$	average value of $\dot{Z}$
$\ddot{Z}_c$	commanded vertical acceleration
$\ddot{Z}_f$	desired vertical acceleration, primary flare
$\ddot{Z}_{ff}$	desired vertical acceleration, start of final falre
$\ddot{Z}_i$	desired vertical acceleration, flight phase i
$\ddot{Z}^p_{ff}$	predicted required vertical acceleration at final flare initiate

α	angle of attack
α_o	α when trim lift coefficient is zero
α_{trim}	estimated trim α
β	sideslip angle
β'	estimated β
β'_f	filtered β'
γ	vehicle flight path angle
γ_g	desired glide path angle
γ_i	value of γ used in θ_{trim} computation
γ_{sg}	required γ, start of glide
γ_{td}	nominal γ at TD
$\dot{\gamma}$	time derivative of γ
$\dot{\gamma}_c$	commanded value of $\dot{\gamma}$
ε	general angular error
ζ_θ	short period pitch damping factor
ζ_ϕ	short period roll damping factor
θ	vehicle pitch angle
θ_c	commanded pitch angle
θ_{trim}	outside pitch trim command
ΔA	error on angle A, where A designates a general angle
$\Delta C_{L/\alpha}$	change in the α induced lift
$\Delta C_{L/\delta_e}$	change in the δ_e induced lift
Δt	computational cycle period
Δt_{sff}	lead time required on pitch at start of final flare
Δt_o	initial time lag in pitch
$\Delta t_{\theta i}$	estimated time required for pitch maneuver, flight phase i
$\Delta t_{\psi o}$	initial decrab time delay

Δt_f^p	predicted time required for primary flare
Δt_{ff}^p	predicted time required for final flare
Δt_{gd}^p	predicted glide time, gear down phase
Δt_{gu}^p	predicted glide time, gear up phase
ΔV_{WF}	filtered value of wind speed component along V vector
ΔV_{WTD}	estimated value of wind speed along V vector at TD
ΔX^p	predicted total X traveled
ΔX_{ef}^p	predicted X traveled during primary flare
ΔX_{ff}^p	predicted X traveled during final flare
ΔX_g^p	predicted X traveled during glide
ΔX_{gd}^p	predicted X traveled, gear down phase of glide
ΔX_{gu}^p	predicted X traveled, gear up phase of glide
ΔX_{td}^p	predicted X error at TD airspeed
ΔZ_{lf}	Z lead compensation for pitch lag during primary flare
ΔZ_{lff}	Z lead compensation for pitch lag during final flare
ΔZ_{li}	Z lead compensation for pitch lag during flight phase i
ΔZ^p	predicted total Z traveled
ΔZ_{ef}^p	predicted Z traveled during primary flare
ΔZ_{ff}^p	predicted Z traveled during final flare
ΔZ_g^p	predicted Z traveled during glide
ΔZ_{td}^p	predicted Z error at TD airspeed
$\Delta \dot{Z}$	sink rate error
$\Delta \alpha i$	required α change for maneuvers during flight phase i
$\Delta \gamma_{lg}$	γ lead compensation
$\Delta \delta_{ai}$	component of δ_{ac} from trimming integrator

$\Delta\delta_{ap}$	component of δ_{ac} from roll rate
$\Delta\delta_{as}$	component of δ_{ac} due to ϕ, β, δ_r
$\Delta\delta_{asl}$	limited $\Delta\delta_{as}$
$\Delta\delta_{a\phi}$	component of δ_{ac} due to bank angle error
$\Delta\delta_{a\phi l}$	limited $\Delta\delta_{a\phi}$
$\Delta\delta_{a\beta}$	component of δ_{ac} due to β
$\Delta\delta_{a\delta_r}$	component of δ_{ac} due to δ_r
$\Delta\delta_{ei}$	component of δ_{ec} from trimming integrators
$\Delta\delta_{e\ max}$	maximum elevator deflection
$\Delta\delta_{e\ min}$	minimum elevator deflection
$\Delta\delta_{eq}$	component of δ_{ec} due to pitch rate
$\Delta\delta_{e\theta}$	incremental elevator command due to pitch error
$\Delta\delta_{e\theta l}$	position limited $\Delta\delta_{e\theta}$
$\Delta\delta_{rr}$	component of δ_{rc} due to yaw rate
$\Delta\delta_{rs}$	component of δ_{rc} due to β or heading error
$\Delta\delta_{rsl}$	limited $\Delta\delta_{rs}$
$\Delta\delta_{r\delta_a}$	component of δ_{rc} for turn coordination
$\Delta\theta_i$	pitch change required for maneuver, flight phase i
$\Delta\dot{\theta}_{eff}$	effective pitch rate
$\Delta\xi_{max}$	maximum allowed heading approach angle
$\Delta\phi_{cyl}$	component of ϕ_c due to limited lateral offset
$\Delta\phi_{c\dot{y}}$	component of ϕ_c due to lateral velocity
δ_a	aileron deflection
δ_{ac}	commanded value of δ_a
δ_{acl}	position limited δ_{ac}

δ_{acrl}	rate limited δ_{acl}
$\delta_{acrl\ prev}$	value of δ_{acrl} from previous computation cycle
$\delta_{a\ max}$	maximum allowable excursion of δ_a
$\delta_{arl\ max}$	largest allowable increment in δ_{acrl} in computation cycle
$\delta_{arl\ min}$	largest allowable decrement in δ_{acrl} in computation cycle
δ_c	general control surface command
δ_e	elevator deflection
δ_{ec}	commanded value of δ_e
δ_{ecl}	position limited δ_{ec}
δ_{ecrl}	rate limited δ_{ecl}
$\delta_{ecrl\ prev}$	value of δ_{ecrl} from previous computation cycle
$\delta_{erl\ max}$	largest increment in δ_{ecrl} allowed per computation cycle
$\delta_{erl\ min}$	largest decrement in δ_{ecrl} allowed per computation cycle
$\delta_{e\ max}$	maximum elevon deflection
$\delta_{e\ min}$	minimum elevon deflection
δ_{gc}	gear lowering command (0 up, 1 down)
δ_i	general control surface deflection
δ_r	rudder deflection
δ_{rc}	commanded value of δ_r
δ_{rcl}	limited δ_{rc}
$\delta_{r\ max}$	maximum allowable δ_r
$\delta r'_c$	δ_{rcl} less the turn coordination component
σ	standard deviation
σ_i	σ of state i (includes i = $X, \dot{X}, Y, \dot{Y}, Z, \dot{Z}, \phi, \psi, V_a$)
σ_{is}	σ of error in estimating state i

σ_{KW}	σ of wind shear magnitude
σ_X	σ of X at trajectory point specified
σ_{XB}	σ of TD error in X due to ground system measurement biases
σ_{XMB}	component of σ_{XB} due to range measurement bias
σ_{XR}	σ of ground system measurement error in X
σ_Y	σ of Y at trajectory point specified
σ_{YB}	σ of TD error in Y due to ground system measurement biases
σ_{YR}	σ of ground system measurement error in Y
σ_Z	σ of Z at trajectory point specified
σ_{ZR}	σ of ground system measurement error in Z
σ_{ur}	σ of gust velocity
$\sigma_{\dot{X}}$	σ of $\dot{X}$ at trajectory point specified
$\sigma_{\dot{Y}}$	σ of $\dot{Y}$ at trajectory point specified
$\sigma_{\dot{Z}}$	σ of $\dot{Z}$ at trajectory point specified
σ_θ	σ of ground system elevation angle error
σ_ψ	σ of ground system localizer angle error
$\sigma_{\psi MB}$	component of σ_{YB} due to azimuth angle bias
$\sigma_{\psi W}$	σ of wind heading to runway
τ	a time constant
τ_q	airspeed filter time constant in gain computations
τ_{ra}	filter time constant on $\Delta\delta_{a\phi l}$
τw	airspeed filter time constant in wind estimation
τ_X	time constant applied to
$\tau_{\dot{X}}$	time constant applied to a time derivative
τ^p_{ff}	predicted τ for exponential final flare
τ_β	β filter time constant
τ_1	time constant of position estimating complementary filter
τ_2	time constant of velocity estimating complementary filter

ϕ	bank angle
ϕ_c	bank command
ϕ_{cl}	limited ϕ_c
ϕ_{cY}	component of ϕ_c due to lateral offset
ϕ_{max}	maximum allowable ϕ
$\overline{\phi}$	average value of ϕ
ψ	heading angle
ψ_c	commanded value of ψ
ψ_{sdc}	heading at start of decrab
ψ_{td}	runway heading
ψ_W	wind direction with respect to runway ($\overline{\psi}_W$=0)
$\dot{\psi}$	yaw rate
$\dot{\psi}_{eff}$	effective decrab rate
$\overline{\psi}$	average ψ
$\overline{\psi}_W$	average wind heading with respect to runway (=0)
ω_θ	short period pitch natural frequency
ω_ϕ	short period roll natural frequency

IV. GUIDANCE CONCEPT

A. General Description of the Guidance System.

This paragraph of Section IV outlines the major features of the guidance system design. The remainder of Section IV is a detailed discussion of this design and the considerations which lead to its formulation. In the flight phase studied, the unconventional problems exist in the longitudinal axis and most of the work reported is concerned with this axis.

1. Longitudinal Guidance

a. In this study, the longitudinal guidance system was specifically designed for the terminal phase of re-entry and landing. The concept, however, can be extended to guidance during the steep descent from re-entry phase. The terminal phase is defined as the phase in which the SSV transitions from the steep re-entry flight path to the conventional glide path and conventional final flare at touchdown.

The specific equations which define the guidance laws are derived in Appendix D.

b. The terminal phase consists of subphases which define the nominal terminal phase trajectory. The nominal trajectory consists of a constant 1.5 g vertical acceleration primary flare, a constant -3 degree flight path angle glide phase, and an exponential final flare with an initial vertical acceleration of 1.1 g and with a nominal time constant of 6 sec. These subphases successively transition the vehicle from the steep descent glide slope to the conventional approach glide slope and then from the conventional glide slope to

the desired sink rate at touchdown with the desired touchdown point as the terminus.

c. The guidance system does not depend upon the use of speed brakes. This was a ground rule imposed at the initiation of the study. The use of landing gear drag to control velocity indicate that speed brakes would greatly improve the precision of the landing of an unpowered vehicle.

The guidance system assumes that the landing gear may be lowered at any time in the terminal approach prior to the initiation of the final flare. The gear is lowered, based on computations in the guidance laws, at the point where the added drag results in the vehicle velocity at touchdown being the desired velocity. The gear, once lowered, is never retracted and is always lowered prior to start of the final flare.

d. In addition to the guidance provided during the terminal phase, the guidance system can also be used to provide an aim point for the system which is used during the prior flight phases. The guidance system developed is a particular form of predictive guidance. The predicted range and altitude required at the start of primary flare defines the aim point. Since this aim point is predicted based on the current vehicle flight conditions, it accounts for the effect of off nominal vehicle conditions due to any prior disturbances.

e. The predictive guidance laws are based on implicit, closed form solutions of the kinematic equations for each of the flareout subphases which were briefly defined in 1 above. The equations are solved backward in time from the desired airspeed, sink rate, range and altitude at touchdown. For each subphase, the kinematic equations utilize the average L/D for that subphase.

The velocity, sink rate, altitude and range from touchdown are computed working backward with the velocity/range computations stopping when the current vehicle velocity is reached and with the altitude/sink rate computations stopping when the current vehicle sink rate is reached. The difference between the computed range and the actual range to touchdown is the range error. The difference between the computed altitude and the actual altitude is the altitude error. These errors are multiplied by simple gain constants and fed to the flight control system as incremental pitch attitude commands.

The pitch attitude changes not only null the predicted range and altitude errors at touchdown but also result in velocity changes due to changes in the vehicle drag and to exchanges of potential and kinetic energy. Nulling the predicted range and altitude errors in this way essentially converts the altitude and range errors into a velocity error at touchdown. The velocity error at touchdown is then controlled by drag modulation. The

L/D values used in the kinematic equations are the values which apply when the landing gear is in the down position. The vehicle, however, actually commences the terminal phase maneuvers with the gear in the retracted position. Therefore, the actual drag is lower than the drag implied by the selected average L/D values. The predicted range to go, computed using the lower L/D ratio and the current vehicle velocity, is less than the actual range which results in a pitch up command to stretch the range. The increased drag decreases the vehicle velocity. At some point in the trajectory the predicted range-to-go and the actual range-to-go become equal. When this occurs, the landing gear is lowered by a guidance command. Since the remainder of the predicted trajectory is based on the L/D values with gear down, the velocity and range are correct for this trajectory at the time of gear lowering. The lowering of the gear is commanded on a one time only basis and no further velocity corrections are made. Altitude and range errors developed subsequent to the gear drop point continue to be corrected as described and converted into residual velocity errors.

f. The principle reason for the choice of predictive guidance for the longitudinal mode is that the vehicle is unpowered. Therefore, the potential and kinetic energy of the vehicle at each instance must be managed to attain the touchdown objectives. The vehicles height, range, sink rate and forward velocity are controlled by taking into account the drag losses of the possible trajectories to the touchdown point. These vehicle states are highly variable with respect to the random winds encountered.

This is the chief advantage of the predictive approach. It was found that if the unpowered NADWO was guided to a fixed aim point for start of the terminal phase in the presence of winds, the vehicle velocity at the aim point could be too much in error to attain the desired touchdown point. In the presence of random winds, the aim point for the start of the terminal phase must be varied to account for the variation of the vehicle velocity with respect to ground due to the winds. The only alternative to changing the aim point (when speed brakes are not available) is to fly a trajectory prior to initiation of the terminal phases which results in the correct velocity when the vehicle reaches the aim point. This implies prior knowledge of the wind since the required maneuver is based on the winds to be encountered at the lower altitudes. The assumption of no knowledge of the wind structure to be encountered was considered more realistic and, therefore, the aim point for start of the terminal phase was varied with the wind conditions.

This formulation of the guidance laws for the terminal phase is tantamount to assuming that a predictive guidance has been employed in the flight phases prior to initiation of the terminal phase.

g. The L/D of the vehicle strongly effects the flight path of an unpowered vehicle. Anticipating the expected vehicle design changes, the predictive guidance laws developed are not tailored to the L/D of the vehicle studied but are generally applicable by simply utilizing the correct average L/D for each flight phase.

2. Lateral Guidance

a. The desired lateral flight path during the terminal phase is simply the runway centerline with a decrab maneuver, when required, designed to align the vehicle with the centerline at touchdown.

b. The lateral guidance laws are not predictive. A bank command is developed which is a function of both the vehicles offset from the runway centerline and the vehicles crosstrack rate. The vehicle is crabbed into winds and a decrab maneuver is performed.

c. Pure roll or deroll maneuvers, pure decrab maneuvers and combined maneuvers were investigated. The early work was directed towards cross wind compensations by combined roll and yaw into the wind. It was subsequently found that to simultaneously satisfy the cross track velocity constraint, the roll angle approximately level requirement and the heading alignment requirement, that the total time remained nearly constant. Whichever mechanization was incorporated, it favored one of those variables at the expense of the others. Therefore, the decrab law was formulated on the basis of the simplest mechanization which was to crab into the crosswinds and decrab based on the maximum rudder directed decrab rate and the existing crab angle, and optimized for least variation in crosstrack rate and lateral offset at touchdown.

B. Organization of the Guidance System.

The longitudinal guidance of Figure II-1 consists of a flareout predictor, logic for selecting the proper longitudinal phase based on information from the flareout predictor and the vehicle states, and predictive longitudinal guidance laws.

To generate a trajectory during the terminal phase, the predictor is used to predict the errors that will exist when the desired touchdown airspeed and sink rate are reached if the remainder of the nominal terminal phase maneuvers is flown from the current vehicle flight conditions. These errors are then used in predictive longitudinal guidance laws which maneuver the vehicle onto a trajectory from which the predicted trajectory intersects the desired touchdown point. For all phases, these laws are of the form,

$$\theta_c = \theta_{trim} + (k_Z \, \Delta Z^p_{td} + k_X \, \Delta X^p_{td} + k_{\dot{Z}} \, \Delta \dot{Z}) \, (1 + k_I/s)$$

where

θ_{trim} = outside trim command

ΔZ^p_{td} = predicted height error at desired touchdown airspeed

ΔX^p_{td} = predicted range error at desired touchdown airspeed

$\Delta \dot{Z}$ = sink rate error

k_Z, etc. = gains

The outside pitch trim command in this law is based on the trim lift required for each flareout maneuver and is computed using sensed airspeed and assumed vehicle characteristics.

As can be seen from this law, pitch is not used for velocity control during the terminal phase. To control the airspeed at touchdown, the lowering of the landing gear is advanced or delayed from the nominal lowering point which is at an airspeed of 396 ft/sec. To do this, the predictor is used to predict the range that will be travelled to the desired touchdown airspeed if the gear is down all the way and when the range to go to touchdown becomes equal to or less than its predicted range, a command to lower the gear is issued.

The lateral guidance of Figure II-1 consists of logic for selecting the lateral guidance mode and lateral guidance laws for the two modes. The two modes are a coordinated turn mode and a decrab mode. The coordinated turn mode is used from flareout initiation to decrab initiation. The decrab is initiated based on estimated time to go and time required to decrab. In the coordinated turn mode, conventional fixed path lateral guidance laws are used. In the decrab mode, a pure decrab maneuver is used where the vehicle is commanded to yaw to a desired touchdown value and to hold wings level.

C. Problems and Requirements.

1. Problems Due to Lack of Power

The guidance and control problems for unpowered vehicle landings differ from those for powered aircraft in several respects. First, the steady state glide path angle and speed on final approach for a given unpowered vehicle are entirely dependent on the L/D that is flown. The L/D that a vehicle can fly is

normally limited on the upper end by the maximum L/D of the vehicle and, on the lower end by the maximum steady state dynamic pressure limit on the vehicle. From a guidance standpoint, the best nominal L/D is midway between these limits because it allows for equal correction capabilities in the presences of disturbances. For the NADWO, the nominal L/D (assuming a dynamic pressure limit of 400 lb/ft^2) is 7.2 (gear up). This results in a nominal glide angle and speed on final approach of -7.25 degrees and 470 ft/sec, respectively. It can be seen that this glide angle is much steeper than is normally flown by conventional powered aircraft on final approach.

Consider the problems associated with a single flare from this glide slope to touchdown. Because of this steep glide slope, a relatively large flare is required prior to touchdown to break the vehicle's sink rate from its terminal glide value to a value acceptable for touchdown. This flareout can also be used to reduce the velocity at the end of flareout to an acceptable value for touchdown. However, studies have shown that either variable acceleration or very low constant acceleration flares are required to do this for typical orbiter vehicles, including the NADWO. From a manual control standpoint, these types of flares are undesirable since they generally cannot be accomplished with simple sensors and displays, are overly sensitive to pilot control tolerances, and start at altitudes which are too high for good visual cues, even in clear weather.

The terminal phase previously described is designed by synthesizing each of the subphases (previously defined). If a constant

acceleration flare is selected such that a simple accelerometer and display can be used for manual control and the nominal acceleration level is set high enough such that the flare is not overly sensitive to pilot control tolerances, the velocity at the end of flare out for typical orbiter vehicles is too hot for touchdown. To reduce the excess velocity, a glide phase is required. The glide angle during this phase must normally be set at three degrees or higher to provide the necessary obstacle clearance during the glide. However, since this glide slope generally results in a sink rate at touchdown which is too high for typical orbiter vehicles, a second or final flare is generally required just prior to touchdown. The lift required during these phases completely determines the angle of attack at which the vehicle must fly. For an unpowered vehicle, the angle of attack must be continuously increased to maintain the required lift as the velocity decreases. Therefore, if the vehicle does not have some other device, such as speed brakes or flaps, for controlling drag, there is no independent control available for controlling speed and and range errors during these phases unless the landing gear itself is used[1].

If the landing gear is not used, independent speed and range errors at flareout initiation simply remain until touchdown

---

(1) This is true if a constant glide slope is flown to final flare. For flights involving "S" type maneuvers in the longitudinal and/or lateral plane, control can be achieved by varying the amplitude of the "S" maneuvers. However, these maneuvers are considered to be unacceptable to pilots.

and the best that can be done is to compromise between them at touchdown. For the NADWO, a 74 foot range error can be corrected at the expense of only a one ft/sec error in touchdown velocity. Since the assumed allowable velocity dispersions at touchdown are ±25 feet/second, range errors of up to ±1850 feet can be corrected if they are converted to touchdown velocity errors. However, since the assumed allowable dispersions in touchdown range are only ±500 feet, velocity errors of only ±7 feet/second can be corrected. Therefore, a guidance system is required that converts range errors from all other sources into velocity errors at touchdown. With this approach, velocity errors of 32 ft/sec and range errors of 2350 feet at terminal phase initiation can be handled without exceeding the allowable touchdown dispersions.

If the landing gear lowering is timed properly during the terminal phase, as previously suggested, the landing gear drag can then be used to eliminate the velocity error. With the drag available from the NADWO landing gear, the allowable dispersions in speed and range errors at terminal phase initiation are about 57 ft/sec and 4200 ft respectively if the nominal trajectory is designed such that the gear is lowered at airspeed halfway between the nominal airspeeds expected at initiation and termination of the glide airspeeds. These errors are corrected by advancing or retarding the time of gear lowering.

From this, it can be seen that an unpowered vehicle must be guided to a rather precise point at flareout initiation since go around is not possible. To accomplish this, energy management

is required during the final approach. This would be a relatively simple task if the vehicle's energy could always be kept constant at terminal phase initiation. However, in the presence of disturbances, the vehicle must make corrective maneuvers which alter the vehicle's energy. For example, in the presence of a headwind, the ground speed of an unpowered vehicle will be lower by the wind speed and the vehicle will drift aft of the nominal final approach if the same L/D is maintained as for the no wind condition.

The L/D of the vehicle can be increased to compensate for the drift but this will cause the ground speed of the vehicle to decrease even further. As a result of this, if the vehicle is guided to a point at a fixed range and altitude (aim point) from touchdown, the vehicle will reach this point at an energy level which is too low to complete a landing without exceeding allowable dispersions. For the NADWO, the allowable dispersions are exceeded when the headwind magnitude is slightly greater than the mean value (a shear defined by 15 knots at an altitude of 10 feet for the assumed wind model). To compensate for winds greater than this, the guidance system could adjust the flare initiation point as required to insure that allowable touchdown dispersions are not exceeded.

As shown in Figure IV-1, two methods of compensating for this wind drift are possible. Both methods guide the vehicle such that the correct energy for the existing wind condition is attained at primary flare initiate. In the first method shown (where the fixed aim point is maintained), the vehicles L/D is increased by an amount which is more than necessary to correct for the drift

NOTE: ILLUSTRATION FOR HEADWIND CASE

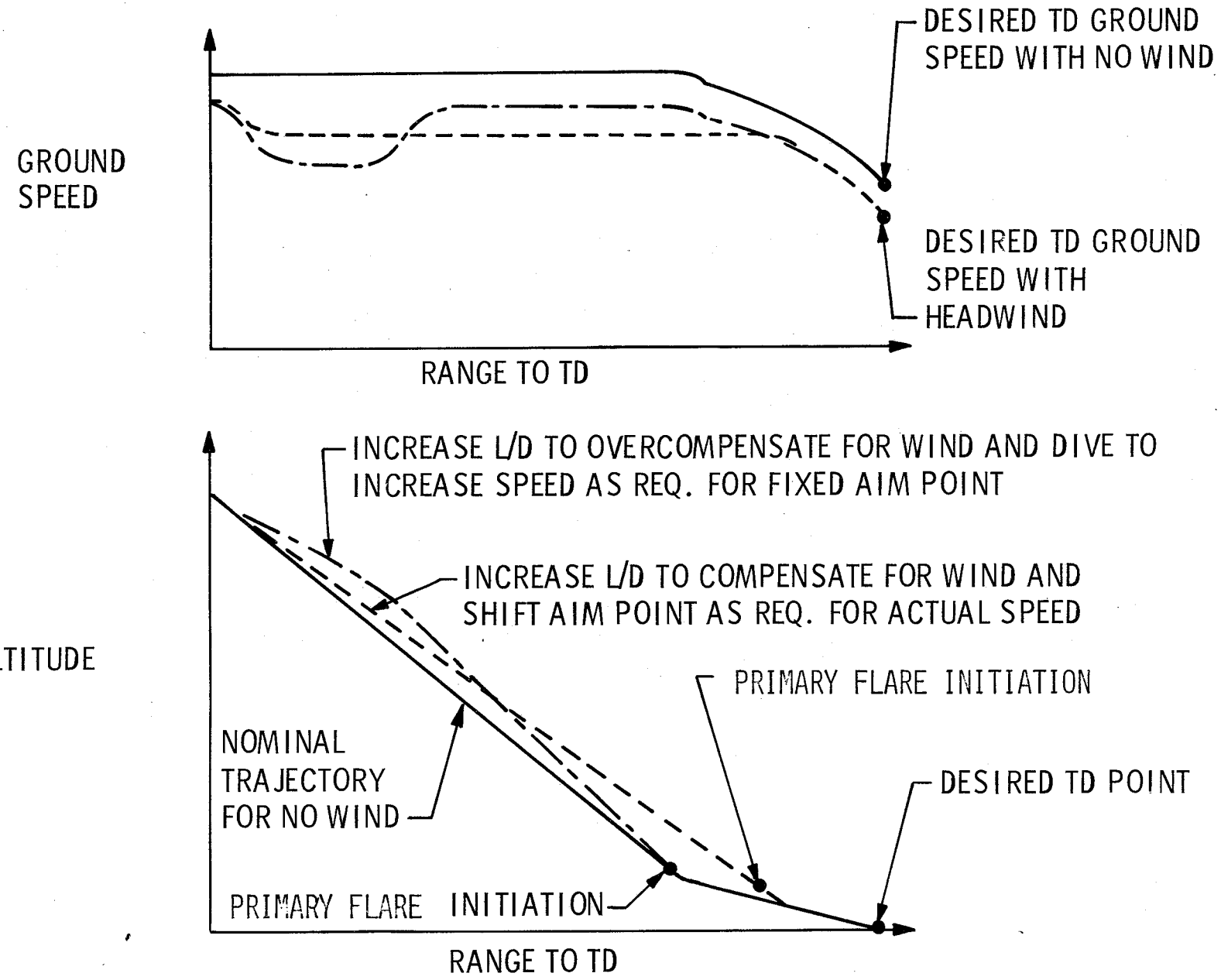

FIGURE IV-1 METHODS OF COMPENSATING FOR WIND

prior to the initiation of primary flare and then decreased sufficiently (diving) to pick up the speed required to make up the proper energy. However, this method requires that a knowledge of the winds to be encountered later in the flight in order to account for the influence of the wind (on the required energy at the fixed flareout initiation point). The second method adjusts the L/D as a function of the actual speed. This results in continuous adjustment of the glide slope and a different aim point for primary flare initiate for different wind conditions. The latter approach is the one selected for this study.

A number of other problems exist for unpowered vehicles stemming from the inability of these vehicles to maintain airspeed. Once the vehicle is in the flareout, the angle of attack must be increased to decrease the glide slope. As soon as this is done, the ground speed and airspeed of the vehicle start to decrease and continue to decrease until touchdown. This is in contrast to the constant indicated airspeed flown by conventional powered vehicles. In addition, since the airspeed decreases, the control power available from the aerodynamic control surfaces decreases as touchdown is approached. For the NADWO, the reduction in control power during flareout is on the order of 2.5 and this results in a significant decrease in the dynamic response of the flight control system if constant gains are used. This presents a significant control problem since it is normally desired to increase the stiffness of the control loops as touchdown is approached. To do this when the control power is decreasing requires variable gains in the flight control system.

In addition, to maintain the required lift, the trim angle of attack must be continuously increased as the airspeed decreases. This results in a significant trimming problem and requires that either high trimming integrator gains or trim feed forward loops be used to prevent large trim errors.

2. Problems Due to Vehicle Characteristics.

There are several aerodynamic characteristics for the NADWO class of vehicles that also result in significant guidance and control problems. The lift coefficients for these vehicles are rather low and, as a result of this, these vehicles must land at either high airspeeds or high angles of attack. The maximum allowable angle of attack at touchdown is normally limited by tail scrape and visibility considerations well before the stall point is reached. These limits normally restrict the airspeed to values above the normal stall speed. For the NADWO, the tail scrape limit on the angle of attack is about 21^{o} assuming near zero glide angle at touchdown and this limits the minimum allowable airspeed at touchdown to 229 ft/sec or 136 knots whereas the stall limit is about 115 knots. Assuming the normal margin of 20% above the minimum airspeed (in this case determined by tail scrape), this angle of attack limit results in a nominal touchdown airspeed of 275 ft/sec or 163 knots.

The low lift coefficient combined with other aerodynamic characteristics of the NADWO class of vehicles also results in a low ratio of the long period change in lift due to a change in angle of attack to the opposing short period change in lift due to the change in trim elevon position required to obtain the change in angle of attack. This ratio is defined as,

$$\frac{\Delta C_{L/\alpha}}{\Delta C_{L/\delta_e}} = \left(\frac{C_{L_\alpha}}{C_{L_{\delta_e}}}\right) \left(\frac{C_{M_{\delta_e}}}{C_{M_\alpha}}\right)$$

where C_{L_α} = slope of lift coefficient due to angle of attack

$C_{L_{\delta_e}}$ = slope of lift coefficient due to elevon

C_{M_α} = slope of pitching moment coefficient due to angle of attack

$C_{M_{\delta_e}}$ = slope of pitching moment coefficient due to elevon.

For control surfaces aft of the c.g., this ratio is negative which means that the initial elevon deflection required to obtain the desired change in angle of attack will result in a short period lift acceleration which is opposite in direction to the long period change in lift acceleration due to the change in angle of attack. Therefore, this ratio provides a useful measure of the destabilizing effect of the elevons on lift. For conventional powered aircraft, this ratio typically has values of from -10 to -30 meaning that the destabilizing lift due to the elevons is small compared to the lift due to the angle of attack. However, forthe NADWO, this ratio is on the order of -1.6 in the landing phase meaning that the destabilizing lift due to the elevons is very significant.

Of course, as the total gain on elevon command is increased above that simply required to trim the vehicle, the destabilizing effect of the elevons will be increased. Although it was found that

guidance laws can be formulated that result in satisfactory control, they cannot eliminate the short period effects of the elevons. This results in a significant problem in controlling the vehicle sink rate near touchdown since any pitch maneuver required to correct the sink rate will result in a significant short period change that is opposite in direction to the desired long period correction. As a result of this, guidance laws are required that do not call for abrupt changes in pitch attitude near touchdown.

In addition to these vehicle characteristics, other vehicle characteristics influence the design of the flight control system and will be discussed in Section V.

3. Nominal Trajectory.

A simple three phase nominal trajectory consisting of a primary flare, a glide, and a final flare was selected for the terminal phase. With this type of trajectory, the primary flare phase is flown from the flareout initiation altitude until the vehicle's glide slope has been reduced to the value desired for the glide phase. The glide phase is then flown to reduce the excess airspeed at the end of primary flare to the magnitude required at the final flare initiation. The final flare phase then reduces the vehicle's sink rate to the desired touchdown value.

For primary flare, a 1.5 "g" constant vertical acceleration flare was selected for the following reasons: (1) it can easily

be flown by a pilot in a manual backup mode; (2) it requires only a simple display of the raw output of the vertical accelerometer on an INS platform for manual control; (3) the acceleration level is well below the three "g" limit on the NADWO but high enough to prevent the flare from being overly sensitive to either manual or automatic control tolerances; (4) the airspeed at the end of this flare is well above the desired touchdown airspeed of 275 ft/sec for all expected flareout initiation conditions and, as a result of this, there is always a float time of at least 10 seconds in the glide phase which is the minimum considered acceptable for the piloted control in the manual backup mode; and (5) the acceleration level is high enough to keep the maximum expected altitude required at flareout initiation to 1400 feet which is low enough to provide good visual cues for manual control in the backup mode.

For the glide phase, a constant three degree glide slope was selected. This glide slope is high enough to provide good obstacle clearance and is compatible with the glide slope flown by conventional powered aircraft on ILS approaches. For the desired touchdown airspeed of 275 ft/sec, this results in a nominal sink rate of about 18 ft/sec as the final flare initiation point is approached.

For the final flare phase, an exponential flare was selected to reduce this sink rate to the desired touchdown value of 3 ft/sec.

The flare has a nominal time constant of 6 sec, and an initial vertical acceleration level of 1.1 g's. This type of flare was selected primarily because it minimizes both the need for any rapid acceleration change near touchdown and the resulting sink rate transient due to the large destabilizing elevon lift. In contrast, a sink rate transient results at the end of a constant acceleration flare in the event of a floater as shown in Figure IV-2.

During the development of the guidance laws, it was decided to use the landing gear as a drag modulation device for controlling airspeed. The nominal point that was selected for lowering the gear was a point where the airspeed reached 396 ft/sec. This point was selected because it is about midway between the nominal airspeed at flareout initiation and the minimum airspeed considered acceptable for lowering the gear based on the assumption that the gear must be lowered at an altitude of 100 feet minimum. This provides about equal capability for correcting airspeed errors on either side of the nominal, by advancing or delaying the lowering of the gear.

In summary, the selected nominal trajectory is specified only in terms of the types of maneuvers flown during the terminal phase (steep re-entry glide slope, constant acceleration primary flare, linear glide slope, exponential final flare). The actual values of altitude and velocity as functions of range or time-to-go are not specified. The trajectory was formulated in this manner because of the limitations of fixed vehicle state trajectories as described in the discussions on energy management and wind problems.

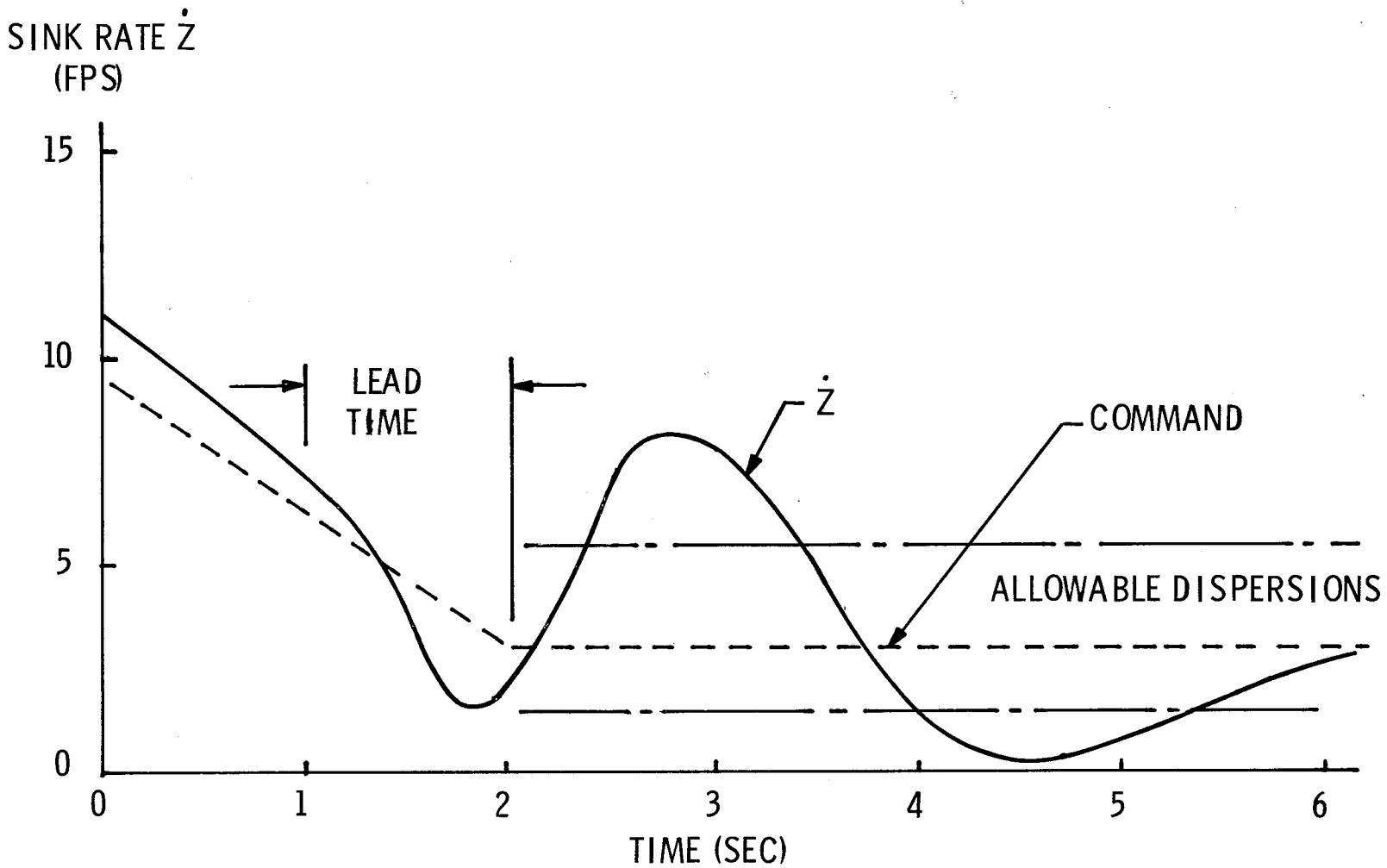

FIGURE IV-2. SINK RATE TRANSIENT AT END OF CONSTANT ACCELERATION FLARE

4. Longitudinal Guidance Design Approach

The approach that was taken in developing the longitudinal guidance laws was first, to develop laws that would determine the altitude and range required at primary flare initiation if the nominal trajectory, described above, were flown from the current vehicle velocity and flight path angle to the desired touchdown conditions. The altitude and range required at primary flare initiation is used prior to flareout initiation to provide an aim point for the final approach guidance system. Since the aim point is based on the current vehicle velocity and flight path angle, it accounts for the effects of changes in these variables on the aim point regardless of whether the changes are due to a maneuver required to correct for a wind or for any other disturbance. In addition, if done repetitively, it accounts for these continuously to the flareout initiation point. Because of this, the maneuvers required to correct for winds and other disturbances are commanded as they occur. Prior knowledge of the disturbance is not required.

Having developed the equations for determining the altitude and range required at primary flare initiation, the second stage in the design was to develop the equations which would be used to determine the altitude and range required at each point after primary flare initiation to touchdown. It was recognized that, the same equations used prior to primary flare initiation to determine the required aim point could also be used to generate the required trajectory from the aim point to touchdown.

A block diagram of the predictive longitudinal guidance system that was designed is shown in Figure IV-3. From this figure, it can be seen that the system is comprised of a longitudinal plane flareout predictor and logic, and longitudinal feedback control laws which initiate each of the three terminal phases and control the vehicle during these phases based on the predicted touchdown information from the flareout predictor.

The flareout predictor was designed to predict the altitude and range that would result if the nominal terminal phase maneuvers were flown from the current vehicle velocity and glide path angle to the desired touchdown airspeed and sink rate. Prior to flare, it was desired to predict the altitude and range that would result if the terminal phase maneuvers were executed from the current vehicle position (shown in Figure IV-4). The required aim point can then be determined simply by subtracting these predicted values from the actual vehicle altitude and range to the touchdown point. For example, if the vehicle is 1100 feet above the runway and the flareout predictor predicts (if the nominal terminal phase maneuvers were executed immediately) the vehicle would be 100 feet above the runway when the desired touchdown airspeed and sink rate are reached, then the required flareout initiation altitude is 1000 feet above the runway.

During the terminal phase, the predictor was designed to compute the height and range errors from the current vehicle position. For example, if the vehicle is part way through the primary flare, the predictor computes the values of the errors that would

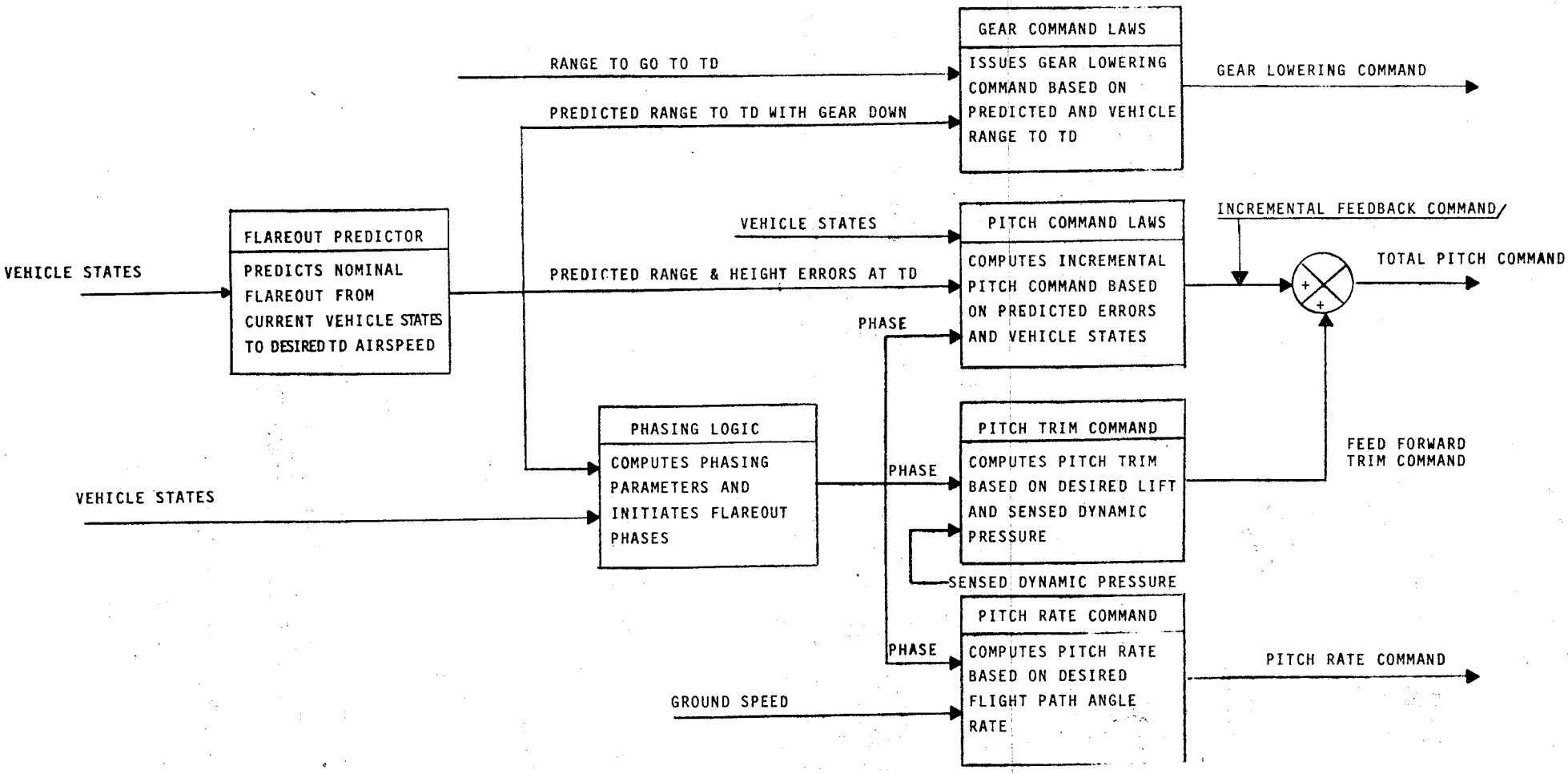

FIGURE IV-3 PREDICTIVE LONGITUDINAL GUIDANCE

FIGURE IV-4 FLAREOUT PREDICTOR

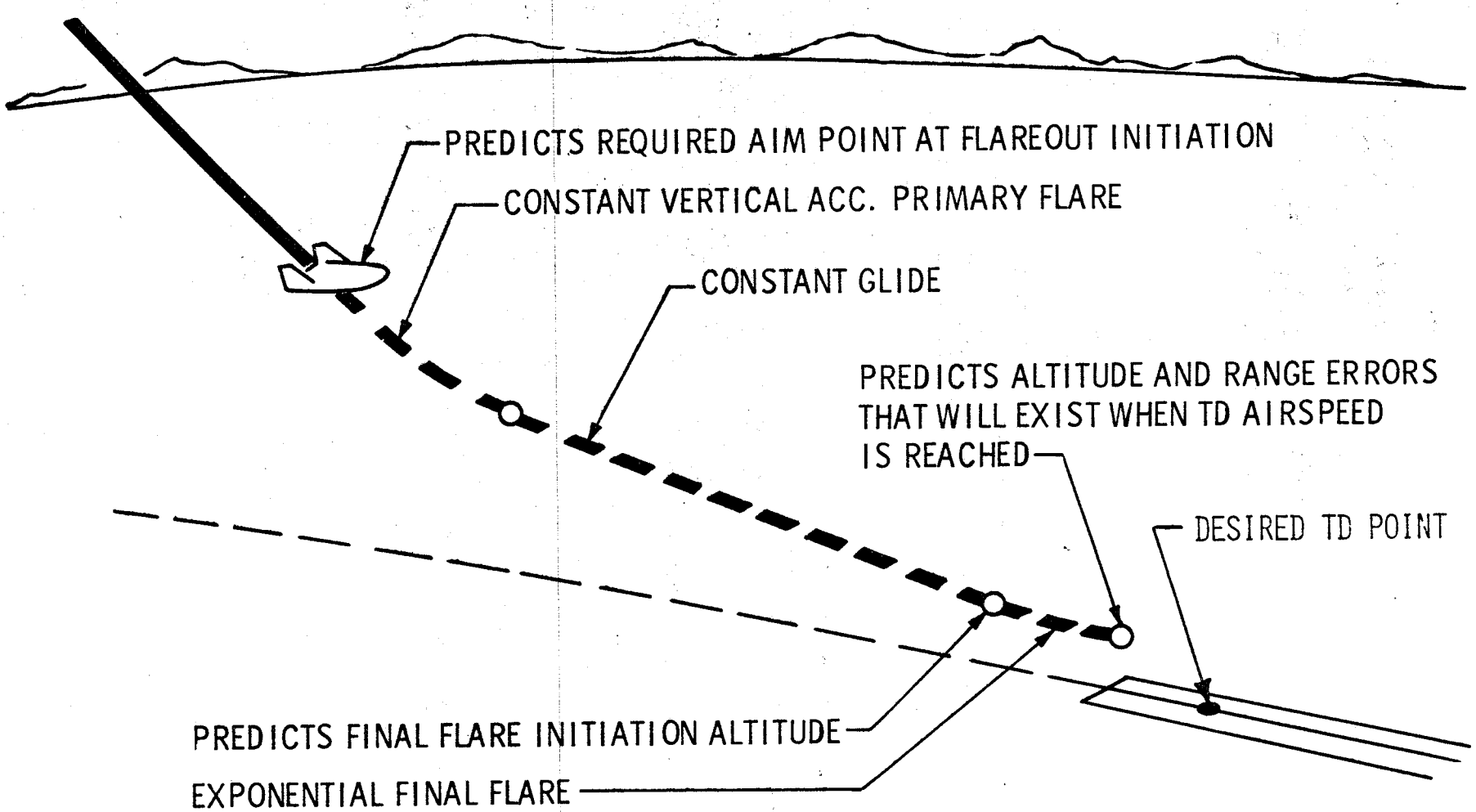

result if the remainder of the nominal primary flare, glide, and final flare maneuvers were flown from the current vehicle velocity and glide path angle. If the vehicle is part way through the glide phase, the predictor calculates the errors if the nominal glide and the final flare maneuver were flown.

In the predictive guidance system, the logic was designed to initiate the flareout phases based on the information from the flareout predictor. The primary flare phase is initiated based on the predicted altitude required at flareout initiation. The final flare phase is initiated based on the predicted altitude required for final flare. The glide phase is initiated based on the desired glide angle. In all cases, lead terms were included on the phase initiation parameters to account for the effect of the destabilizing elevon lift during the required pitch maneuver at the start of each phase.

The longitudinal feedback laws were designed to use the predicted altitude and range at the desired touchdown airspeed to command pitch attitude changes that will cause the vehicle to fly a trajectory that will intersect the desired touchdown point both at the desired sink rate and velocity. This was done by resolving the altitude and range errors into an equivalent altitude error normal to the desired glide slope during the glide phase as shown in Figure IV-5. As shown in this figure, if the pitch guidance law is used to drive this error to zero, the vehicle will be on a trajectory that, under ideal conditions, will intersect the runway at the desired point and at the desired sink rate and velocity. The pitch guidance laws convert errors from all sources during flareout into a velocity error at touchdown as desired.

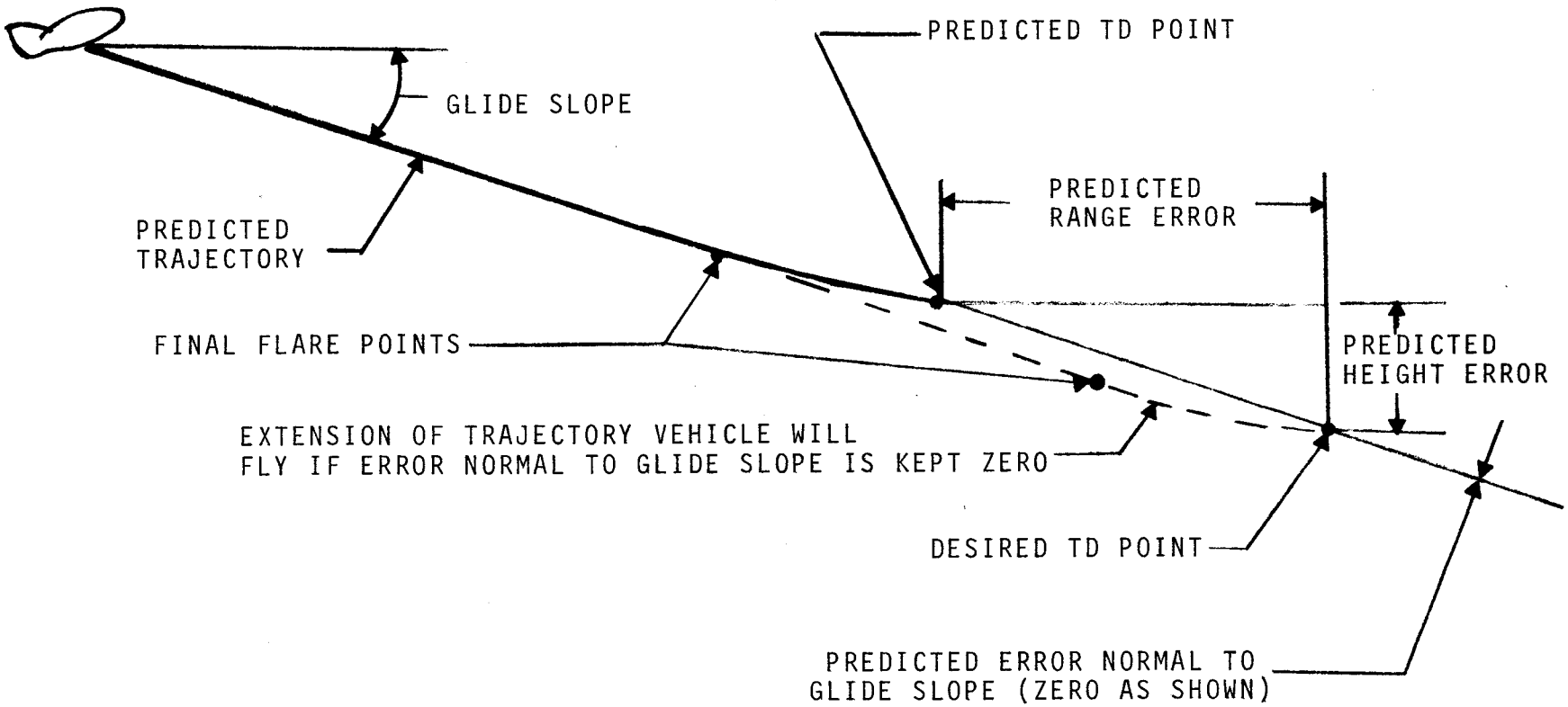

FIGURE IV-5 RANGE-HEIGHT CONTROL TECHNIQUE

If the actual range to touchdown and the range determined by the predictor differ, the vehicle will be guided to the actual touchdown point but with a speed which differs from the desired speed. This is shown in Figure IV-6, which shows the trajectories resulting from off nominal initial conditions. As shown in this figure, all touchdown errors were insignificant except for the velocity error.

To control this velocity error, the flareout predictor was also designed to predict the range that would be travelled to the desired touchdown airspeed if the landing gear were down all the way after primary flare. Since the longitudinal guidance predictor was designed to estimate the range required at terminal phase initiation for a nominal glide maneuver where the gear is lowered at an airspeed of 396 ft/sec during the glide, the vehicle will nominally reach this point after primary flare where the range to touchdown is greater than that predicted with the gear down all the way. However, as the vehicle is guided towards the touchdown point with the gear up, the range to touchdown will decrease faster than that predicted with gear down, and eventually the predicted range with gear down will be equal to the actual range to go. This of course if the time when the vehicle landing gear should be lowered. Gear command laws were designed to compare these ranges and issue a command to lower the gear when this situation occurs.

To cope with the large pitch trim changes required due to the changes in airspeed during flareout, the pitch laws were designed to compute a pitch trim command. This command is fed forward

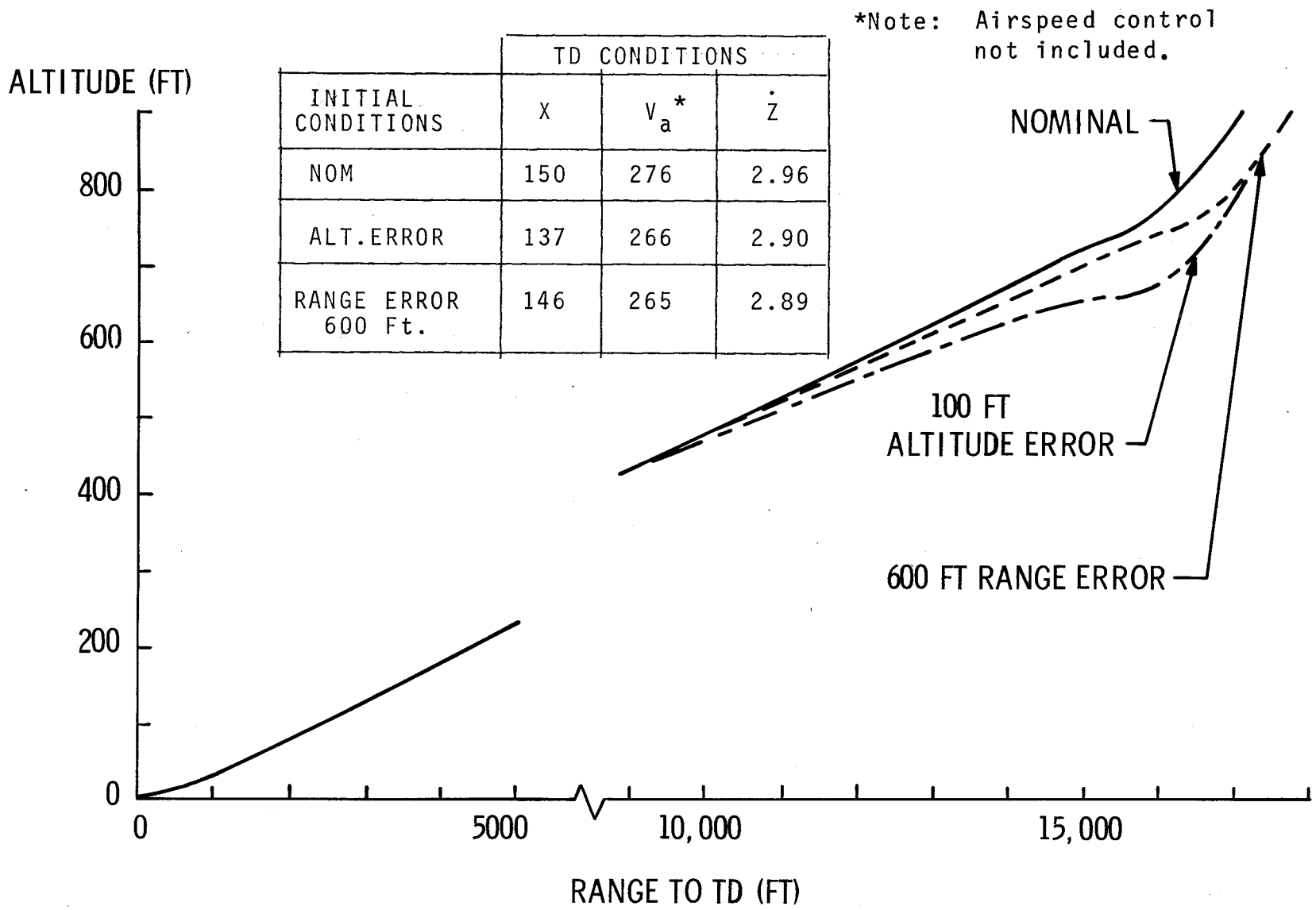

INITIAL CONDITIONS	TD CONDITIONS X	V_a*	$\dot{Z}$
NOM	150	276	2.96
ALT.ERROR	137	266	2.90
RANGE ERROR 600 Ft.	146	265	2.89

FIGURE IV-6 PREDICTIVE GUIDANCE TRAJECTORIES FOR NOMINAL AND OFF NOMINAL INITIAL CONDITIONS

into the pitch command channel and greatly reduces the load on the pitch trimming integrator. To reduce the load on the elevon trimming integrator in the flight control laws, the pitch laws were also designed to compute a pitch rate command and to feed this forward into the flight control laws.

5. Lateral Guidance Design Approach.

a. General

The laws required for the lateral guidance may be classified into two distinct phases. These are the laws required before and after the initiation of the final runway alignment maneuver. The final runway alignment maneuver is the transition from the far range lateral guidance to that required for touchdown. At far ranges it is sufficient to direct and maintain the vehicle's velocity vector in the vertical plane which contains the runway centerline. At touchdown, ideally, the vehicle's heading and velocity vector should be aligned with the runway centerline and the wings should be level. (Note: Landing gear which may be aligned to the runway centerline independently of the vehicle heading are not being considered.) In practice, compromises in these ideals must be accepted. The alignment maneuver may be:

(1) Decrab. With the velocity vector aligned with the runway and the sideslip angle held to zero, the vehicle is initially heading into the relative wind (crabbing). The vehicle is yawed (decrab) so that its heading is aligned with the runway to within acceptable limits at TD.

(2) Deroll. With the velocity vector and heading aligned with the runway, the vehicle is initially rolled into the crosswind. The vehicle is derolled so that the roll angle is within acceptable limits at TD.

(3) Combined. This is a combination of the first two. By partially crabbing and partially rolling into crosswinds, both the heading and roll angle misalignments are reduced.

(4) Predictive. Utilizing any of the above approaches, the guidance orients the velocity vector and lateral flight path such that an apparent lateral drift and offset from the runway centerline exists. The magnitude of the drift and offset are based on predicted runway alignment transients. The alignment maneuver is executed such that the predicted net drift and offset at TD is zero. (Note: This maneuver is generally considered unacceptable to pilots.)

b. Summary of Selected Systems

The lateral guidance laws used prior to the final runway alignment maneuver were conventional fixed path laws since neither the lack of control power nor the NADWO characteristics presented any unusual problems prior to runway alignment. These laws were based on bank commands proportional to both the lateral offset and the crosstrack rate with respect to the runway centerline. (Appropriate gain changes with range and limiters were also included, see section IV.D.3.(c)).

Prior to the runway alignment maneuver, the flight control system was designed to weather cock the vehicle into the wind as required to coordinate the turns and, therefore, the selected

runway alignment maneuver was a pure decrab. The system was designed to command the required heading for runway alignment and to command wings level (zero roll angle). During this phase, the flight control system was designed to operate in a yaw and roll hold mode.

The system was designed to initiate the decrab maneuver based on time to go and time to decrab. The time to go is based on the current vehicle height and an average commanded sink rate. Commanded sink rate was selected over actual sink rate for determining this parameter because it was found that the destabilizing elevon lift produced sink rate transients that were large enough to prematurely initiate the decrab maneuver. The time to decrab is based on the magnitude of the decrab angle and the available yaw control power.

c. Decrab Discussion

During the decrab maneuver, the large changes in lateral characteristics with angle of attack and the strong coupling of yaw into roll present several problems for the NADWO. When the decrab maneuver, described above, was executed, it was found that the sideslip buildup during the decrab could result in severe roll transients unless properly compensated. In addition, it was found that, if the decrab maneuver was performed fast enough such that no appreciable lateral velocity was built up, the resulting sideslip angle in the 3 sigma cross wind produced a rolling moment that required the full aileron deflection of 12.5 deg. (aileron saturation).

Further studies showed that the sideslip induced rolling moment could be adequately compensated by crossfeeding

estimated sideslip directly into the aileron controls. This is discussed in Section V. In addition, the aileron saturation problem was relieved by decrabing slowly and allowing the vehicle to build up lateral velocity and/or by not fully decrabing. The amount that the aileron saturation problem can be relieved is limited by the maximum allowable touchdown dispersions in the lateral parameters and this in turn limits the maximum cross wind that the vehicle can land in. For the selected touchdown dispersions and no gusts, this limit is about 30 knots for the NADWO. Since some aileron control power must be reserved to compensate for gusts and other disturbances, the effective limit is about 15 knots based on the simulation studies.

d. Deroll Discussion

Before settling on the pure decrab alignment maneuver, the deroll and combined maneuvers were investigated. (Predictive alignment maneuvers were rejected because of unacceptability to pilots.)

It was found that the sideslip induced roll transient problem could be eliminated if pure deroll laws were used. The vehicle was first gradually aligned with the runway by sideslipping and rolling into the wind and then derolled to zero at an appropriate point prior to touchdown. However, the roll transient problem was replaced by a roll trim problem prior to deroll. Since full aileron deflection was required to compensate for the sideslip induced rolling moment in a 15 knot crosswind, this left no margin for gusts and other corrections.

It was further found that it was not desirable to allow the lateral velocity to build up and decrease the sideslip angle prior to the deroll maneuver since this lateral velocity build up could exceed that resulting from the decrab maneuver. The resultant total lateral velocity after deroll was, therefore, higher even though the time to deroll was less.

Figure IV-7 compares pure decrab and deroll maneuvers.

e. Combined Maneuver Discussion

Combined decrab and deroll laws were also studied where the vehicle was first partially weather cocked and partially rolled into the wind and then decrabed and derolled at an appropriate point prior to touchdown. As expected, this relieved the aileron saturation problem prior to decrab and deroll but at the expense of a potential roll transient problem during the partial decrab maneuver. In addition, it did not relieve the aileron saturation problem during the decrab and deroll maneuver. This is illustrated in Figure IV-8 for a combined maneuver in the 15 knot crosswind.

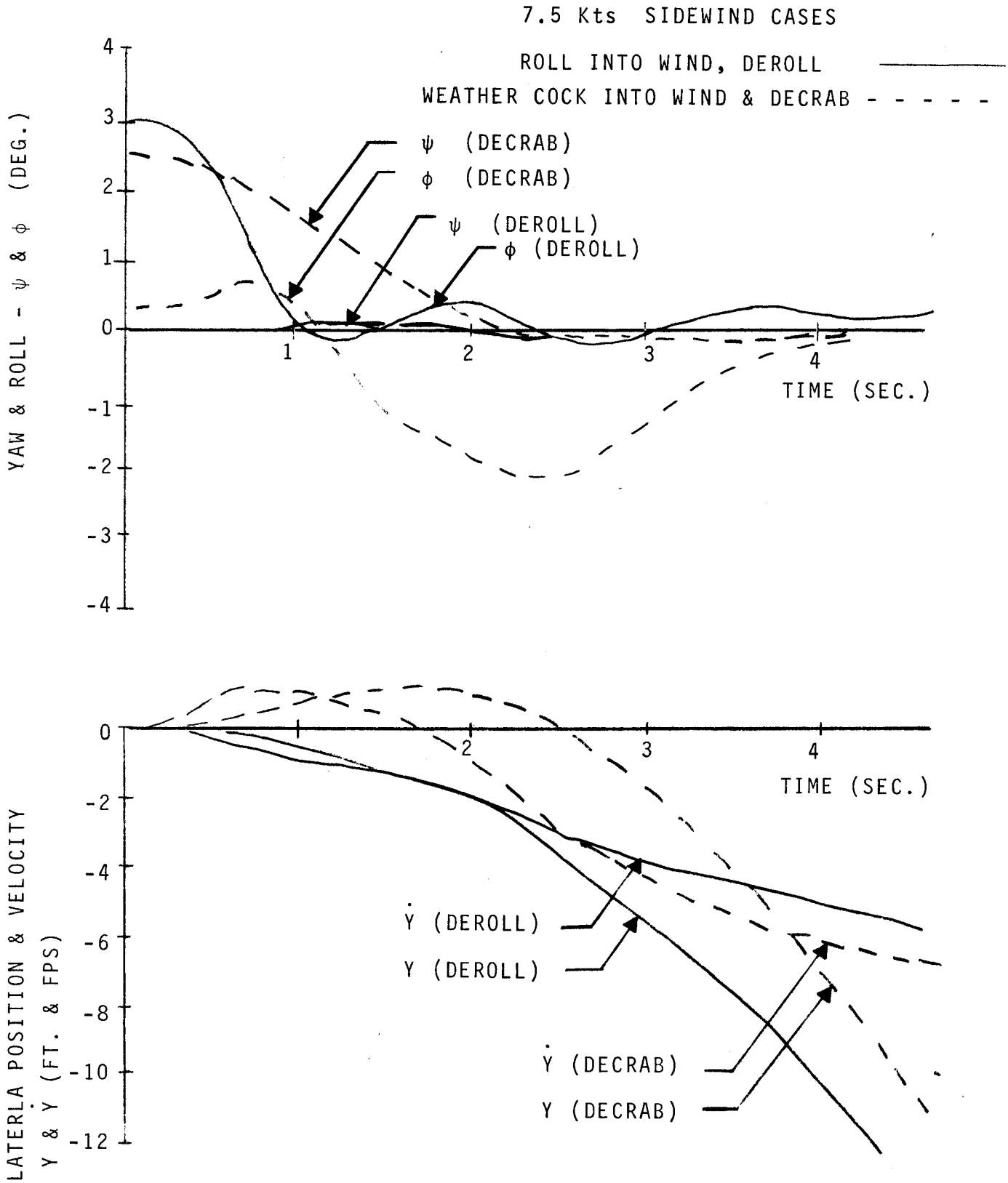

FIGURE IV-7. DECRAB AND DEROLL MANEUVERS PRIOR TO TD.

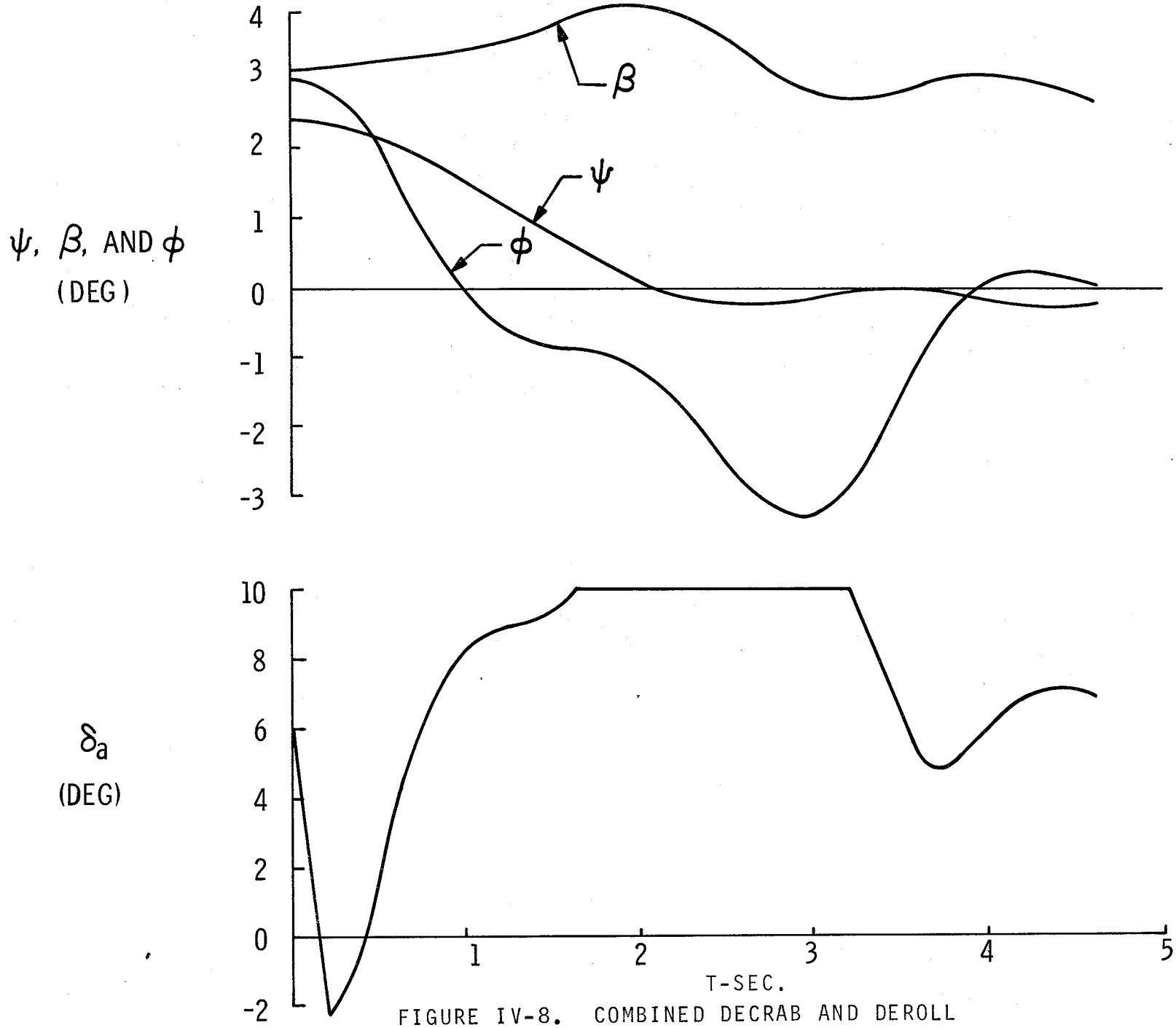

FIGURE IV-8. COMBINED DECRAB AND DEROLL MANEUVER IN 15 KNOT CROSSWIND

D. Detailed Description.

1. Flareout Predictor.

The flareout predictor predicts the altitude and range that would result when the touchdown velocity and sink rate are reached if the nominal flareout maneuvers were flown from the current vehicle velocity and glide path angle to touchdown. It does this by solving a set of implicit equations for each of the nominal flareout maneuvers; i.e., primary flare, glide, and final flare. The equations for the primary and final flare maneuvers are solved first using the current vehicle flight conditions and the desired touchdown velocity and sink rate as boundary conditions respectively. The necessary boundary conditions at the start and end of the glide maneuver are then established from these solutions and the equations for the glide maneuver are solved for.

The equations for the constant vertical acceleration primary flare maneuver are,

$$\dot{Z} = -V \sin \gamma$$

$$\dot{Z}^p_{ef} = -V^p_{ef} \sin \gamma_g$$

$$\Delta t^p_f = -(\dot{Z} - \dot{Z}^p_{ef})/\ddot{Z}_f$$

$$\Delta Z^p_{ef} = -\dot{Z}\,\Delta t^p_f - .5\,\ddot{Z}_f\,(\Delta t^p_f)^2$$

$$V^p_{EF} = V - \frac{(-\ddot{Z}_f + g)\,\Delta t^p_f}{(L/D)_{f\ avg}} + \frac{g\,(\dot{Z} + .5\,\ddot{Z}_f\,\Delta t^p_f)\,\Delta t^p_f}{.5\,(V + V^p_{ef})}$$

$$\Delta X^p_F = .5\,(V \cos\gamma + V^p_{ef} \cos\gamma_g)\,\Delta t^p_f$$

where:

$(L/D)_{f\ avg}$ = average lift to drag ratio during primary flare with gear up (nominally 8.0 for the NADWO)

V = current vehicle ground speed (ft/sec)

$\dot{Z}$ = current vehicle sink rate (+ down, ft/sec)

$\ddot{Z}_f$ = desired vertical acceleration for primary flare maneuver (nominally -16 ft/sec^2)

V^p_{ef} = predicted ground speed at end of primary flare (ft/sec)

$\dot{Z}^p_{ef}$ = predicted sink rate at end of primary flare (ft/sec)

Δt^p_f = predicted time required for primary flare (sec)

ΔX^p_f = predicted range traveled during primary flare (ft)

ΔZ^p_{ef} = predicted height traveled during primary flare (ft)

γ = current vehicle glide path angle (- down, rad)

γ_g = desired glide path angle during glide maneuver (nominally -3 deg)

The equations for the exponential final flare maneuver are,

$$\dot{Z}^p_{eg} = -V^p_{eg} \sin\gamma_g$$

$$\tau^p_{ff} = \dot{Z}^p_{eg}/\ddot{Z}_{ff}$$

$$\Delta t^p_{ff} = \tau_{ff} \ln(\dot{Z}^p_{eg}/\ Z_{td})$$

$$\Delta Z^p_{ff} = \frac{(\dot{Z}^p_{eg})^2}{\ddot{Z}_{ff}} \left(1 - e^{-(\Delta t^p_{ff}/\tau^p_{ff})}\right)$$

$$V^p_{eg} = V_{td} + \frac{(-\ddot{Z}_{ff} + g)\ \Delta t^p_{ff}}{(L/D)_{ff\ avg}} - 0.5g\ (\sin \gamma_g - \dot{Z}_{td}/V_{td})\ \Delta t^p_{ff}$$

$$\Delta X^p_{ff} = 0.5\ (V^p_{eg} \cos \gamma_g + V_{td})\ \Delta t^p_{ff}$$

where $(L/D)_{ff\ avg}$ = average lift to drag ratio during final flare with gear down (nominally 5.2 for NADWO)

V_{td} = desired touchdown ground speed (ft/sec)

V^p_{eg} = predicted ground speed required at end of glide (ft/sec)

$\dot{Z}_{td}$ = desired touchdown sink rate (nominally 3 ft/sec)

$\ddot{Z}_{ff}$ = desired vertical acceleration at start of exponential final flare maneuver (nominally -3 ft/sec^2)

$\dot{Z}^p_{eg}$ = predicted sink rate at end of glide (ft/sec)

Δt^p_{ff} = predicted time required for exponential final flare (sec)

ΔX^p_{ff} = predicted range traveled during final flare (ft)

ΔZ^p_{ff} = predicted height traveled during final flare (ft)

τ^p_{ff} = predicted time constant for exponential final flare (sec)

The desired touchdown ground speed in these equations is computed as,

$$V_{td} = V_{a\ td} - \Delta V_{w\ td},$$

where: $V_{a\ td}$ = desired touchdown airspeed (nominally 275 ft/sec)

$\Delta V_{w\ td}$ = estimated wind speed along ground speed velocity vector at touchdown (ft/sec).

The estimated wind speed at touchdown is assumed to be one half of the current wind speed as computed from sensed airspeed and inertial ground speed. This factor was included to account for the effect of the expected wind shear during flareout on the wind speed at touchdown and on the corresponding ground speed required to obtain the desired touchdown airspeed. It was found that deviations in the expected wind shear did not result in significant errors with this assumption.

The equations for the portion of the glide phase with the gear up are:

$$V^p_{a\ ef} = V^p_{ef} + \Delta V_{wf}$$

$$V^p_{a\ gd} = V_{a\ gd\ nom}, \text{ if } V_{a\ gd\ nom} < V^p_{a\ ef}$$

$$= V^p_{a\ ef}, \text{ if } V_{a\ gd\ nom} \geq V^p_{a\ ef}$$

$$\Delta V_{wf} = \frac{V_a - V}{\tau_w s + 1}$$

V_a is sensed airspeed

τ_w is filter time constant

$$(L/D)^p_{ef} = 8.76 - 0.041\ (V^p_{a\ ef} - 396)$$

$$(L/D)^p_{gu} = 8.76 - 0.041\ (V^p_{a\ gd} - 396)$$

$$(L/D)^p_{gu\ avg} = .5\left[(L/D)^p_{ef} + (L/D)^p_{gu}\right]$$

$$V^p_{gd} = V^p_{a\ gd} - \Delta V_{wf}$$

$$\Delta t^p_{gu} = \frac{(V^p_{ef} - V^p_{gd})}{g/(L/D)_{gu\ avg} + g \sin \gamma_g}$$

$$\Delta X^p_{gu} = .5\ (V^p_{ef} + V^p_{gd})\ \Delta t^p_{gu},$$

where $(L/D)^p_{ef}$ = predicted lift to drag ratio at end of primary flare with gear up

$(L/D)^p_{gu}$ = predicted lift to drag ratio with gear up just prior to gear lowering point

$(L/D)^p_{gu\ avg}$ = average predicted lift to drag ratio during portion of glide with gear up

$V_{a\ gd\ nom}$ = airspeed at which gear is nominally lowered (nominally 396 feet/sec)

$V^p_{a\ ef}$ = predicted airspeed at end of primary flare (ft/sec)

$V^p_{a\ gd}$ = predicted airspeed at nominal gear lowering point (ft/sec)

V^p_{gd} = predicted ground speed at nominal gear lowering point (ft/sec)

ΔV_{wf} = filtered value of current wind speed along ground velocity vector (feet/sec)

Δt^{p}_{gu} = predicted time for portion of glide with gear up (sec)

ΔX^{p}_{gu} = predicted range traveled during portion of glide with gear up

The equations for the portion of the glide maneuver with the gear down are,

$$V^{p}_{a\ eg} = V^{p}_{eg} + \Delta V_{wf}$$

$$(L/D)^{p}_{gd} = 7.9 - 0.035\ (V^{p}_{a\ gd} - 320)$$

$$(L/D)^{p}_{eg} = 7.9 - 0.035\ (V^{p}_{a\ eg} - 320), \text{ if less than } 6.8$$

$$= 6.8\ , \text{ if greater than } 6.8$$

$$(L/D)^{p}_{gd\ avg} = .5\left[(L/D)^{p}_{gd} + (L/D)^{p}_{eg}\right]$$

$$\Delta t^{p}_{gd} = \frac{(V^{p}_{gd} - V^{p}_{eg})}{g/(L/D)^{p}_{gd\ avg} + g \sin \gamma_{g}}$$

$$\Delta X^{p}_{gd} = .5\ (V^{p}_{gd} + V^{p}_{eg})\ \Delta t^{p}_{gd},$$

where $(L/D)^{p}_{gd}$ = predicted lift to drag ratio with gear down just after gear lowering point

$(L/D)^{p}_{eg}$ = predicted lift to drag ratio with gear down at end of glide

$(L/D)^{p}_{gd\ avg}$ = predicted average lift to drag ratio for portion of glide with gear down

$V^p_{a\ eg}$ = predicted airspeed at end of glide maneuver (ft/sec)

Δt^p_{gd} = predicted time required for portion of glide with gear down (sec)

ΔX^p_{gd} = predicted range traveled during portion of glide with gear down (ft)

The total predicted range traveled during the glide is,

$$\Delta X^p_g = \Delta X^p_{gu} + \Delta X^p_{gd} \quad ,$$

and the predicted height traveled during the glide is,

$$\Delta Z^p_g = -\Delta X^p_g \sin \gamma_g$$

It can be seen from the predictor equations for the glide maneuver that, in predicting the airspeeds at the nominal gear lowering point and at the end of glide, it is assumed that the wind speed is the same as the current wind speed. This is because most of the expected wind shear occurs during the final flare phase. Deviations from the expected wind shear were not found to result in significant errors mainly because the predicted airspeeds are only used to predict lift to drag ratios which are not overly sensitive to small changes in airspeed. Conversely, it was found that, when the effect of airspeed on lift to drag was ignored entirely and average lift to drag ratios were used as in the primary and final flare equations, the prediction errors in the glide phase were significant. This is because the changes

in airspeed at the beginning of glide that result from maneuvers required for wind compensation do have a significant effect on the lift to drag ratio in the glide phase. Although these changes also have the same effect on the lift to drag ratio for the primary flare phase, ignoring them here does not result in significant errors in the total prediction since the primary flare phase is short compared to the glide phase for the NADWO.

The total height and range traveled during the flareout maneuvers are simply the sum of the increments from each phase.

$$\Delta Z^p = \Delta Z^p_{ef} + \Delta Z^p_g + \Delta Z^p_{ff}$$

$$\Delta X^p = \Delta X^p_{ef} + \Delta X^p_g + \Delta X^p_{ff}$$

The predicted height and range from the desired touchdown point that will result when the desired touchdown airspeed and sink rate are reached are then:

$$\Delta Z^p_{td} = Z - \Delta Z^p$$

$$\Delta X^p_{td} = |X| - \Delta X^p \ ,$$

where: X = current range from desired touchdown point (ft)

Z = current height above desired touchdown point (+ down, ft.)

Prior to flareout initiation and during the primary flare, the predictor equations are solved in the form presented.

However, when the vehicle is in the glide phase, two changes are made. First, the prediction of the primary flare maneuver is bypassed. This is done by setting the predicted height and range increments for this phase to zero and by setting the predicted ground speed at the end of this phase to the current vehicle ground speed. Second, the range traveled during the glide phase is predicted with the gear down all the way as discussed previously under guidance design. This is done by bypassing the glide equations for the gear up portion of the glide and by setting the range traveled during this portion to zero and the airspeed and ground speed at the beginning of the gear down portion to the current vehicle values.

In both cases, it can be seen that the predictor equations are implicit in terms of the predicted ground speeds and require an iterative solution. It was found that real time iteration techniques, in which the previous values of the predicted ground speeds are simply used on the right hand side of the implicit equations, result in solutions with sufficient accuracy as long as solution rates of about 10 times per second are used.

2. Phase Selection Logic

The logic for selecting the flareout phase is as follows:

If $Z < Z^p_{sf}$, final approach phase

If $Z \geq Z^p_{sf}$, primary flare phase

If $\gamma \geq \gamma_{sg}$, glide phase

If $Z \geq Z^p_{sff}$, final flare phase

where: Z^p_{sf} = predicted height required at start of primary flare (ft)

γ_{sg} = glide path angle required at start of glide (rad)

Z^p_{sff} = predicted height required at start of final flare (ft)

The predicted heights required at the start of primary and final flare are computed as,

$$Z^p_{sf} = Z - Z^p_{td} + \Delta Z_{lf}$$

$$Z^p_{sff} = \Delta Z^p_{ff} + \Delta Z_{lff}$$

where: ΔZ_{lf} and ΔZ_{lff} = lead terms used to account for effect in vehicle pitch response at start of maneuver (ft.).

The lead terms are computed as

$$\Delta Z_{li} = -\dot{Z}\Delta t_{\theta i}$$

where: $\Delta t_{\theta i}$ = estimated time required to perform required pitch maneuver (sec).

The estimated time is computed as,

$$\Delta t_{\theta i} = \Delta t_o + \Delta\theta_i / \dot{\theta}_{eff}$$

where: Δt_o = initial pitch time delay (nominally 0.8 sec)

$\Delta\theta_i$ = pitch change required at start of maneuver (deg)

$\dot{\theta}_{eff}$ = effective pitch rate (nominally 4 deg/sec).

The pitch change required at the start of the maneuver is estimated as,

$$\Delta\theta_i \cong \Delta\alpha_i$$

$$\cong \frac{-\dddot{Z}_i}{Q(S/m)C_{L_\alpha}}$$

where: $\dddot{Z}_i$ = desired vertical acceleration at start of maneuver ($\ddot{Z}_f$ for primary flare, $\ddot{Z}_{ff}$ for final flare)

Q = sensed dynamic pressure (lb/ft^2)

(S/m) = assumed vehicle reference area to mass ratio (nominally 0.92 ft^2/slug)

C_{L_α} = assumed vehicle trim lift coefficient slope (nominally 0.026/deg).

The glide path angle γ_{sg}, at which the glide phase is initiated is computed as,

$$\gamma_{sg} = \gamma_g + \Delta\gamma_{lg}$$

where: γ_{lg} = lead term used to account for effect of lag in vehicle pitch response during pitch down maneuver at start of glide (rad)

The flight path angle lead term is computed as,

$$\Delta\gamma_{lg} = \dot{\gamma}\Delta t_{\theta g}$$

where: $\dot{\gamma}$ = rate of change of vehicle flight path angle (rad/sec)

$\Delta t_{\theta g}$ = estimated time required to perform pitch down maneuver (sec)

The rate of change of the vehicle flight path angle is estimated as,

$$\dot{\gamma} = -\ddot{Z}_f/V$$

and the time required, $\Delta t_{\theta g}$, is estimated in the same manner as for the pitch maneuver at the start of primary flare since the acceleration change required is the same.

In the phase selection logic, locks are provided that lock the guidance into each phase as it is entered and prevent the previous phases from being reentered. In the airbore system, a reset switch should be provided to unlock all of the locks in the event that a system malfunction causes a premature lock into one of the flareout phases.

In addition to setting the locks at the start of each phase, certain additional prediction functions are done at the start of the final flare. In the flareout predictor, the height required for exponential final flare is predicted based on the current vehicle ground speed and the desired glide path angle during glide. However, if the vehicle's glide path angle is off nominal, the acceleration level must be changed to accomplish the exponential flare from the same height as predicted for the nominal glide angle. Therefore, to account for the effect of off nominal glide path angle, the acceleration level required to accomplish the exponential flare from the nominal glide path angle height is predicted at the start of the final flare based on the actual vehicle glide path angle. This was done here instead of in the flareout predictor because it was found that accounting for glide path angle deviations in the flareout predictor resulted in a noisy final flare initiation altitude and that the effect of these deviations could easily be compensated for by slight changes in the acceleration level.

The prediction equations for doing this are,

$$\ddot{Z}^{p}_{ff} = \frac{\dot{Z}^{2}}{\Delta Z^{p}_{ff}} \left(1 - e^{-(t/\tau)}\right)$$

$$\dot{Z} = -V \sin \gamma$$

$$(t/\tau) = \dot{Z}/\dot{Z}_{td}$$

3. Feedback Laws

(a) Longitudinal

The pitch command feedback law for all flareout phases is,

$$\theta_c = \theta_{trim} + k_{vg} \left[-k_{zi} (Z_{ci} - Z) - k_{xi} \Delta X^p_{td} - k^{\cdot}_{zi} (\dot{Z}_{ci} - \dot{Z}) \right] \left[1 + k_{zI/s} \right]$$

where:

k_{vg} = variable gain (function of range)

k_{zi} = height error gain (deg/ft)

k_{xi} = range error gain (ft/ft)

$k^{\cdot}_{zi}$ = sink rate error gain (deg/ft/sec)

k_{zI} = pitch trimming integrator gain (nominally 0.1/sec)

Z_{ci} = height command (ft)

$\dot{Z}_{ci}$ = sink rate command (ft/sec)

θ_{trim} = estimated pitch attitude required for trim (deg)

During the primary flare, the pitch feedback law parameters are set as follows:

$k_{xi} = k_x - \sin\gamma_g$ (nominally 0.053 deg/ft)

$k_{zi} = k_z$ (nominally 0.128 deg/ft)

$k^{\cdot}_{zi} = 0$

$Z_{ci} = Z - \Delta Z^p_{td}$

Three things should be noted here. First, the feedback law in this phase is truly predictive since only the predicted errors in height and range are being fed back. Second, the predicted

height and range errors at touchdown are first converted into an equivalent height error normal to the glide slope and then multiplied by the height error gain. As discussed previously, this causes the guidance system to guide the vehicle along a path where the predicted height error at touchdown and the equivalent height error due to the predicted range error at touchdown cancel each other out and such a path is one that intersects the runway at the desired touchdown point. By doing this, errors from all sources are being converted into a velocity error which can then be corrected by advancing or delaying the lowering of the landing gear. The third thing to note is that no sink rate error term is fed back during this phase. This is because the flareout predictor predicts the primary flare phase based on the actual vehicle glide path angle and, therefore, the effect of sink rate is automatically accounted for in the predicted errors at touchdown.

During the glide phase, the pitch feedback law parameters are set as follows,

$$k_{xi} = k_x - \sin\gamma_g$$

$$k_{zi} = k_z$$

$$k_{zi}^{\cdot} = k_z^{\cdot} \quad \text{(nominally 0.106 deg/ft/sec)}$$

$$Z_{ci} = Z - Z_{td}^{p}$$

$$\dot{Z}_{ci} = -V \sin\gamma_g$$

It can be seen that these are the same as for the primary flare phase with the exception that a sink rate error term is included in this phase. This is because the flareout predictor predicts the glide phase based on the desired glide path angle and, therefore, the effect of sink rate is not accounted for in the predicted errors at touchdown during this phase. This approach was taken because it was found that the effect of sink rate on the predicted errors during this phase is small, is difficult to account for in the flareout predictor, and is easily compensated for by a simple rate damping loop.

During the final flare phase, the pitch feedback loop parameters are set as follows,

$$k_{xi} = 0$$

$$k_{zi} = k_z$$

$$k_{\dot{z}i} = k_{\dot{z}}$$

$$Z_{ci} = Z_{sff} + \dot{Z}_{ci}/s$$

$$\dot{Z}_{ci} = (\dot{Z}_{sff} + \ddot{Z}_c/s) \geq \dot{Z}_{td}$$

$$\ddot{Z}_c = \ddot{Z}^p_{ff} \, (\dot{Z}_c/\dot{Z}_{sff}), \text{ if } (t-t_{sff}) \geq \Delta t_{lff}$$

$$= 0 \qquad , \text{ if } (t-t_{sff}) < \Delta t_{lff}$$

where: t = current flight time (sec)

t_{sff} = time at which final flare was started (sec)

Δt_{lff} = lead time for required pitch maneuver as start of of final flare ($\Delta t_{\theta i}$) at start of final flare)

$\dot{Z}_{sff}$ = sink rate as start of final flare (sec)

Two things should be noted here. First, no range error loop is included in pitch feedback law during this phase. This is because the flight time during this phase is small and, therefore, very little can be done to correct range if it is not correct at the start of this phase. In addition, without an independent device for controlling range errors, what control is possible can only be accomplished through pitch changes which also induce sink rate transients. This is not desirable since the prime purpose of this phase is to brake the vehicle's sink rate to the desired value for touchdown.

Second, it can be seen that the height and sink rate commands during this phase are generated as open loop time functions of the required acceleration which is predicted at the start of final flare only. This is done simply by commanding an acceleration that is proportional to the predicted start acceleration times the ratio of the commanded sink rate to the sink rate at the start of the flare and integrating this acceleration with respect to time to obtain the commanded sink rate and height. It should be noted that, during the initial lead time for the final flare, the commanded acceleration is held at zero to give the vehicle time to pitch to the attitude required to obtain the initial acceleration. It should also be noted that the sink rate command is limited to being not less than the desired touchdown sink rate.

Therefore, it can be seen that the pitch feedback law in the final flare is based on predicting only the start of the final flare and continuous prediction during the maneuver is not used as it is in the primary flare and glide phases. This type was used because it was found that continuous prediction resulted in a stiffer loop for the same gains. Although this is normally desired, for the NADWO it results in an amplification of the destabilizing elevon lift and of the short period sink rate transients caused by it. Although this can be tolerated in the primary flare and glide phases, it cannot be tolerated in the final flare phase where it is desired to control the sink rate to a precise value.

In the pitch command feedback law, a variable gain is used on the total incremental command due to errors. This gain is computed as,

$$k_{vg} = \left(\frac{4000}{|X|}\right) \leq 1.0$$

and is used to lower the system gain at long ranges. This was done to prevent the system from commanding unnecessarily severe maneuvers to correct errors at long range when there is plenty of time to correct them.

It can also be seen from the pitch command feedback law that a pitch trim command is used in all phases. This command is computed as,

$$\theta_{trim} = \alpha_{trim} - \gamma_i$$

where: α_{trim} = estimated trim angle of attack (deg)

γ_i = γ(deg) , if in primary flare

= γ_g(deg) , if in glide

= $-57.3\ (\dot{Z}_c/V) + 1$, if in final flare

The γ_i, ideally, shall be with respect to the air mass but inertial flight path angles are used as approximations.

The angle of attack required for trim is estimated as,

$$\alpha_{trim} = \frac{-\ddot{Z}_i + g}{Q_f\ (S/m)\ C_{L_\alpha}} + \alpha_o$$

where: $Q_f = Q/(.655s+1)$

$\ddot{Z}_i = \ddot{Z}_f$, if in primary flare

= 0 , if in glide

$= \ddot{Z}^p_{ff}\ (\frac{\dot{Z}_c - \dot{Z}_{td}}{\dot{Z}_{sff} - \dot{Z}_{td}})$, if in final flare.

This pitch trim command is fed forward into the pitch command feedback law. It was included because it was found that when only a pitch trimming integrator was used, the gains required to keep up with the large changes in pitch trim during flareout resulted in stability problems in the presence of disturbances. In computing this command, it can be seen that a filtered value of sensed dynamic pressure is used. The filter was included to

prevent the system from commanding changes in pitch trim which are faster than the flight control system can respond to and which were found to amplify the effects of the destabilizing elevon lift. To compensate for the lag error introduced by this filter, a one degree pitch trim bias is added to the pitch trim command during final flare as shown in the equation for γ_i.

To further compensate for the large rate of change of pitch trim required as touchdown is approached, a required pitch rate command is also estimated in the guidance section and fed forward into the flight control system. This command is estimated as,

$$q_c \cong \dot{\gamma}_c$$

$$\cong -\ddot{Z}_i/V$$

where: $\ddot{Z}_i$ = vertical acceleration during each phase (same as for α_{trim} estimation).

(b) Gear Command Law.

The gear command law is,

$\delta_{gc} = 0$, if in primary flare phase

$= 0$, if after primary flare and $\Delta X^p_{td} > 0$ and $Z < -100$

$= 1$, if after primary flare and $\Delta X^p_{td} \leq 0$ or $Z \geq -100$

It can be seen that, after primary flare, this law commands the gear to be lowered when the predicted range error at touchdown with gear down all the way becomes less than or equal to zero. A height override is also included. If the gear lowering command has not been issued by the time the vehicle is 100 feet above the runway, this override commands the gear to be lowered regardless of whether the predicted range error is less than zero or not. In addition, a lock is also included which locks the gear lowering command once it has been issued. This was included to prevent chattering on the command due to noise.

(c) Lateral.

Prior to decrab, the lateral guidance law is,

$$\phi_c = k_{vg} \left(\Delta \phi_{cyl} + \Delta \phi_{c\dot{y}} \right)$$

where: k_{vg} = variable gain (function of range)

$\Delta\phi_{cyl}$ = limited incremental roll command due to lateral offset from fixed center line (deg)

$\Delta\phi_{c\dot{y}}$ = incremental roll command due to lateral velocity.

To prevent this law from commanding excessive roll angles, the command is limited as follows:

$$\phi_{cl} = -\phi_{max}, \quad \text{if } \phi_c \leq -\phi_{max}$$

$$= \phi_c, \quad \text{if } -\phi_{max} < \phi_c < \phi_{max}$$

$$= \phi_{max}, \quad \text{if } \phi_c \geq \phi_{max}$$

where: ϕ_{max} = maximum roll angle limit (nominally 30 deg.)

The incremental roll command to lateral offset is computed as,

$$\Delta\phi_{cyl} = k_y Y_l ,$$

where: k_y = lateral offset gain (nominally .128 deg/ft.)

Y_l = lateral offset from fixed centerline (ft) used for computations; same as actual offset but limited to a maximum magnitude.

The lateral offset is limited to prevent approaching the centerline at excessive heading angles. The limit is defined as,

$$Y_{max} = V \sin \Delta\xi_{max} \, (\dot{k}_y / k_y),$$

where V = total inertial speed (ft/sec)

$\dot{k}_y$ = lateral velocity gain (deg/ft/sec)

$\Delta\xi_{max}$ = maximum desired heading approach angle (nominally 30 deg.)

The lateral offset is then simply limited as follows:

$$Y_l = -Y_{max}, \qquad \text{if } Y \leq -Y_{max}$$

$$= Y, \qquad \text{if } -Y_{max} < Y < Y_{max}$$

$$= Y_{max}, \qquad \text{if } Y \geq Y_{max}$$

To prevent the incremental roll command due to lateral offset from saturating the roll command and cancelling out the lateral velocity damping term, this term is also limited before being added to the incremental roll command due to lateral velocity.

$$\Delta\phi_{cyl} = -\phi_{max}, \qquad \text{if } \phi_{cy} \leq -\phi_{max}$$

$$= \phi_{cy}, \qquad \text{if } -\phi_{max} < \phi_{cy} < \phi_{max}$$

$$= \phi_{max}, \qquad \text{if } \phi_{cy} \geq \phi_{max}$$

The incremental roll command due to lateral velocity is computed as,

$$\Delta\phi_{c\dot{y}} = \dot{k}_y \dot{Y}$$

where $\dot{k}_y$ = lateral velocity gain (deg/ft/sec)

$\dot{Y}$ = lateral velocity normal to fixed centerline (ft/sec).

The variable gain that is used in this lateral law is the same as is used in the longitudinal laws.

During the decrab maneuver, the lateral guidance laws are simply,

$$\psi_c = \psi_{td} + .25\ (\psi_{sdc} - \psi_{td})$$
$$\phi_c = 0.$$

where ψ_{td} = runway heading attitude

ψ_{sdc} = yaw attitude at start of decrab

It can be seen from the yaw command yaw that the vehicle is only being commanded to decrab through 75% of the angle required to line up with the runway. As discussed previously, this was done to relieve the aileron saturation problem during decrab. Although it results in landing with a crab angle, the angle is well within the allowable dispersion that was selected even in the presence of a 3 sigma cross wind.

The logic for initiating the decrab is as follows. If the vehicle is in any phase prior to the final flare phase, the guidance law prior to decrab is used. If the vehicle is in the final flare phase, a time to touchdown and time to decrab are computed and the decrab is initiated based on these times as follows:

If $t_{ttd} > t_{tdc}$, use guidance prior to decrab.

If $t_{ttd} \leq t_{tdc}$, use decrab laws

The time to touchdown is computed as,

$$t_{ttd} = \frac{-Z}{.5\ (\dot{Z}_c + \dot{Z}_{td})}$$

where Z = current vehicle height above runway (ft).

$\dot{Z}_c$ = commanded sink rate from longitudinal guidance section (ft/sec).

$\dot{Z}_{td}$ = desired touchdown sink rate (ft/sec).

The time to decrab is computed as,

$$t_{tdc} = \Delta t_{\psi 0} + \frac{|\psi - \psi_{td}|}{\dot{\psi}_{eff}}$$

where $\Delta t_{\psi 0}$ = initial decrab time delay (nominally 0.8 sec.)

$\dot{\psi}_{eff}$ = effective decrab rate (nominally 1.5 deg/sec).

As in the longitudinal phase selection logic, once the decrab maneuver has been initiated, the guidance is locked into this mode to prevent system noise from causing chattering.

V. CONTROL.

A. History and Description of the Flight Control System.

This paragraph of Section V summarizes the historical evolution of the Flight Control System (FCS) design and describes the resulting design in general terms. The remainder of Section V discusses in detail the design and the factors which lead to it. A summary of the history of FCS may be itemized as follows:

1. The longitudinal and lateral channels were designed "first cut" by independent 3 DOF simulations with assumed surface limits and rates.

2. NASA/AMES determined that the allowable aerodynamic surface rate limits were lower than the assumed values (See Appendix C, Data Base for actual specifications). This, coupled with the fact that the elevator and aileron are a single surface, lead to instability due to surface rate saturation when the two axes were cross-coupled in the 6 DOF simulation and when combined pitch and roll commands were developed. The problem occurred at the lowest vehicle airspeeds near touchdown because the control authority was least and because both flare (elevator action) and decrab (aileron action) were occurring simultaneously. (The surface rate could not be increased because severe penalties would be imposed by the larger actuator system designs.) Although the instability resulted only when combined maneuvers existed, the FCS designs were considered acceptable because it was felt that combined maneuvers could be minimized by designing sufficient separation time between the flare and decrab maneuvers.

3. When gusts were introduced, the assumption that combined aileron and elevator action could be separated was no longer valid. The FCS design was modified to eliminate the instability which is most severe at the low dynamic pressures.

4. The FCS initially was designed to utilize direct measurements of α (angle of attack), β (side slip angle), and airspeed (Pitot tube). It was later decided that, because of the thermal effects on re-entry, it was not practical to consider a design based on measurements utilizing α, β vanes. Therefore, the FCS was modified to eliminate the requirement for α, β measurements. The airspeed measurement, due to less stringent constraints on sensor location, was considered to be available. An estimate of β was obtained by utilizing an accelerometer to measure side forces. Due to the fact that the rudder also develops side forces which are also measured by the accelerometer, positive feedback resulted which was excessive and destabilizing. A computation based on the average side force coefficient due to rudder was incorporated to subtract the rudder side force from the accelerometer readings. The adjusted accelerometer output was found to be an adequate estimation of β.

The need for the α vane was eliminated. For this flight phase, the flight path angle (which is known), and the airspeed (Q) measurements was sufficient to approximate the α required.

5. When evaluating performance with heavy turbulence, the variation of airspeed affected the guidance loop (see Section VII, Results), but did not significantly effect the FCS design. This is because the measurement of airspeed (Q) was used only to adjust autopilot gains.

6. A final modification to the FCS system was required because the force due to the elevons (when functioning as elevators) increased the sink rate dispersion at touchdown in severe gusts. When the elevons were commanded to pitch the vehicle to counteract the effects of gusts on lift, the initial vehicle acceleration due to elevon forces is in the direction of reinforcing the adverse gust lift. A moderate decrease FCS system gain was found to reduce the variance in sink rate at touchdown.

7. As shown in Figure II-1, System Block Diagram, the flight control section consists of elevon, aileron, and rudder flight control laws. The elevon law is a simple pitch error law. The aileron law consists of a roll error law plus direct sideslip and rudder compensation. The rudder law consists of a sideslip or yaw error law (sideslip for coordinated turn mode and yaw for decrab) plus turn compensation for the coordinated turn mode. The angular error laws for all channels are of the form,

$$\frac{\delta_c}{\Delta A} = (k_A + k_{\dot{A}}\, s)\ (1 + k_{Ai}/s).$$

where δ_c = general surface command

ΔA = general angular error

k_A, etc. = flight control gains.

Due to the large loss in airspeed during flareout, the gains k_A and $k_{\dot{A}}$ in each channel are varied inversely with the square of sensed airspeed to account for the resulting loss in control power. In addition, limits are included on the stiffness terms, $k_A\ \Delta A$, to prevent these terms from saturating the commands against the hard

surface limits and eliminating the damping terms, $k_A s\ \Delta A$. Limits are also included on the trimming integrator terms, k_{Ai}/s, to prevent these terms from continuing to integrate when the commands are against the hard limits.

The sideslip and rudder compensation terms in the aileron channel are included to compensate for the large coupling of sideslip and rudder into roll that occurs for the NADWO. These terms are based on assumed vehicle characteristics and are computed such that they ideally command an aileron deflection that exactly compensates for the rolling moment produced by sideslip and rudder.

In the coordinated turn mode, a turn coordination term is added into the rudder channel. This term is based on the roll error and is used to quicken the turn.

B. Problems Due to Vehicle Characteristics.

This section details the FCS problems stemming from specific vehicle characteristics.

The lateral characteristics for this vehicle are highly dependent on angle of attack. This vehicle becomes directionally unstable ($C_{N_\beta} < 0$) at angles of attack above 20°. The results of the simulation studies showed that the vehicle did not reach these high angles under automatic control during the terminal phase of landing. However, to assume that this was not a problem was felt to be misleading. The FCS design logically must proceed on the assumption that the control system would be used in the earlier flight phases. Further, it is mandatory to consider the possibility of manual flying as a preference or a backup mode. It should not be assumed that the

manual system will be as precise at the automatic system. Both considerations admit the possibility of higher angles of attack.

To cope with the directional instability, an angular direction feedback loop was incorporated in the rudder channel of the flight control system. The changes in the lateral characteristics with angle of attack can also result in significant changes in the dynamic response of the lateral loops; especially near touchdown where the angle of attack is relatively larger. For example, during a decrab maneuver, the decrease in directional stability of the vehicle can cause the overall stiffness of the yaw loop to decrease to an unacceptable value if too low a gain is used on the angular direction feedback. To prevent this, the gains in the flight control system must be made high enough to overshadow the changes in lateral characteristics with angle of attack. If these gains are too high, the flight control system must be designed to compensate for the changing lateral characteristics.

In addition to the dependency of the lateral characteristics on angle of attack, the NADWO also has significant coupling of yaw into roll. For example, the rolling moment induced by sideslip requires about two degrees of aileron to compensate for the moment induced by a degree of sideslip. This presents a significant control problem during the decrab maneuver when the vehicle is purposely being sideslipped to line up with the runway. To prevent this, either a high gain roll error feedback loop or a sideslip feed forward loop is required in the aileron control channel. The same problem also exists for the rolling moment induced by rudder but to a lesser degree.

Both the lateral and longitudinal control problem is further complicated by the fact that the NADWO has relatively low control power. As a result of this relatively high flight control gains are required to obtain satisfactory angular responses for normal maneuvers. These gains can result in surface saturation in the presence of disturbances or errors which require large corrective maneuvers. In these cases, the desired response cannot be obtained and the guidance gains must either be low enough or the guidance commands limited enough to insure that the increased lag in the flight control system does not drive the guidance system unstable. In addition, in the presence of large angular commands, the angular error stiffness terms can completely cancel any angular rate damping terms that are required. Since this can result in poorly damped or even unstable angular responses, limits must be included on the angular error stiffness terms where rate damping is required.

The proposed control surface actuator design for the NADWO also results in control problems in both the lateral and longitudinal channels. In the proposed design, elevons are used together as elevators and differentially as ailerons. With the proposed actuator, the total rate limit on each surface is 20°/sec. However, since the surfaces are used as both elevators and ailerons, this requires appropriate limiting on each command to prevent the surface commands from one axis from saturating the other axis. Although it is possible to plan the landing phase such that planned pitch and roll maneuvers do not occur simultaneously, it is not possible to prevent pitch and roll maneuvers required to compensate for disturbances, such as wind

gusts, from occurring at the same time. Therefore, if the flight control gains are too high, the effective reduction in surface rates can drive the flight control system unstable even though it is stable for independent maneuvers. To cope with this, the flight control gains must either be made low enough to provide stability with the reduced rates or programmed as a function of the type of maneuver; i.e., high gains for independent maneuvers and low gains for combined maneuvers. It was decided to use the lower gain system.

Another undesireable vehicle characteristic is the reverse lift due to elevons (described in item 6 of the historical summary of Section V.A.). This problem straddled the area of guidance and control. Its influence on guidance and a detailed discussion of the effect is included in Section IV, Guidance Concept. When correcting gust disturbance near touchdown, the initial lift due to elevon causes the vehicle to move opposite to the direction that is intended. This increases the number of hard landings and increases the touchdown errors. This is a guidance problem. However, the corrective action required is to adjust the gains in the pitch axis of the flight control system to minimize the touchdown errors due to gusts. This is a flight control problem.

C. FCS Design Philosophy.

The basic approach that was taken in developing the flight control laws was to develop laws that would meet the selected response criteria and would keep these responses invariant with changing flight conditions. To do this, the system was first designed by linearized analysis techniques. For this analysis, a desired damping ratio of

0.7 was selected for both the pitch and roll responses. Based on the flight control system criteria specified in MIL-C-18244A (WEP), "Control and Stabilization Systems: Automatic, Piloted Aircraft, General Specifications for", a frequency response of 2.9 rad/sec in pitch and 1.5 rad/sec in roll were the design goals.

The natural frequency initially achieved was 3.4 rad/sec in pitch and 2.5 rad/sec in roll. When severe turbulence was introduced, sink rate dispersion increased because of the initial reverse lift of the elevons when making pitch corrections and because of surface velocity saturation. (This problem is discussed as a guidance problem in Section IV.). The gains were reduced which resulted in natural frequencies of 2.5 rad/sec and 1.7 rad/sec in roll. In the modified system (see Section VIII), a natural frequency of 3.4 rad/sec in pitch and 2.5 rad/sec in roll was achieved because the higher airspeed at landing reduced the surface saturation problem.

A basic flight control law of the form,

$$\frac{\delta_i}{A_i} = (k_A + k_A^{\cdot}s),$$

where δ_i and A_i are general control surface deflections and attitudes respectively, was selected for stabilization. The laws were derived using the linearized characteristic equations for the raw vehicle. The flight control gains required to meet the desired response characteristics were then determined from the closed loop characteristic equations. It was found that the gains required to obtain the desired responses resulted in control stiffness and damping terms that were significantly larger than the natural vehicle

stiffness and damping terms except for the vehicle yaw coupling terms into roll. It was necessary to design the flight control system to compensate for both the changes in control power with flight conditions and the yaw coupling into roll in order to obtain responses that were invariant with flight conditions. In addition, it was also necessary to compensate for certain actuator nonlinearities for maneuvers requiring actuator motions outside of the linear range.

The flight control system design that evolved during the study is shown in Figures V-1, V-2 and V-3 for the pitch, roll, and yaw channels respectively. The most significant aspects of this design are discussed in the following sections.

To compensate for the changes in control power with flight conditions, the system was designed with variable gains (functions of Q_F) as shown in Figures V-1 through V-3. Since the dominant change in control power was due to the loss in airspeed during flareout, it was only necessary to make the flight control gains inversely proportional to sensed dynamic pressure. The influence of this gain compensation can be seen by comparing the basic flight control system responses[1] at primary flare initiation in Figure V-4 with those at final flare initiation in Figure V-5 where the dynamic pressure is nominally only 40% of that at primary flare initiation. In both cases, the responses are shown for the nominal flareout maneuvers and for maneuvers twice as large as nominal. (The difference in the size of

---

[1] Compensation for yaw coupling into roll not included at this point.

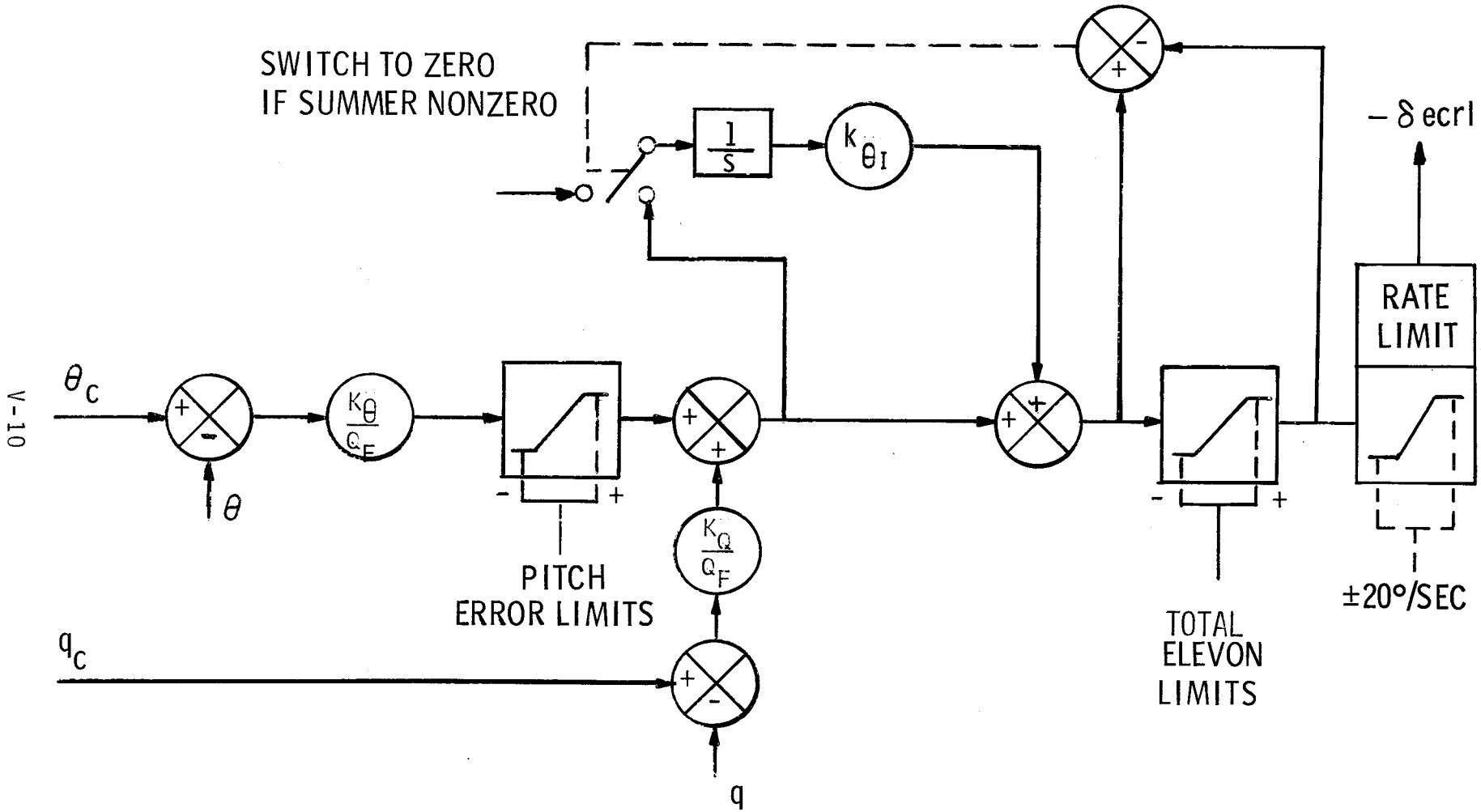

Figure V-1. Pitch Control Channel

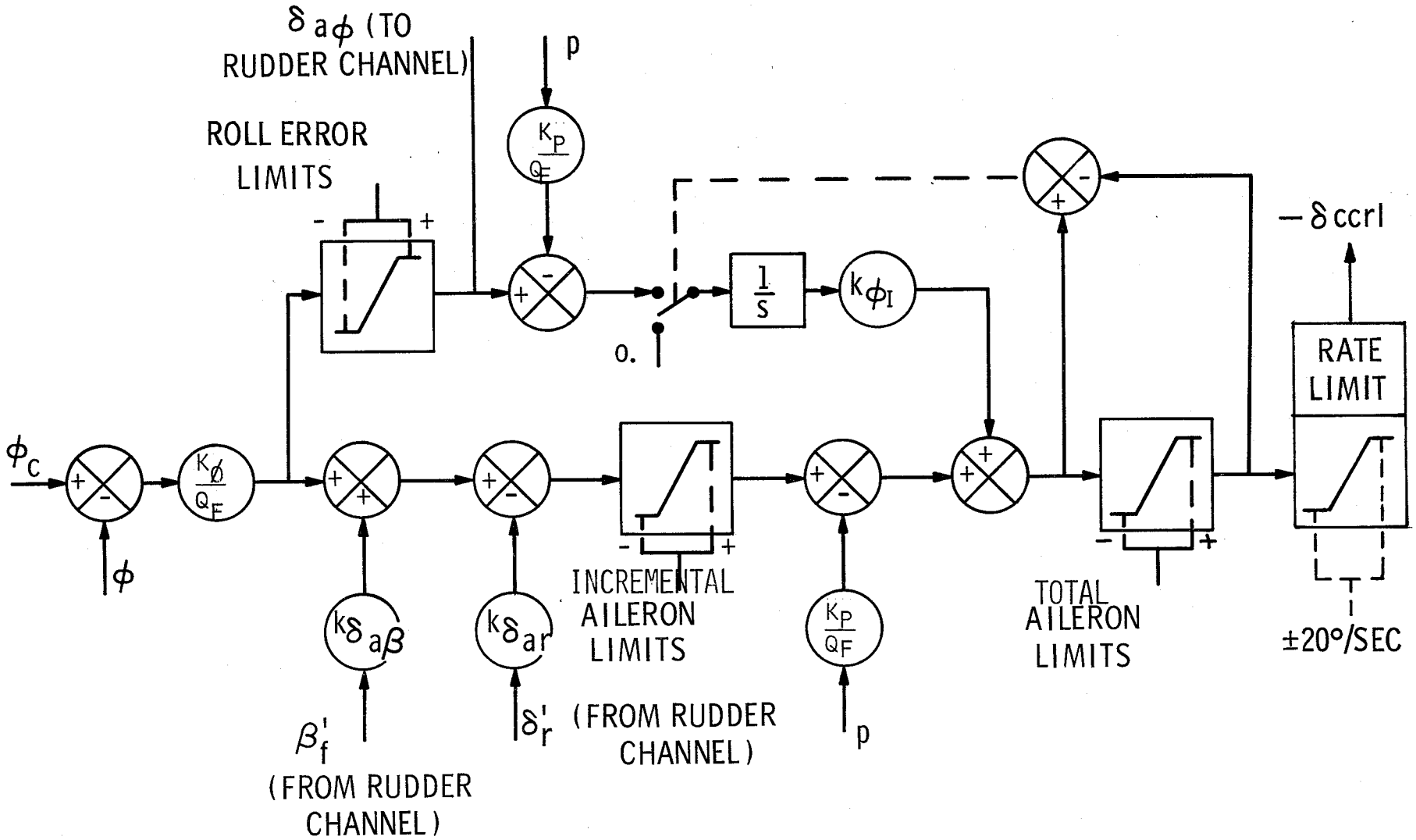

Figure V-2. Aileron Channel - Roll

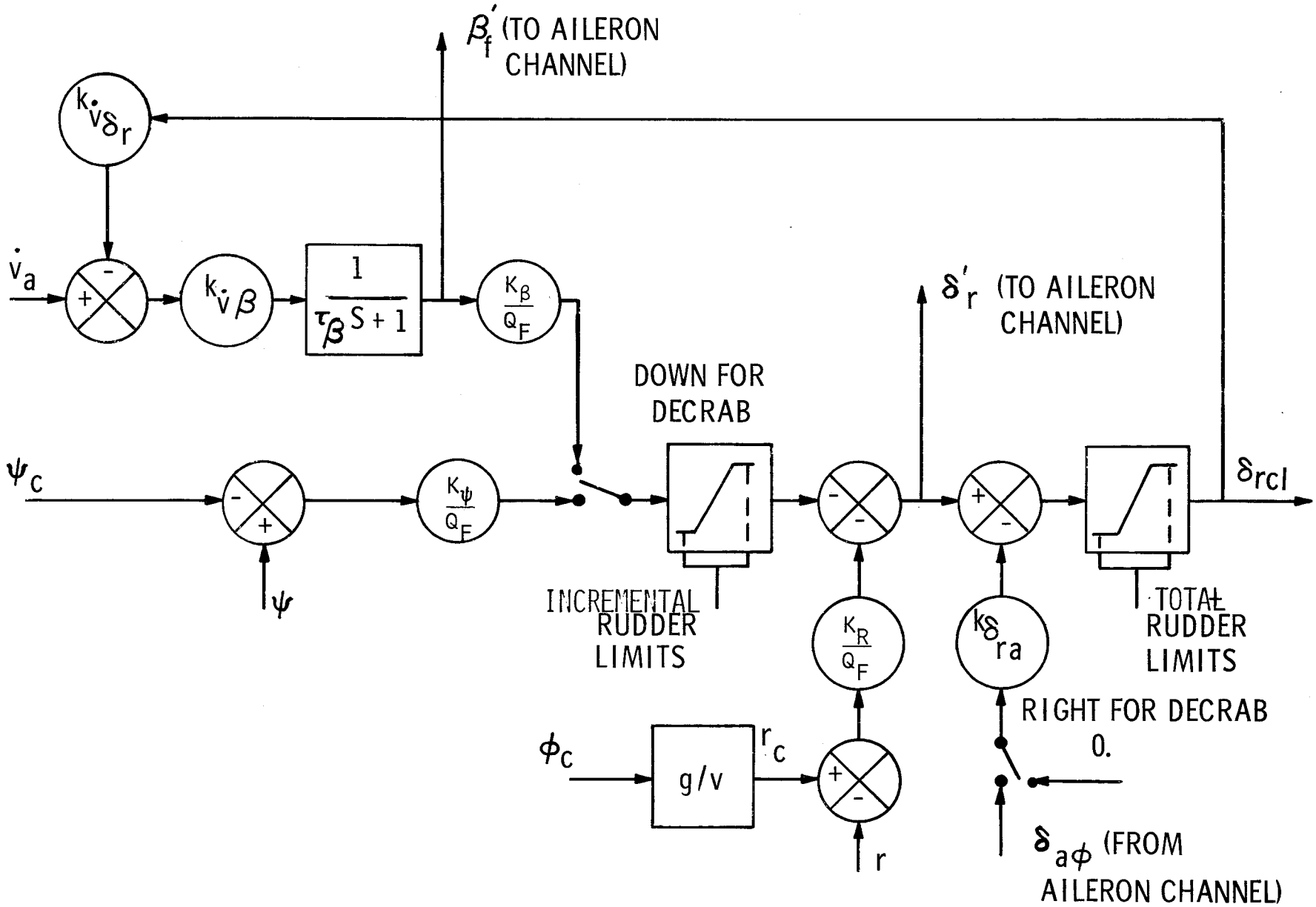

Figure V-3. Rudder Channel - Yaw

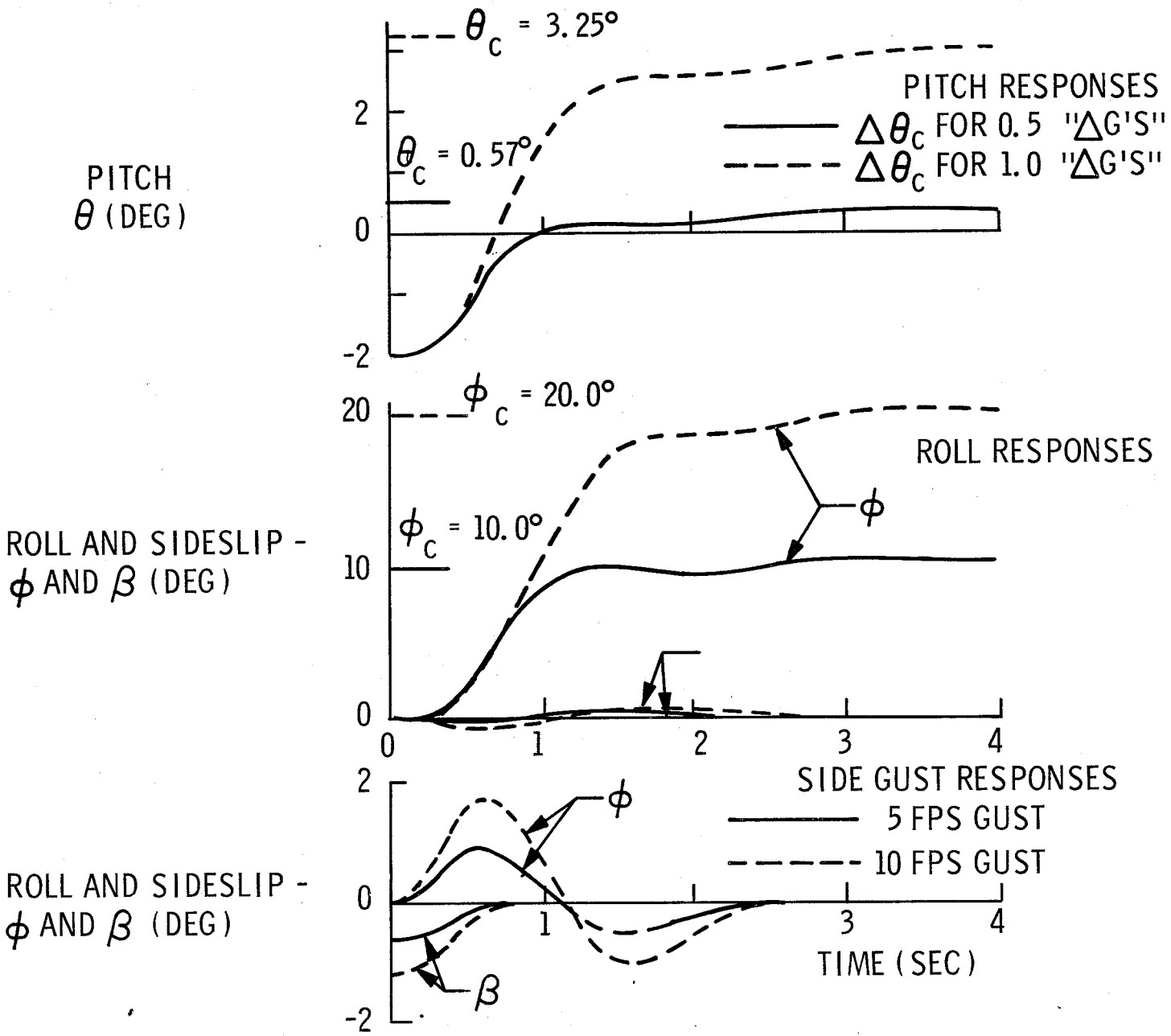

Figure V-4. Flight Control System Responses at Primary Flare Initiation

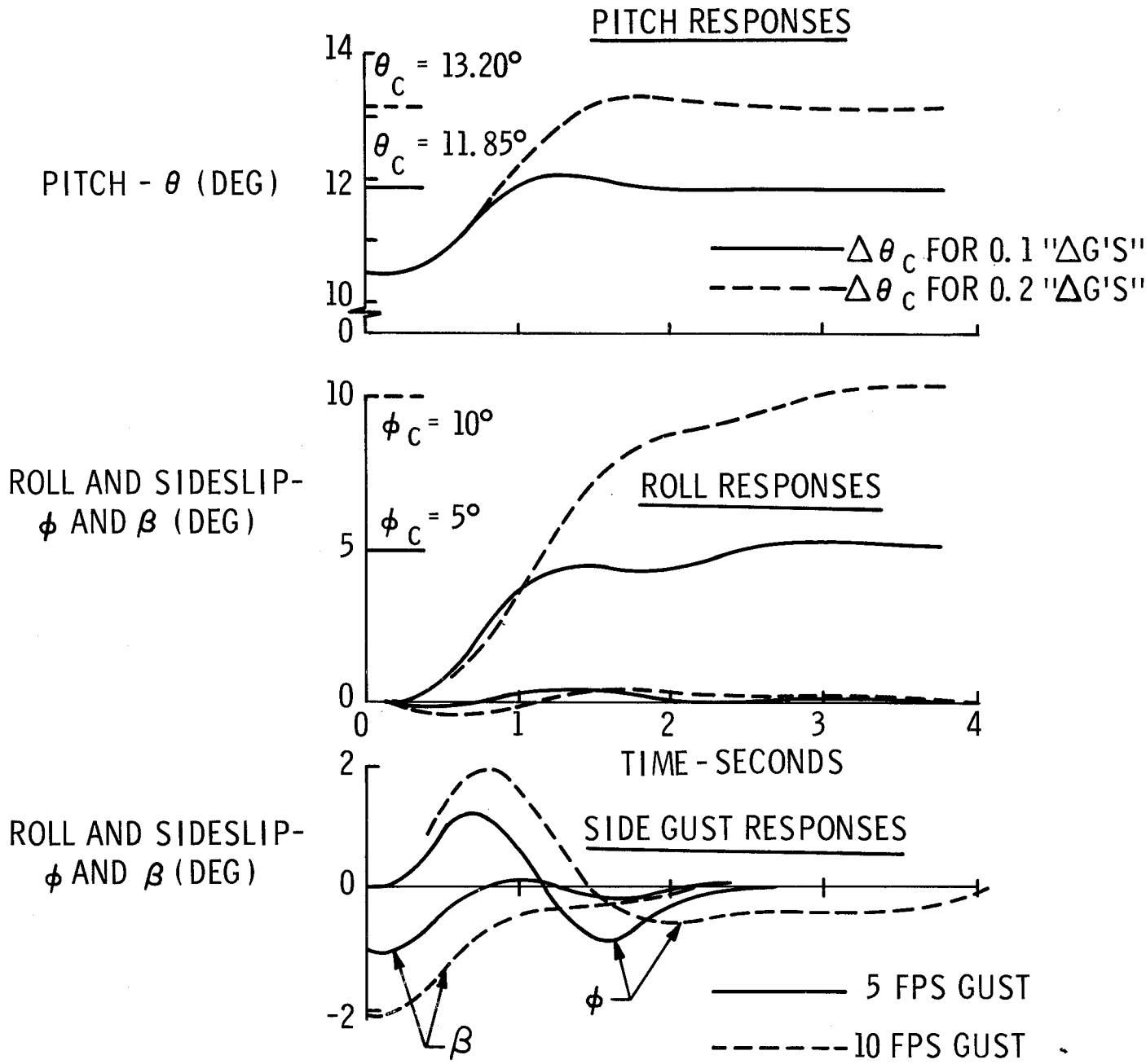

Figure V-5. Flight Control System Responses at Final Flare Initiation

the step inputs in these figures is due to difference in size of the nominal commands at these two flight conditions.) For surface saturation evaluation, the most realistic comparison is made when the input magnitudes are nominals. The pitch and roll responses are almost invariant with flight conditions although there is some deterioration for the larger maneuvers due to control surface saturation. Also, the roll and sideslip responses to a step sidegust are somewhat less invariant to flight conditions due to the strong coupling of yaw into roll.

To compensate for the effects of yaw coupling into roll, the system was designed to use direct compensation in the roll channel. The most significant rolling moments due to yaw terms were those due to rudder deflections and sideslip. Therefore, as shown in Figure V-2, these terms are fed directly into the roll channel. The gains on these terms are based on assumed vehicle characteristics and are set such that, under ideal conditions they will command an aileron deflection which will exactly compensate for the rolling moments induced by rudder deflection and sideslip.

The influence of this compensation on the flight control system response to a step roll command and a step sidegust disturbance at final flare is shown in Figure V-6. It can be seen from this figure that this compensation reduces the roll transient induced by a step sidegust. This effect is even more pronounced during the decrab maneuver when the vehicle is purposely being sideslipped into the wind to obtain alignment with the

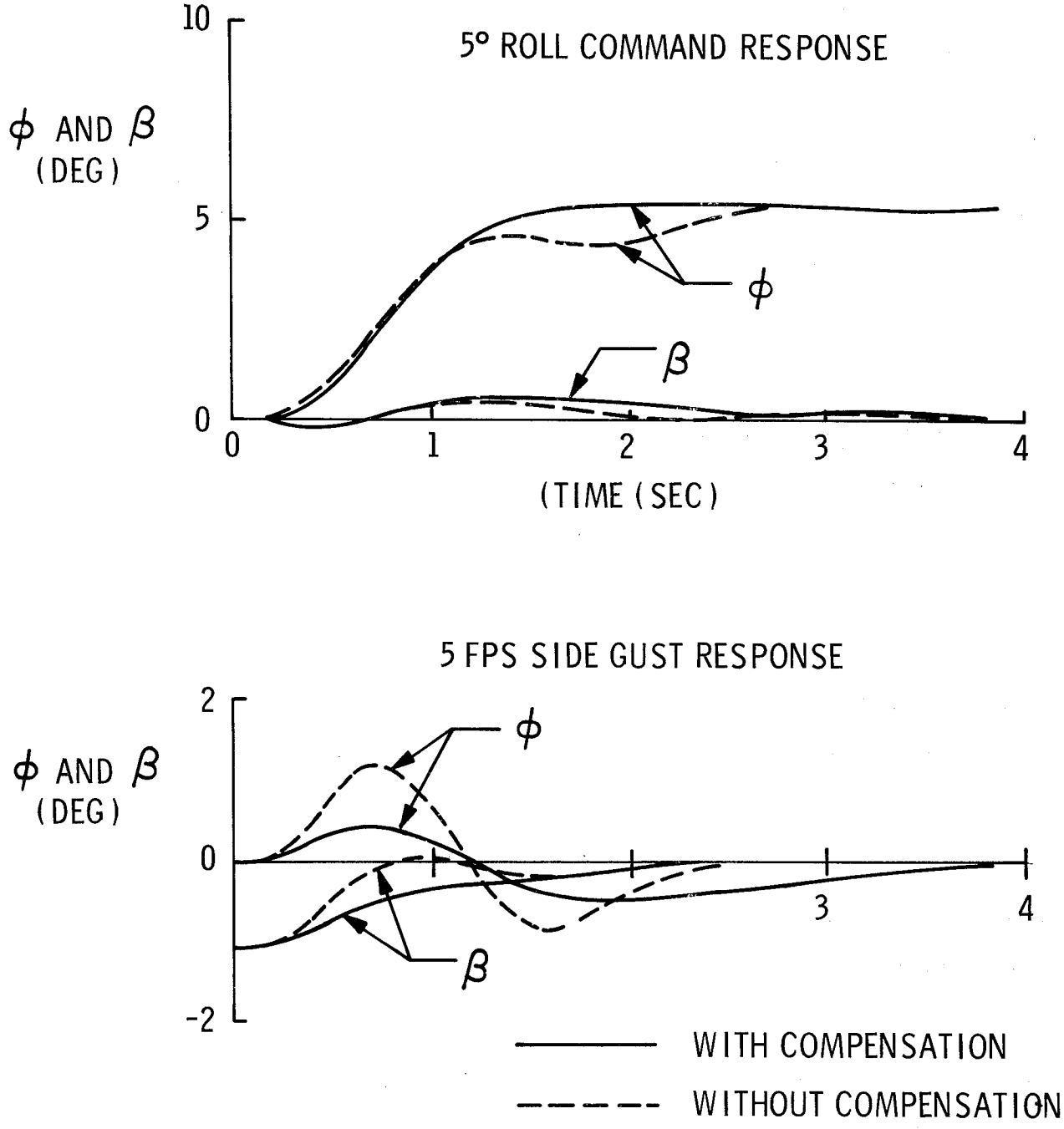

Figure V-6. Influence of Direct Aileron Compensation on Responses at Final Flare

runway. The improvement obtained is shown in Figure V-7 for a decrab maneuver in a 12.5 fps crosswind.

As shown in Figures V-1 and V-2, the pitch and roll flight control laws were designed to follow pitch and roll commands from the guidance system. During the decrab maneuver, the yaw control law is also designed to follow the required runway alignment yaw command from the guidance system as shown in Figure V-3. However, prior to decrab, the yaw flight control law was designed to null the sideslip angle. This approach was selected because it results in coordinated turns, compensates for wind drifts, and prevents large sideslip induced rolling moments. In both cases, the control stiffness gain required to meet the desired yaw response results in a control stiffness term which is significantly larger than the natural vehicle stiffness term as discussed previously. As a result of this, the fact that the natural vehicle is directionally unstable (negative stiffness as a result of negative C_{N_β}) at angles of attack above 20° did not present any design problem in itself since the overall closed loop stiffness of loop (control plus natural) remains positive as required for stability even when the natural vehicle stiffness becomes negative. However, the ruling that a sideslip sensor would not be practical on the NADWO did present a problem since the yaw control law had been designed to use sensed sideslip in the weather cocking mode. To cope with this, the system was redesigned to obtain an estimate of aerodynamic sideslip from sensed lateral acceleration along the y body axis. At first it was assumed that the dominant side force would be due to sideslip

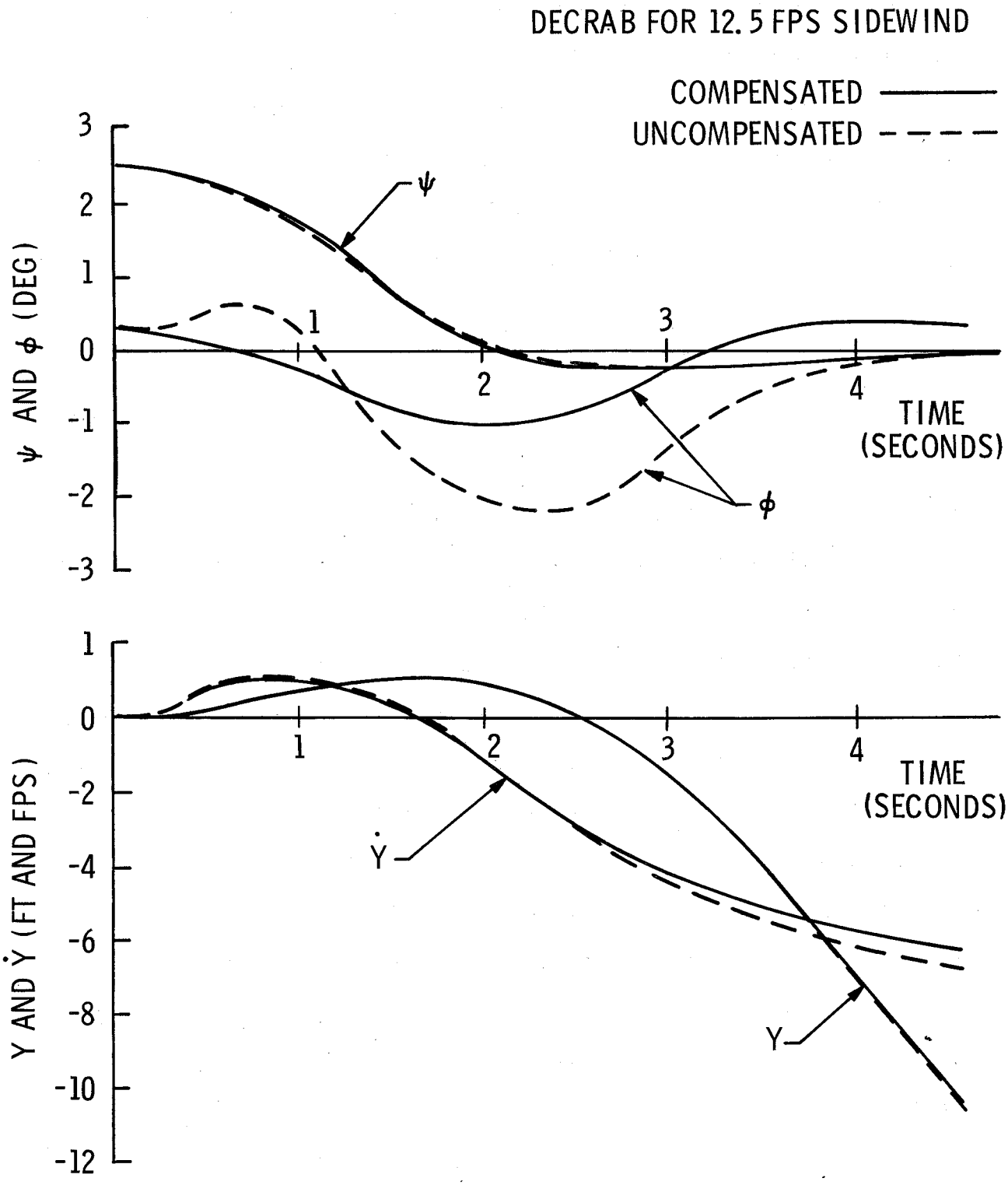

Figure V-7. Influence of Direct Aileron Compensation on Decrab Responses

(C_{Y_β} term) and therefore that sideslip could be estimated directly from the total sensed lateral acceleration. However, it was found that the destabilizing side force from the rudder resulted in a positive feedback of rudder into rudder with a magnitude so large that the overall closed loop stiffness term became negative. The resulting unstable response is shown in Figure V-8. Although it was found that the control stiffness term could be made positive by reducing the yaw stiffness gain, the magnitude of the control stiffness term was not sufficient to keep the overall closed loop stiffness term positive at angles of attack above 20°. To compensate for this positive feedback effect, the system was designed to subtract out the component of lateral acceleration due to the rudder ($C_{Y_{\delta_r}}$ term) from the total sensed lateral acceleration.

Ideally, both the gain on the subtracted term and the coefficient used to estimate the sideslip angle from the compensated acceleration should be functions of aerodynamic angle of attack since they are both based on vehicle coefficients that change with angle of attack. However, it was decided to base these gains on constant coefficients. Coefficients were selected at an angle of attack of 15° for two reasons; (1) they do not vary significantly at angles of attack below this value, and (2) the angle of attack during the majority of the nominal flareout trajectory is below this value. Figure V-9 shows a comparison of the roll responses to a 5° roll command at final flare for the measured β approach and the compensated lateral acceleration approach. It is apparent from this figure that the compensated lateral acceleration approach is nearly as good as the

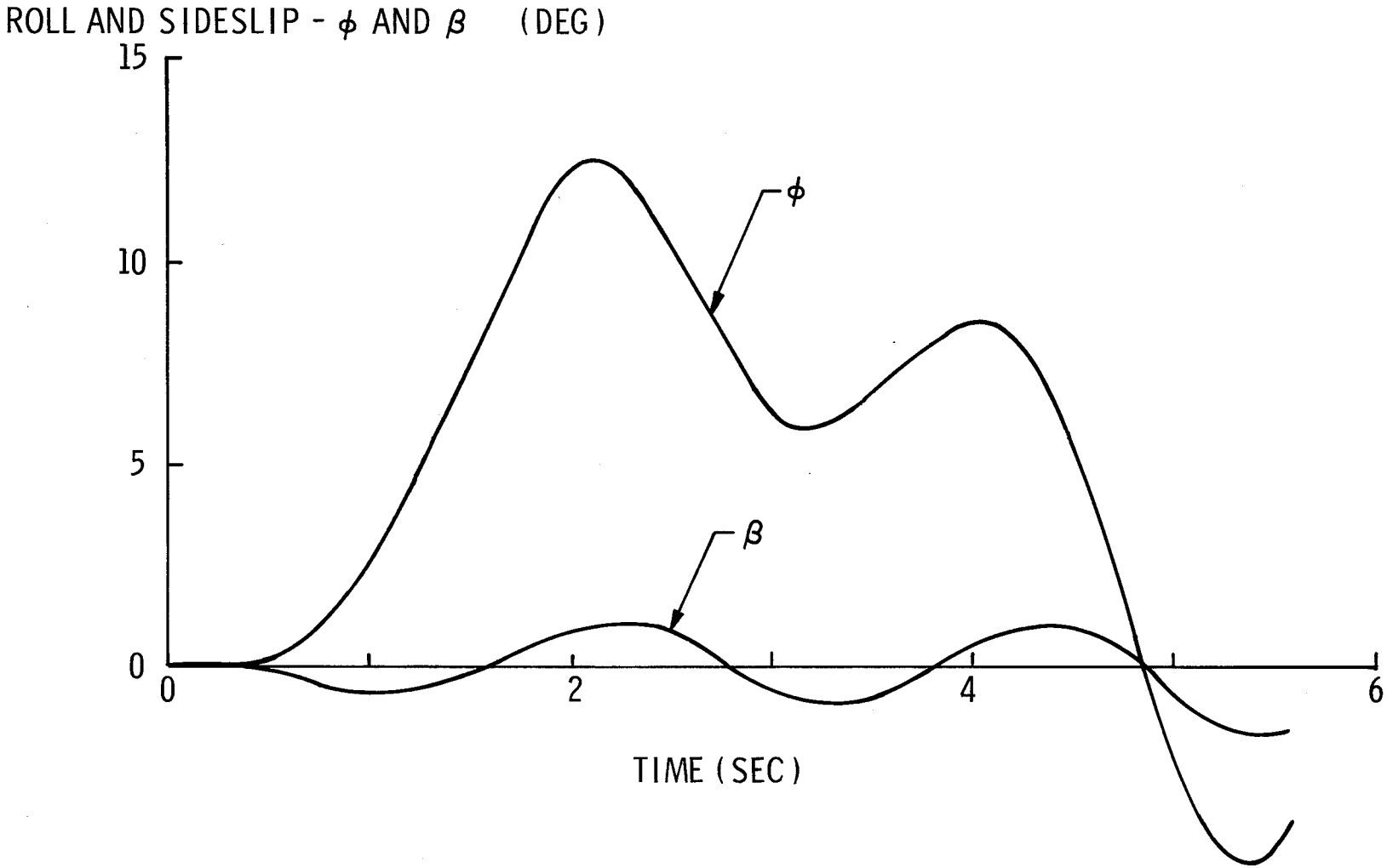

Figure V-8. Roll Response at Final Flare for FCS Using Lateral Acceleration Directly

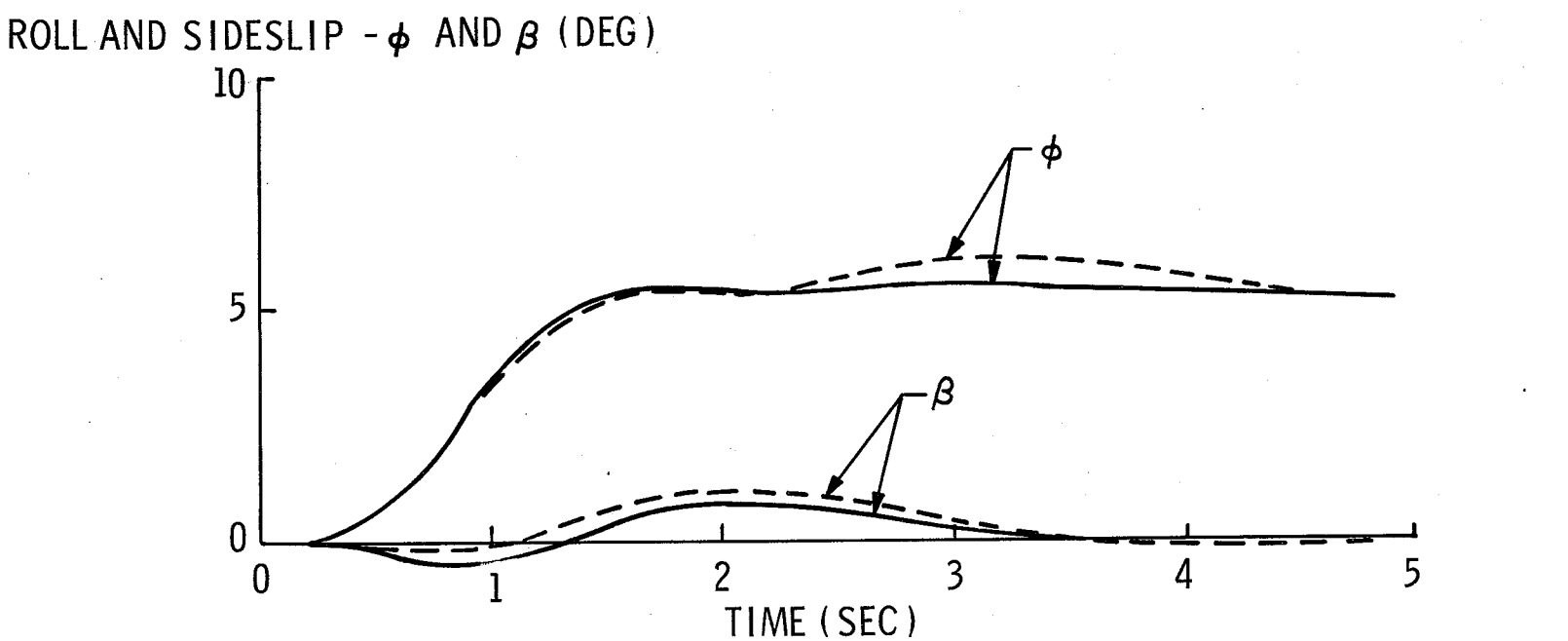

Figure V-9. Comparison of Roll Responses at Final Flare for FCS Using Either Sensed Sideslip or Compensated Lateral ACC

sensed sideslip approach. This is because the angle of attack on this run was between 13.5° and 16.0°, and, therefore, the assumed constant coefficients that were used to compensate the lateral acceleration were close to the ones used in the simulation of the vehicle.

Runs were also made at higher angles of attack to determine if the compensated lateral acceleration approach was satisfactory in cases where the assumed coefficients were significantly different from those used in the vehicle simulation and where the vehicle is naturally divergent in yaw. Figure V-10 shows a comparison of the roll responses to a 5° roll command at an initial angle of attack of 20°. At the end of this run, the angle of attack was 30° and, at this value, the assumed effect of rudder on lateral acceleration was 60% higher than that in the vehicle simulation. The response deteriorates but is still stable. By further adjustment of the flight control law gains, it was possible to reduce the sideslip angles shown in this figure by about 25%.

To compensate for the steady pitch rate required during the flares and the steady yaw required during turns, the system was designed to use rate commands in the pitch and yaw channels as shown in Figures V-1 and V-3. The pitch rate command is computed in the guidance section (page IV-58). The yaw rate command is computed from the roll command in the flight control laws. The resulting yaw rate error term in this channel is commonly called a $\dot{\beta}$ damper. No rate command was included in the roll channel since the normal roll maneuvers during flareout do not require a steady roll rate. To obtain quicker turn coordination, the system was also designed to use roll command compensation in the yaw channel.

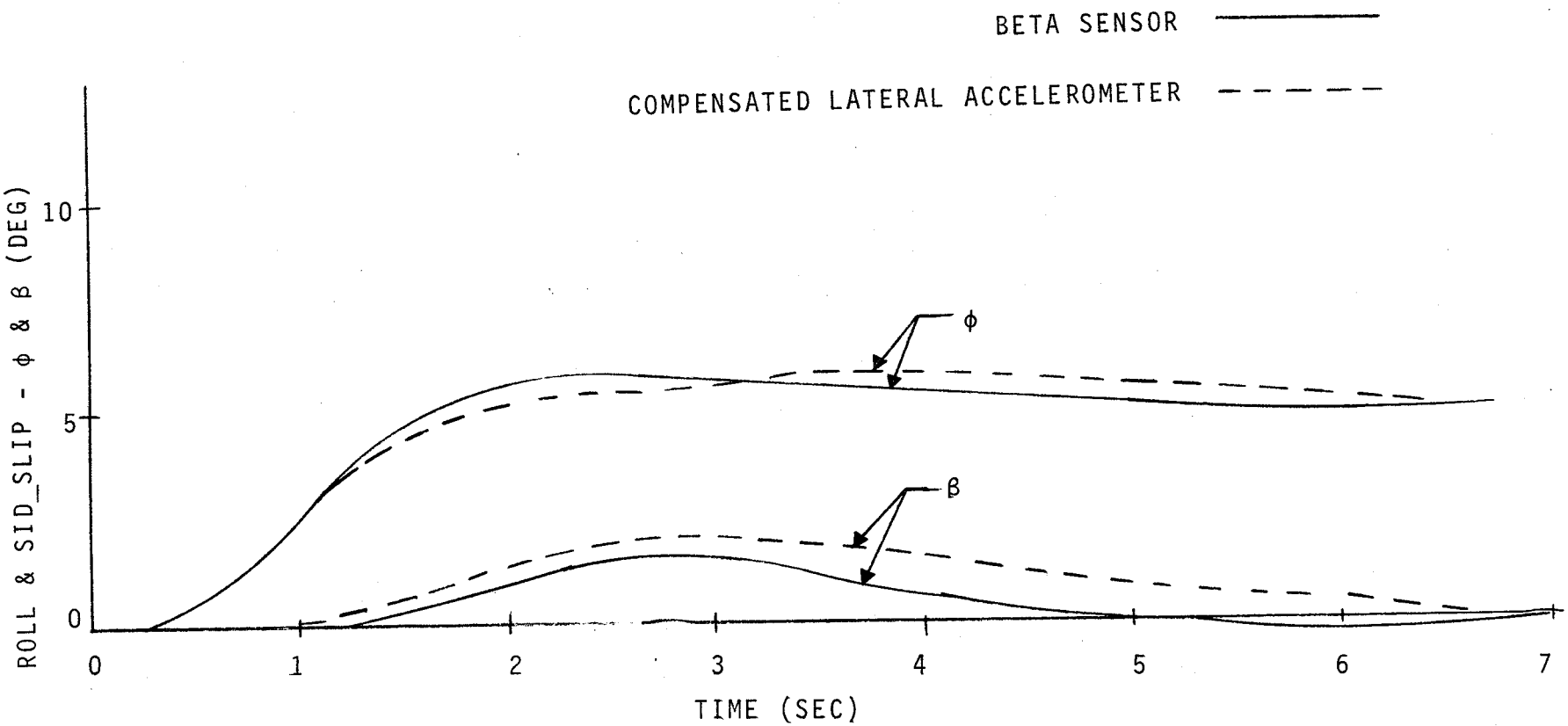

FIGURE V-10 COMPARISON OF ROLL RESPONSES AT HIGH ANGLE-OF-ATTACK FOR FCS USING EITHER SIDESLIP OR COMPENSATED LATERAL ACC.

To compensate for the large elevon trim changes required due to the loss of airspeed during flareout and for any residual aileron trim that might be required due to errors in the yaw coupling compensation and/or other disturbances, the system was designed with trimming integrators in the pitch and roll channels. Limits were included on these integrators to prevent them from saturating the commands when the commands are against the hard surface limits.

D. Detailed Description of the Flight Control System

1. Pitch Channel

The elevon command law for all phases is,

$$\delta_{ec} = \Delta\delta_{e\theta\ell} + \Delta\delta_{eq} + \Delta\delta_{ei},$$

where $\Delta\delta_{e\theta\ell}$ = limited incremental command due to pitch error (deg)

$\Delta\delta_{eq}$ = incremental command due to pitch rate error (deg)

$\Delta\delta_{ei}$ = incremental command from elevon trimming integrator (deg)

To prevent the system from commanding elevon deflections greater than the hard limits on the surfaces, the elevon command is limited as follows:

$$\delta_{ec\ell} = \delta_{e\ min}, \quad \text{if } \delta_e \leq \delta_{e\ min}$$

$$= \delta_{ec}, \quad \text{if } \delta_{e\ min} < \delta_{ec} < \delta_{e\ max}$$

$$= \delta_{e\ max}, \quad \text{if } \delta_{ec} \geq \delta_{e\ max}$$

where: $\delta_{e\ max}$ = maximum elevon delfection (nominally 15 deg)

To prevent the elevon command from saturating the elevons at the assumed 20^{o}/sec rate limit, a further rate limit is imposed. This is required since surface rate saturation due to elevon commands, if allowed, leave no differential elevon rate available for aileron control. The rate limiting is as follows:

$$\delta_{ecrl} = \delta_{erl\ min}, \text{ if } \delta_{ecl} < \delta_{erl\ min}$$

$$= \delta_{ecl}, \text{ if } \delta_{erl\ min} \leq \delta_{ecl} < \delta_{erl\ max}$$

$$= \delta_{erl\ max}, \text{ if } \delta_{ecl} \geq \delta_{erl\ max}$$

$$\delta_{erl\ min} = \delta_{ecrl\ prev} - 20\ \Delta t$$

$$\delta_{erl\ max} = \delta_{ecrl\ prev} + 20\ \Delta t$$

where: $\delta_{ecrl\ prev}$ = previous value of δ_{ecrl} from last cycle

Δt = computational cycle period

$\delta_{e\ min}$ = minimum elevon deflection (nominally -45 deg)

The incremental command due to pitch error is

$$\Delta\delta_{e\theta} = -k_{\theta}\ (\theta_c - \theta),$$

where: k_{θ} = pitch error gain (nominally 1.92 $(250/Q_f)$ deg/deg)

θ_c = pitch command from guidance (deg)

To prevent this term from saturating the elevon command and cancelling out the pitch rate damping term, it is limited as follows:

$$\Delta\delta_{e\theta\ell} = -\Delta\delta_{e\ max}, \qquad \text{if } \Delta\delta_{e\theta} \leq -\Delta\delta_{e\ max}$$

$$= \Delta\delta_{e\theta}, \qquad \text{if } -\Delta\delta_{e\ max} < \delta_{e\theta} < \Delta\delta_{e\ max}$$

$$= \Delta\delta_{e\ max}, \qquad \text{if } \Delta\delta_{e\theta} \geq \Delta\delta_{e\ max}$$

where : $\Delta\delta_{e\ max}$ = maximum desired incremental elevon command due to pitch error (nominally 12.5 deg.)

The incremental command due to pitch rate error is,

$$\Delta\delta_{eq} = -k_q\ (q_c - q),$$

where : k_q = pitch rate damping gain (nominally 0.96 $(250/Q_f)$ deg/deg/sec)

q = current vehicle pitch rate (deg/sec)

q_c = pitch rate command from guidance (deg/sec)

If the total elevon command is not against the hard limits ($\delta_{ec\ell} = \delta_{ec}$), the incremental command from the elevon trimming integrator is,

$$\Delta\delta_{ei} = \frac{k_{\theta i}}{s}\ (\Delta\delta_{e\theta\ell} + \Delta\delta_{eq})$$

where k_{θ_i} = elevon trimming integrator gain (nominally 0.2 deg/deg/se

If the elevon command is against the hard limits ($\delta_{ec\ell} \neq \delta_{ec}$), the input to the trimming integrator is set to zero to prevent saturation build up.

2. Roll Channel

The aileron command law for all phases is,

$$\delta_{ac} = \Delta\delta_{as\ell} + \Delta\delta_{ap} + \Delta\delta_{ai},$$

where: $\Delta\delta_{as\ell}$ = limited incremental command due to all stiffness terms (deg)

$\Delta\delta_{ap}$ = incremental command due to roll rate (deg)

$\Delta\delta_{ai}$ = incremental command from roll trimming integrator (deg).

As in the pitch channel, the total command is limited to prevent commanding deflections greater than the hard surface limits.

$$\delta_{ac\ell} = -\delta_{a\ max}, \quad \text{if } \delta_{ac} \leq -\delta_{a\ max}$$

$$= \delta_{ac}, \quad \text{if } -\delta_{a\ max} < \delta_{ac} < \delta_{a\ max}$$

$$= \delta_{a\ max}, \quad \text{if } \delta_{ac} \geq \delta_{a\ max}$$

where: $\delta_{a\ max}$ = aileron surface limit (nominally 12.5 deg.)

To prevent the aileron command from saturating both elevons at the assumed 20^{o}/sec rate limit at high command rates, thereby leaving no further elevon rate available for pitch control, the position limited aileron command is further rate limited as follows:

$$\delta_{acrl} = \delta_{arl\ min}, \text{ if } \delta_{acl} \leq \delta_{arl\ min}$$

$$= \delta_{acl}, \text{ if } \delta_{arl\ min} < \delta_{acl} < \delta_{arl\ max}$$

$$= \delta_{arl\ max}, \text{ if } \delta_{acl} \geq \delta_{arl\ max}$$

$$\delta_{arl\ min} = \delta_{acrl\ prev} - 20\ \Delta t$$

$$\delta_{arl\ max} = \delta_{acrl\ prev} + 20\ \Delta t$$

where: $\delta_{acrl\ prev}$ = previous value of δ_{acrl} from last cycle

Δt = computational cycle period

The incremental command due to all stiffness terms is,

$$\Delta\delta_{as} = \Delta\delta_{a\phi} + \Delta\delta_{a\beta} + \Delta\delta_{a\delta_r} ,$$

where: $\Delta\delta_{a\phi}$ = increment due to roll error (deg)

$\Delta\delta_{a\beta}$ = increment for sideslip compensation (deg)

$\Delta\delta_{a\delta_r}$ = increment for rudder compensation (deg).

As in the pitch channel, the total stiffness term is limited to prevent it from saturating the aileron command and cancelling out the roll rate damping term.

$$\Delta\delta_{as\ell} = -\delta_{a\ max}, \qquad \text{if } \Delta\delta_{as} \leq -\delta_{a\ max}$$

$$= \Delta\delta_{as}, \qquad \text{if } -\delta_{a\ max} < \Delta\delta_{as} < \delta_{a\ max}$$

$$= \delta_{a\ max}, \qquad \text{if } \Delta\delta_{as} \geq \delta_{a\ max}$$

The stiffness term increment due to roll error is,

$$\Delta\delta_{a\phi} = k_{\phi}\ (\phi_c - \phi) ,$$

where: k_{ϕ} = roll error gain (nominally 0.64 $(2.50/Q_f)$deg/deg)

ϕ = current vehicle roll attitude (deg)

ϕ_c = commanded roll attitude from guidance (deg)

The stiffness term increment for sideslip compensation is,

$$\Delta\delta_{a\beta} = k_{\delta_a\beta}\ \beta'_f$$

where: $k_{\delta_a\beta}$ = gain on sideslip compensation into aileron (nominally $-L_{\beta}/L_{\delta_a} \cong 2.0$ deg/deg)

β'_f = filtered value of estimated sideslip from rudder channel (deg.)

The stiffness term increment for rudder compensation is,

$$\Delta\delta_{a\delta_r} = k_{\delta_a\delta_r}\,\delta'_{rc}\ ,$$

where: $k_{\delta_a\delta_r}$ = gain on rudder compensation into aileron (nominally $-L_{\delta_r}/L_{\delta_a} \cong -0.5$ deg/deg)

δ'_{rc} = total rudder command from rudder channel except for turn coordination term (deg)

The increment in aileron command due to roll rate is,

$$\Delta\delta_{ap} = -k_p\,p,$$

where: k_p = roll rate gain (nominally 0.33 $(250/Q_f)$deg/deg/sec)

p = current vehicle roll rate (deg/sec)

If the aileron command is not against the hard limits ($\delta_{ac\ell} = \delta_{ac}$), the incremental aileron command from the aileron trimming integrator is,

$$\Delta\delta_{ai} = \frac{k_{\phi i}}{s}\,(\Delta\delta_{a\phi\ell} + \Delta\delta_{ap})\ ,$$

where:

$$\Delta\delta_{a\phi\ell} = -\delta_{a\ max}, \qquad \text{if } \Delta\delta_{a\phi} \leq -\delta_{a\ max}$$

$$= \Delta\delta_{a\phi}\ , \qquad \text{if } -\delta_{a\ max} < \Delta\delta_{a\phi} < \delta_{a\ max}$$

$$= \delta_{a\ max}, \qquad \text{if } \Delta\delta_{a\phi} \geq \delta_{a\ max}$$

As in the pitch channel, if the aileron command is against the hard limits ($\delta_{ac\ell} \neq \delta_{ac}$), the input to the trimming integrator is set to zero to prevent saturation build up.

3. Yaw Channel.

The rudder command law for all phases is,

$$\delta_{rc} = \Delta\delta_{rs\ell} + \Delta\delta_{rr} + \Delta\delta_{r_{\delta_a}}$$

where: $\Delta\delta_{rs\ell}$ = limited incremental command due to stiffness term (deg)

$\Delta\delta_{rr}$ = incremental command due to yaw rate error (deg)

$\Delta\delta_{r\delta_a}$ = incremental command for turn coordination (deg)

As in the other channels, the total command is limited to prevent commanding deflections greater than the hard surface limits.

$$\delta_{rc\ell} = -\delta_{r\ max}, \qquad \text{if } \delta_{rc} \leq -\delta_{r\ max}$$

$$= \delta_{rc}, \qquad \text{if } -\delta_{r\ max} < \delta_{rc} < \delta_{r\ max}$$

$$= \delta_{r\ max}, \qquad \text{if } \delta_{rc} \geq \delta_{r\ max}$$

where: $\delta_{r\ max}$ = rudder surface limit (nominally 10 deg.)

The incremental rudder command due to the stiffness term is

$$\Delta\delta_{rs} = k_\beta\ \beta'_f \qquad \text{, if in weather cocking mode}$$

$$= k_\psi\ (\psi_c - \psi), \qquad \text{if in decrab mode}$$

where: k_β = sideslip gain (nominally -4.3 $(250/Q_f)$ deg/deg)

k_ψ = yaw error gain (nominally -4.3 $(250/Q_f)$deg/deg)

β'_f = filtered value of estimated sideslip (deg)

ψ = current vehicle yaw attitude (deg)

ψ_c = yaw command from guidance (deg)

The sideslip filter is,

$$\beta_f' = \beta'/(\tau_\beta s + 1),$$

where β' = estimated aerodynamic sideslip

τ_β = filter time constant (nominally 0.5 sec)

The sideslip angle is estimated from sensed lateral acceleration along the vehicle Y body axis, $\dot{v}_a$, as follows:

$$\beta' = \frac{\dot{v}_a - Q\,(S/M)'\,C_{Y_{\delta_r}}'\,\delta_{rc\ell}}{Q\,(S/M)'\,C_{Y_\beta}'}$$

where C_{Y_β}' = assumed slope of sideslip side force coefficient (nominally -0.0075/deg)

$C_{Y_{\delta r}}'$ = assumed slope of rudder sideforce coefficient (nominally -0.0040/deg)

Q = sensed dynamic pressure

$(S/M)'$ = assumed reference area to mass ratio for vehicle (nominally 0.92 ft^2/slug)

$\delta_{rc\ell}$ = total limited rudder command (deg)

It can be seen from this expression that the lateral acceleration due to rudder is first being estimated and subtracted from the sensed lateral acceleration. As discussed previously in the flight control system design, this is done to compensate for the destabilizing side force from the rudder.

In both the weather cocking and decrab modes, the incremental rudder stiffness term is limited to prevent it from saturating the rudder command and cancelling out the yaw rate damping term.

$$\Delta\delta_{rs\ell} = -\delta_{r\ max}, \qquad \text{if } \Delta\delta_{rs} \leq -\delta_{r\ max}$$

$$= \Delta\delta_{rs}, \qquad \text{if } -\delta_{r\ max} < \Delta\delta_{rc} < \delta_{r\ max}$$

$$= \delta_{r\ max}, \qquad \text{if } \Delta\delta_{rs} \geq \delta_{r\ max}$$

where : $\delta_{r\ max}$ = maximum rudder deflection (nominally 10 deg).

The incremental rudder command due to yaw rate error is,

$$\Delta\delta_{rr} = k_r\ (r_c - r)$$

$$r_c = (g/V)\ \phi_c\ ,$$

where : k_r = yaw rate error gain (nominally 4.0 $(250/Q_f)$ deg/deg/sec for weather cocking mode; 2.5 $(250/Q_f)$ deg/deg/sec for decrab mode)

V = current vehicle speed (ft/sec), inertial

r = current vehicle yaw rate (deg/sec)

The incremental rudder command for quickening the turn coordination in the weather cocking mode is,

$$\Delta\delta_{r_{\delta_a}} = k_{\delta_r\delta_a} \frac{\Delta\delta_{a\phi\ell}}{\tau_{ra}\ s + 1}\ ,$$

where: $K_{\delta_r \delta_a}$ = gain on aileron command into rudder (nominally 0.4 deg/deg)

$\Delta\delta_{a\phi\ell}$ = limited incremental aileron command due to roll error from roll channel (deg)

τ_{ra} = filter time constant (nominally 0.2 sec)

VI. NAVIGATION.

A. Background.

Discussions between NASA/Ames and BAC indicated that a number of approaches could be adopted to attain the objectives of the study. One extreme approach assumed a generalized data source which supplied the vehicle state variables, introduced measurement errors into these variables and performed the Task II and Task III tests of the contract with the result that the allowable bounds on the measurement errors would be established. From these results, hardware configurations which fell within these bounds could be defined. The other extreme approach was to select various hardware configurations, establish error models for each subsystem and then perform the tests of Task II and Task III. These configurations would then be ranked in order of performance.

When the detailed tasks required to pursue these approaches were examined, it became apparent that the problem had another dimension; namely, the dependency of the final conclusions on the blending algorithms selected. It was assumed at the outset that the final system would utilize data from the on-board Inertial Navigation System (INS) which would be updated by the external landing system hardware. Thus, altering the update algorithm and/or update frequency could vary the allowable errors determined for each of the subsystems.

The approach which was adopted is described in the following sequence of steps.

1. The system would be based on guidance and control laws which would utilize parameters measured by an INS and blended with parameters measured by other landing system devices.

2. Candidate hardware configurations for the other landing system devices would be selected from existing hardware, (examples: ILS, GSN-5, radar altimeter) or from hypothetical hardware whose specifications were within the state-of-the-art (SC117 Scanning Beam System).

3. Error models would be developed for the subsystems in each of the candidate configurations.

4. The form of the blending algorithm for the navigation data would be selected and held invariant for all candidate systems. In this way, comparison between systems would be valid. Although the form would not change, the parameters within this form would be adjusted to optimize the blending for each specific landing system. This is to prevent biasing of results by selectively tuning the blending algorithm.

A quadratic lag complementary filter was selected for the blending algorithm with the time constants adjusted for each hardware system. A 3 DOF simulation during the second month of the study indicated that the algorithm resulted in estimation errors which were sufficiently small such that the performance would not be significantly altered by the choice of other methods of estimating states.

5. Hardware system configurations which have obvious deficiencies would be eliminated to allow more time for evaluating realistic candidates.

6. The selected systems would be evaluated in accordance with the requirements of Task II. One system would be selected for detailed evaluation.

7. The selected landing system would be evaluated in accordance with the Monte Carlo tests of Task III.

B. Ground Based Reference System Considerations.

Over forty concepts for landing systems have been proposed or reduced to hardware. (See "A Survey of Instrument Landing Systems" by D. J. Marino and A. E. Ward, MTR-954, The Mitre Corporation). This number of concepts, along with possible permutations of these systems appeared to create a large number of combinations as potential candidates for evaluation. However, the total number of landing system candidates was reduced by classifying the concepts into types and then selecting the best representative of that type.

The major mechanization categories were:

1. Fixed Crossed beam
2. Scanning Beam
3. Tracking Radar-Ground Based
4. Tracking Radar-Airborne
5. Multiple Range Measurements

In choosing the best candidates within each class, and in eliminating classes, it was necessary to formulate selection ground rules. The rules adopted were:

(1) Concentrate on systems which are in active use or have a high potential for coming into active use.

(2) Classify systems into their mechanization categories and determine the state of the art parameters.

(3) Exclude candidates inferior in accuracy.

(4) Exclude operationally irrational candidates.

(5) Bizzarre composites were rejected. This ground rule eliminated from consideration hypothetical systems formed by combining bits and pieces of other systems, systems which involve large numbers of elements or systems which required peculiar arrangements (spacing, locations, distributions, etc.) of components.

(6) Favor systems which have the potential for guidance throughout the flight regime.

(7) Favor systems which have potential for raw data guidance with partial or complete system failures. Redundancy was not a valid solution to the failure problem for purposes of this study.

The subsection which immediately follows describes the six systems which were selected for study under Task II. A number of configurations employing ILS were studied even though being a narrow, fixed beam with limited range violates rule (6) above. However, the widespread usage of this system (rule (1) above) was considered overriding.

Scanning beam systems have wider coverage but are essentially one-directional and of limited range, and may be considered weak from the point of view of rule (6). But rule (1) was considered overriding in view of the proposed SC117 Scanning Beam System.

Systems based on range only measurement were totally rejected if trilateration only were considered. These are readily demonstrated to result in large errors, or, alternatively, to require peculiar arrangements (violations of rules (3) and (5) above). Range measurements utilizing Kalman Filtering to update the INS and auxilliary Z axis compensation are being investigated by NASA/Ames which eliminate the difficulties inherent in the trilateration system. See "Navigation for Space Shuttle Approach and Landing Using an Inertial Navigation System Augmented by Data from a Precision Ranging System or a Microwave Scanning Beam Landing Guidance System", by L. A. McGee, et. al., Dec. 28, 1970, Ames Research Center.

The Precision Ranging System violates rule (7) but the high potential for guidance in orbit and higher segments of the trajectory was considered overriding. Since the added complexity of this system would have required an investigation beyond the scope of this study, a compromise was necessary to include this system. It was decided to assume that an unlimited number of ground DMEs were available such that range information could theoretically be obtained from a DME which is optimally located with respect to the coordinate being measured. Thus, the X_R, Y_R, Z_R coordinate as measured

instantaneously by the ground reference system (DME) and associated processing were assumed to have only the basic bias and noise errors of the DME.

It will be noted that no candidate from the airborne radar category was selected or even seriously considered because a direct one-to-one comparison between this and the ground based radar could be made and the airborne radar readily eliminated. The ground-based radar has a clear advantage on a performance basis. It is not restricted in power output (restrained by power consumption in the vehicle) as is the airborne radar. This results in both improved range and accuracy. The ground antenna may be of any size required to obtain the desired beamwidth unlike the airborne radar which is space and form factor limited. Since the ground-based radar is looking up at a radar target (corner reflector or beacon) surrounded by the area of the vehicle, noise effects from multiple reflections are in the order of magnitude of the vehicle's dimension. The airborne radar looks at a beacon on the ground which is surrounde by the earth with multiple reflectors. The multipath error in this case may at times result in the radar tracking a reflected source which is a large distance from the true source. Since the ground-based radar is stationary, the line of sight angle measurements are more accurate than for the airborne radar. The airborne radar will have vehicle pitch, roll and yaw motions as noise inputs which will result in additional angle errors due to the dynamics of the tracking loops.

In addition, the spatial region which can be searched by an airborne radar is strongly restricted by the antenna location on the vehicle. The airborne radar may not be able to acquire the ground beacon except in certain orientation of the vehicle with respect to the line of sight to the beacon. The ground-based radar does not suffer this restriction and may acquire the vehicle at any point of its trajectory from orbit.

For these reasons, a decision to use airborne radar in preference to ground-based radar would need to be based on factors outside the scope of this study.

All landing systems were compared with the same INS and Pitot Tube error models. When used, the same Radar Altimeter error model was used. A complete description of all the error models is contained in Appendix C and should be reviewed.

The following ground based portions of the landing system were compared:

(1) Precision Tracking Radar

(2) Scanning Beam System

(3) Precision Ranging System

(4) ILS with Radar Altimeter-Configuration 1

(5) ILS with Radar Altimeter-Configuration 2

(6) ILS with INS only - Configuration 1

All of the ILS systems were considered to have unuseable elevation beam information below 100 feet of altitude. For systems (4) and (5) above, a radar altimeter was used to update the INS Z axis after data dropout. For system (6), only the INS was used in

all axes. Systems (4) and (6), which are labeled as Configuration 1, placed the localizer beam on the projection of the glide slope to the runway. This was a favorable location for the lateral updates (shorte distance to vehicle) but required that data from both beams be dropped out at 100 feet. System (5), labeled Configuration 2, was more conventional in that the localizer antenna was located at the stop end of the runway. This permitted lateral updates throughout the landing.

C. Blending Algorithm.

The measured position from the hardware systems were converted into vehicle X, Y, Z coordinates and a blending algorithm used to combine these with the INS data. It was considered adequate for the purposes of this study to develop an algorithm which reduces the errors in estimation of states to a value sufficiently small so as to contribute negligibly to the touchdown errors. More sophisticated estimation techniques could not significantly reduce the touchdown errors if the algorithm resulted in estimation errors which were small compared with the touchdown errors due to maneuvers.

The Blending Algorithm is a quadratic, complementary filter. In the coordinate system described above, the position coordinates of the vehicle as measured by the INS are designated as X_N, Y_N, Z_N. The position measured by the external hardware subsystem is converted to this same coordinate system (X_R, Y_R, Z_R). Then the estimate of the vehicle position, X, and velocity, $\hat{X}$, is given by the following with the Y and Z coordinates being treated in a like manner

$$\hat{X} = \frac{X_R + \tau_1 \dot{X}_N + 0.5 \tau_1^2 \ddot{X}_N}{1 + s\tau_1 + 0.5s^2 \tau_1^2}$$

$$\hat{\dot{X}} = \frac{S \hat{X} + \tau_2 \ddot{X}_N}{1 + s \tau_2}$$

S is the Laplace operator and τ_1, τ_2 are preselected time constants.

The estimate, $\hat{X}$, is obtained by filtering the measurement X_R which in general contains accurate position data but is corrupted by higher frequency noise. The filter is a quadratic lag which is well damped irrespective of the choice for the time constant, τ_1, and, therefore, gives good high frequency attenutation. The lag introduced into the estimate of $\hat{X}$ by the quadratic filter is compensated by adding back the position change during the lag interval, τ_1, as estimated from the INS measured velocities and accelerations ($\dot{X}_N$, $\ddot{X}_N$). The short term changes in velocity and acceleration information from the INS are good with the principal error in the INS being due to a relatively slow drift which result in poor long term INS position error. The algorithm, in summary, averages the external measurement of position and corrects for the averaging process by utilizing the velocity and acceleration changes obtained from the INS. Note that if X_R, $\dot{X}_N$, $\ddot{X}_N$ were error free, $\dot{X}_N = \dot{X}_R$ and $\ddot{X}_N = \ddot{X}_R$ and the algorithm reduces exactly to $\hat{X} = X_R$.

The estimate of velocity $\hat{\dot{X}}$ is based upon differentiating the best estimate of X, namely $\hat{X}$. A first order lag filter with time constant, τ_2, is used to smooth the differentiation. The error due to filter lag is compensated by addition of the term

$\tau_2 \ddot{X}_N$ where $\ddot{X}_N$ is the best information on vehicle acceleration. Note that $\hat{\dot{X}} = \dot{X}_R$ for the error free case as desired.

The constants τ_1, τ_2, which differ between hardware configurations, were selected based upon the errors associated with the external subsystem (radar, ILS, etc.) used to update the INS. Since τ_1, τ_2 are tailored to best fit the subsystem, the algorithm will result in blending that is not biased in favor of a particular system.

It was found from preliminary runs that, for the best combination of blending time constants, the accuracy of the estimated position signal, $\hat{X}$, was limited by the accelerometer bias error in the INS. To correct this, an update loop was added to the INS. This loop is of the form:

$$\ddot{X}_{NU} = \ddot{X}_N + K\,(\hat{\dot{X}} - \dot{X}_N)$$

where $\ddot{X}_{NU}$ = updated acceleration

K = update gain.

The values for the constants were empiracally determined to be

$\tau_1 = \sqrt{0.75\ \sigma_{XR}}$ but not less than 1.0 secs.

$\tau_2 = 2\tau_1$

$K = 0.2$

where σ_{XR} is the assumed standard deviation of the ground referenced position error. For the Y and Z axes, σ_{YR} and σ_{ZR}, respectively, are used. It should be noted that where an angular error is the basic error, such as ILS beam bending, then σ_{ZR} and σ_{YR} are $X\sigma_\theta$ and $X\sigma_\psi$, respectively, where σ_θ, σ_ψ are the standard deviations of the elevation and azimuth angle errors.

D. Blending Algorithm, Discussion of Results.

Preliminary results prior to the simulations of Task II and III indicated that the estimation errors using the complementary filter were sufficiently small such that more sophisticated estimation techniques would not strongly affect the conclusions concerning touchdown errors. To confirm the validity of this approach, a review of the estimation errors resulting from the simulation work is presented in this section.

The questions of interest are:

1. How significant were the estimation errors with respect to the touchdown errors?
2. How close were the estimates to the best attainable?
3. How much do winds and gusts effect the estimation?

The scanning beam system evaluated in Task II will be used to investigate questions (1) and (2). Table VI-1 lists the results obtained from Figure VII-8 along with the position TD errors expected from measurement bias. Recognizing that the theoretical limit on position accuracy is determined by the biases in the ground based measuring system, the measurement bias columns depict the least RMS error that can be attained with the assumed hardware error model. The term RMS bias means the RMS value of the long term bias, an error that is a constant within the time span of one landing but may be expected to vary from landing to landing.

To obtain the total touchdown bias error for X,

$$\sigma_{XB}^2 = \sigma_{XMB}^2 + (\gamma_{td})^{-2} (R_\theta \sigma_{\theta MB})^2$$

TABLE VI-1

SBS BLENDING AND TOUCHDOWN ERRORS (RMS)

1. SBS Configuration of Task II
2. Hardware errors only

VARIABLE	T.D. ERROR	ESTIMATION ERROR	TD ERROR EXPECTED FROM MEASUREMENT BIAS	ERROR IN ESTIMATION EXPECTED FROM MEASUREMENT BIAS
X	205 ft.	16.2 ft.	160 ft.**	10 ft.
Y	2.4 ft.	2.1 ft.	1.26 ft.	1.26 ft.
Z	0 ft.*	1.9 ft.	0 ft.*	1.64 ft.
$\dot{X}$	3.5 ft/sec.	0.73 ft/sec.	-	-
$\dot{Y}$	0.59 ft/sec.	0.27 ft/sec.	-	-
$\dot{Z}$	0.36 ft/sec.	0.31 ft/sec.	-	-

*Touchdown is defined by the wheels touching the ground plane. Therefore, by definition, there is no touchdown error in the Z coordinate of the vehicle.

**See text for calculations.

where σ_{XB} is the RMS TD error in X that is expected from total measurement bias, σ_{XMB} is the RMS error due to range measurement bias, γ_{td} is the nominal glide slope at touchdown which is expressed in radians as the ratio of the nominal sink rate (3 ft/sec) and the nominal speed (275 ft/sec), R_θ is the range from the elevation scanner to the TD point, and $\sigma_{\theta MB}$ is the RMS error due to elevation angle measurement bias.

For the scanning beam system studied in Task II,

σ_{XMB} = 10 ft, R_θ = 2000 ft., $\sigma_{\theta MB}$ = 0.87 mr yielding

σ_{XB} = 160 feet.

Similarly for Y, the RMS error expected from the assumed error model biases is:

$$\sigma_{YB} = R_\psi \sigma_{\psi MB}$$

where σ_{YB} is the RMS Y error expected because of measurement system bias, R_ψ is the range from the azimuth scanner to the TD point and $\sigma_{\psi MB}$ is the RMS error due to azimuth angle measurement bias. For the system studied in Task II, R_ψ = 2000 feet, $\sigma_{\psi MB}$ = 0.63 mr yielding σ_{YB} = 1.26 feet.

Note that there is no Z touchdown error since by definition TD occurs when Z = 0. Similarly, there is no Z touchdown error due to bias. This is converted into X error as shown in the expression for σ_{XB}.

From Table VI-1, the following conclusions are drawn when only hardware errors are present.

1. The major component of X dispersion is due to Z (altitude) errors.

2. Because of 1, the major component of X error is due to elevation angle measurement bias and is not reducible by any estimation technique.

3. Errors in estimating range with the blending algorithm are negligible in terms of effect on TD errors.

4. The lateral error at TD is due almost entirely to the estimation error. It is negligibly small and 60% of it is due to measurement bias errors which cannot be reduced.

5. The blending algorithms estimation of velocity errors is adequate. The errors are either small compared with the total error or the total error is small, conditions which preclude consideration of improving the algorithm. Note that the estimation error of $\dot{X}$ is small compared with the $\dot{X}$ error, the estimation error of $\dot{Y}$ is one-half of the $\dot{Y}$ error and the estimation error of $\dot{Z}$ is about the same as the $\dot{Z}$ error with the actual $\dot{X}$, $\dot{Y}$, $\dot{Z}$ errors decreasing in this order. As the actual TD errors become smaller, the estimation errors become a greater part of the error. Although the vehicle is undergoing vertical deceleration during the final flare which increases the dynamic errors in the blending computation, an adequate estimation of $\dot{Z}$ is still attained.

How much do winds and gusts effect the estimation provided by the Blending Algorithm? This was the third question asked at the beginning of this section. It is important because the frequency content of the vehicle states differ between a system with only hardware noise and one with wind and gust induced dynamics. The blending algorithm is a digital computation performed 10 times per second. Though the gust frequencies are generally low so that negligible fold-over (aliasing) of high frequency noise into the low frequency region would be expected, the modeling of the vertical gust (see Appendix C, Data Base) in Task III required the gust spectrum to spread from 2.75 radians/second to 27.5 radians/second in the last 100 feet. This gave accelerations with frequency content well up in the region where fold-over in the sampling process could increase the apparent low frequency noise. To minimize this problem, a 0.1 sec first order filter was included on the vertical acceleration measurement and the computation of the blending algorithm was maintained at 10 SPS. (Increasing the rate could also get around the fold-over problem. Since the algorithm would be mechanized on an airborne computer, it was realistic to emulate the airborne digital computation and not raise the computation rate.)

Though the foldover problem resulting from sampling the NASA/Ames defined vertical gust spectrum was real, the question of whether the assumed spectrum itself was realistic is outside the scope of this study.

To investigate the possible effects of turbulence, the results of the SC117 scanning beam system are shown in Table VI-2, for the K_W = 2 crosswind and σ_{ur} = 6.8 ft/sec gust case. This system differs from the one studied in Task II in that σ_{XMB} = 2 ft and R_ψ = 8000 ft. The conclusions which may be drawn from this table are:

1. Further improvement in the blending algorithm is unjustified. The influence of winds and gusts significantly increase the TD errors, but only midly affect the estimation errors.

2. Increasing the DME accuracy for the SBS by reducing the RMS bias error from 10 feet to 2 feet is unjustified.

Table VI-1 shows that with an RMS bias error of 10 feet in range measurement (DME) and the angle errors specified in Appendix C. Data Base, the error in estimating the X coordinate at touchdown was 16.2 feet RMS and the touchdown error in X was 205 feet RMS. Table VI-2 shows that with the RMS bias reduced to 2 feet and the same angle errors, the estimation error was 3.9 feet RMS and the touchdown error was 440 feet RMS. Neither the error in the DME or the resulting error in estimate was significant with respect to the actual TD error.

3. The larger TD error in the case depicted in Table VI-2 is, of course, due to the addition of high winds and gusts. The ratios of estimation errors in X to the assumed DME bias errors is about the same for the high gust cases of Table VI-2 and the "hardware errors only" case of Table VI-1 and is, further, seen to be less than two.

TABLE VI-2

SC117 BLENDING AND TOUCHDOWN ERRORS (RMS)

1. SBS Configuration of Task III
2. Hardware errors
3. K_W = 2 crosswind, σ_{ur} = 6.8 ft/sec gusts

VARIABLE	T.D. ERROR	ESTIMATION ERROR	TD ERROR EXPECTED FROM MEASUREMENT BIAS	ERROR IN ESTIMATION EXPECTED FROM MEASUREMENT BIAS
X	440 ft	3.9 ft.	160 ft.	2.0 ft.
Y	16.2 ft.	5.6 ft.	5.04 ft.	5.04 ft.
Z	0 ft.	1.7 ft.	0 ft.	1.64 ft.
$\dot{X}$	12.6 ft/sec.	0.7 ft/sec.	-	-
$\dot{Y}$	6.5 ft/sec.	0.54 ft/sec.	-	-
$\dot{Z}$	1.7 ft/sec.	0.7 ft/sec.	-	-

4. Similarly, the estimation error in Y of 5.6 feet is nearly the minimum expected which is that due to the azimuth angle bias error. Note the 5.04 ft that would result from bias error alone.

5. The added maneuvering in Y due to decrab for these heavy crosswind runs does deteriorate the estimation of $\dot{Y}$ at TD since very little averaging time before end of flight is available.

6. The actual $\dot{Y}$ error is more than 10 times larger than the $\dot{Y}$ estimation error and, hence, improving the algorithm is unjustified.

7. The deterioration in the estimation of $\dot{Z}$ is about the same degree as that of $\dot{Y}$; namely, the error in both cases is about twice as large as the error in the no wind case.

8. There is evidence of a weak influence on the estimation errors of the presence of wind gust and shears. However, the growth of the estimation error is small compared with the growth of the touchdown errors due to the vehicle disturbances caused by these winds and gusts.

9. Since the scanning beam system of Task II was somewhat different than the SC117 system, the results of Task III may be used to estimate the results that could be expected for the SC117 system under Task II conditions for a more exact comparison of hardware errors. Note that the error in the DME bias played no significant role in the X error in either Task II or III. The X error was in fact largely due to the estimation error in Z.

Note, further, that the estimation errors in Z were about the same (see Tables VI-1 and VI-2). Therefore, the X TD error with either system will be the same, namely 205 ft RMS.

Note that without winds and gusts, the Y error is about the same as the estimation error. Since in Task III the estimation error approached the minimum determined by azimuth bias, a good estimate of the Y error that would result from the SC117 system without winds and gusts is the estimation error, namely 5.6 feet.

Since the estimation errors are about the same in $\dot{X}$ and since the major velocity error without winds is due to vehicle and control loop dynamics, the assumption is made that there would be no differences between the velocities of the SC117 system and the one studied in Task II.

The SC117 error in $\dot{Y}$ does not seem to reflect the added lever arm that affected the Y estimate. This can be seen by noting that the $\dot{Y}$ estimation error is only 2 times worse in the SC117 case than in the Task II scanning beam case in spite of a 4 times increase in lever arm plus decrab maneuver dynamics and 6.8 ft/sec standard deviation gusts. The presumption is that the SC117 without gusts and winds would give an error of 0.59 ft/sec just as the other system.

Since there is no difference between the Z axes, the SC117 system would give a $\dot{Z}$ error of 0.36 ft/sec., RMS, due to hardware errors alone.

VII. SIMULATION RESULTS.

A. Task II.

The first part of Task II evaluated the sensitivity of the guidance and flight control system to deterministic variations in vehicle parameters, wind shears and initial conditions. Due to the strong influence of gusts, a limited Monte Carlo evaluation of gust effects was also found necessary to refine the control laws.

The second purpose of Task II was to evaluate by limited Monte Carlo runs the candidate hardware systems and recommend a landing system for the SSV program.

Descriptions of the models used for both Task II and Task III are contained in Appendix C, Data Base.

1. System Sensitivities to Initial Condition (I.C.) Errors.

With the guidance and flight control laws finalized, the sensitivity of the system to deterministic perturbations was investigated.

Figure VII-1 lists for reference purposes the nominal initial conditions at the primary flare start point used for Task II.

Figure VII-2 tabulates the effects at touchdown of initial condition (I.C.) errors at the start of primary flare. These are errors in the nominal conditions listed in Figure VII-1 for the no wind case. The row labeled Nominal in Figure VII-2 lists the touchdown conditions for no disturbances or initial condition errors. The nominal touchdown point was selected as

FIGURE VII-1

NOMINAL INITIAL CONDITIONS

WIND SHEAR	h (Ft.)	X (Ft.)	Y (Ft.)	V (Ft/Sec)	γ (Degrees)	$\dot{\gamma}$ (Ft/sec)
MEAN HEADWIND	555	10,907	0	381	-7.07	0
MEAN CROSSWIND OR NO WIND	1085	20,841	0	470	-7.27	0
MEAN TAILWIND	1310	24,790	0	506	-7.35	0

MEAN WIND SHEAR PROFILE FROM APPENDIX C			
h (feet)	WIND VELOCITY IN KNOTS		
	HEADWIND	CROSSWIND	TAILWIND
10	12.5	7.5	5.0
100	19.4	11.6	7.8
1000	26.3	15.8	10.5

FIGURE VII-2

INFLUENCE OF I.C. ERRORS

ERRORS AT FLARE INITIATE	TOUCHDOWN VALUES							
	X	V	$\dot{Z}$	Y	$\dot{Y}$	α	ϕ	ψ
NOMINAL	150	276	2.90	0	0	14.8	0	0
+ 1000 = ΔX	**143**	275	2.90	0	0	14.9	0	0
+ 20 = ΔV	145	**279**	**2.91**	0	0	**14.6**	0	0
+ 200 = ΔY	147	276	2.90	**-0.2**	**0.1**	14.8	**-0.16**	-0.02
$+1.15^{o}$ = $\Delta\xi$	151	276	2.90	0	**0.1**	14.8	-0.08	**0.05**

ΔX range error, ft.

ΔV velocity error, ft/sec

ΔY lateral offset error, ft.

$\Delta\xi$ velocity vector misalignment with respect to runway centerline, degrees

X = 150 feet long bacause, when disturbances are added, the system tends to land short. It is the intent to bias the nominal TD point such that the statistical average in the presence of random disturbances is zero. It should be noted that the exact value of the nominal aim point is ultimately determined by the results of the Monte Carlo runs of Task III.

The numbers which are enclosed by squares in Figure VII-2 designate the largest change from the nominal of the variables listed. The largest change in X was 7 feet from the nominal and resulted when the initial value of X was 1000 feet longer than the nominal. The largest change in touchdown airspeed, V, was 3 feet per second faster than nominal and resulted from starting 20 feet per second too fast. The largest change in sink rate, $\dot{Z}$, was 0.01 feet per second and again resulted from the start velocity being 20 feet per second too fast. The largest lateral error, Y, resulted from starting 200 feet off the centerline with the error being 0.2 feet in magnitude. Two I.C. errors resulted in 0.1 feet/second lateral velocity error, these being the 200 foot off-centerline start and starting with the velocity vector misaligned by 1.15^{o} from the centerline. The largest change in angle of attack was 0.2^{o} from nominal and this occurred for the 20 foot per second velocity error case. The largest roll angle error at touchdown was 0.16^{o} and occurred for the case of the 200 foot lateral offset at primary flare start. The largest error in heading angle, 0.05^{o}, occurred

for the case when the velocity vector at primary flare start was misaligned by 1.15^{o} from the runway centerline. There were no unexpected developments in this deterministic investigation with the influences at touchdown being predictable from the assumed initial condition error. More importantly, the touchdown errors were small when compared with the I.C. errors.

2. System Sensitivities to Vehicle Characteristics.

The sensitivity of the design to uncertainties in the vehicle parameters was investigated. Figures VII-3 and VII-4 list the effects at touchdown of a 5% deterministic variation in key vehicle parameters without revising the flight control or guidance laws. The first row in Figure VII-3 restates the nominal touchdown conditions for reference purposes. The numbers that are enclosed by squares in Figure VII-3 designate the largest change from the nominal of the variable listed. The largest changes in X (60 feet and 59 feet short) were due to a 5% increase in weight $(\frac{S}{M})$ and to a 5% decrease in the pitch control power respectively. A 5% decrease in the lift to drag ratio (L/D) resulted in the largest change in touchdown airspeed (9 feet/second). The 5% increase in weight also resulted in the greatest sink rate change, namely an increase of 0.13 feet/second. The largest change in angle of attack was 0.8^{o} and resulted from a 5% decrease in (L/D).

FIGURE VII-3

INFLUENCE OF VEHICLE CHARACTERISTICS

	X	V_a	$\dot{Z}$	Y	$\dot{Y}$	α	ϕ	ψ
NOMINAL	150	276	2.90	0	0	14.8	0	0
-5% (S/M)	90	283	3.03	0	0	14.8	0	0
-5% (L/D)	103	267	2.93	0	0	15.6	0	0
-5% PITCH CP	91	278	3.00	0	0	15.0	0	0
+5% ELEVON LIFT	110	274	2.92	0	0	15.3	0	0
DENSITY $\Delta\rho = -5\%\rho$	152	282	2.90	0	0	14.9	0	0

FIGURE VII-4

INFLUENCE OF LATERAL CONTROL POWER VARIATIONS
WITH MEAN CROSSWIND

CONTROL POWER VARIATION	$\dot{Y}$	ϕ	ψ
NOMINAL CP	-4.8	-.54	-.35
-5% ROLL CP	-4.9	-.71	-.36
-5% YAW CP	-4.8	-.62	-.39

See Figure VII-1 for Mean Crosswind Shear Profile.

To determine the effect of decreasing the roll and yaw control power, these must be compared with the case for a mean crosswind shear with nominal control power. This is shown in Figure VII-4. In Figure VII-4, the first row shows the results for nominal control power with the mean cross wind shear. It is seen that the effect at touchdown is to develop a cross track velocity of 4.8 feet/sec, a roll angle of 0.54 degrees and a yaw angle with respect to runway centerline of 0.35 degrees. Reducing the roll control power by 5% increased the cross track rate at touchdown by 0.1 feet/sec, the roll angle by 0.17 degrees and the heading error by 0.01 degrees. Decreasing the yaw control power by 5% did not degrade the crosstrack velocity but resulted in an increase both in roll angle (0.08 degrees) and in the heading error (0.04 degrees).

The small effects shown for decreased control power are deceptive. In the absence of disturbances, the system is not severely taxed and does not call for full control power except for brief periods. A decrease in maximum control power, therefore, does not appreciably effect results since maximum power is generally not required. Under gust conditions, a greater deterioration would have resulted.

3. System Sensitivity to Winds.

a. Mean Wind Shears and Rotations.

Appendix C describes the wind shears and wind rotation models.

Figure VII-5 illustrates the influence at touchdown of a variety of wind shears. The results show that the greatest change in X is 92 feet short and occurred for the HW shear. The greatest change in V_a is 6 feet/second slower and occurred for the HW Rotation. This case also resulted in the greatest change in sink rate which was 0.14 feet/second light. The crosswind shear resulted in the largest error in Y, $\dot{Y}$ and ψ (3.5 feet, 4.8 feet/second, and 0.35°, respectively). The HW Rotation resulted in the largest change in angle of attack, α (0.5°). The TW Rotation resulted in the biggest roll angle (1.01°).

b. Gusts Influence.

The influence of gusts on system statistics at touchdown is illustrated in Figure VII-6. These results were based on statistics obtained from a 20 run sample.

The gust model used is described in Appendix C. σ_{ur} = 3.4 feet/second for the Task II evaluations.

The results show that the vehicle became "heavy" in the presence of gusts. The average touchdown range, $\bar{X}$, is shorter and the average sink rate, $\bar{\dot{Z}}$, is higher. In addition, the dispersion of all variables is significant even with mean gust levels.

FIGURE VII-5

INFLUENCE OF WIND SHEARS (NO GUSTS)

	X	V_a	$\dot{Z}$	Y	$\dot{Y}$	α	ϕ	ψ
NOMINAL	150	276	2.90	0	0	14.8	0	0
MEAN HEADWIND	58	273	2.80	0	0	15.1	0	0
MEAN TAILWIND	182	279	2.92	0	0	14.5	0	0
MEAN CROSSWIND	139	276	2.94	-3.5	-4.8	14.8	-0.54	-0.35
MEAN HEADWIND +0.045°/FT (ROTATION	72	270	2.76	1.2	2.4	15.3	0.89	0.23
MEAN TAILWIND +0.045°/FT (ROTATION)	191	280	2.87	-1.1	-2.3	14.4	-1.01	-0.19
MEAN CROSSWIND +0.045°/FT (ROTATION)	118	278	2.93	-2.9	-4.5	14.6	-0.63	-0.34

See Table VII-2 for wind shear profiles and Appendix C for the wind shear model and description of wind rotation.

FIGURE VII-6

INFLUENCE OF GUSTS
(20 SAMPLE STATISTICS)

	$\overline{X}$ Feet	σ_x Feet	$\overline{\dot{Z}}$ Ft/Sec	σ_z Ft/Sec	σ_y Feet	$\sigma_{\dot{y}}$ Ft/Sec	σ_ϕ Degrees	σ_ψ Degrees
NOMINAL (no gusts)	150	0	2.9	0	0	0	0	0
MEAN GUSTS (σ_{ur}=3.4 ft/sec)	43.2	180	3.5	0.58	3.5	2.3	1.55	0.30

σ_{ur} is defined in Appendix C under WIND MODEL.

As discussed in Appendix C, there was a difference between the vertical gust models used in Task II and Task III. The bandwidth of the spectrum was held constant for the last 100 feet of altitude for Task II but was inversely proportional to altitude for the last 100 feet for Task III.

4. Influence of Hardware Errors.

a. General Approach.

The total landing system was divided into ground based measurement hardware (commonly referred to as Landing Systems) which give vehicle position measurements with respect to an earth coordinate system and the airborne portion which included the INS, Pitot Tube, and Radar Altimeter. The airborne components were used as required by the system being studied. All computations were assumed to be performed in an airborne digital computer with the computation rates and computations restricted to be consistent with programming state of the art airborne computers.

The hardware error models are defined in Appendix C and the selection criteria for the ground based measuring systems was discussed in Section VI.

The basic concept was to convert the position measurements into the X, Y, Z coordinates of the vehicle with respect to the touchdown point. The X-axis is the runway centerline, the Z-axis is the local vertical and the Y-axis completes the orthogonal set. These coordinates would be combined with the INS outputs to

form best estimates of X, Y, and Z, and $\dot{X}$, $\dot{Y}$, and $\dot{Z}$. The combining scheme was termed the Blending Algorithm and was described in Section VI.

The purpose of Task II was to recommend the ground based measurements system. The recommendation was to be based on limited Monte Carlo evaluations of the touchdown error resulting from hardware errors only (no winds or gusts). As discussed in Section VI, the candidate systems were reduced to:

(1) Precision Tracking Radar (TR)

(2) Scanning Beam Systems (SBS)

(3) Conventional ILS

(4) Conventional ILS and Radar Altimeter

(5) Precision Ranging System (PRS)

For the PRS, as described in Appendix C, idealized locations of the ground based beacons (DME) were assumed; i.e., the measurement error in the X, Y, Z position coordinates was assumed to be the same as the basic DME ranging error.

b. Limited Monte Carlo Evaluation Results.

The results for touchdown (TD) errors and blending algorithm errors is summarized in Figures VII-7 through VII-10. The results are based on twenty runs for each system.

FIGURE VII-7 RADAR

RADAR ERRORS	VARIABLE	R	θ	ψ				
	NOISE (1σ)	8 ft.	0.3 mr	0.3 mr				
	BIAS (1σ)	1 ft.	0.3 mr	0.3 mr				
BLENDING ERRORS AT TD	VARIABLE	X	Y	Z	$\dot{X}$	$\dot{Y}$	$\dot{Z}$	
	RMS	1.9 ft	0.57 ft	0.71 ft	0.23 fps	0.13 fps	0.16 fps	
TD ERRORS	VARIABLE	X	V_a	Y	$\dot{Y}$	$\dot{Z}$	ϕ	ψ
	RMS	83 ft.	1.7 fps	1.4 ft	0.30 fps	0.29 fps	0.26 deg	0.18 deg

FIGURE VII-8 SCANNING BEAM SYSTEM

SCANNING BEAM ERRORS	VARIABLE	R	θ	ψ				
	NOISE (1σ)	75 ft.	0.61 mr	0.39 mr				
	BIAS (1σ)	10 ft	0.87 mr	0.63 mr				
BLENDING ERRORS AT TD	VARIABLE	X	Y	Z	$\dot{X}$	$\dot{Y}$	$\dot{Z}$	
	RMS	16.2 ft	2.1 ft	1.9 ft	0.73 fps	0.27 fps	0.31 fps	
TD ERRORS	VARIABLE	X	V_a	Y	$\dot{Y}$	$\dot{Z}$	ϕ	ψ
	RMS	205 ft	3.5 fps	2.4 ft	0.59 fps	0.36 fps	0.42 deg	0.23 deg

FIGURE VII-9

ILS SYSTEMS

ILS ERRORS

VARIABLE	R	θ	ψ
NOISE (1σ)	75 ft.	1.26 mr	1.4 mr
BIAS (1σ)	10 ft.	1.26 mr	1.4 mr

ESTIMATION ERRORS (ILS DROP OUT @ h=100 FT, ESTIMATION ERRORS AT TD)

VARIABLE	X	Y	Z	$\dot{X}$	$\dot{Y}$	$\dot{Z}$
(1) RMS ERROR	38.2	5.9	13.3	1.06	0.57	1.06
(2) RMS ERROR	36.7	6.1	1.6	1.04	0.55	0.21
(3) RMS ERROR	39.2	12.9	1.7	1.01	0.89	0.19

TD ERRORS

VARIABLE	X	V_a	Y	$\dot{Y}$	$\dot{Z}$	ϕ	ψ
(1) RMS ERROR	896	34.9	6.4	0.58	2.04	0.34	0.19
(2) RMS ERROR	156	4.0	6.5	0.60	0.56	0.31	0.16
(3) RMS ERROR	161	3.9	13.6	1.03	0.57	0.32	0.18

(1) INS ONLY AFTER ILS DROPOUT AT h=100 FT - CONFIGURATION 1

(2) RADAR ALTIMETER AFTER ILS DROPOUT - CONFIGURATION 1

(3) RADAR ALTIMETER AFTER ILS DROPOUT - CONFIGURATION 2

(See Appendix C, Data Base, for definition of Configurations)

FIGURE VII-10. PRS SYSTEM

DME ERRORS	VARIABLE	X	Y	Z				
	NOISE (1σ)	1.5 ft	1.5 ft	1.5 ft				
	BIAS (1σ)	1.0 ft	1.0 ft	1.0 ft				
BLENDING ERRORS AT TD	VARIABLE	X	Y	Z	$\dot{X}$	$\dot{Y}$	$\dot{Z}$	
	RMS	1.1 ft	0.9 ft	0.8 ft	0.42 fps	0.13 fps	0.15 fps	
TD ERRORS	VARIABLE	X	V_a	Y	$\dot{Y}$	$\dot{Z}$	ϕ	ψ
	RMS	108 ft	2.6 fps	1.4 ft	0.39 fps	0.41 fps	0.41 deg	0.19 deg

In these figures, the bias and noise errors of the hardware system being evaluated are listed in the first row, the blending algorithm errors in estimating the state at touchdown is in the second row, and the actual TD errors are in the third row.

Figure VII-11 compares the various hardware systems in terms of dispersions. It can be seen that the TR, SB, ILS with INS and Radar Altimeter update (both configurations) are acceptable. The ILS without Radar Altimeter augmentation is unacceptable. Note that the PRS system would rank second, just behind the TR, in this evaluation. However, because the DME is optimally located for each vehicle state update, the results are considered inconclusive. Also, the SB system was evaluated with the localizer antenna located 2000 feet beyond the nominal touchdown point. If the localizer antenna is moved to the stop end of the runway, σ_y will vary proportional to the distance between the localizer and the TD point. Since a four-fold increase is still acceptable, the conclusion that the SB is acceptable remains valid.

The somewhat better performance of the TR when compared with the PRS aided by ideal DME locations was unexpected. The tracking radar (TR) is somewhat better than the Precision Ranging System primarily because the data near touchdown is the most important.

FIGURE VII-11

COMPARISON OF HARDWARE SYSTEMS

	σ_X	σ_{V_a}	$\sigma_{\dot{Z}}$	σ_Y
TR	83	1.7	0.29	1.4
SB	205	3.5	0.36	2.4
PRS	108	2.6	0.41	1.4
ILS (Config. 1) (INS, h < 100')	896	34.9	2.04	6.4
ILS (Config. 1) (Radar Alt, h < 100')	156	4.0	0.56	6.5
ILS (Config. 2) (Radar Alt, h < 100')	161	3.9	0.57	13.6

(See Appendix C for definition of ILS Configurations 1 and 2)

At TD, the PRS system cannot improve upon the 1 foot bias error which is basic to the DME while the limitation of the radar system is determined by the 0.3 mr angular bias error. Since the radar can be placed close to the TD point, this results in a smaller position error measurement. Even at the assumed range (2000 feet) for the study, which is larger than actually required, the bias is only 0.6 feet.

Figure VII-11 should be compared with Figure VII-6. This suggests, based on the limited number of runs made to obtain these data, that mean gusts will cause the same order of magnitude errors as the hardware system errors.

B. Task III - Monte Carlo Results

1. General.

Based on the results of Task II, NASA/AMES decided that the proposed SC117 scanning beam system, because of its planned widespread usage in the future, should be the major system studied in Task III. It was further decided, in order to obtain the maximum information from the limited number of runs allowed by the program's budget, that high wind cases be examined in detail. For this reason, Task III was subdivided into two parts. The first part is reported in this section and consisted of a set of tests as follows:

a. model the SC117 scanning beam system as described in Appendix C, randomly selecting the noise and bias as indicated.

b. randomly choose the initial states, X_{ic}, Y_{ic}, Z_{ic}, $\dot{X}_{ic}$, $\dot{Y}_{ic}$, $\dot{Z}_{ic}$ as described in Appendix C.

c. randomly choose the initial errors in "estimate" of the state as described in Appendix C.

d. model the INS and Pitot tube as described in Appendix C.

e. deterministically select σ_{ur} to be 6.8 ft/sec or 4.6 ft/sec as shown in Table VII-1 below. (NOTE: σ_{ur} is the standard deviation in the gust model described in Appendix C. σ_{ur} is less than 6.8 ft/sec 99% of the time according to this model and σ_{ur} is less than 4.6 ft/sec 88% of the time. The gusts themselves are randomly selected from the distribution having the selected σ_{ur}).

f. deterministically select the wind shear direction in the wind model described in Appendix C to be headwinds (HW), crosswinds (CW) and tailwinds (TW) where ψ_W = 0, 90^o, 180^o, respectively.

g. deterministically select the wind shear magnitude for the wind model described in Appendix C to be K_W = 2 and K_W= 1-1/3 as shown in Table VII-1 below. According to the model, the shear magnitudes will be less than these levels 99.8% and 84% of the time respectively.

h. the number of runs and the deterministic winds were in accordance with Table VII-1 below resulting in a total of 600 runs.

TABLE VII-1

WIND MAGNITUDES

Set. No.	Number of Runs	σ_{ur}*	ψ_W*	K_W*
1	50	6.8	0°	2
2	50	6.8	90°	2
3	50	6.8	180°	2
4	50	4.6	0°	2
5	50	4.6	90°	2
6	50	4.6	180°	2
7	50	4.6	0°	1-1/3
8	50	4.6	90°	1-1/3
9	50	4.6	180°	1-1/3
10	50	6.8	0°	1-1/3
11	50	6.8	90°	1-1/3
12	50	6.8	180°	1-1/3

*Defined in Appendix C, Data Base.

The second part of Task III was a true Monte Carlo where turbulence magnitude (σ_{ur}), wind direction (ψ_W) and wind magnitude (K_W) were also randomly selected from their models. These runs better define the center of the distributions of the key touchdown parameters. In addition, the "true" Monte Carlo was repeated for the Precision Tracking Radar as well as the SBLGS. The SC117 scanning beam system and the Precision Tracking Radar were each run 50 times.

Prior to initiating these "true" Monte Carlo runs, it was found necessary to make a change in the incremental drag coefficient due to ground effects, ΔC_a, and to decrease the allowable pitch attitude at touchdown. This resulted in an improved system termed the Modified System which is discussed in Section VIII.

The remainder of this section discusses the results for the original system. These results are essentially conservative as can be seen by reading Section VIII which discusses the Modified System. The changes resulted in a better system but the trends exhibited by the high wind and high gust Monte Carlo runs with the original system are considered valid.

2. SC117 Scanning Beam System Results.

Appendix A contains the histograms of the key vehicle states which resulted from the Monte Carlo runs outlined in Table VII-1. The means (bar over the variable) and standard

deviations (σ) of these variables were computed from the histograms and are listed in Table VII-2. The trends depicted in the histograms of Appendix A are discussed in the sections which follow.

In table VII-2 and in the following, the variables are defined as:

HW = headwind

CW = crosswind

TW = tailwind.

The variables are the touchdown values with respect to a nominal TD point with coordinates X = 0, Y = 0, Z = 0.

X = longitudinal distance

$\dot{X}$ = forward ground speed

V_a = air speed

Y = lateral displacement

$\dot{Y}$ = cross track velocity

$\dot{Z}$ = sink rate

ψ = heading angle with respect to centerline

θ = pitch attitude

ϕ = roll attitude

β = sideslip angle

K_W, ψ_W and σ_{ur} are defined in Appendix C.

TABLE VII-2
MEANS AND STANDARD DEVIATIONS OF TD VARIABLES

WINDS AND GUSTS K_W	ψ_W	σ_{ur}	$\bar{X}$	σ_X	$\bar{\dot{X}}$	$\sigma_{\dot{X}}$	$\bar{V}_a$	σ_{V_a}	$\bar{Y}$	σ_Y	$\bar{\dot{Y}}$	$\sigma_{\dot{Y}}$	$\bar{\dot{Z}}$	$\sigma_{\dot{Z}}$
2	HW	4.6	152	232	228	7.7	270	8.2	0.6	5.0	.5	2.1	3.59	1.31
2	TW	4.6	110	328	302	7.3	285	8.0	1.8	8.1	.3	2.1	2.95	.97
2	CW	4.6	48	254	276	7.0	276	7.2	-13.6	12.9	-8.7	4.4	3.46	1.23
2	HW	6.8	37	402	230	13.5	271	14.1	0	8.6	- .8	4.0	4.29	1.58
2	TW	6.8	86	388	302	8.4	282	9.4	1.9	8.7	.3	3.6	3.86	1.55
2	CW	6.8	16	446	276	11.7	275	12.6	-13.5	16.3	-6.6	6.5	4.26	1.72
1-1/3	HW	6.8	56	410	244	13.3	271	14.7	- .2	8.0	- .2	4.2	4.51	1.76
1-1/3	TW	6.8	-20	362	296	8.7	283	9.9	.7	8.0	.7	3.4	3.98	1.74
1-1/3	CW	6.8	-19	343	278	9.5	278	10.9	- 9.0	11.9	-4.9	3.9	4.10	1.69
1-1/3	HW	4.6	111	250	243	8.5	269	9.7	- 0.9	6.3	-0.7	2.6	4.15	1.29
1-1/3	TW	4.6	54	281	294	6.7	283	6.7	.3	6.4	- .4	2.0	3.25	1.15
1-1/3	CW	4.6	84	245	276	6.1	275	7.6	- 9.1	9.3	-5.2	3.3	3.53	1.08

WINDS AND GUSTS K_W	ψ_W	σ_{ur}	$\bar{\psi}$	σ_ψ	$\bar{\theta}$	σ_θ	$\bar{\phi}$	σ_ϕ	$\bar{\beta}$	σ_β
2	HW	4.6	.1	.5	14.5	.8	- .1	1.4	0	.8
2	TW	4.6	0	.3	13.5	.6	0	1.1	0	.8
2	CW	4.6	1.4	.6	14.1	.6	- .7	1.6	1.8	.8
2	HW	6.8	- .2	.7	14.4	1.3	.1	2.2	- .1	1.0
2	TW	6.8	0	.7	13.5	.7	.6	1.9	0	1.3
2	CW	6.8	1.9	1.4	14.0	.9	- .3	2.5	1.7	1.3
1-1/3	HW	6.8	0	1.0	14.4	1.1	- .2	2.6	.2	1.1
1-1/3	TW	6.8	.1	.6	13.5	.9	.4	1.7	- .1	1.3
1-1/3	CW	6.8	1.1	.7	13.9	.8	- .2	2.4	1.1	1.1
1-1/3	HW	4.6	-0.1	0.6	14.6	0.9	-0.1	1.4	0.2	0.8
1-1/3	TW	4.6	0	.3	13.7	.5	0	1.4	0	.6
1-1/3	CW	4.6	, .9	.6	14.1	.7	- .4	1.3	1.4	.8

The TD criteria when all conditions are randomly selected are specified in Appendix C, Data Base. The histograms depicted in Appendix A, however, are the results of extreme conditions of low probability. The motivation behind these tests was to investigate potential crash conditions. The TD criteria, therfore, do not apply directly without interpretation. For purposes of examining potential crash cases, upper limits for the variables defined as crashes have been established. These assumed crash values are listed in the following discussion of the histograms.

a. Crash X is defined as X exceeding 2000 feet. This is based on landing on a 10,000 foot runway and 6,000 feet of rollout allowed. The histograms show no problems. Under no combination of wind shear or gusts did the landing exceed X = ±1250 feet. The guidance was very effective in controlling this parameter.

b. The crash value of the airspeed will be taken as steady state values of less than 229 feet/second, based upon a tail scrape of 21^{o} required to maintain lift at this speed. (Note that for the Modified System of Section VIII these numbers were changed but in mutually compensating directions. The conclusion that no problem exists is still valid.) No upper limit is set on air speed as this appears to be no problem. In no case did the airspeed exceed 315 feet/second which is actually below the nominal airspeed proposed by other studies. Since gusts may induce

short term changes in airspeed, it is important even in the low airspeed at TD case, to note whether it persisted sufficiently long to effect the flight path or altitude before classifying it as a crash.

The lowest airspeed found was one case between 215 and 225 feet/second. This was for the $K_W = 2$ headwind case with the $\sigma_{ur} = 6.8$ feet/second shear. This was also the case which produced the largest airspeed which was a single case between 305 and 315 feet/second. It is interesting to note these cases on Figure A-1. The two extreme cases are separated from the main body of the distribution. These were caused by head and tail gusts which arose just before touchdown in the high gust condition. The tail gust persisted long enough to require attitude change since Figure A-3 shows that almost 20^o pitch up was attained.

The variable $\dot{X}$ which represents ground speed is not directly controlled. Since the predictive guidance system attempts to maintain airspeed, then the ground speed variation must simply reflect the average wind. The ground speed, $\dot{X}$, is important for setting the specifications on the vehicle's braking system employed after touchdown. In this respect, only the high speed is important. The highest noted were in Figure A-7 and Figure A-16. The ground speed in both cases was less than 325 feet/second. The winds were $K_W = 2$ tailwinds. This is considered a low speed for the SSV application.

c. The crash value of Y will be taken to be 50 feet if there is no $\dot{Y}$ (or a favorable $\dot{Y}$) component since this value places one wheel of the vehicle studied on the edge of a 150 foot wide runway.

Figure A-5 shows that one case between 50 and 60 feet occurred. This is for the K_W = 2 crosswind and σ_{ur} = 6.8 ft/sec gusts. These wind cases require a large decrab due to the crosswind and demand high surface activity to buck the high wind gusts. Under these conditions, the surface rate and position limits are frequently exceeded. In addition, the decrab law which utilizes a computation of time to initiate the decrab which is based on the crab angle, gives erroneous time to decrab results if a yaw rate component also exists; that is, the time to decrab is incorrect. The touchdown values of Y and $\dot{Y}$ are extremely sensitive to errors in this estimate. In fact, one of the recommendations for further study (see Section X) is to modify this law to include yaw rate. For the case shown in Figure A-5, a yaw rate component due to gusting resulted in overcorrection of the crab angle, and with the high crosswind, an excessive Y error at TD developed.

The next worse case which occurred was a case where Y was between 40 and 50 feet. This was on Figure A-14 which is again a high crosswind shear case but with σ_{ur} = 4.8 feet/second gusts.

All the Y histograms show the distinct shift of the mean value for crosswinds as expected. The shift in the mean is approximately linearly related to the magnitude of the crosswind component.

Tailwinds and headwinds do not pose a lateral control problem to the system even in the high gust cases.

d. The crash value of $\dot{Y}$ is assumed to be 20 feet/second which is derived from the TD criteria (defined in Appendix C) which defines 4° of heading misalignment as safe; that is, $\dot{Y}$ = 20 ft/sec $\simeq$ 300 sin 4° (where 300 ft/sec is the touchdown speed). This appears to be a conservative definition of crash since it is based on side velocities which could be obtained under conditions which have been defined as safe.

The worst results occurred, as expected, in the crosswind cases. In Figure A-5, a K_W = 2 crosswind and σ_{ur} = 6.8 ft/sec gust, 3 cases occurred between 15 and 20 ft/sec. In Figure A-14, K_W = 2 crosswind and σ_{ur} = 4.6 ft/sec, 2 cases occurred between 15 and 20 ft/sec. In Figure A-32, a K_W = 1-1/3 crosswind and σ_{ur} = 6.8 ft/sec gust, one case occurred between 15 and 20 feet/second. None of these is considered a crash. The strong shift of mean value with crosswind is again apparent.

The headwind and tailwind cases presented no problems even with severe gusts.

e. The crash value of sink rate was taken to be 10 ft/sec., based on the impact design criteria of MIL-A08862(ASG).

In Figure A-2, one case occurred between 8 and 9 feet/second. This was a K_W = 2 headwind and σ_{ur} = 6.8 ft/sec gust. This is the case where the airspeed dropped due to a persistant tail gust which arose near the time of touchdown. This resulted in loss of airspeed and consequently loss of lift. It should be noted that in these high gust cases, the adverse lift of the elevators which initially re-enforces the gust, increases the dispersion in sink rate near T.D.

In Figure A-29, these observations are confirmed. This was a case where K_W = 1-1/3 headwind and σ_{ur} = 6.8 ft/sec gust. One case between 8 and 9 feet/second was recorded. Again the combination of lower airspeed plus a large tail wind gust resulted in a heavy landing.

In Figure A-32, a K_W = 1-1/3 crosswind and σ_{ur} = 6.8 ft/sec gust, one landing between 8 and 9 ft/sec was recorded. In this case, the effect is isolated and the hard landing is separated from the main distribution.

None of these reached the sink rate defined as a crash (10 ft/sec). It should be noted that all of these cases occurred with the highest wind gust (σ_{ur} = 6.8 ft/sec) and the effect of heavy turbulence biased the landings in the heavy landing direction. This trend is evident in Figure VII-14.

f. The crash specification on heading misalignment with respect to the runway centerline is heavily dependent upon the design of the landing gear. Designs based on the caster principle

will tolerate any degree of misalignment and a number of operational aircraft do not have a constraint on the crab angle at TD. In view of a 4^{o} misalignment being defined as an acceptable landing, a crash is arbitrarily defined as 10^{o}. Only the crosswind cases are of interest and these show no cases above 8^{o}.

Figure A-6, a $K_W = 2$ crosswind and $\sigma_{ur} = 6.8$ ft/sec gust, shows a cluster of landings which have separated from the main population consisting of 4 cases between 5^{o} and 8^{o}.

In Figure A-15, a $K_W = 2$ crosswind and $\sigma_{ur} = 6.8$ ft/sec gust, one case between 4^{o} and 5^{o} was recorded. For the $K_W = 1\text{-}1/3$ crosswinds, no misalignment greater than 4^{o} was observed.

The four cases between 5^{o} and 8^{o} recorded with the highest crosswind and highest gusts were again examples of an overcompensated decrab where an existing yaw rate (result of correction with high gusts) was not taken into account in the "time to decrab" compensation. Overcorrection resulted in surface saturation and, thus, excess yaw. This is supported by the roll angles recorded in Figure A-6. These show the separation of two cases of roll angle from the main distributions due to the saturated aileron attempting to correct the strong roll transient induced by the overcorrected sideslip and rudder.

g. The crash pitch attitude has been defined as 21^{o} which gives tail scrape. (Again, note that for the Modified System of Section VIII airspeed and tailscrape angle were changed in a mutually compensating manner. The conclusions are still valid.)

No landings exceeded this number, though as described above, one case between 19^{o} and 20^{o} was recorded (Figure A-3) which was the result of low airspeed followed by a tail gust just prior to touchdown.

h. It is known that pilot's do not object to touching down with reasonable roll angles in crosswind landings. To define a crash, it was decided that the roll angle must be such that one wing touches the runway. (It should be restated that extreme conditions are being discussed.) Based on drawings supplied with the data package, this number is about 12^{o}.

As expected, the crosswind case was the most troublesome. Figure A-6 records one landing with roll angle between 7^{o} and 8^{o} and another landing with a roll angle between 9^{o} and 10^{o}. These were the cases discussed in g above where excess decrab induced sideslip and rudder moments which saturated the aileron channel. No other roll angles recorded exceeded 7^{o}.

i. In summary, the high wind and gust investigation shows that, in 600 flights, one case of crash due to excess Y displacement from the centerline. This was a landing between 50 and 60 feet (center of vehicle to runway centerline distance) which occurred during the maximum crosswind, maximum gust cases. Since a 150 ft wide runway is assumed, one wheel would be off the runway edge.

In general, the lateral performance came closest to crash conditions. This was due to (1) a "time to decrab" computation which did not account for yaw rates but was based on

crab angle only, (2) excess roll moment coupling due to rudder and sideslip angle for this vehicle design, and (3) aileron saturation when maneuvers induced by the transients of (1) and (2) are experienced.

These resulted in a number of marginal cases in heading alignment, roll attitude, crosstrack rate and off-center landings.

3. SC117 Scanning Beam System - Analysis of Results.

Although the means and standard deviations do not provide as much information as the histograms discussed, they do provide a clearer picture of the various trends with respect to wind direction, wind magnitude and gust level. To illustrate this, the means and standard deviations for the most significant touchdown parameters were plotted with respect to the various wind conditions used in this sequence of Monte Carlo runs.

Figure VII-12 shows the variation in the mean and standard deviation of the touchdown miss distance, X, with respect to the various wind conditions. It can be seen that mean miss distance moves aft for the higher gust levels in all cases. This is due to the fact that deviations from the nominal which are high have not resulted in touchdowns when the nominal range has been reached but deviations which are low have resulted in touchdowns. This argument applies in the flight path region just prior to touchdown when the time-to-go is too short for significant guidance corrections to be effective. Thus, if there are equal numbers of high and low cases in this near touchdown region, the probability of the wheels actually touching is biased in favor of the short, hard landing.

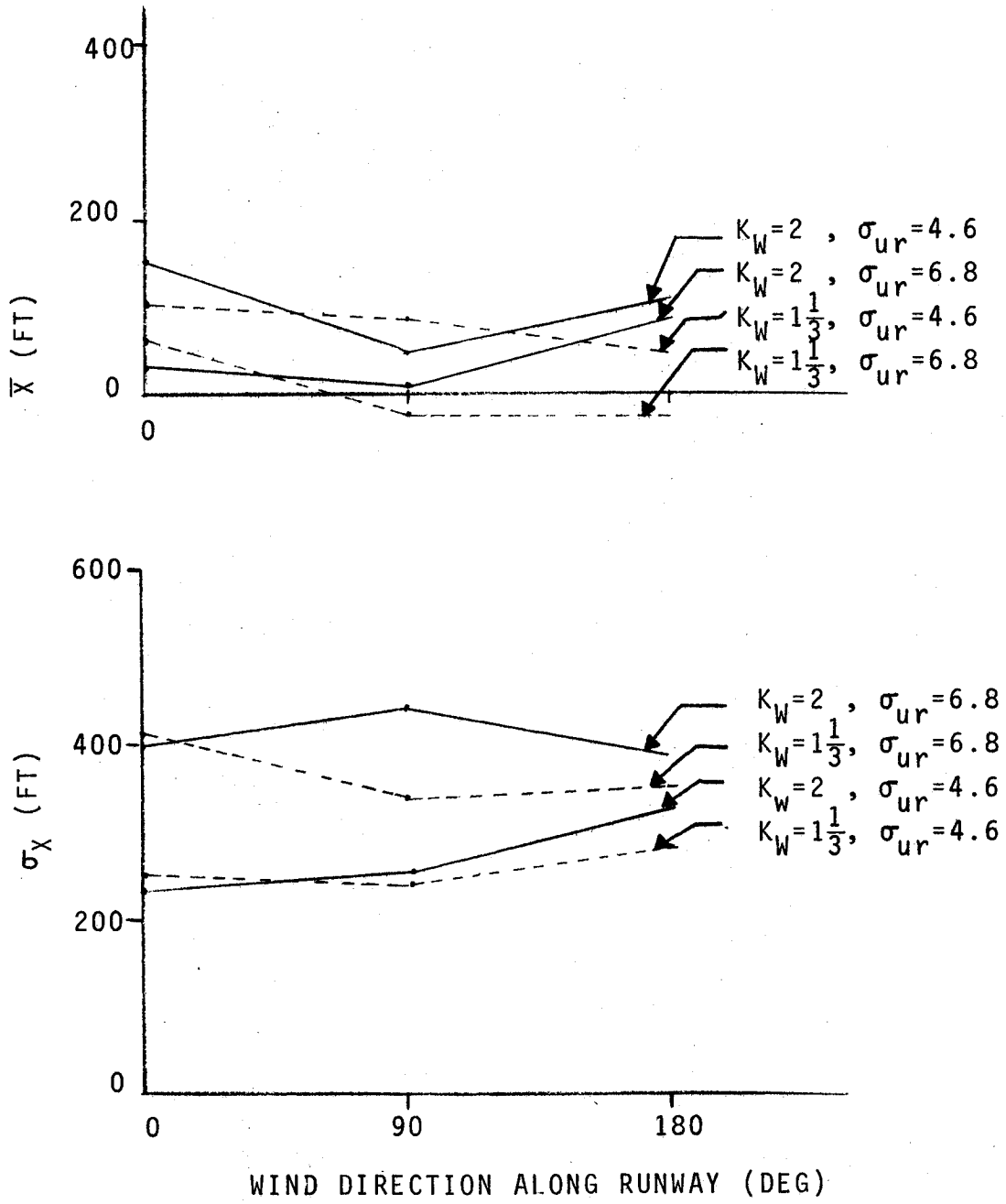

FIGURE VII-12. MONTE CARLO MISS DISTANCE STATISTICS FOR SCANNING BEAM SYSTEM

It can also be seen from Figure VII-12 that the mean miss distance is relatively insensitive to wind direction and magnitude. This indicates that the predictive guidance laws used adequately compensate for the mean wind along the runway.

From the plot of the standard deviation in this figure, it can be seen that the standard deviation of the miss distance is mainly dependent on the gust level and relatively insensitive to the wind direction and magnitude. This was expected since the gust levels in the wind model that was used were independent of wind direction and magnitude.

The variation in the mean and standard deviation of the touchdown airspeed with the various wind conditions is shown in Figure VII-13. It can be seen from this figure that the mean touchdown airspeed is mainly dependent on the wind direction and increases slightly for a tail wind and decreases slightly for a head wind as one might expect. This indicates that the predictive guidance laws did not compensate quite enough for the effect of the mean wind and shear on the touchdown airspeed.

From the plot of the standard deviation of the touchdown airspeed, it can be seen that the standard deviation is proportional to the gust level and relatively insensitive to wind magnitude as one might expect. However, it can also be seen that the standard deviation in general decreases from the headwind case to the tailwind case. This is due to the increase in control power that results from the increase in the mean airspeed from the headwind to the tailwind case.

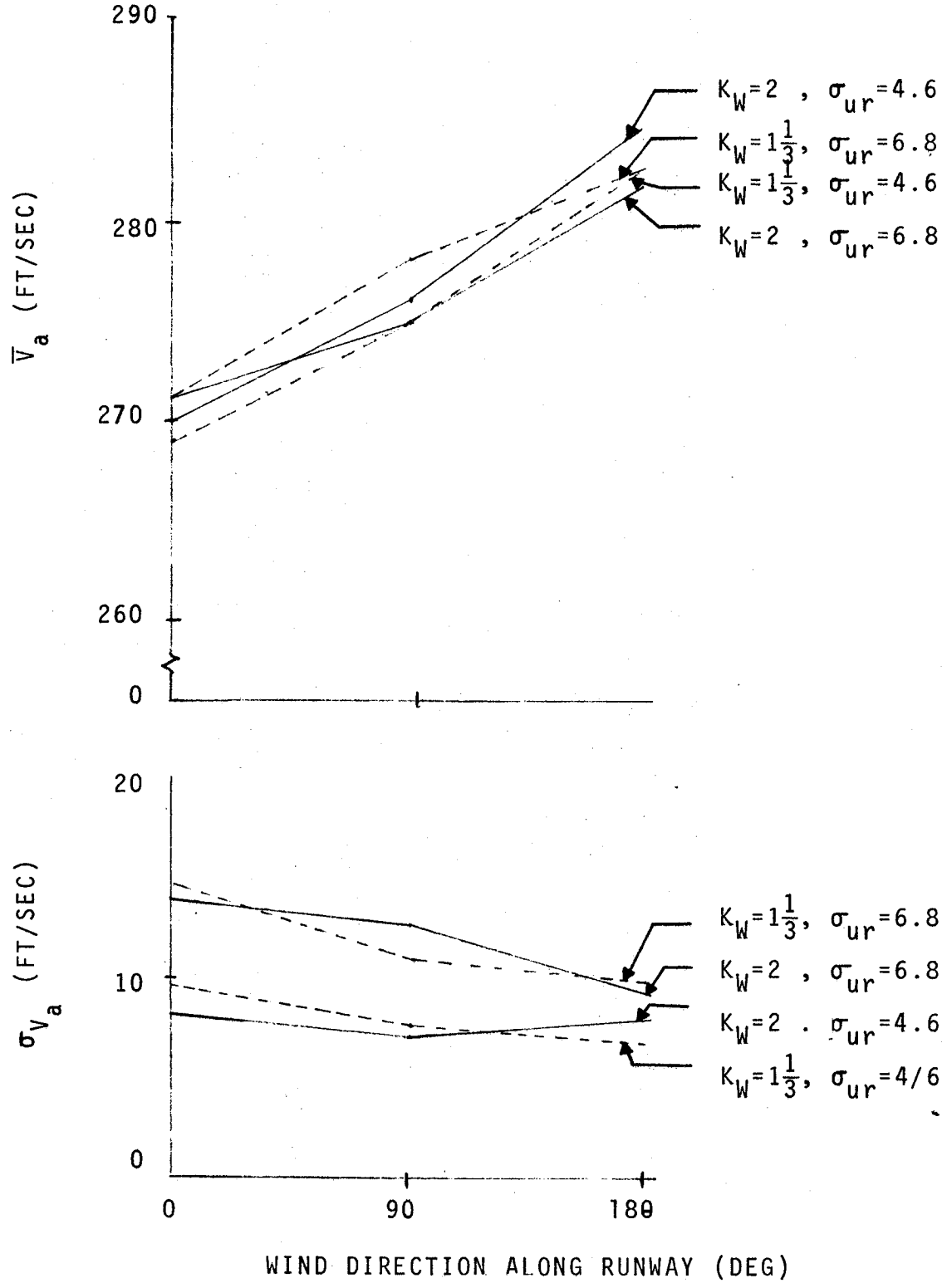

FIGURE VII-13 MONTE CARLO AIRSPEED STATISTICS FOR SCANNING BEAM SYSTEM

Figure VII-14 shows the variation in the mean and the standard deviation of the touchdown sink rate with the various wind conditions. From the plot of the mean touchdown sink rate, it can be seen that the mean sink rate increases with the gust level and is relatively insensitive to the wind magnitude. The increase in the mean sink rate with gust level is explained by the same phenomenon which explained the short landings (namely, the higher probability of touching down on transients which drive the vehicle below the nominal trajectory). Note that the wheels can touch down only when the sink rate is positive. As a result of this, as the gust level is increased, landings occur at higher and higher sink rates.

It can also be seen that the mean sink rate at touchdown decreases from the headwind to the tailwind case. This was found to be due to the nonlinear effect of the surface rate limits on the ability of the system to compensate for wind shear. For the wind model used, the mean shear results in a incremental loss in airspeed for the headwind case and an incremental increase in the tailwind case. However, since there is also an incremental loss in airspeed in both cases due to the mean drag and since the mean headwind shear is greater in magnitude than the tailwind shear in the wind model used, the mean rate of loss of airspeed in the headwind case is greater than that in the tailwind case. As a result of this, the system must pitch the vehicle up faster in the headwind case to compensate for the mean shear than in the tailwind case. Now, as

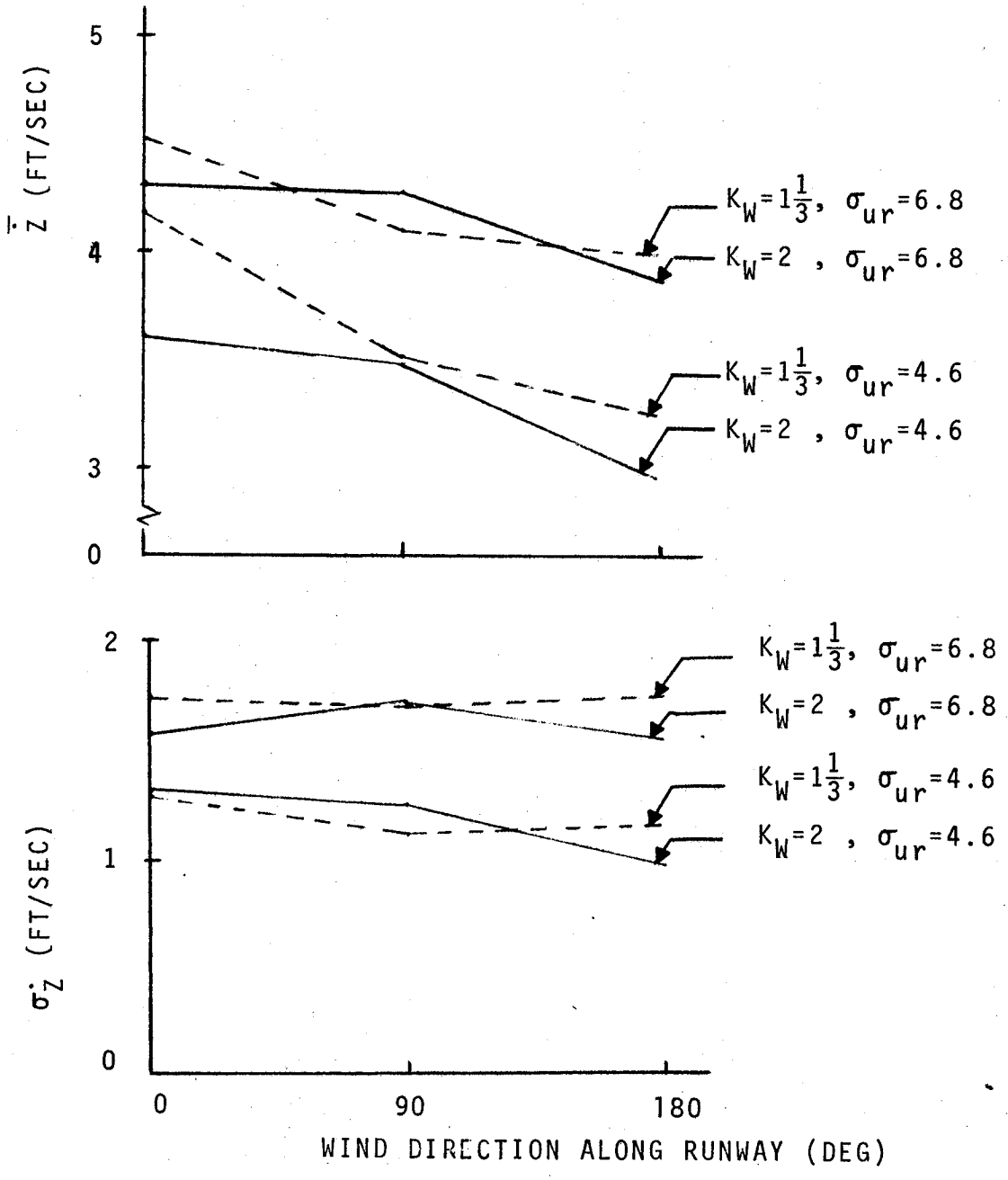

FIGURE VII-14. MONTE CARLO SINK RATE STATISTICS FOR SCANNING BEAM SYSTEM

long as the surface rates required to obtain this pitch rate do not exceed the limits, the wind shear has very little effect on the sink rate as shown previously in the deterministic results for winds with no gusts. However, when gusts are included, the surface rates required to compensate for the total shear can exceed the limits and they will be exceeded more times in the headwind case than in the tailwind case since the mean shear will cause the maximum shear to be greater in the headwind case. Since the maximum shear in this case results in a loss of airspeed, the surface rate limits restrict the ability of the vehicle to pitch up to compensate for it which in turn results in harder landings.

From the plot of the standard deviation of the sink rate at touchdown, it can be seen that the standard deviation is proportional to the gust level and relatively insensitive to the wind magnitude as one might expect. It can also be seen that the standard deviation in general decreases somewhat from the headwind to the tailwind case. Again, this is due to the nonlinear effect of the surface rate limits on the ability of the system to compensate for wind shear.

The variations in the means and standard deviations of the lateral offset and velocity at touchdown with the various wind conditions are shown in Figures VII-15 and VII-16 respectively. It can be seen from these figures that the mean lateral offset and velocity at touchdown is near zero for the headwind and tailwind

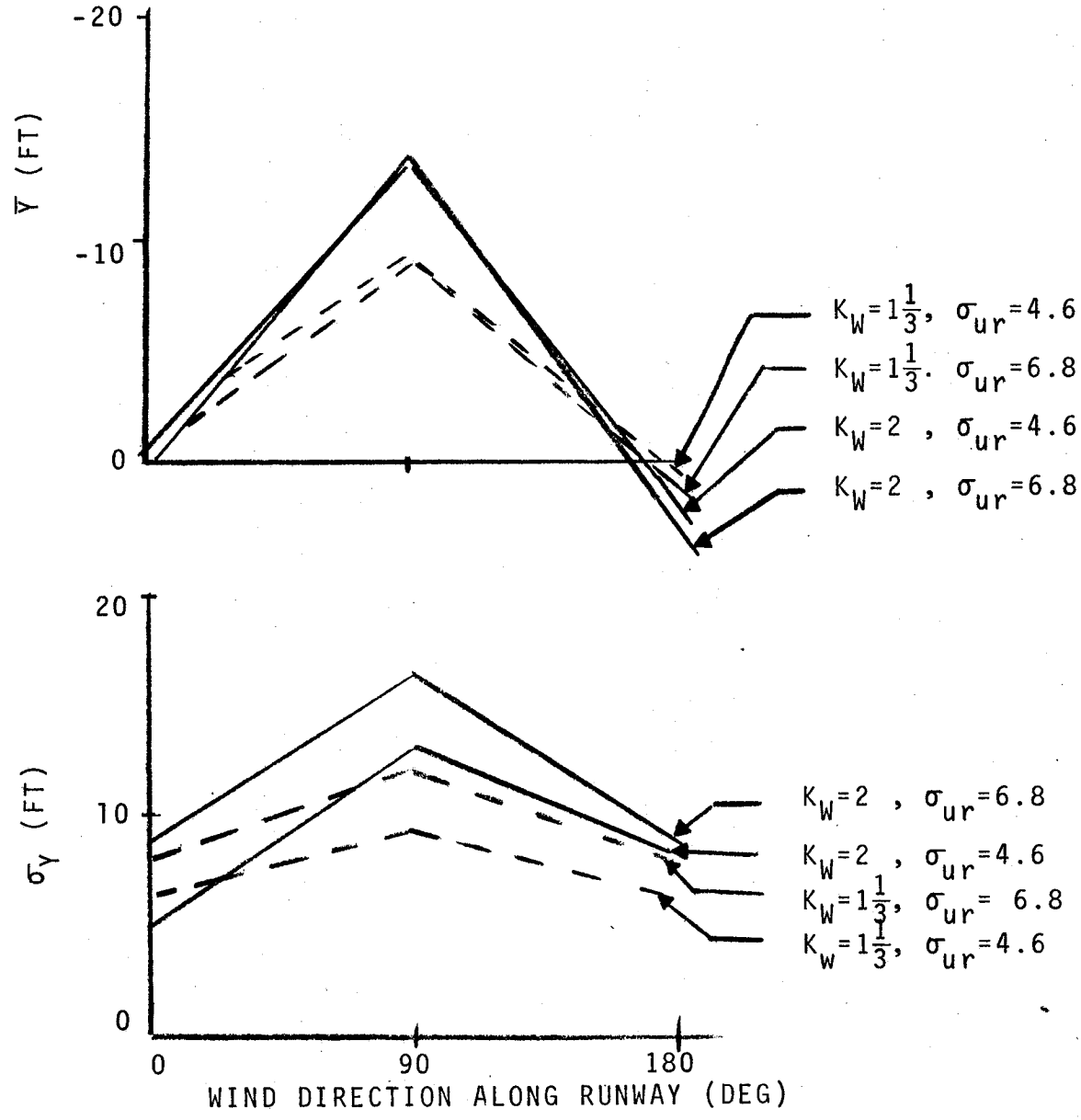

FIGURE VII-15 MONTE CARLO LATERAL OFFSET STATISTICS FOR SCANNING BEAM SYSTEM

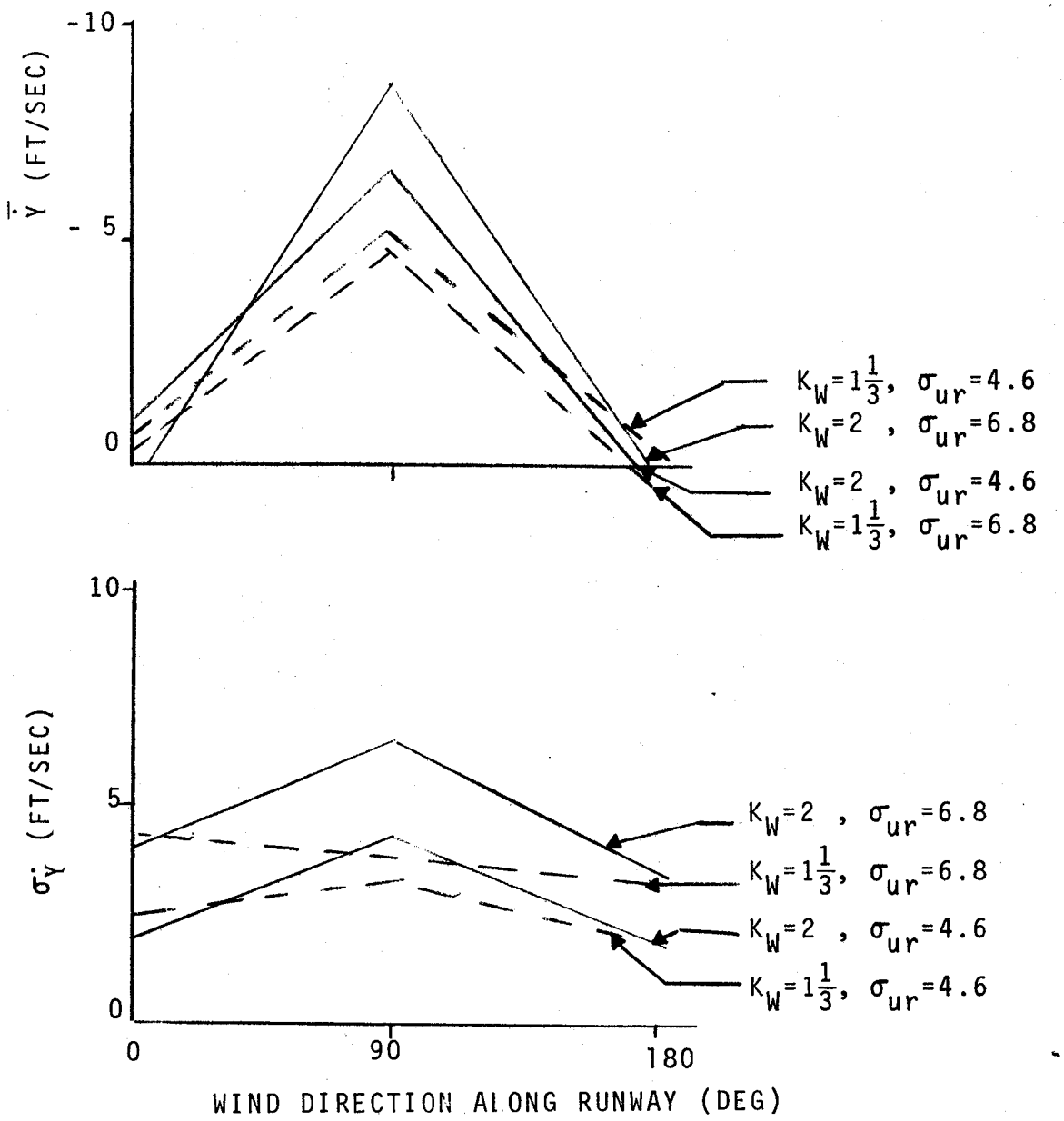

FIGURE VII-16 MONTE CARLO LATERAL VELOCITY STATISTICS FOR SCANNING BEAM SYSTEM

cases as one would expect. For the cross wind case, the mean lateral velocity and offset are proportional to the wind magnitude and relatively insensitive to the gust level.

From the plots of the standard deviations in these figures, it can be seen that standard deviations of the lateral offset and velocity is proportional to the gust level and relatively insensitive to the wind magnitude except for the crosswind case. In this case, the higher cross wind magnitude combined with gusts results in aileron surface saturation against the hard limits during the decrab maneuver on some landings which increases the lateral dispersions at touchdown. It can also be seen from Figure VII-16 that the standard deviation of the lateral velocity at touchdown is somewhat less in the tailwind case than in the headwind case. This again is due to the increased control power that results from the increased mean airspeed in the tailwind case. This effect is most pronounced on the short period variables since control power has the fastest influence on these. A significant portion of the standard deviation in all cases is due to the assumed random bias error in the scanning beam localizer which amounts to a lateral offset error at the desired touchdown point of about 5 ft RMS.

Figure VII-17 shows the variation in the mean and the standard deviation of the yaw attitude at touchdown with the various wind conditions. It can be seen from the plot of the mean yaw attitude at touchdown that the mean for the headwind and tailwind

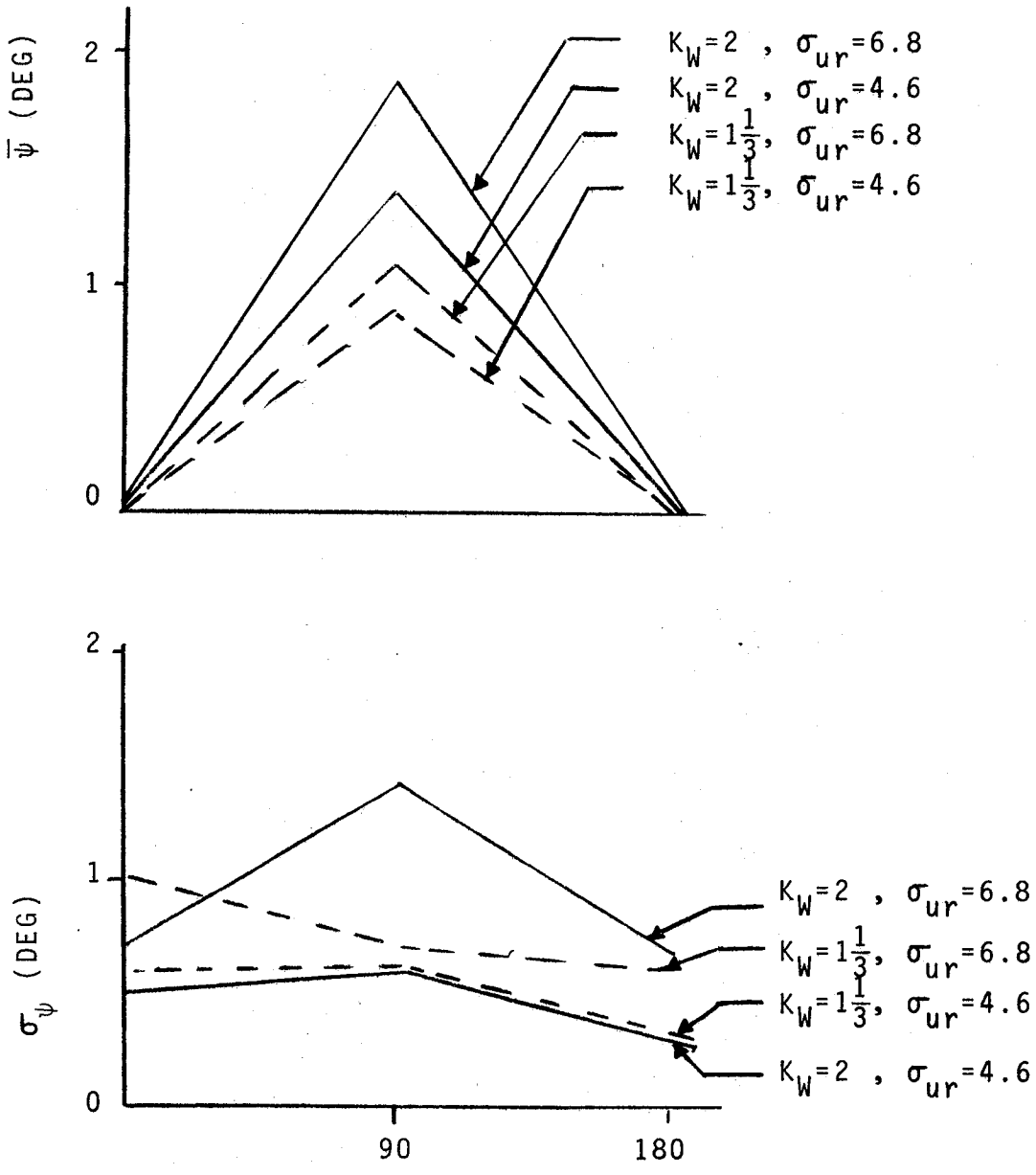

FIGURE VII-17. MONTE CARLO YAW ATTITUDE STATISTICS FOR SCANNING BEAM SYSTEM

conditions is near zero as would be expected. For the crosswind case, the mean increases with the wind magnitude as one would expect. However, it can also be seen that the mean also increases with the gust level. This is due again to increase in number of short landings which occur with disturbances. Since the landings are shorter, the actual time from the point of initiation of the decrab to touchdown is shorter than the estimated time to go to touchdown. As a result of this, the vehicle does not have time to fully complete the commanded decrab maneuver and this results in an increased yaw attitude at touchdown.

From the plot of the standard deviation of the yaw attitude at touchdown, it can be seen that the standard deviation is proportional to the gust level and relatively insensitive to the wind magnitude except in the cross wind case. In this case, the higher cross wind magnitude combined with gusts results in rudder saturation against the hard limits during the decrab maneuver on some landings and this increases the yaw dispersions at touchdown. It can also be seen that the standard deviation is somewhat less in the tailwind case than in the headwind case. Again, this is due to the increased control power that results from the increased mean airspeed at touchdown in the tailwind case.

The mean and the standard deviation of the roll attitude at touchdown with the various wind conditions is shown in Figure VII-18. From the plot of the mean roll attitude at touchdown, it can be seen that the mean is quite small in all cases.

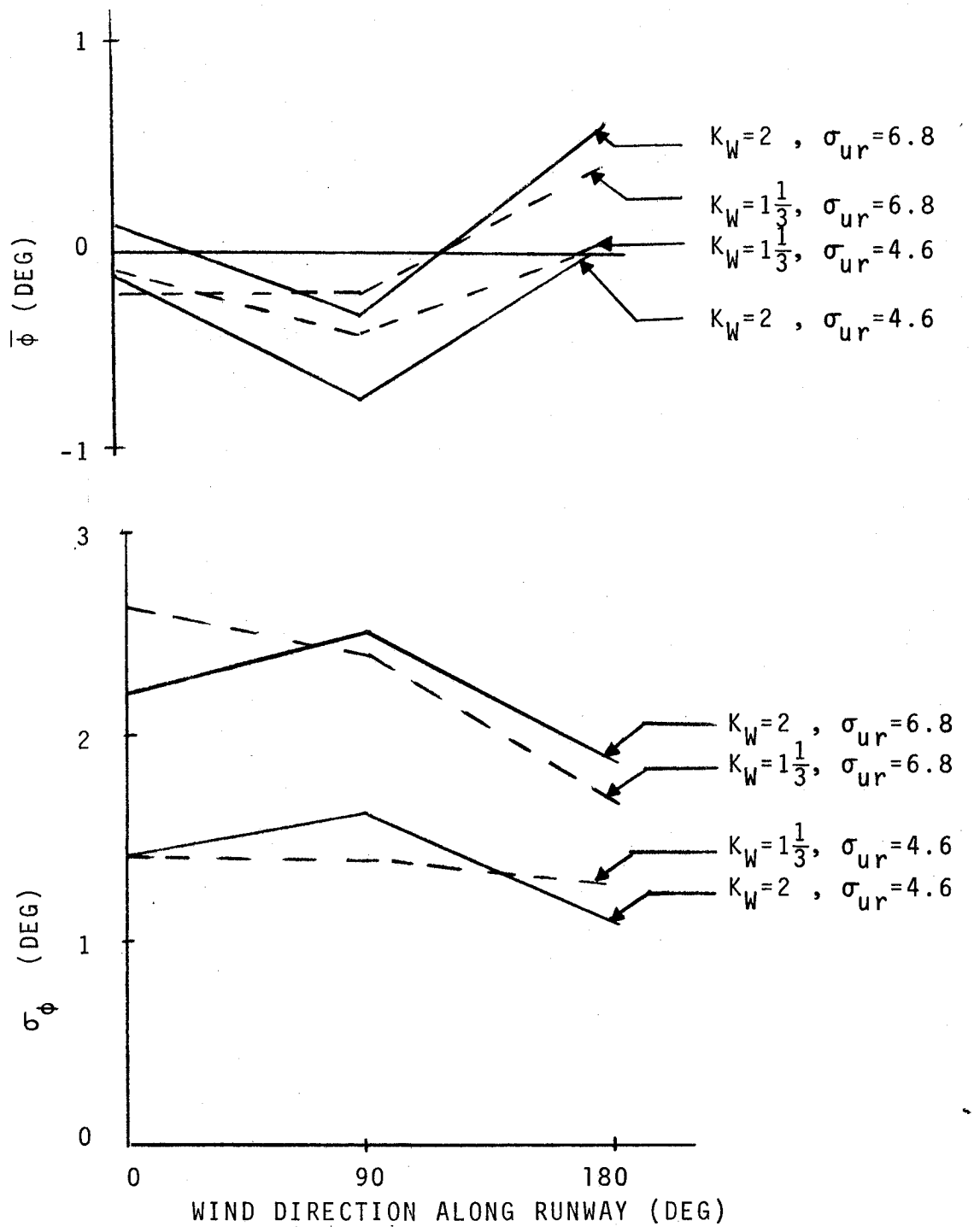

FIGURE VII-18 MONTE CARLO ROLL ATTITUDE STATISTICS FOR SCANNING BEAM SYSTEM

The slight negative shift for the cross wind cases is caused by the sideslip during decrab which produces a negative rolling moment for the wind direction selected for these runs. This indicates that the direct sideslip compensation loop that was included in the aileron channel of the flight control system is not compensating quite enough for the effect of sideslip.

From the plot of the standard deviation of the roll attitude at touchdown, it can be seen that the deviation is proportional to gust level and relatively insensitive to wind magnitude as one would expect. The slight decrease in the deviation from the headwind to the tailwind case is due to the increased control power that results from the increased mean touchdown airspeed in the tailwind case. The slight increase for the higher cross wind case is due to aileron saturation against the hard limits in these cases.

VIII. MODIFIED SYSTEM.

A. Introduction.

It was discovered late in the program that some of the basic assumptions that had been made earlier in the study were incorrect. First, it was discovered during discussions after the final oral review at NASA-Ames that, due to the lack of a clear pitch reference line on the preliminary NADWO drawing, the tail scrape angle was selected as 21 degrees. It was subsequently determined that it should have been 17 degrees. Second, it was discovered during telephone discussions after the final oral review at NASA-Ames that, due to the lack of a coordinate system definition on the ground effects data and subsequent interpretation problems in discussions with NASA-Ames, the direction of the drag due to ground effects was incorrectly selected. It was assumed that ground effects would increase the total vehicle drag whereas it should have decreased the total vehicle drag.

Both of these have strong implications on the system performance. First, as a result of selecting too high a tail scrape angle, the selected touchdown airspeed used in the original system was too low and resulted in a margin of only about 1.08 times the minimum allowable airspeed for a 17 degree tailscrape instead of the desired margin of 1.2. It can be seen from the Monte Carlo histograms in Appendix A that this resulted in many landings where the pitch attitude is close to the limit of 17 degrees and one landing where it is above this limit.

Second, since the drag due to ground effects is very significant near touchdown (about 50% of the gear down trim drag without ground effects at an altitude of 12 feet), the sign error in this drag component resulted in a significant error in the lift to drag ratio of the vehicle. Furthermore, since the guidance system that was developed uses a flareout predictor which contains an approximate model of the vehicle in terms of lift to drag ratio, the sign error also resulted in errors in the approximate lift to drag ratio model in the flareout predictor. This resulted in significant guidance system errors when the ground effects drag was corrected in the vehicle because the flareout predictor was computing the required trajectory for a vehicle with a significantly lower lift to drag ratio near touchdown. In addition, since the ground effects drag data used was in the body axis coordinate system, reversing the sign on this data also resulted in significant change in the stability axis lift component due to this drag. The sign change was such that the total stability axis lift was increased. Both this and the decrease in drag resulted in a significant decrease in the rate of loss of airspeed near touchdown and in the steady pitch rate required to maintain constant lift. Since the guidance system that was developed uses a pitch trim command which was developed to compensate for a large rate of loss of airspeed near touchdown, changing the sign of the ground effects drag in the vehicle also resulted in significant guidance pitch trim errors.

Since the guidance errors resulting from these incorrect assumptions were found to be significant, it was decided to modify the system before making the true Monte Carlo runs on the scanning beam and tracking radar landing systems. These modifications are described in Part B of this section. The influence of these modifications on the flareout initiation conditions is discussed in Part C. A comparison of the performance of the modified and old system is shown in Part D. The results of the true Monte Carlo evaluation of the scanning beam and tracking radar landing systems are presented in Part D of this section. The term "true" Monte Carlo evaluation is used to identify runs where the wind magnitude (KW), wind direction (ψ_W) and the standard deviation of the gust level (σ_W) are also randomly selected. This is in contrast with the runs specified in Section VII, where these were deterministically selected to assess the effects of extreme winds and turbulence.

B. Modifications to Guidance and Flight Control Systems.

To cope with the change in sign on the body axis drag due to ground effects and the lower allowable tail scrape angle at touchdown, the following modifications were made to the guidance and flight control systems: (1) the assumed vehicle lift to drag ratios used in the guidance system flareout predictor were modified to account for the effect of the ground effect drag sign change on the vehicle lift to drag ratio; (2) the pitch trim computation in the guidance system was modified to account for both the corresponding sign change in the lift component of the body axis ground effect drag and for the affect of this drag sign change on the rate

of loss of airspeed; (3) the time to go computation which is used in the decrab initiation logic in the guidance system was modified to account for the effects of the above on the actual sink rate during final flare; (4) the desired airspeed at touchdown was increased to account for the reduction in the tail scrape angle at touchdown, and (5) certain guidance and flight control system gains were increased to utilize the additional control power at touchdown resulting from the increase in the desired touchdown airspeed.

The modifications to the assumed lift to drag ratios used in the flareout predictor are as follows. The equations used to compute the assumed lift to drag ratios during the gear down portion of the glide phase on Page IV-44 are replaced with the following equations:

$$(L/D)^p_{gd} = 7.9 - 0.035\,(V^p_{a\ gd} - 320), \text{ if less than } 6.8$$

$$= 6.8 \quad \text{, if greater than } 6.8$$

$$(L/D)^p_{eg} = 7.9 - 0.035\,(V^p_{a\ eg} - 320), \text{ if less than } 6.8$$

$$= 6.8 \quad \text{, if greater than } 6.8$$

$$(L/D)^p_{gd\ avg} = .5\left[(L/D)^p_{gd} + (L/D)^p_{eg}\right], \text{ if } V^p_{a\ eg} \geq 351.4 \text{ ft/sec}$$

$$= \Big[.5\left((L/D)^p_{gd} + (L/D)^p_{eg}\right)\left(V^p_{a\ gd} - 351.4\right)$$

$$+ (L/D)^p_{eg}\left(351.4 - V^p_{a\ eg}\right)\Big] / \left(V^p_{a\ gd} - V^p_{a\ eg}\right),$$

$$\text{if } V^p_{a\ eg} < 351.4 \text{ ft/sec.}$$

In addition, the nominal value for average lift to drag ratio during final flare, $(L/D)_{ff\ avg}$, that is used in the final flare prediction equations on Page IV-41 is changed from 5.2 to 8.4.

The modifications to the pitch trim computations is as follows. The equation for computing the trim angle of attack, α_{trim}, on page IV-57 is replaced by the following equation.

$$\alpha_{trim} = \frac{-\ddot{Z}_i + g}{Q_f\ (S/m) C_{L_\alpha}\ (1 + .0015\ (Z_1 + 100))} + \alpha_0$$

where: $Q_f = Q/(.665\ s + 1)$

$Z_1 = Z$, if $Z \geq -100$ feet

$= -100$, if $Z < -100$ feet

$\ddot{Z}_i = \ddot{Z}_f$, if in primary flare

$= 0$, if in glide

$= \ddot{Z}^p_{ff} \dfrac{(\dot{Z}_c - \dot{Z}_{td})}{(\dot{Z}_{sff} - \dot{Z}_{td})}$, if in final flare

α_0 = zero trim lift angle of attack (nominally 1.2 degrees).

The time to touchdown computation on Page IV-63 is modified as follows:

$$t_{ttd} = \frac{-Z}{0.5\ (\dot{Z}_c + \dot{Z}_{td})}$$, unmodified

$$= \frac{-Z}{0.41\ (\dot{Z}_c + \dot{Z}_{td})}$$, modified

To compensate for the reduction in the tail scrape pitch angle from 21 to 17 degrees, the desired touchdown airspeed, $V_{a\ td}$, which is used to compute the desired touchdown ground speed on Page IV-42 of this report, is increased from 275 to 300 ft/sec.

To utilize the additional control power resulting from the increased touchdown airspeed, the following system gains are increased as shown.

Gain	System	Old Value	Increased Value
k_z	Guidance	0.128 deg/ft	0.2 deg/ft
$k_{\dot{z}}$	Guidance	0.106 deg/fps	0.133 deg/fps
k_θ	Flight Control	1.92 $(250/Q_f)$	3.0 $(250/Q_f)$
k_q	Flight Control	0.96 $(250/Q_f)$	1.2 $(250/Q_f)$
k_ϕ	Flight Control	0.64 $(250/Q_f)$	1.0 $(250/Q_f)$
k_p	Flight Control	0.33 $(250/Q_f)$	0.41$(250/Q_f)$

C. Influence on Flareout Initiation Conditions.

The nominal trajectory phases and maneuvers for the modified system are the same as for the original system described in Section IV. However, the numerical value of the initial conditions for the modified system have been changed to reflect the effects of the change in sign on the body axis drag due to ground effects and the increased touchdown airspeed on the actual flight conditions along the nominal trajectory. It was found that the overall effect of the ground effects drag and airspeed changes was to decrease the float time available during the glide phase when the nominal initial

conditions described in the body of this report were used. In the 3σ headwind case, this decrease was enough to lower the float time below the minimum acceptable value of 10 sec that was assumed.

To obtain the necessary float time in this worse case wind condition, the nominal velocity at flareout initiation for the no wind condition was increased from 470 to 493 ft/sec. This resulted in an increase in the initial velocity in the 3σ head wind case of from 320 to 343 ft/sec and an acceptable float time of 15 sec.

Table VIII-1 lists the increased flareout initiation velocities for the modified system in the no wind and in the 3σ headwind, crosswind, and tailwind cases. The equilibrium glide path angle and the required attitude and range at flareout initiation associated with these increased velocities are also listed in this table. For winds between those listed, straight line interpolation may be used to determine the flareout initiation conditions.

D. Comparison of Performance.

It was suspected that the performance of the modified system would be better than that shown for the system described in the body of this report for two reasons: (1) the increased touchdown airspeed required for the new tail scrape limit resulted in an increase in the control power available and certain of the system gains were increased to take advantage of this; and (2) the change in sign of the body axis drag due to ground effects resulted in less drag and more lift near touchdown; both of which

TABLE VIII-1

VARIATION IN FLAREOUT INITIATION CONDITIONS WITH WIND
FOR MODIFIED SYSTEM

WIND	V	γ	h	X	(L/D)	α	δ_e
3σ HEADWIND (KW = 2)	343	-10.4	487	8258	7.45	7.73	-6.17
NOMINAL AND 3σ CROSSWIND	493	-10.4	1343	25216	5.60	5.45	-3.67
3σ TAILWIND	553	-10.4	1763	31596	5.00	4.87	-3.02

reduce the steady state rate at which the vehicle must pitch up to maintain constant lift. To verify that these factors would improve the performance of the modified system, simulation runs on the modified system were made for deterministic variations in those parameters that the unmodified system was most sensitive to. The touchdown conditions on these runs for the two systems are compared in Table VIII-2. As shown in this table, the sensitivity of the modified system to variations in the flareout initiation conditions is about the same. This was expected since these errors are eliminated in both systems well before a point is reached where the modified ground effects or increased touchdown airspeed become significant.

However, the sensitivity of the modified system to variations in the mean wind is definitely improved. This was found to be primarily due to the decreased sensitivity of the airspeed and the required pitch trim attitude for the modified vehicle to variations in the range that must be traveled to touchdown. The airspeed lost and the required pitch trim change per unit time is significantly less due to the decreased drag. This decreased sensitivity of the pitch trim attitude was further found to result

TABLE VIII-2

COMPARISON OF SYSTEM SENSITIVITY TO
DETERMINISTIC VARIATIONS

VARIATION	SYSTEM	X	V_a	Y	$\dot{Y}$	$\dot{Z}$	ψ	ϕ
NOMINAL	OLD	150	276	0	0	2.90	0	0
	MOD	0	301	0	0	2.51	0	0
+1000 ΔX	OLD	143	275	0	0	2.90	0	0
	MOD	-4	301	0	0	2.52	0	0
+20 ΔV	OLD	145	279	0	0	2.91	0	0
	MOD	-6	301	0	0	2.51	0	0
MHW	OLD	58	273	0	0	2.80	0	0
	MOD	-25	302	0	0	2.47	0	0
MCW	OLD	139	276	-3.5	-4.8	2.94	-0.35	-0.54
	MOD	-4	300	-2.7	-4.1	2.58	0.48	0.35
MTW	OLD	182	279	0	0	2.92	0	0
	MOD	9	301	0	0	2.51	0	0

in better control of the vertical channel which, of course, reflects in a reduced X dispersion at touchdown.

To determine the sensitivity of the modified system to random disturbances and errors, one set of the Monte Carlo runs specified in Section VII.B was repeated with the modified system. This set of runs (3σ cross wind level (K_W = 2) and a rms gust level of 6.8 ft/sec) was selected because it was one of the most severe conditions in the Task III evaluation. The means and dispersions of the touchdown parameters on these runs for the two systems are compared in Table VIII-3. As shown in this table, the sensitivity of the modified system to random disturbances and errors is also definitely improved. This is especially noticeable on the sink rate statistics and on the roll and yaw attitude statistics at touchdown. This was found to be primarily due to the increased control power available near touchdown for the modified system and the resulting allowable increase in guidance and flight control gains. This tends to verify the reason for the decreased dispersions shown for the tailwind Monte Carlo cases discussed in Section VII.B since the mean airspeed at touchdown was also higher in these cases.

E. True Monte Carlo Comparison of SC117 Scanning Beam and Precision Tracking Radar.

To better define the center of the distributions of the key touchdown parameters for the SC117 scanning beam system and to

TABLE VIII-3

COMPARISON OF SYSTEM PERFORMANCE ON SET NO. 2
OF MONTE CARLO RUNS

SYSTEM	STAT	X	$\dot{X}$	V_a	Y	$\dot{Y}$	$\dot{Z}$	ψ	θ	ϕ
OLD	MEAN	16	276	275	-13.5	-6.6	4.26	1.9	14.0	-0.3
	RMS	445	11.7	12.6	16.3	6.5	1.72	1.4	0.9	2.5
MOD.	MEAN	-117	299	297	-14.8	-8.5	3.72	1.6	12.0	0.1
	RMS	451	6.0	8.3	15.8	4.6	1.03	0.9	0.8	1.8

enable a precision tracking radar system to be compared with it under the most probable landing conditions, true Monte Carlo evaluations of the two landing systems were made. The runs for both the SBLGS and TR were made with the modified system. The set up procedure for these runs was the same as that described for the Monte Carlo runs in Section VII.B except that: (1) the wind magnitude, K_W, was randomly selected from a Gaussian distribution with a mean of 1.0 and a standard deviation of 0.333, (2) the wind direction, ψ_W, was randomly selected from a Gaussian distribution with a mean of zero (headwind condition) and a standard deviation of 60 degrees, and (3) the standard deviation of the gust level, σ_W, was randomly selected from a Rayleigh distribution with a probability of being less than 6.8 ft/second 99% of the time. The models used for the precision tracking radar and the SC117 scanning beam system are described in Appendix C (Data Base).

The results of these evaluations are illustrated in the form of histograms in Appendix B. Several things can be noted from these histograms. First, they are nearly identical for both systems even though the radar system was about eight times more accurate in Y and three times more accurate in Z than the SC117 scanning beam system. This supports the other results and verifies the conclusion that the primary cause of the touchdown dispersions is due to gusts and not due to hardware system errors.

Second, it can be seen that the distributions of the touchdown parameters for both systems appear to be Gaussian in shape except for sink rate distributions which appear to be more like a Rayleigh distribution. This shape is caused by the fact that touchdowns can only occur at positive sink rates as discussed in Section VII.B. It can also be seen that the means of the distributions of the touchdown parameters for both systems are close to the nominal touchdown parameters shown in Table VII-2, except for the touchdown miss distance and sink rate. These are shifted aft and up respectively by the effects of the wheels touching down early in the presence of gusts as discussed previously in Section VII.B.

Third, it can be seen that, based on the criteria used in Section VII.B of this report, there were no crashes for either systems in 50 landings under the most probable gust conditions. However, it can be seen that for both systems, there is one landing where the roll attitude at touchdown is well separated from the main distribution. Even under probable gust conditions, roll attitude at touchdown will be difficult to control because of the large sideslip rolling moments, the effects of the combined elevon/aileron rate limits and the maximum available aileron control power.

The means and standard deviations of the touchdown parameters that resulted in the true Monte Carlo evaluation of the

SC117 scanning beam and precision tracking radar systems are listed in Table VIII-4. Although these do not provide as much information as the histograms, they do provide a clearer comparison of the two systems. As a result of the better Y information from the radar, the lateral dispersion at touchdown is decreased somewhat. Due to the lower noise in the Y information from the radar, the roll attitude dispersion at touchdown is also decreased somewhat. As a result of the better Z information from the radar, the miss distance (X) dispersion at touchdown is also decreased. The dispersions and means for all other parameters are about the same for both systems.

TABLE VIII-4

COMPARISON OF TRUE MONTE CARLO EVALUATION STATISTICS FOR SC117 SCANNING BEAM AND PRECISION TRACKING RADAR SYSTEMS

LANDING SYSTEM	STAT	X	$\dot{X}$	V_a	Y	$\dot{Y}$	$\dot{Z}$	ψ	θ	ϕ
SC117 SBS	MEAN	-74	290	301	0.9	0.5	2.78	-0.1	11.8	0.2
	RMS	238	9.9	4.0	8.9	3.5	0.88	0.7	0.5	1.4
PTR	MEAN	-61	289	302	0.7	0.2	2.88	0	11.8	-0.1
	RMS	176	9.1	3.4	6.5	4.0	0.85	0.6	0.4	1.1

IX. CONCLUSIONS.

1. The following landing systems are recommended choices for the SSV landing mission:

Precision Tracking Radar

SC117 Scanning Beam System

The touchdown errors expressed in terms of standard deviation due to hardware errors only in the recommended systems are:

	σ_X (ft)	$\sigma_{\dot{X}}$ (ft/sec)	σ_Y (ft/sec)	$\sigma_{\dot{Y}}$ (ft/sec)	$\sigma_{\dot{Z}}$ (ft/sec)
Precision Tracking Radar	83	1.7	1.4	0.3	0.3
SC117 Scanning Beam System	205	3.5	5.6	0.7	0.4

2. The effect of winds and gusts on touchdown errors is more significant than the effects of landing system hardware errors. The influence of winds and gusts on touchdown errors expressed in terms of standard deviation may be assessed by comparison in the following table.

Wind Shear KW*	Wind Gust σ_{ur}*	Hardware Error	σ_X (ft)	σ_Y (ft)	$\sigma_{\dot{Y}}$ (ft/sec)	$\sigma_{\dot{Z}}$ (ft/sec)
0 (no shear)	0	SC117	205	5.6	0.7	0.4
0 (no shear)	3.4 ft/sec	None	180	3.5	2.3	0.6
2 headwind	6.8 ft/sec	SC117	400	8.5	4.0	1.6
2 crosswind	6.8 ft/sec	SC117	440	16.1	6.5	1.7
2 tailwind	6.8 ft/sec	SC117	390	8.9	3.6	1.55

*(Note: KW, σ_{ur} are defined in Appendix C, Data Base)

Of particular significance are the high wind shear, high gust cases which are the conditions likely to produce a crash landing.

3. For the vehicle studied and the SC117 SBS, one crash and a number of marginal landings resulted for the high crosswind shear and high gust combinations of wind conditions of Task III. This was primarily due to excess lateral offset in heavy crosswind landings. The presumption is that a 150 foot wide runway is used. Use of 200 foot runways or setting maximum crosswind restrictions on allowable landing sites readily reduces the crash probability.

4. The system factors which contributed to the marginal landings in the high crosswind shear, high turbulence cases are:

a. the high crosscoupled roll moment due to both sideslip and rudder for the vehicle studied.

b. elevon surface rate saturation and aileron position limiting during combined maneuvers when simultaneous decrabs, and flare and/or heavy gust corrections are required.

c. decrab computation which did not include vehicle yaw rate in estimating time to decrab (note: this required improvement to the decrab laws became apparent only after the Monte Carlo runs were evaluated and, therefore, too late to incorporate into the system).

5. The Precision Ranging System results were inconclusive. Minimizing the number of DME's, optimal location of DME's and possible auxilliary vertical axis updating should be investigated.

6. The use of the currently existing ILS is acceptable provided guidance into the beam is provided by some other system and Radar Altimeter update of the vertical axis is available when the ILS elevation beam becomes unreliable below 100 feet.

This conclusion is valid for a relatively high L/D vehicle (Note; NADWO L/D > 9) where the flight path in the terminal phase is straight. For lower L/D vehicles (L/D < 5) higher curvature of the terminal phase would take the vehicle outside the linear range of the narrow beam conventional ILS. In the latter case, auxilliary measurement information would be required to initiate the primary flare.

7. The system's sensitivity to deterministic variations in parameters is negligible. 5% variations in both major vehicle parameters and initial condition errors and the influence of mean winds without gusts do not yield significant touchdown errors. These results are felt to be deceptive, particularly with respect to pitch and roll control power, in that the system is not taxed until gusts are included.

8. Operational factors are more important in making a selection between realistic candidate systems than the touchdown errors resulting from system measurement errors since the large errors (i.e., the significant errors) are due to wind shears and gusts. (See Section X, Recommendations for Future Study, for listing of possible factors.)

9. A quadratic lag complementary filter was found to be adequate for the systems studied. More sophisticated techniques

for blending the ground measurement data (landing system) with the inertial navigation system (INS) are not required for the terminal landing. The effect of winds and gusts and vehicle dynamics dominate in determining touchdown errors.

10. It is concluded that the unpowered SSV vehicle should incorporate speed brakes. The effectiveness of utilizing the landing gear drag to control the airspeed at touchdown is the basis for this conclusion. In this study the gear is lowered once and only once since it is vital to flight safety to be sure the gear is in the down position. A much better speed control system would result if continuous modulation of drag by means of speed brakes was possible.

X. RECOMMENDATIONS FOR FUTURE STUDY.

1. Blending Algorithms Study.

Because of the success of the simple algorithms used to combine the INS data with the landing system (ground based measuring system), it is recommended that this be investigated for applicability for the precision ranging system being investigated by NASA/Ames.

It is particularly recommended to base comparisons on closed loop performance with gust environment.

2. Revision of G&C Laws for Updated Vehicle.

This self evident recommendation suggests that the study be repeated, with the advantage of the insights gained during this study, for the finalized vehicle.

3. Study of Guidance from Higher Altitudes.

The dependency of the study on guidance from the higher regions of the trajectory was evident throughout the study. Repeated re-evaluation was required of the trim conditions and vehicle states for the varying winds resulting from the earlier flight phases. The subject of how the designed guidance system blended with the guidance of the other flight segments was not specifically treated though it was known that the predictive technique could be readily extended. It is recommended that a study extending the guidance laws to 20,000 feet of altitude be undertaken.

4. Revised Predictive Guidance for Fixed Aimpoint.

As described in Section IV, the predictive guidance used in this study assumed a similar guidance scheme was in effect in the higher trajectory regions of the flight. This resulted in different altitudes, ranges and airspeeds for the varying conditions of wind at the start of primary flare. It is feasible to revise the predictive guidance laws such that a fixed aimpoint (altitude and range) is used to define start of the primary flare. In the latter system, the glide path angle required to attain the necessary equilibrium velocity for the fixed aimpoint would be predicted.

As pointed out in Section IV, which should be read for details, the advantages of a fixed aimpoint are that it is easy to monitor the flight since the point does not change as a function of winds and it gives a constant length straight glide path for all wind conditions. The disadvantages are that the system requires prior knowledge of the wind. It is recommended that a study leading to a comparison of the two techniques be undertaken and a possible combination of the two be synthesized for further improvement in guidance.

5. Modified Decrab Time Computation.

The time to initiate decrab maneuvers in the system developed was based on the crab angle only. In high crosswind shears and high gusts, a sizeable yaw rate component exists prior to decrab. If not taken into account, the decrab may be over-compensated or the decrab time may be incorrect. The crosstrack

velocity and the lateral touchdown error are critically dependent on decrab time. The lateral touchdown error increases as the square of the time.

Since this is only a problem in the high crosswind, high gust cases, the problem was not apparent until the results of Task III were analyzed. Revision of the decrab computation and rerunning the Monte Carlo tests to verify results was not feasible within the remaining budget.

It is recommended that the decrab law be modified and a limited Monte Carlo high crosswind, high gust evaluation be conducted.

6. Reverse Elevon Compensation Study.

One of the contributers to increasing the sink rate dispersion at touchdown in this vehicle was the large positive feedback due to the elevon lift which is used to produce the pitch moment to compensate for vertical errors. Initially the elevon lift causes an acceleration in a direction which increases the error being corrected by the pitch rotation. This is a physical phenomenon which cannot be removed by the control system design. However, feeding back the additional error caused by the elevon lift is destabilizing. Smaller sink rate dispersions in heavy turbulence are attained by reducing the feedback gains.

This problem is similar to the problem experienced with the rudder side force. A computation of this force had to be subtracted from the lateral accelerometer reading when the lateral accelerometer was incorporated to measure sideslip (See Section V). This same technique may be applied to the elevon. The destabilizing

lift may be computed out such that short period vertical acceleration from this source is removed from the feedback enabling the use of higher gains (tighter control).

With a vehicle with as large an elevon lift as the one considered, a study leading to the possible application of this concept is recommended.

7. Monte Carlo with Random Vehicle Perturbations.

In evaluating the system's sensitivities to deterministic changes in vehicle parameters and deterministic mean wind shears, it was established that the system was insensitive to 5% changes in key parameters. It is evident, however, that under these conditions, parameters such as control surface power, are not strongly exercised and, therefore, the conclusions may be optimistic. That is, if the test conditions are such that the full control power is rarely required, then a 5% decrease in the maximum control power would not show significant changes. The best way of assessing the effect is under random conditions of gust which require a realistic demand on maximum control power. Under these conditions, the system's sensitivity to a reduction in control power may be assessed more realistically. A similar argument may be made for variations in L/D, elevon lift, air density uncertainties, vehicle weight and inertia.

Each parameter should be changed singly and a limited Monte Carlo evaluation made with gusts to assess the true sensitivity of the system performance to the parameter uncertainty.

8. Study of Operational Factors and Functional Requirements.

Because of the conclusions that all landing systems (ground based measurement system) could be used for the SSV landing missions, it is apparent that the final choice must be based on Operational Factors and Functional Requirements. These are such considerations as:

a. systems angular and range coverage
b. ease of set-up and calibration
c. capability of providing a raw data backup mode
d. vehicle effects in terms of added on-board weight or external attached hardware (the latter poses problems of breaking through the vehicle's skin (structural integrity problems) or of protecting the external hardware thermally during re-entry)
e. on-board computer problems imposed by computational requirements
f. availability of the selected hardware at the candidate landing sites
g. availability of the selected hardware within the SSV schedule time span.

This study did not address these questions as a major task. It is evident that considerations of these factors will play a major role in the system selection.

9. Actual Site Wind Studies.

Because of the strong dependence of the conclusions on the wind models, it is recommended that precise wind models be developed which closely represent the conditions at the prime candidate sites for the SSV landings. Comparison of these wind models with the one used in this study and some limited additional simulations should be performed to more precisely estimate the touchdown parameters for the prime sites.

10. Flight Simulations.

It is strongly urged that flight test of the guidance concepts which have evolved be performed utilizing aircraft to simulate the SSV.

11. Simplified Systems.

In order to increase overall system reliability without imposing excessive redundancy, a study of the limitations of simpler systems is suggested. In particular, the use of a landing system directly and not blended with the output of an Inertial Navigation System should be investigated since less hardware is required. The trade-off between decreased precision and increased reliability should be evaluated for potential for a better system.

12. Speed Brake Study

The feasibility of employing speed brakes with appropriate actuators for continuously modulating drag should be investigated. If the SSV design can accommodate these devices, a study leading to an improved speed control system should be conducted.

APPENDIX A

HISTOGRAMS FOR TASK III HIGH WIND AND HIGH GUST RUNS

APPENDIX A

HISTOGRAMS FOR TASK III HIGH WIND AND HIGH GUST RUNS

This appendix contains the histograms of the results of the high wind and high turbulence simulations of Task III which are discussed and analyzed in Section VII.

The histograms are coded in terms of the touchdown variable as listed in Table A-1. The meaning of gust magnitude, σ_{ur}, and wind shear magnitude, K_W, are defined in Appendix C, Data Base.

The symbols used in this appendix are:

HW = headwind

CW = crosswind

TW = tailwind.

The variables are the touchdown values with respect to a nominal TD point with coordinates X=0, Y=0, Z=0.

X = longitudinal distance

$\dot{X}$ = forward ground speed

V_a = airspeed

Y = lateral displacement

$\dot{Y}$ = cross track velocity

$\dot{Z}$ = sink rate

ψ = heading angle with respect to centerline

θ = pitch attitude

ϕ = roll attitude

Table A-1

HISTOGRAMS LIST

Figure No.	Set No. (Table VII-1)	Variables	σ_{ur} Gust Magnitude	Wind Direction and Magnitude
A-1	1	$X, \dot{X}, V_a$	6.8 ft/sec	K_W = 2 HW
A-2	1	$Y, \dot{Y}, \dot{Z}$	6.8	K_W = 2HW
A-3	1	ψ, θ, ϕ	6.8	K_W = 2 HW
A-4	2	$X, \dot{X}, V_a$	6.8	K_W = 2 CW
A-5	2	$Y, \dot{Y}, \dot{Z}$	6.8	K_W = 2 CW
A-6	2	ψ, θ, ϕ	6.8	K_W = 2 CW
A-7	3	$X, \dot{X}, V_a$	6.8	K_W = 2 TW
A-8	3	$Y, \dot{Y}, \dot{Z}$	6.8	K_W = 2 TW
A-9	3	ψ, θ, ϕ	6.8	K_W = 2 TW
A-10	4	$X, \dot{X}, V_a$	4.6	K_W = 2 HW
A-11	4	$Y, \dot{Y}, \dot{Z}$	4.6	K_W = 2 HW
A-12	4	ψ, θ, ϕ	4.6	K_W = 2 HW
A-13	5	$X, \dot{X}, V_a$	4.6	K_W = 2 CW
A-14	5	$Y, \dot{Y}, \dot{Z}$	4.6	K_W = 2 CW
A-15	5	ψ, θ, ϕ	4.6	K_W = 2 CW
A-16	6	$X, \dot{X}, V_a$	4.6	K_W = 2 TW
A-17	6	$Y, \dot{Y}, \dot{Z}$	4.6	K_W = 2 TW
A-18	6	ψ, θ, ϕ	4.6	K_W = 2 TW
A-19	7	$X, \dot{X}, V_a$	4.6	K_W = 1-1/3 HW
A-20	7	$Y, \dot{Y}, \dot{Z}$	4.6	K_W = 1-1/3 HW
A-21	7	ψ, θ, ϕ	4.6	K_W = 1-1/3 HW

TABLE A-1 (CONTINUED)

Figure No.	Set No. (Table VII-1)	Variables	σ_{ur} Gust Magnitude	Wind Direction and Magnitude
A-22	8	$X, \dot{X}, V_a$	4.6 ft/sec	K_W = 1-1/3 CW
A-23	8	$Y, \dot{Y}, \dot{Z}$	4.6	K_W = 1-1/3 CW
A-24	8	ψ, θ, ϕ	4.6	K_W = 1-1/3 CW
A-25	9	$X, \dot{X}, V_a$	4.6	K_W = 1-1/3 TW
A-26	9	$Y, \dot{Y}, \dot{Z}$	4.6	K_W = 1-1/3 TW
A-27	9	ψ, θ, ϕ	4.6	K_W = 1-1/3 TW
A-28	10	$X, \dot{X}, V_a$	6.8	K_W = 1-1/3 HW
A-29	10	$Y, \dot{Y}, \dot{Z}$	6.8	K_W = 1-1/3 HW
A-30	10	ψ, θ, ϕ	6.8	K_W = 1-1/3 HW
A-31	11	$X, \dot{X}, V_a$	6.8	K_W = 1-1/3 CW
A-32	11	$Y, \dot{Y}, \dot{Z}$	6.8	K_W = 1-1/3 CW
A-33	11	ψ, θ, ϕ	6.8	K_W = 1-1/3 CW
A-34	12	$X, \dot{X}, V_a$	6.8	K_W = 1-1/3 TW
A-35	12	$Y, \dot{Y}, \dot{Z}$	6.8	K_W = 1-1/3 TW
A-36	12	ψ, θ, ϕ	6.8	K_W = 1-1/3 TW

K_W = 2 HW, σ_{ur} = 6.8 FT/SEC.

FIGURE A-1

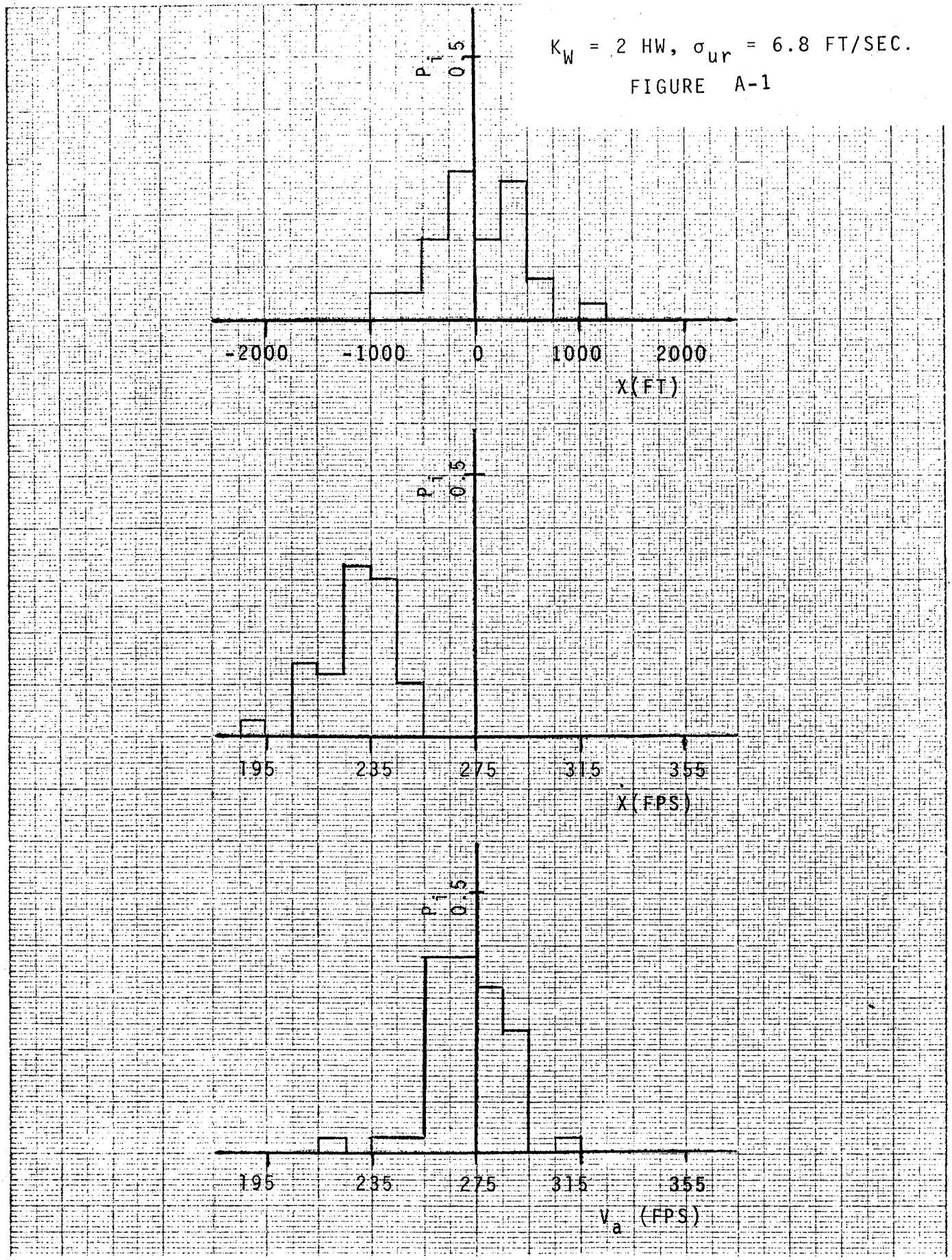

K_W = 2 HW, σ_{ur} = 6.8 FT/SEC.

FIGURE A-2

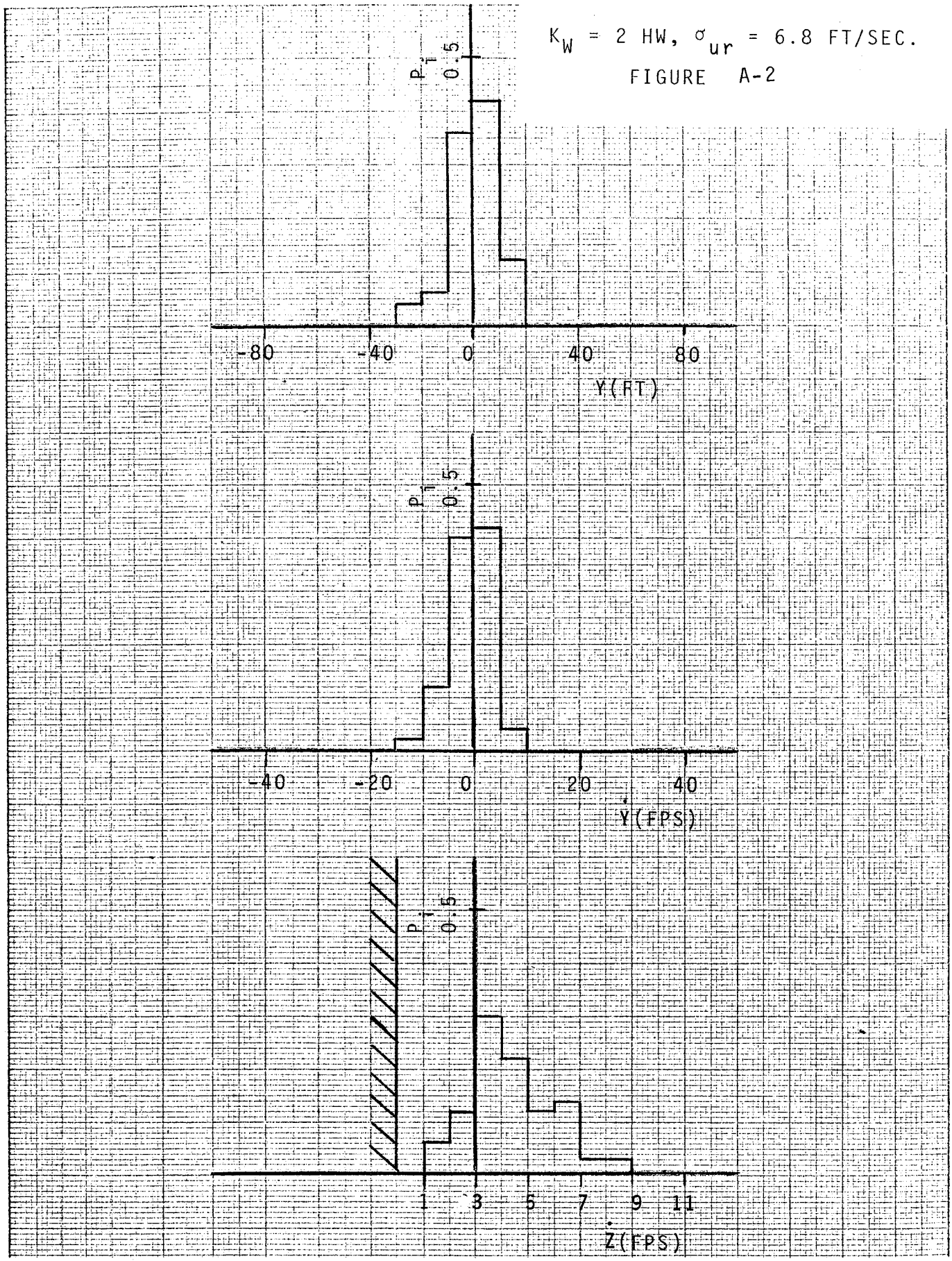

K_W = 2 HW, σ_{ur} = 6.8 FT/SEC

FIGURE A-3

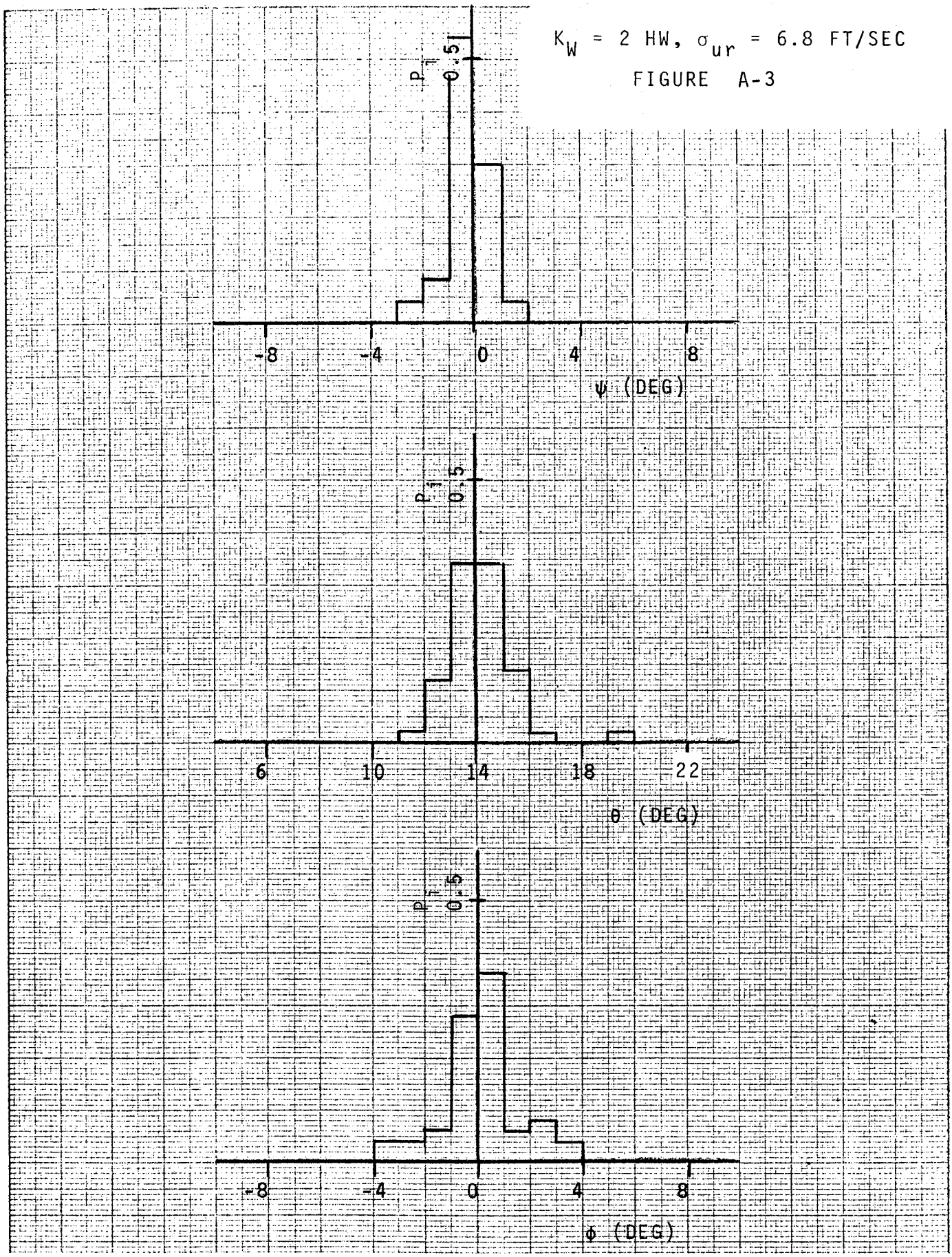

K_W = 2 CW, σ_{ur} = 6.8 FT/SEC

FIGURE A-4

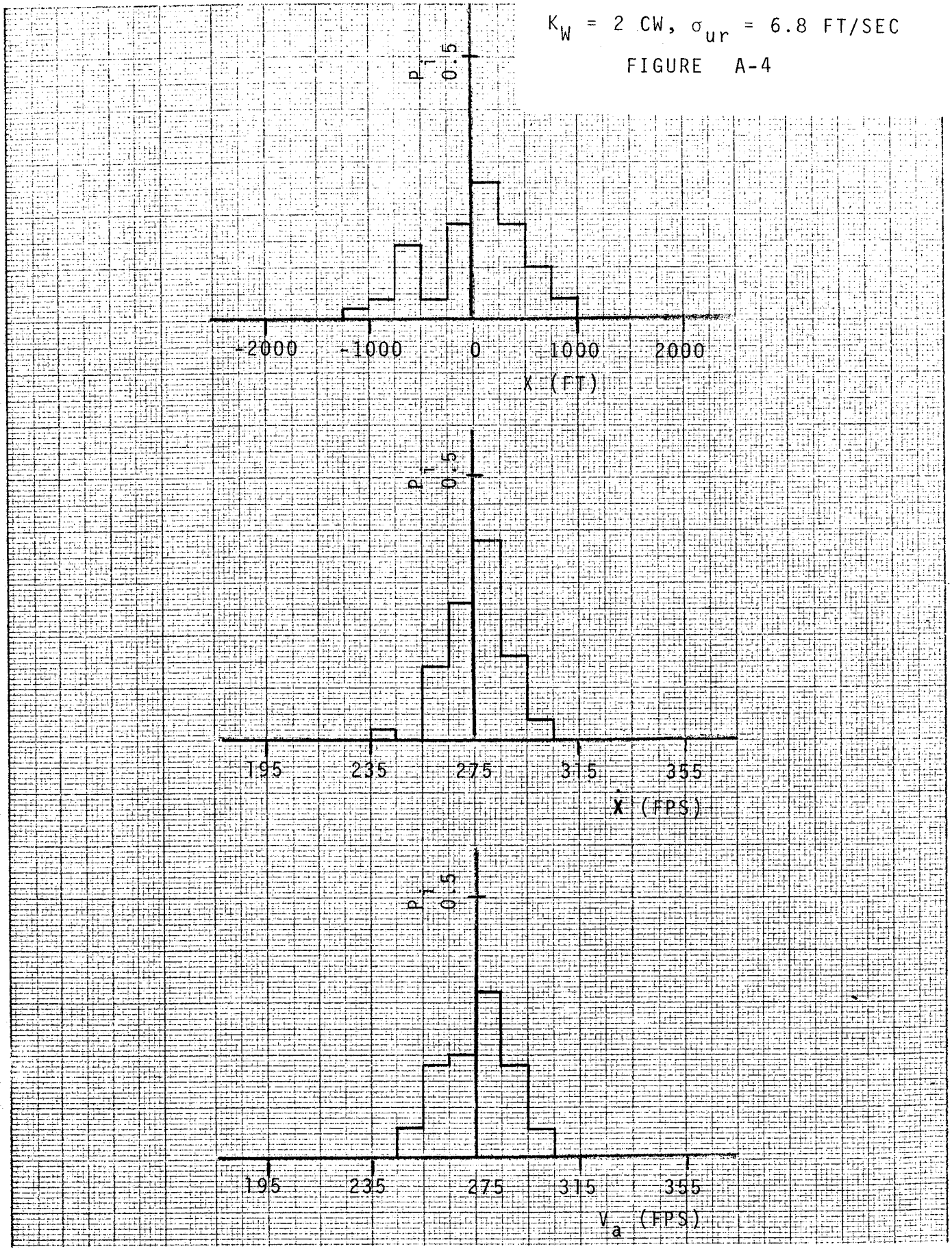

K_W = 2 CW, σ_{ur} = 6.8 FT/SEC

FIGURE A-5

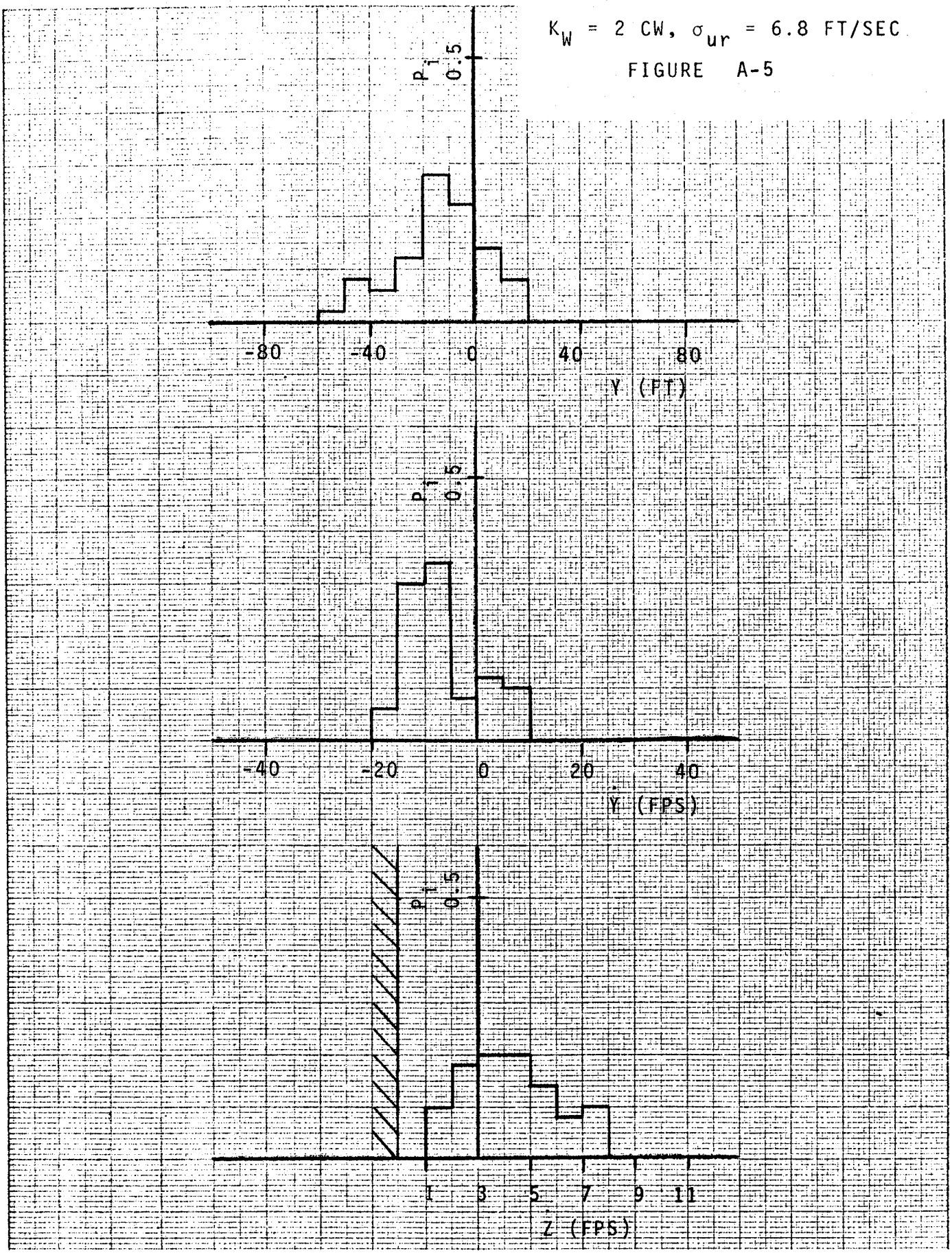

K_W = 2 CW, σ_{ur} = 6.8 FT/SEC.

FIGURE A-6

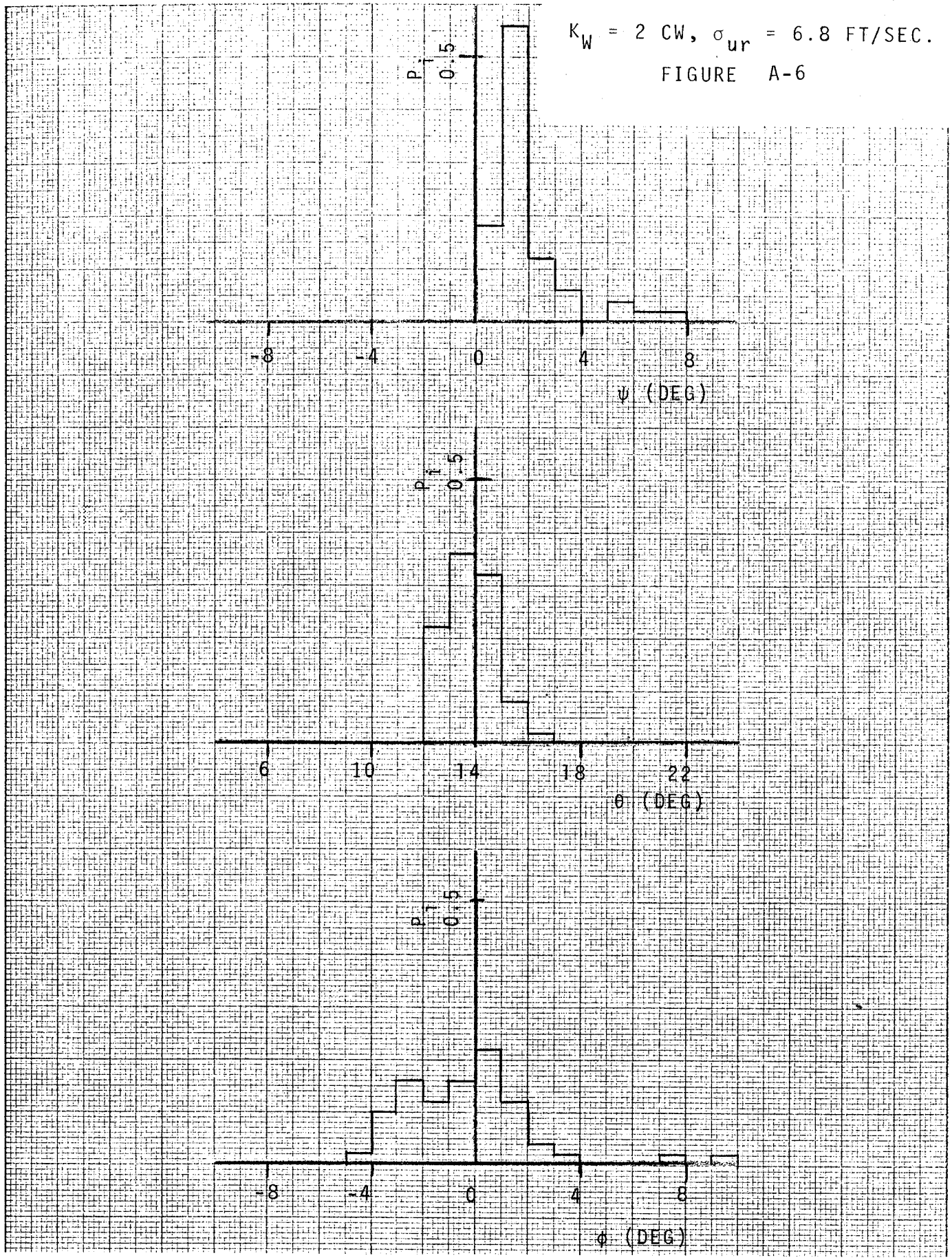

K_W = 2 TW, σ_{ur} = 6.8 FT/SEC

FIGURE A-7

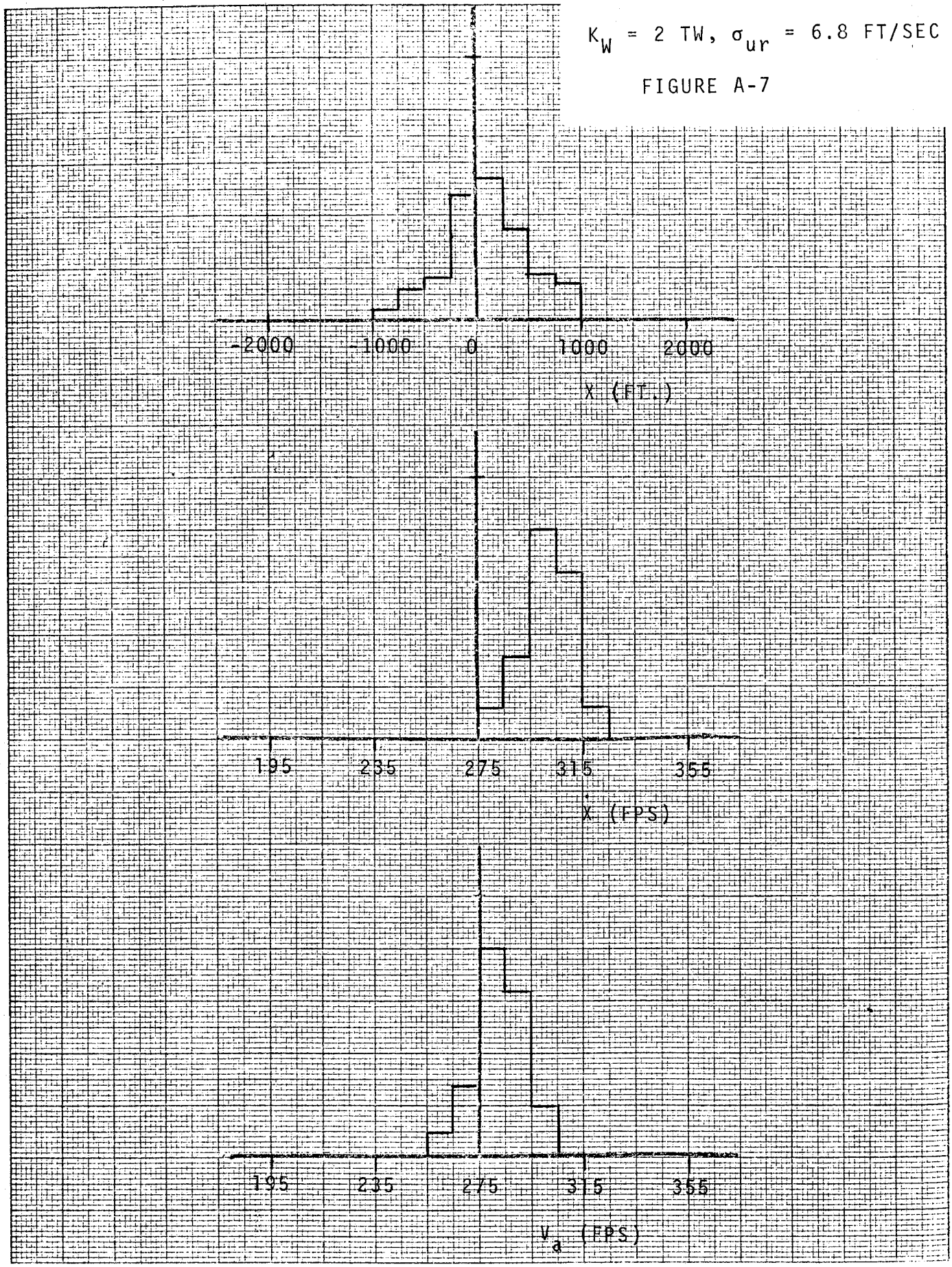

K_W = 2 TW, σ_{ur} = 6.8 FT/SEC

FIGURE A-8

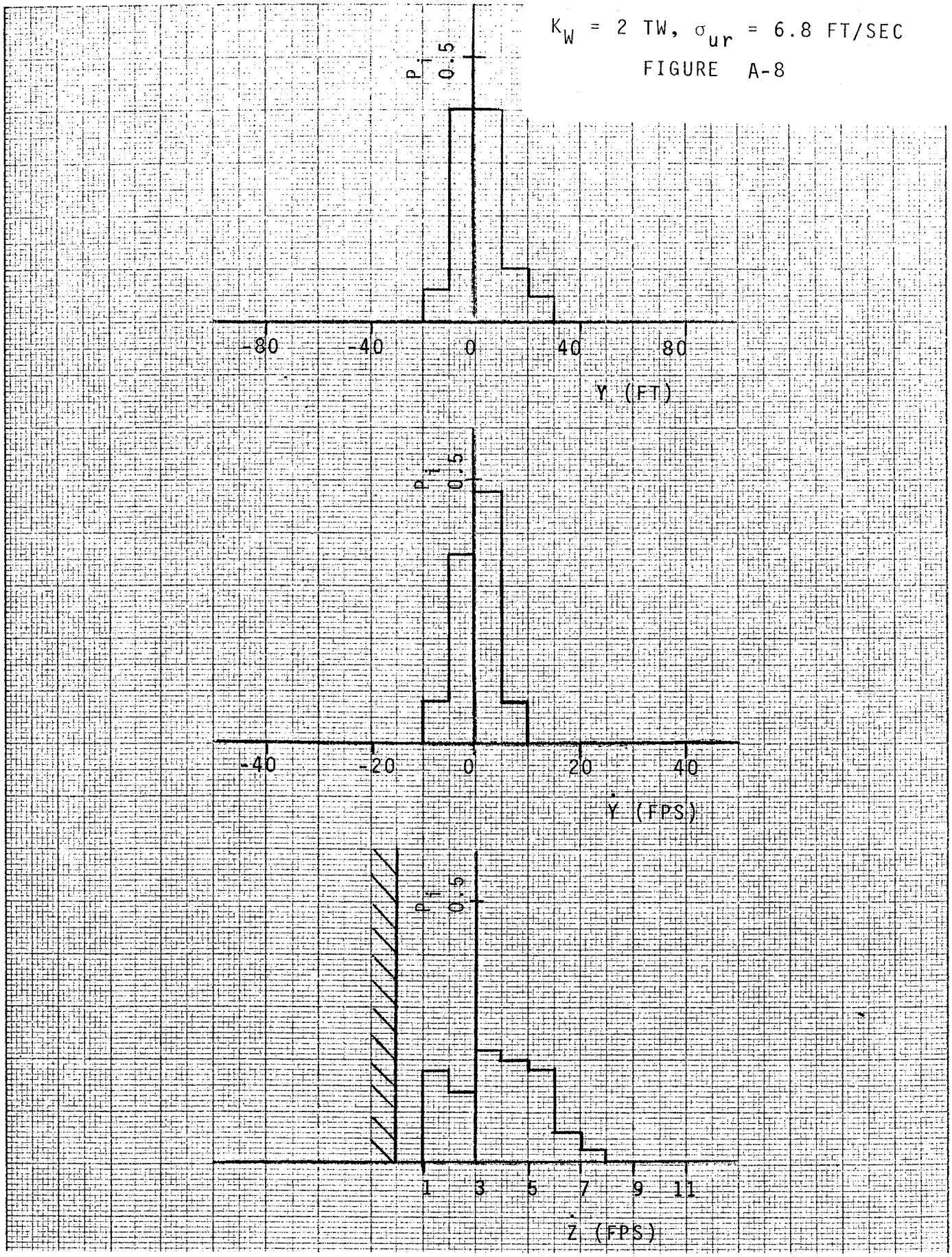

K_W = 2 TW, σ_{ur} = 6.8 FT/SEC.

FIGURE A-9

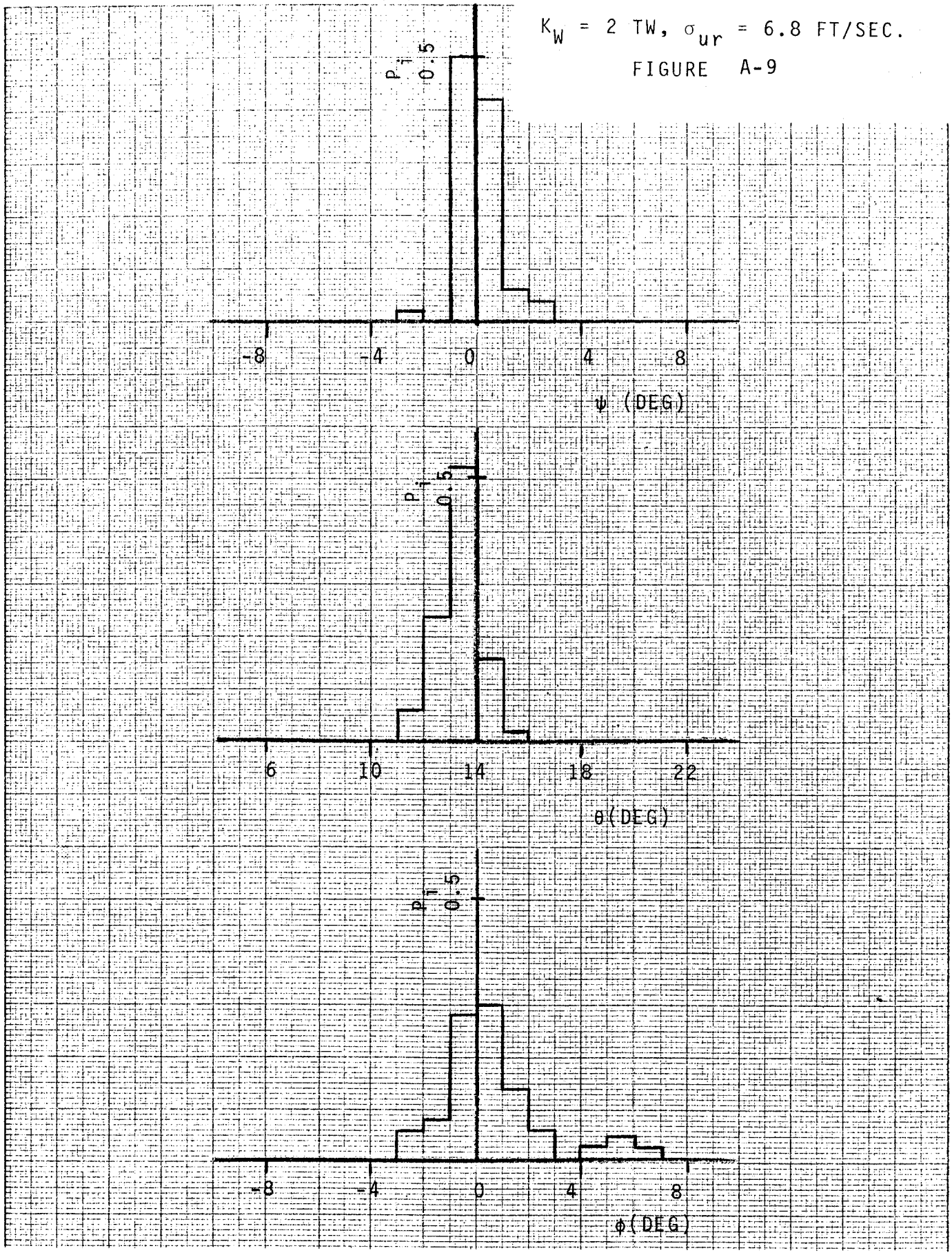

K_W = 2 HW, σ_{ur} = 4.6 FT/SEC

FIGURE A-10

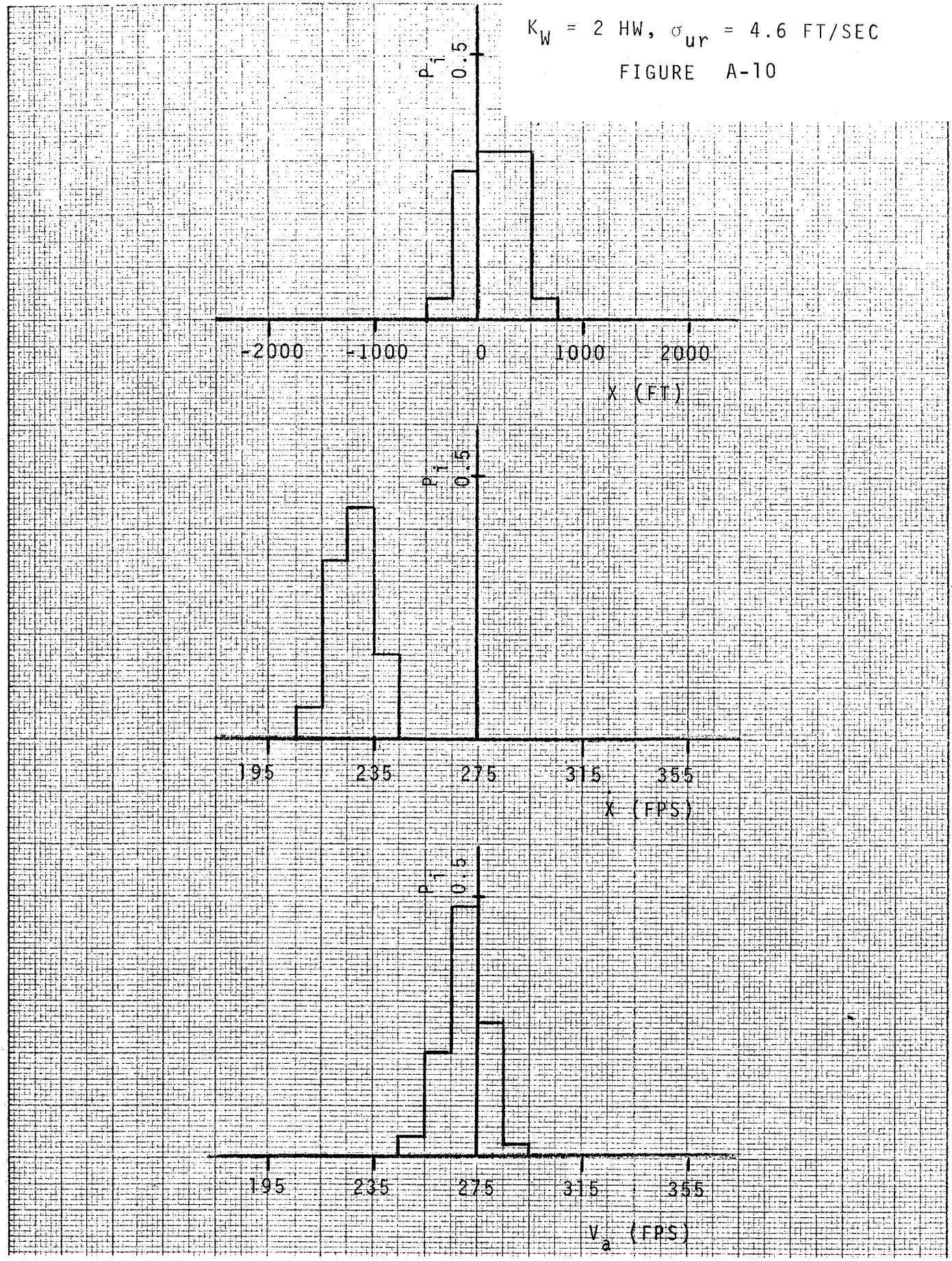

K_W = 2 HW, σ_{ur} = 4.6 ft/sec

FIGURE A-11

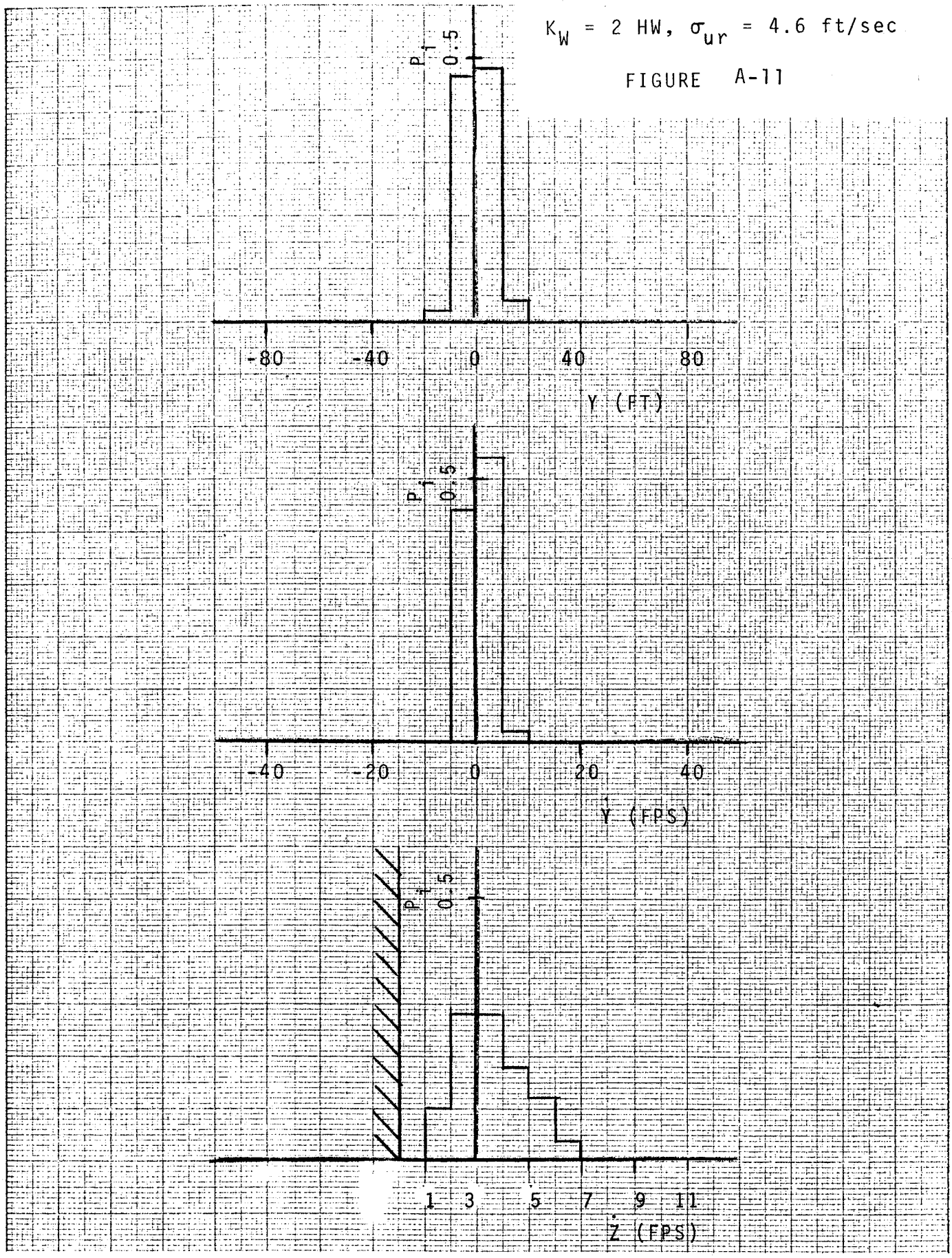

K_W = 2 HW, σ_{ur} = 4.6 FT/SEC

FIGURE A-12

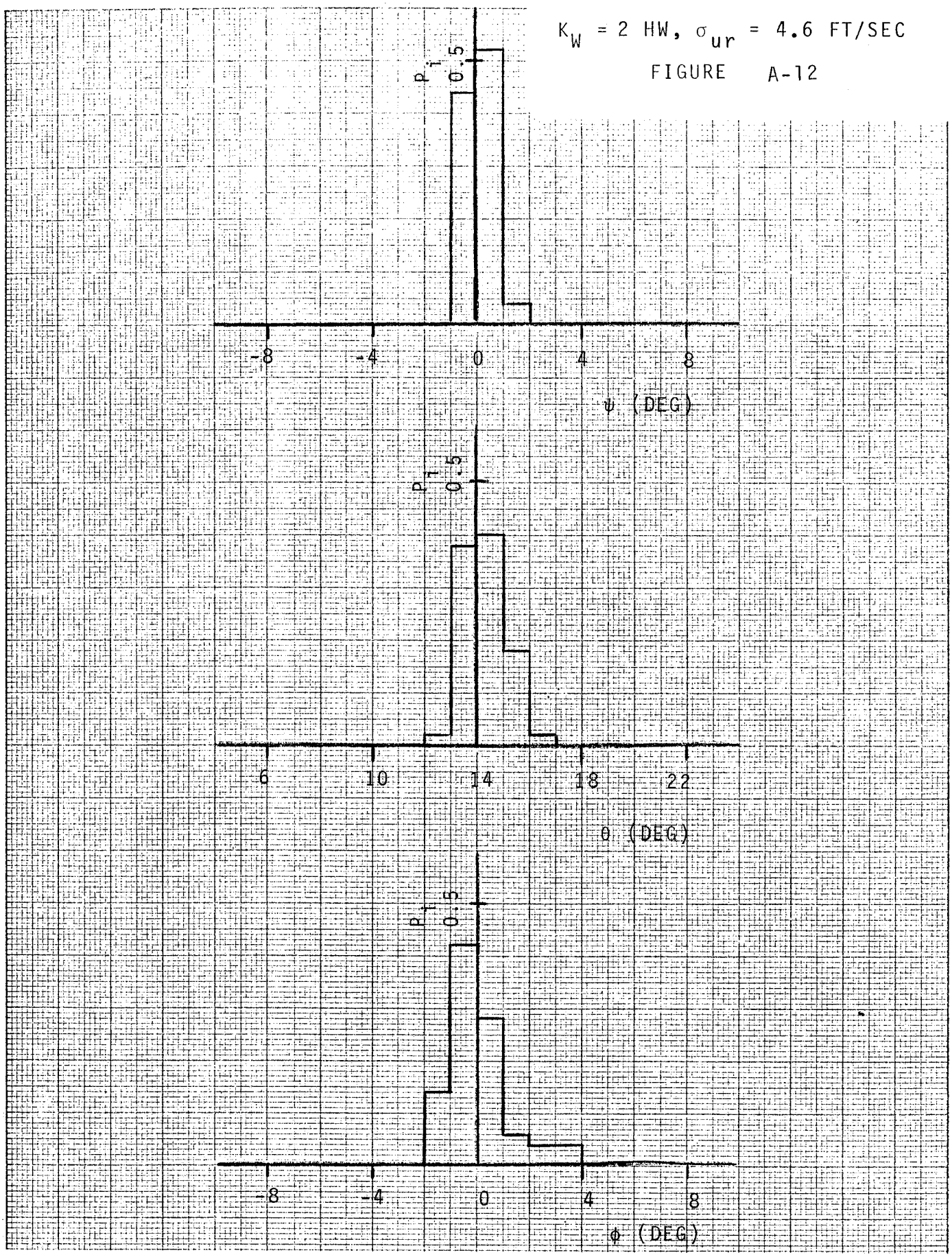

K_W = 2 CW, σ_{ur} = 4.6 FT/SEC

FIGURE A-13

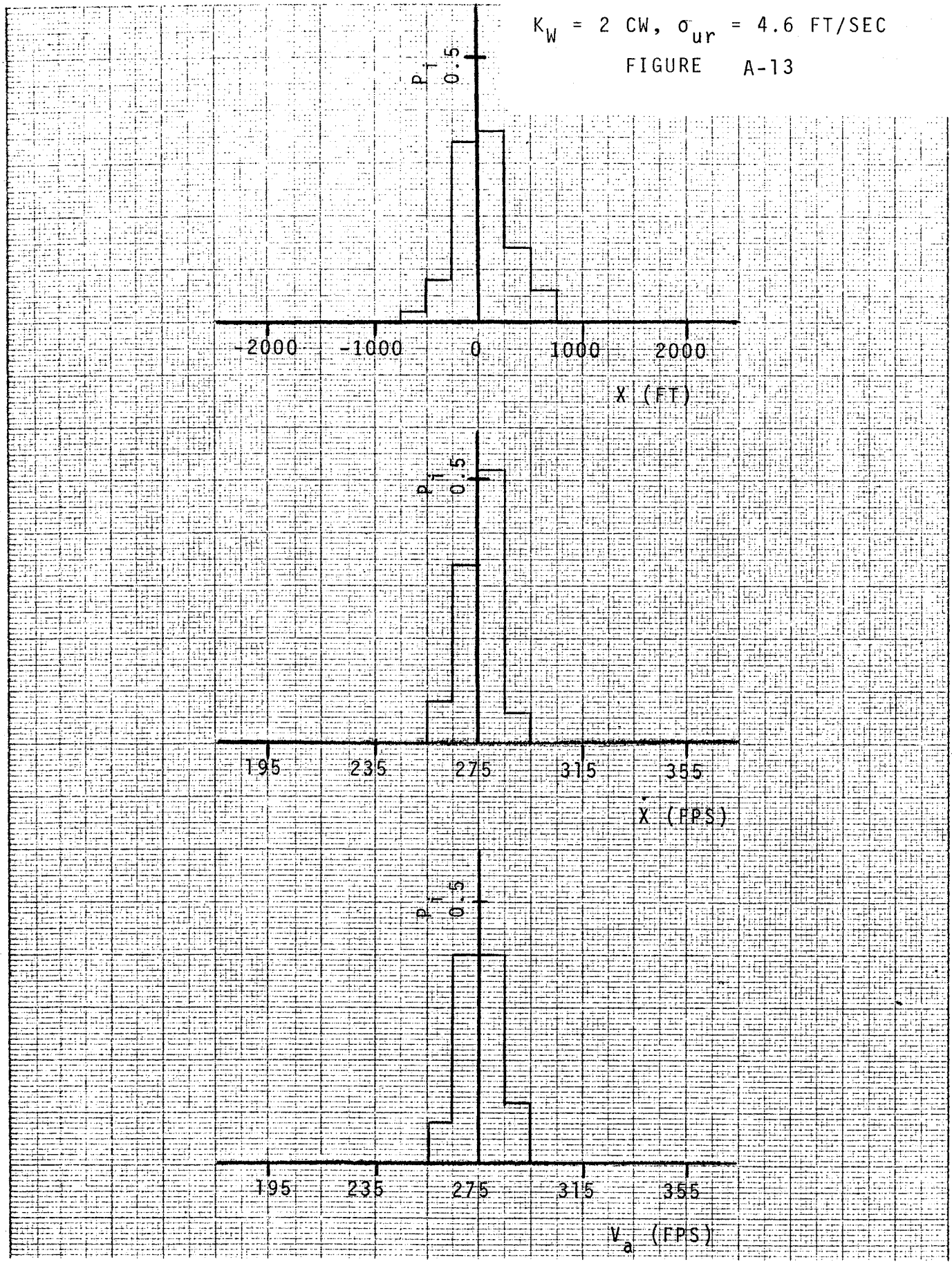

K_W = 2 CW, σ_{ur} = 4.6 FT/SEC

FIGURE A-14

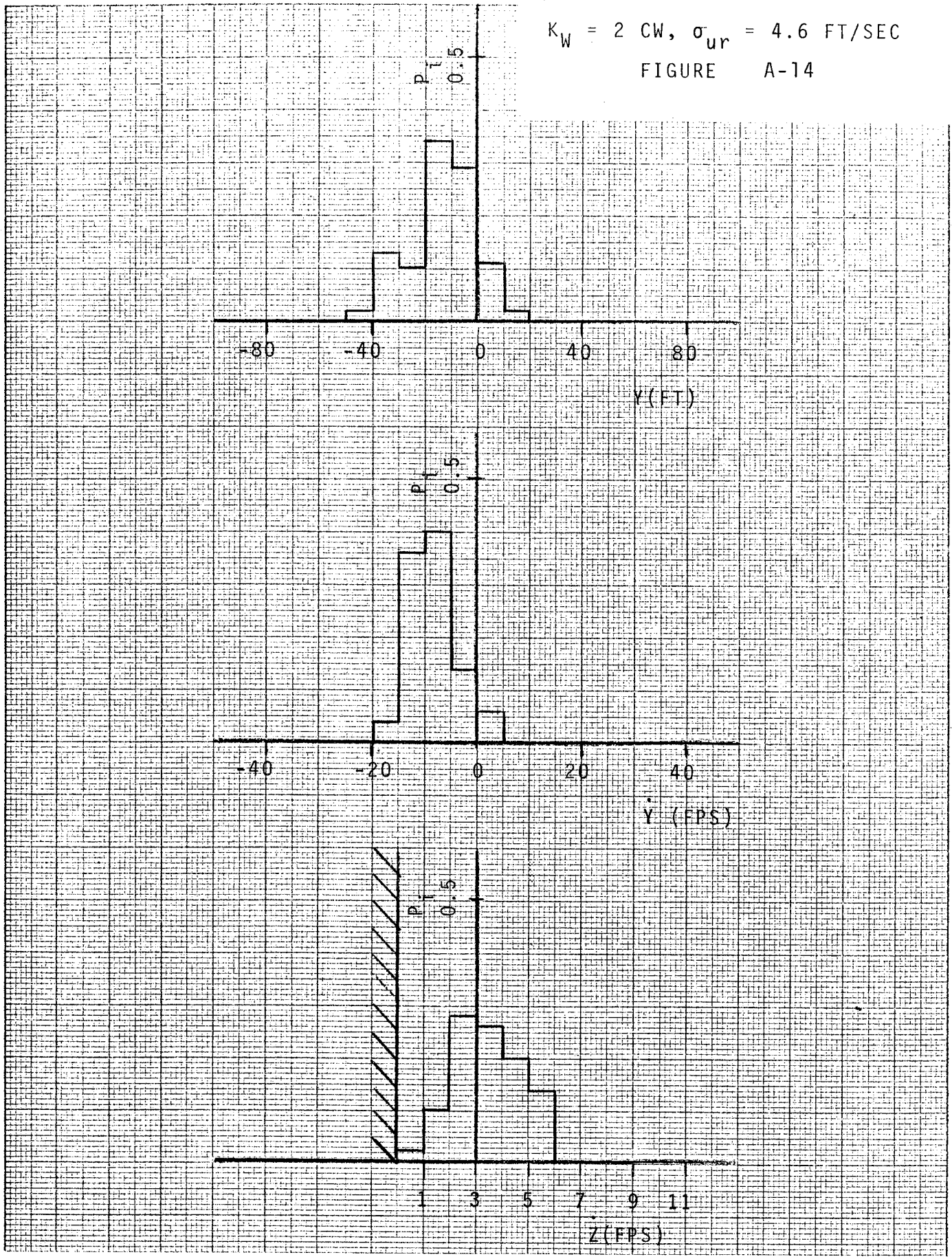

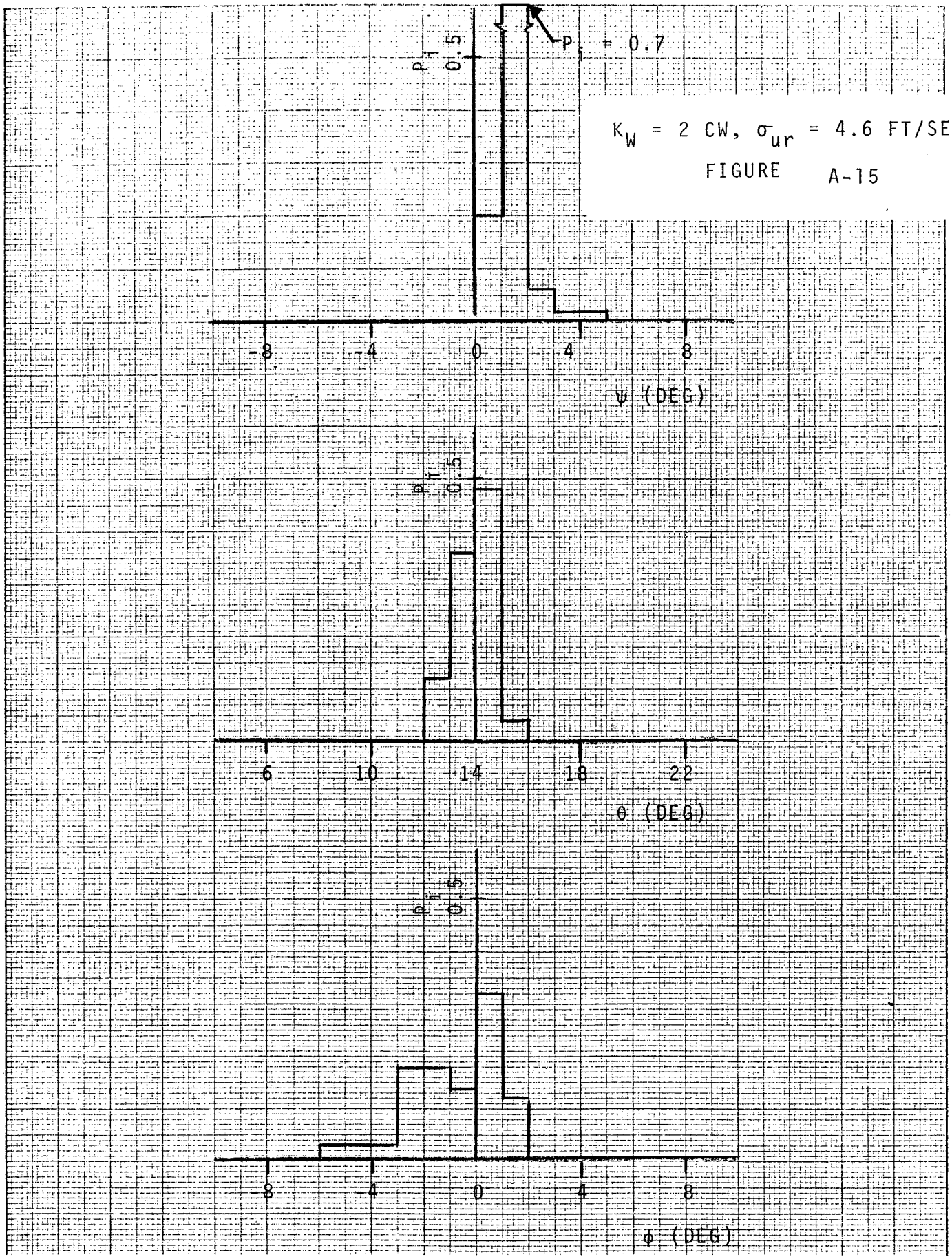

K_W = 2 CW, σ_{ur} = 4.6 FT/SEC

FIGURE A-15

K_W = 2 TW, σ_{ur} = 4.6 FT/SEC.

FIGURE A-16

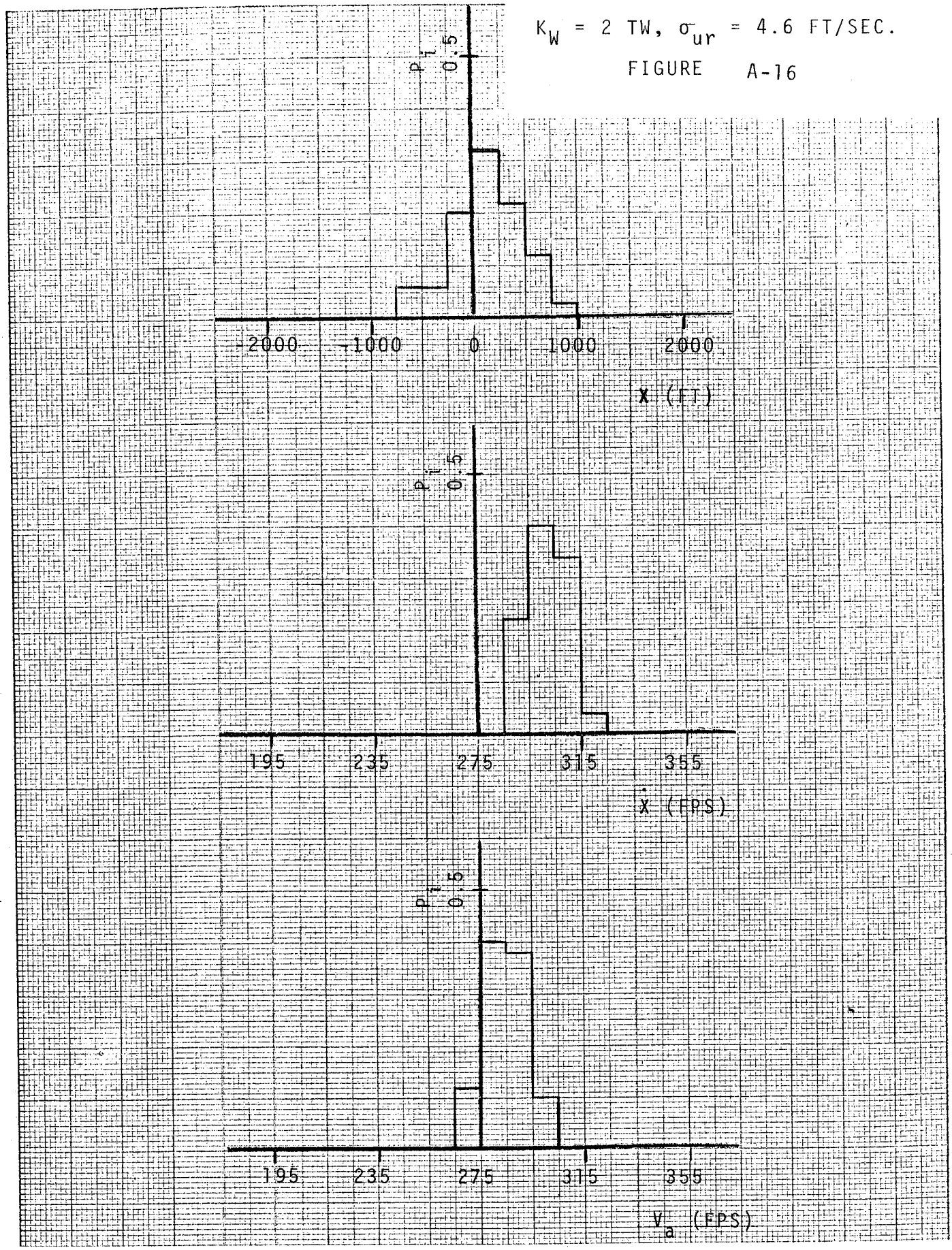

K_W = 2 TW, σ_{ur} = 4.6 FT/SEC.

FIGURE A-17

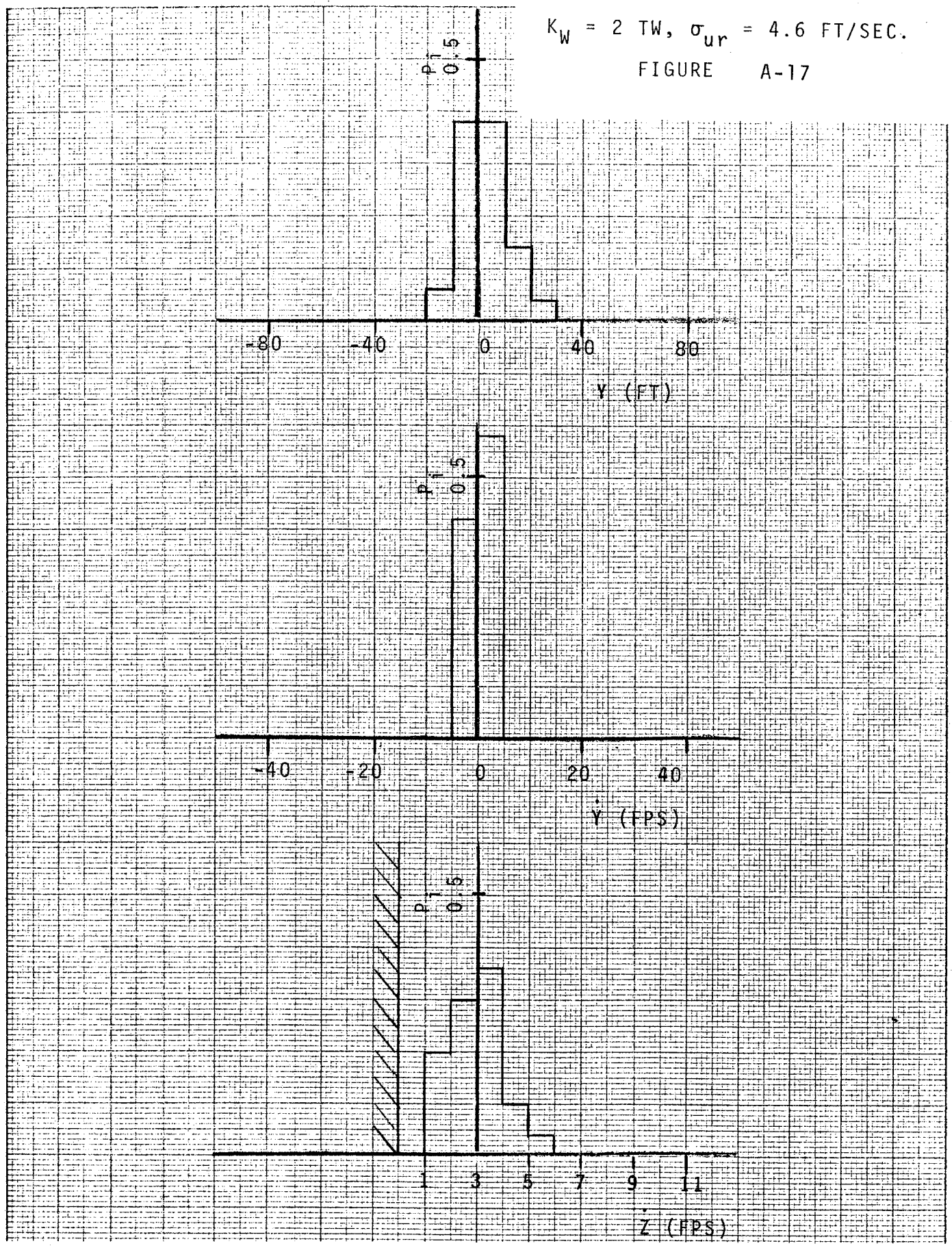

K_W = 2 TW, σ_{ur} = 4.6 FT/SEC.

FIGURE A-18

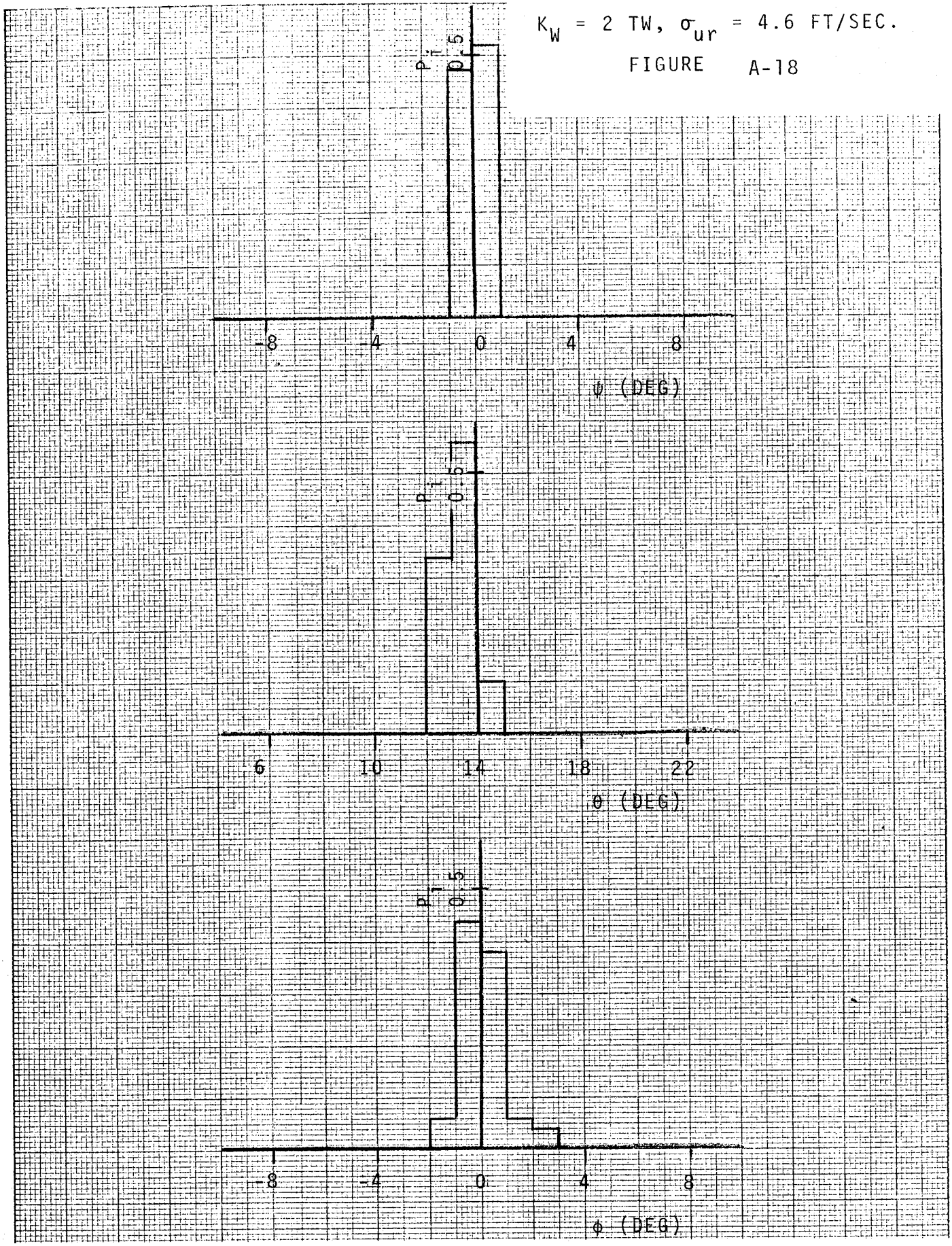

$K_W = 1\frac{1}{3}$ HW, σ_{ur} = 4.6 FT/SEC.

FIGURE A-19

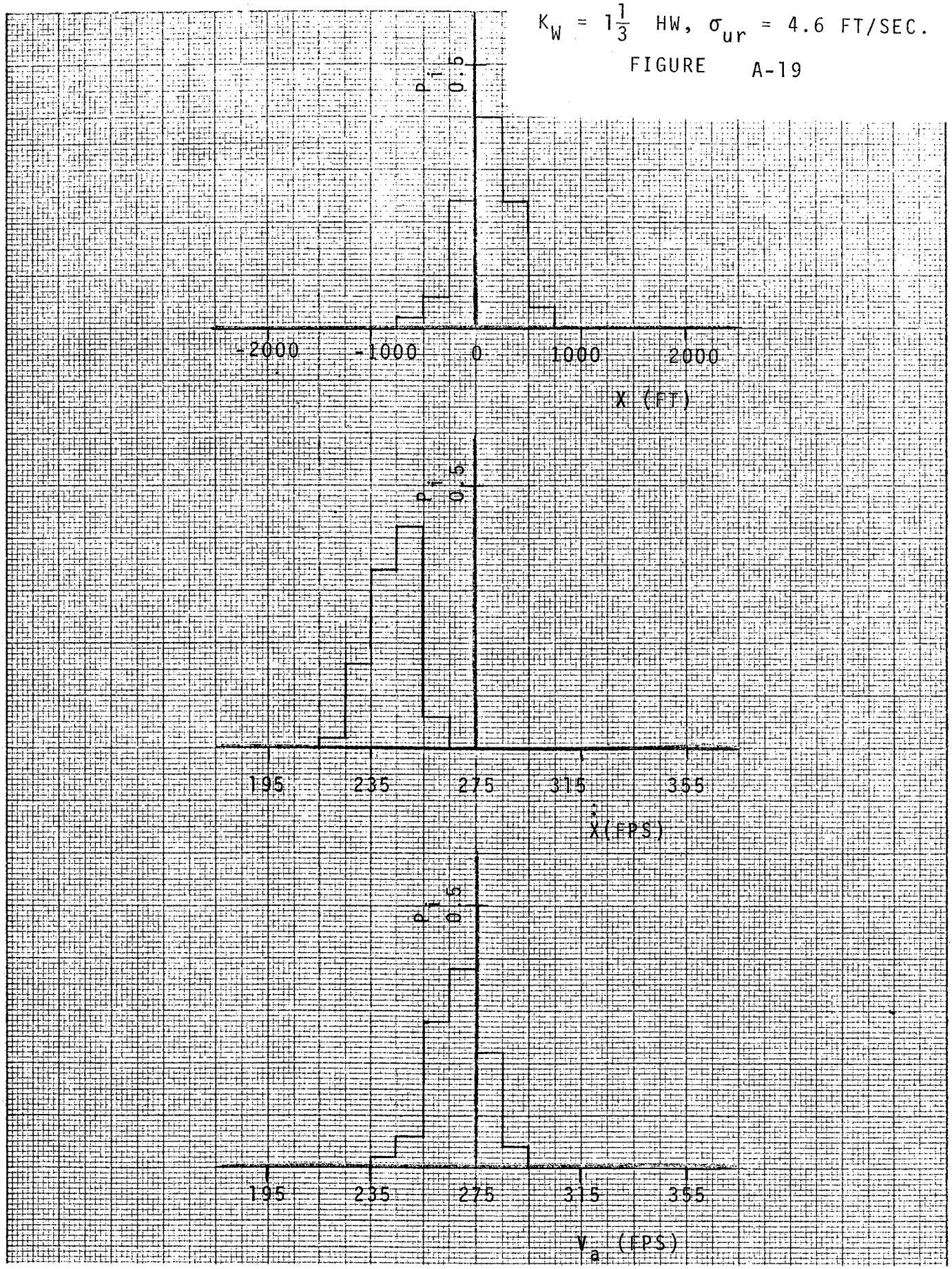

$K_W = 1\frac{1}{3}$ HW, σ_{ur} = 4.6 FT/SEC.

FIGURE A-20

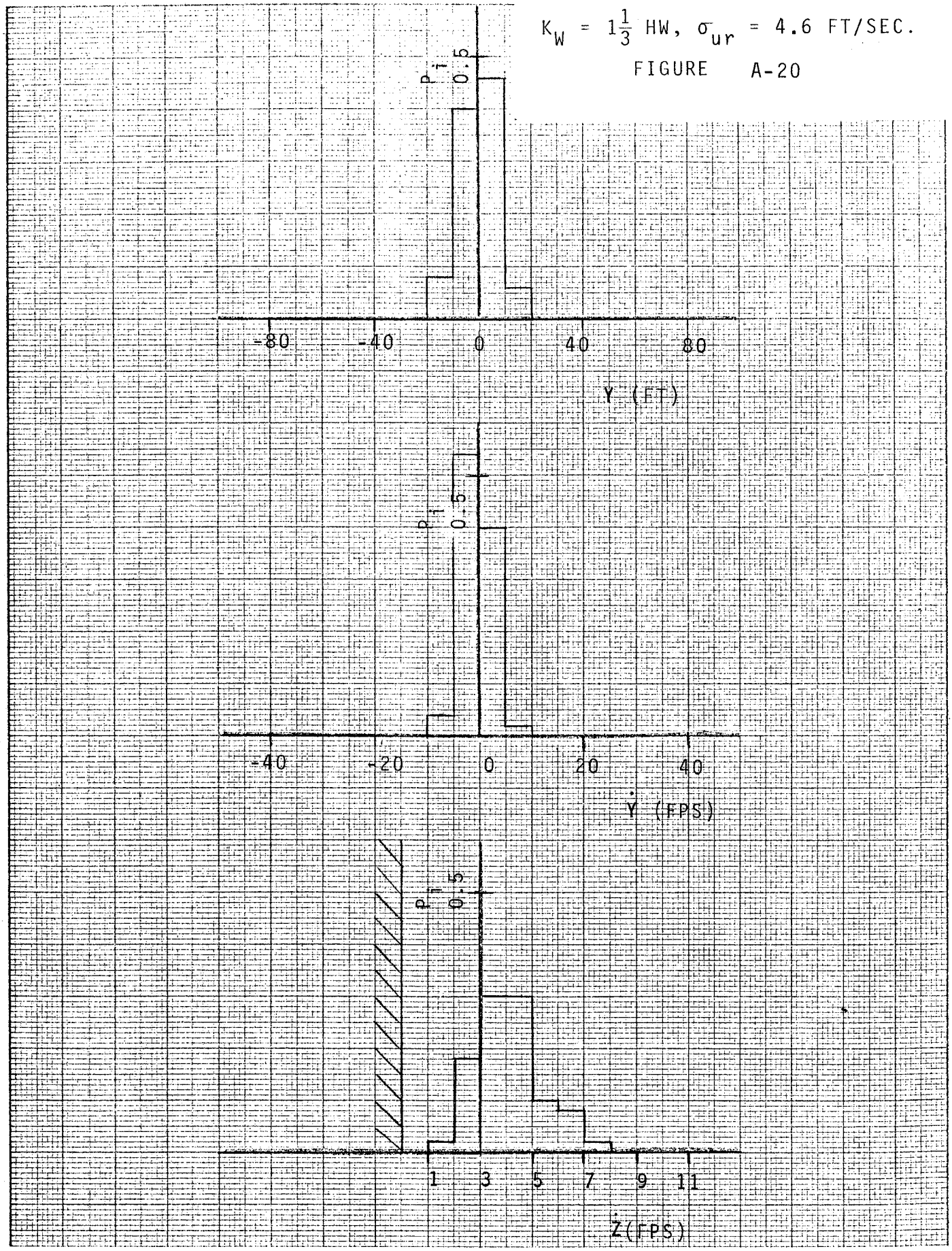

$K_W = 1\frac{1}{3}$ HW, σ_{ur} = 4.6 FT/SEC.

FIGURE A-21

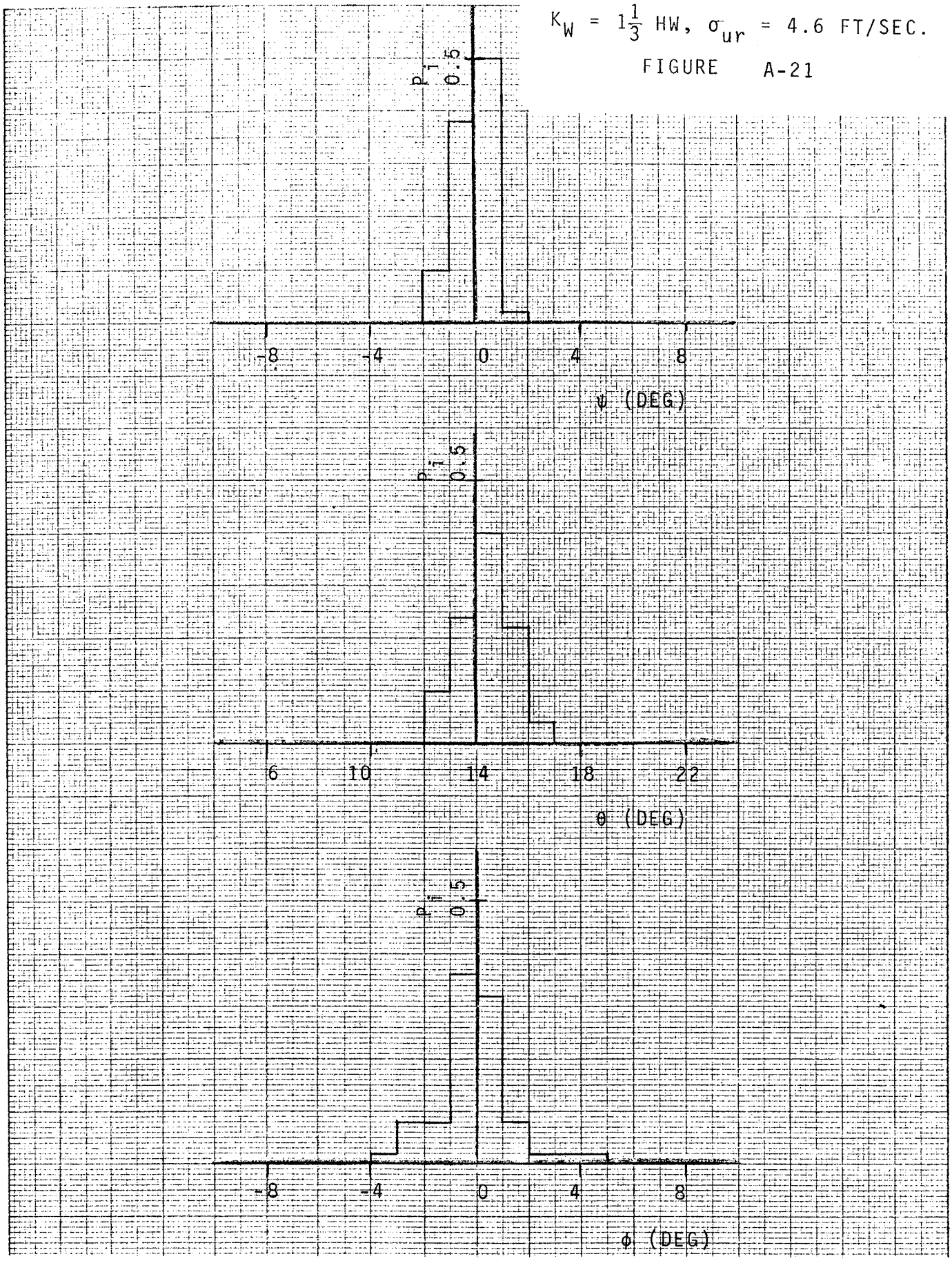

$K_W = 1\frac{1}{3}$ CW, σ_{ur} = 4.6 FT/SEC.

FIGURE A-22

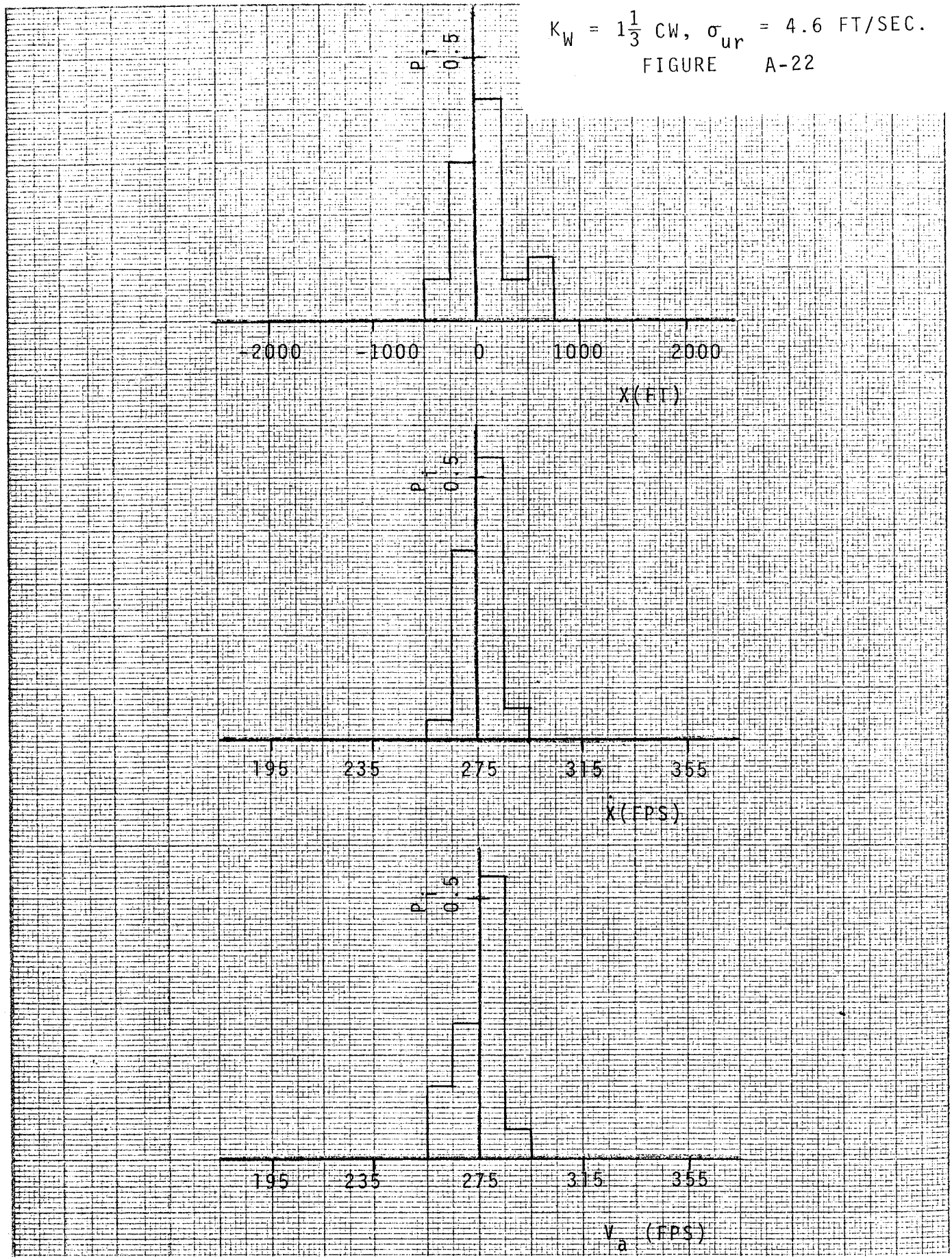

$K_W = 1\frac{1}{3}$ CW, σ_{ur} = 4.6 FT/SEC

FIGURE A-23

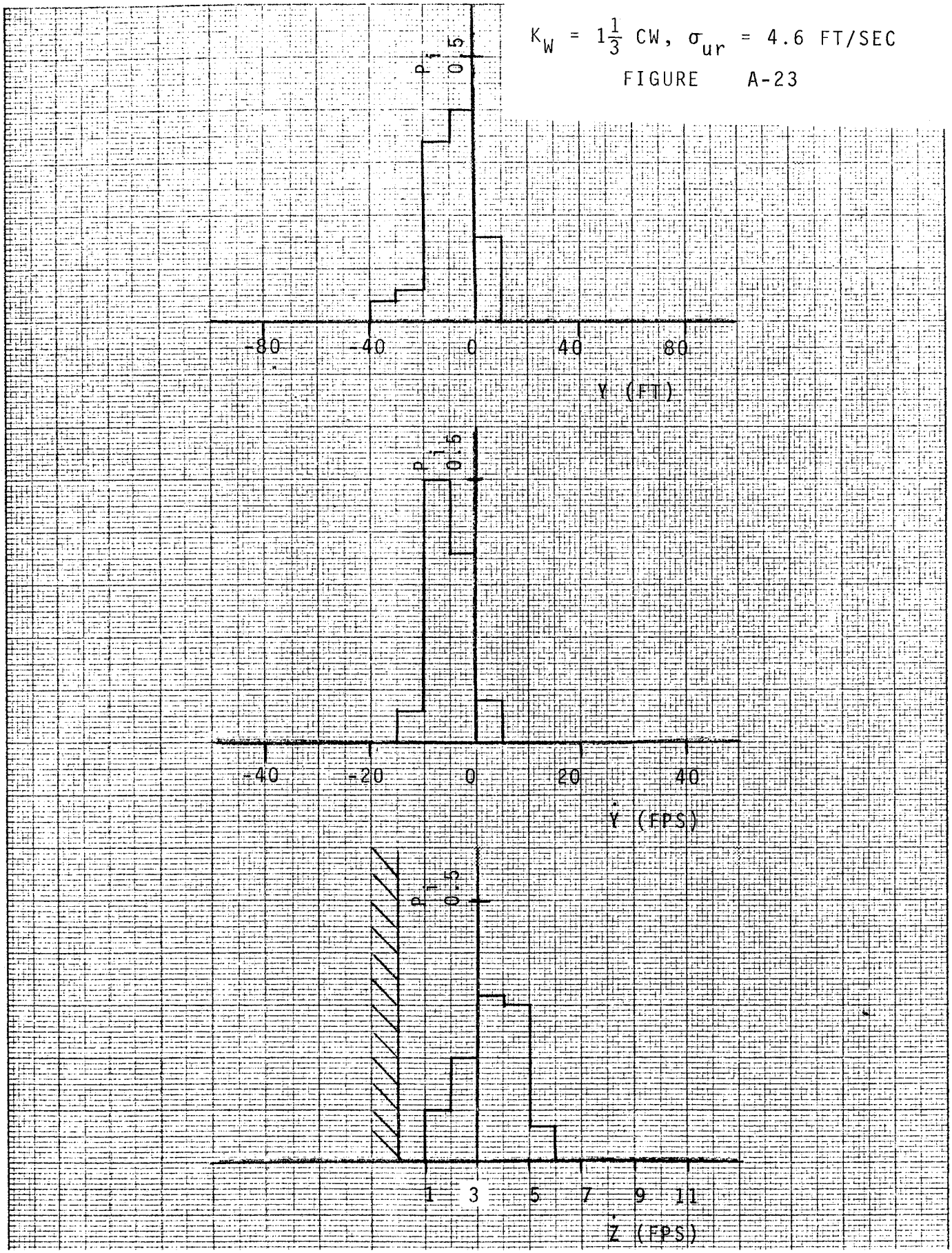

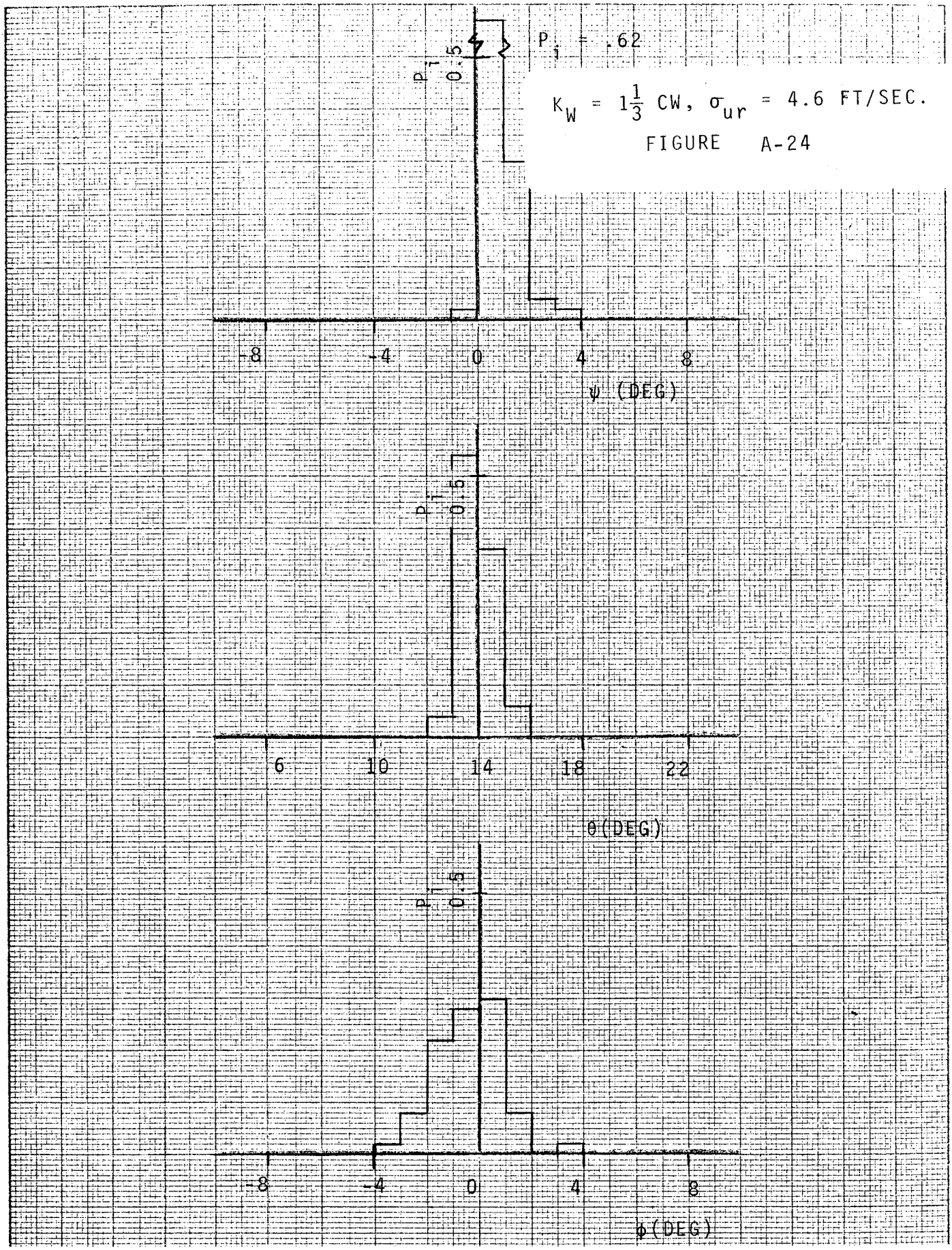
$P_i = .62$
$K_W = 1\frac{1}{3}$ CW, $\sigma_{ur} = 4.6$ FT/SEC.
p_i 0.5
-8
-4
0
4
8
ψ (DEG)
p_i 0.5
6
10
14
18
22
θ(DEG)
p_i 0.5
-8
-4
0
4
8
φ(DEG)

FIGURE A-24

$K_W = 1\frac{1}{3}$ TW, σ_{ur} = 4.6 FT/SEC.

FIGURE A-25

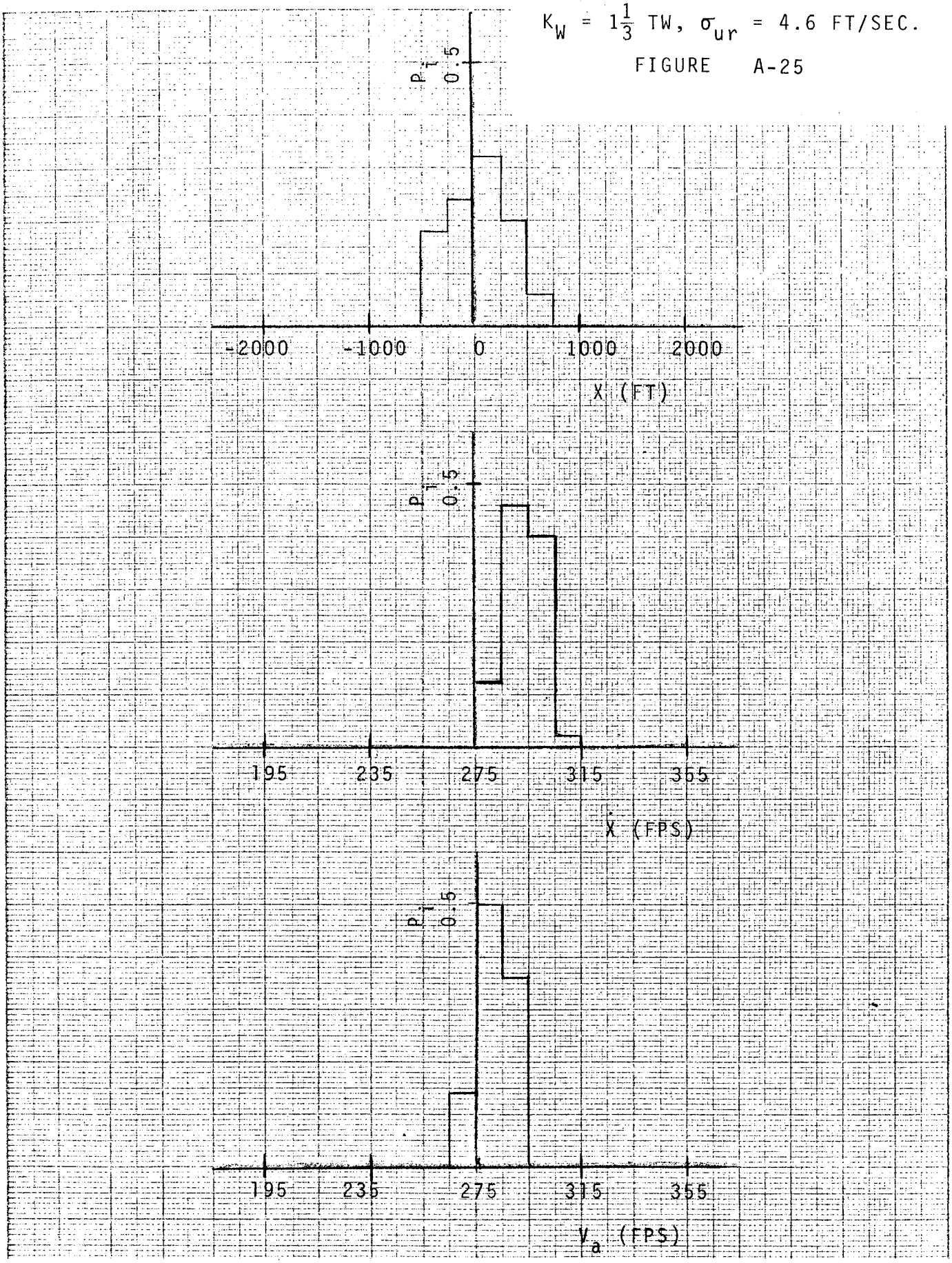

$K_W = 1\frac{1}{3}$ TW, σ_{ur} = 4.6 FT/SEC.

FIGURE A-26

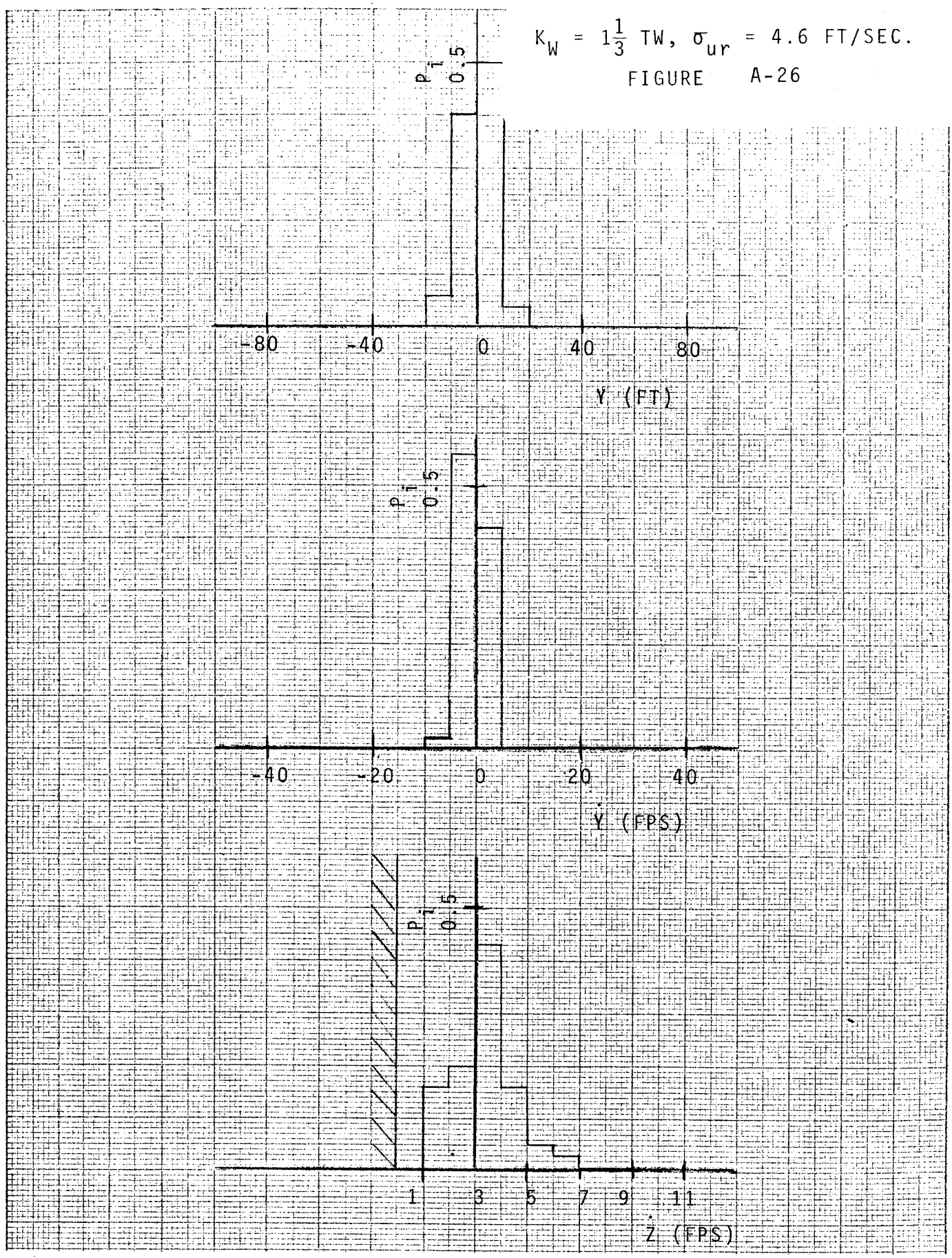

$K_W = 1\frac{1}{3}$ TW, σ_{ur} = 4.6 FT/SEC.

FIGURE A-27

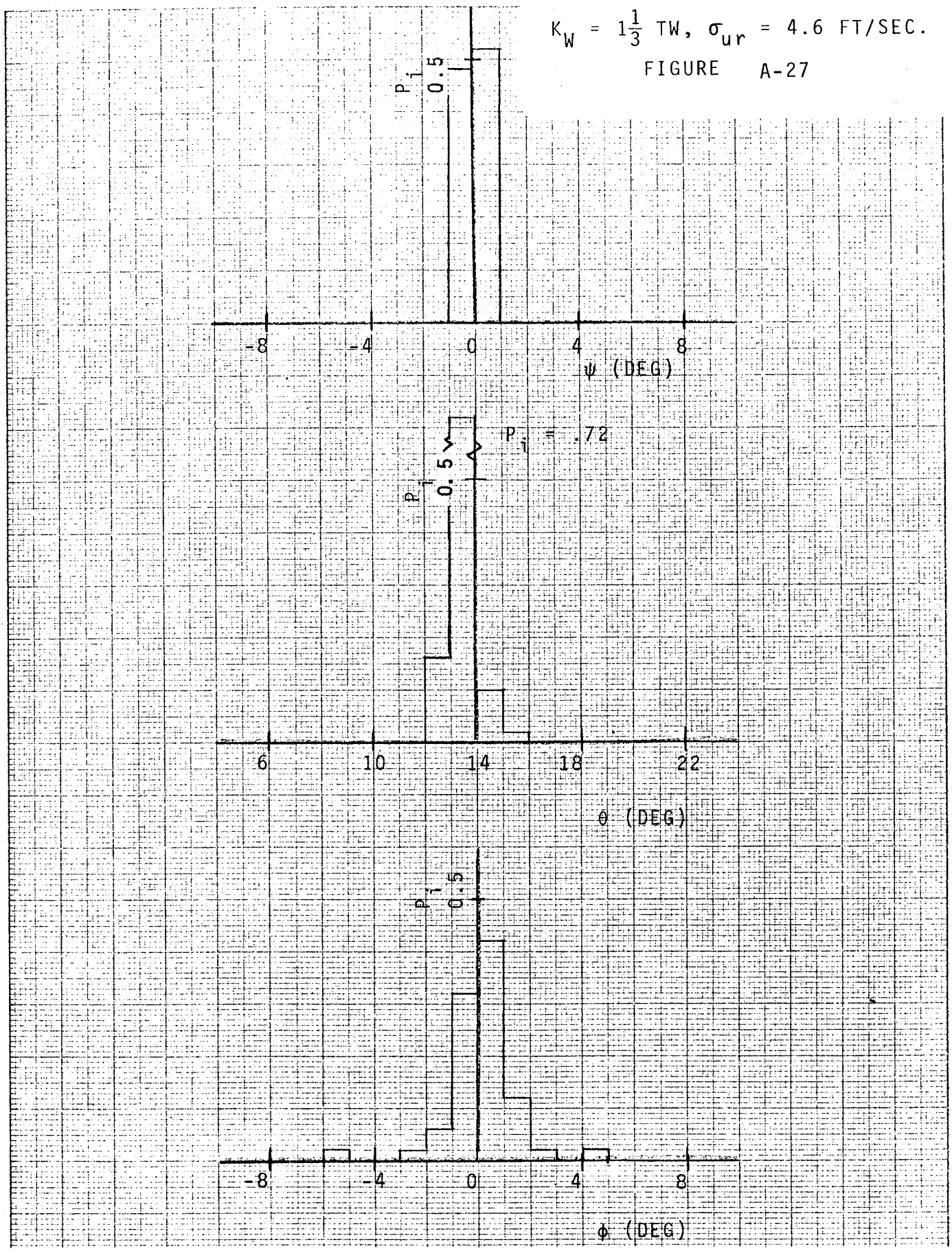

$K_W = 1\frac{1}{3}$ HW, σ_{ur} = 6.8 FT/SEC.

FIGURE A-28

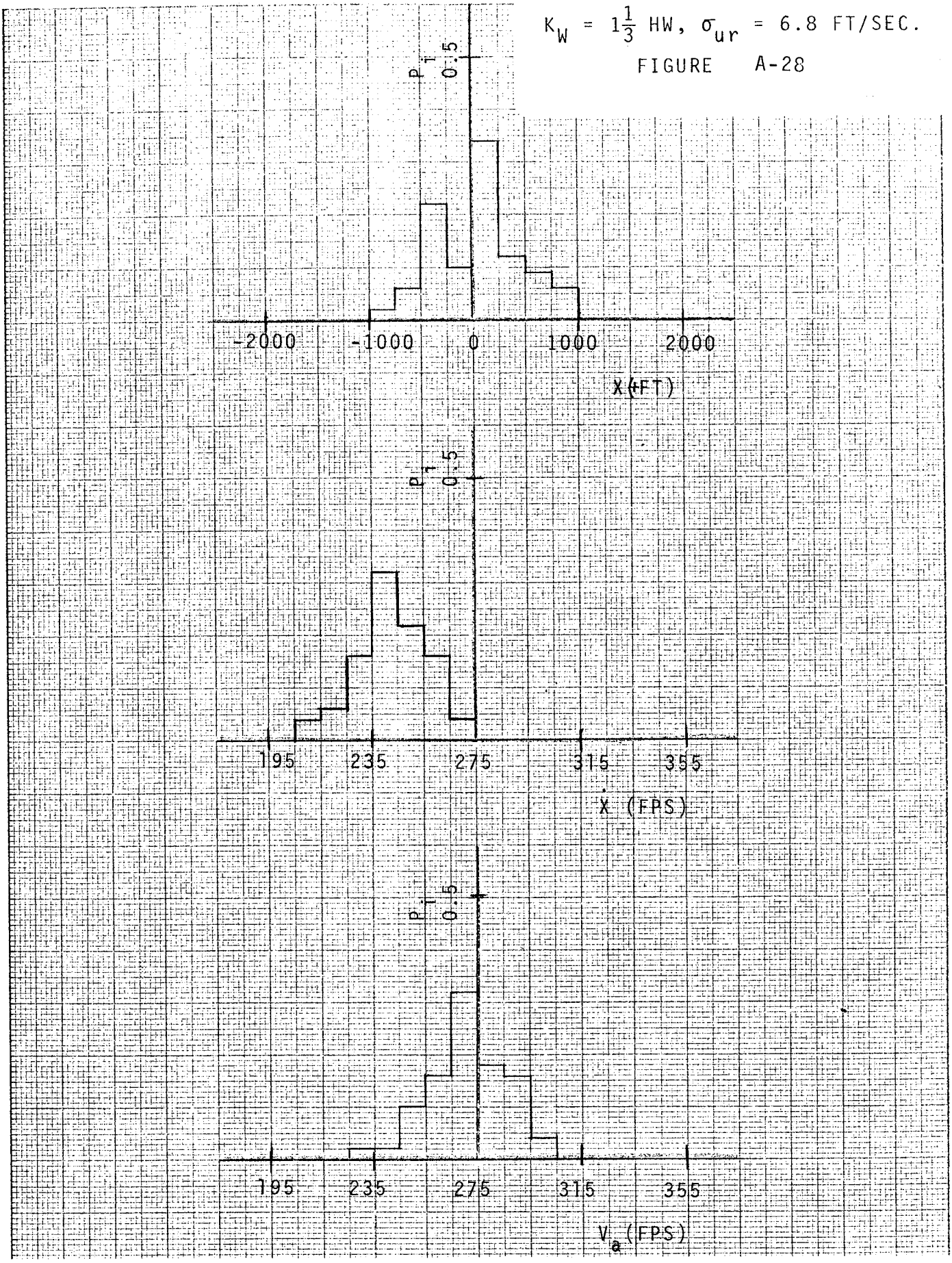

$K_W = 1\frac{1}{3}$ HW, σ_{ur} = 6.8 FT/SEC.

FIGURE A-29

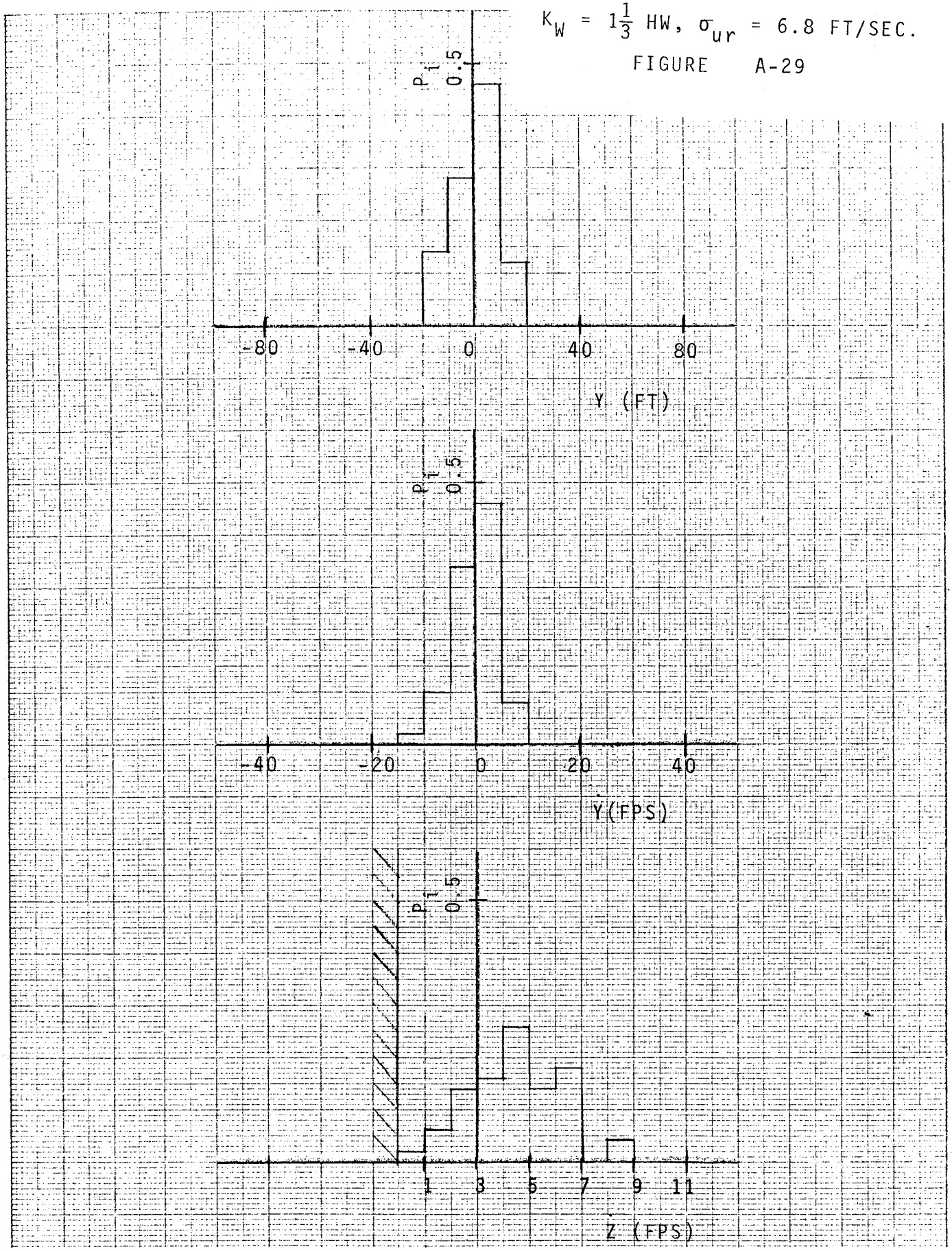

$K_W = 1\frac{1}{3}$ HW, σ_{ur} = 6.8 FT/SEC.

FIGURE A-30

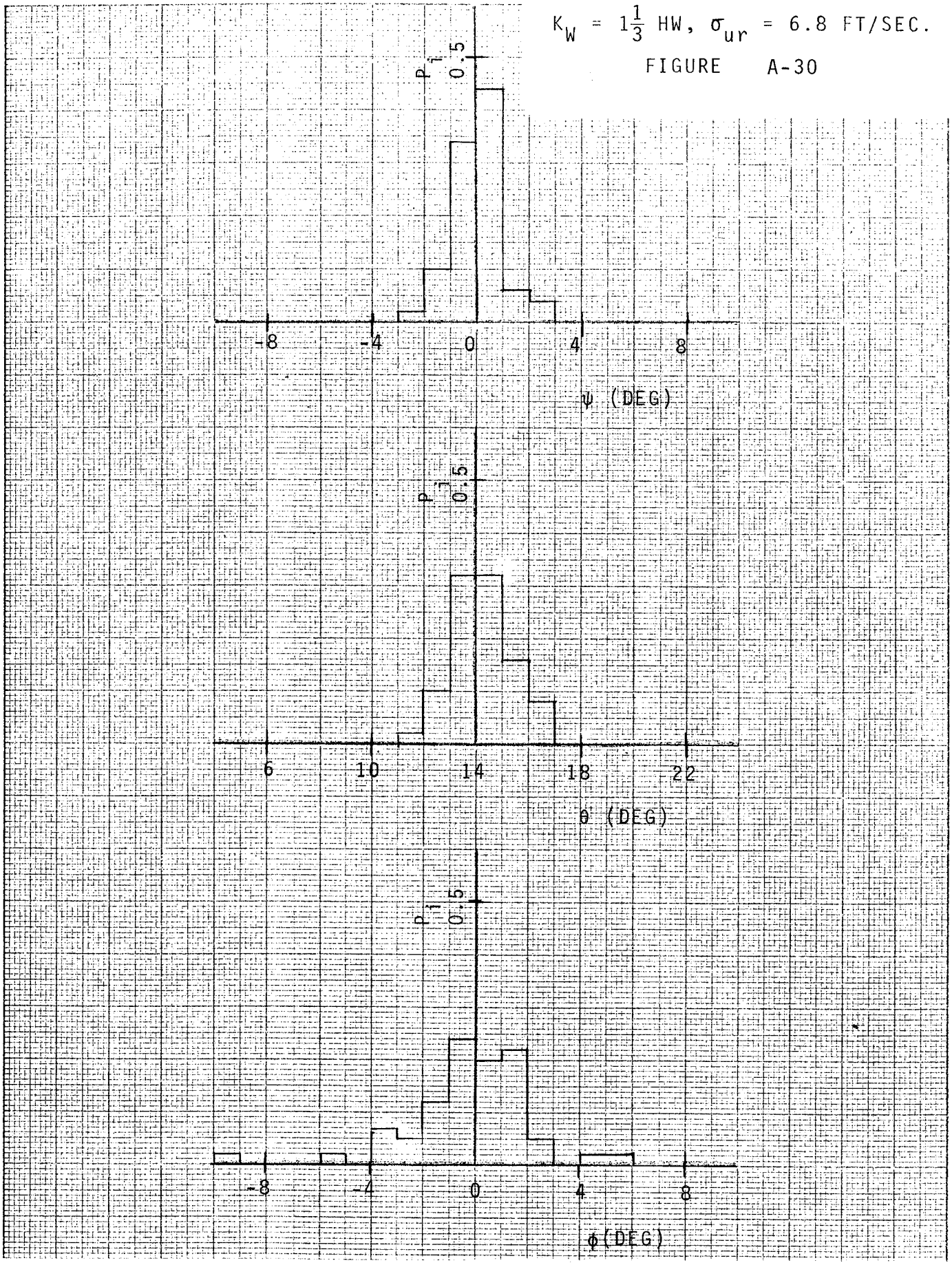

$K_W = 1\frac{1}{3}$ CW, σ_{ur} = 6.8 FT/SEC.

FIGURE A-31

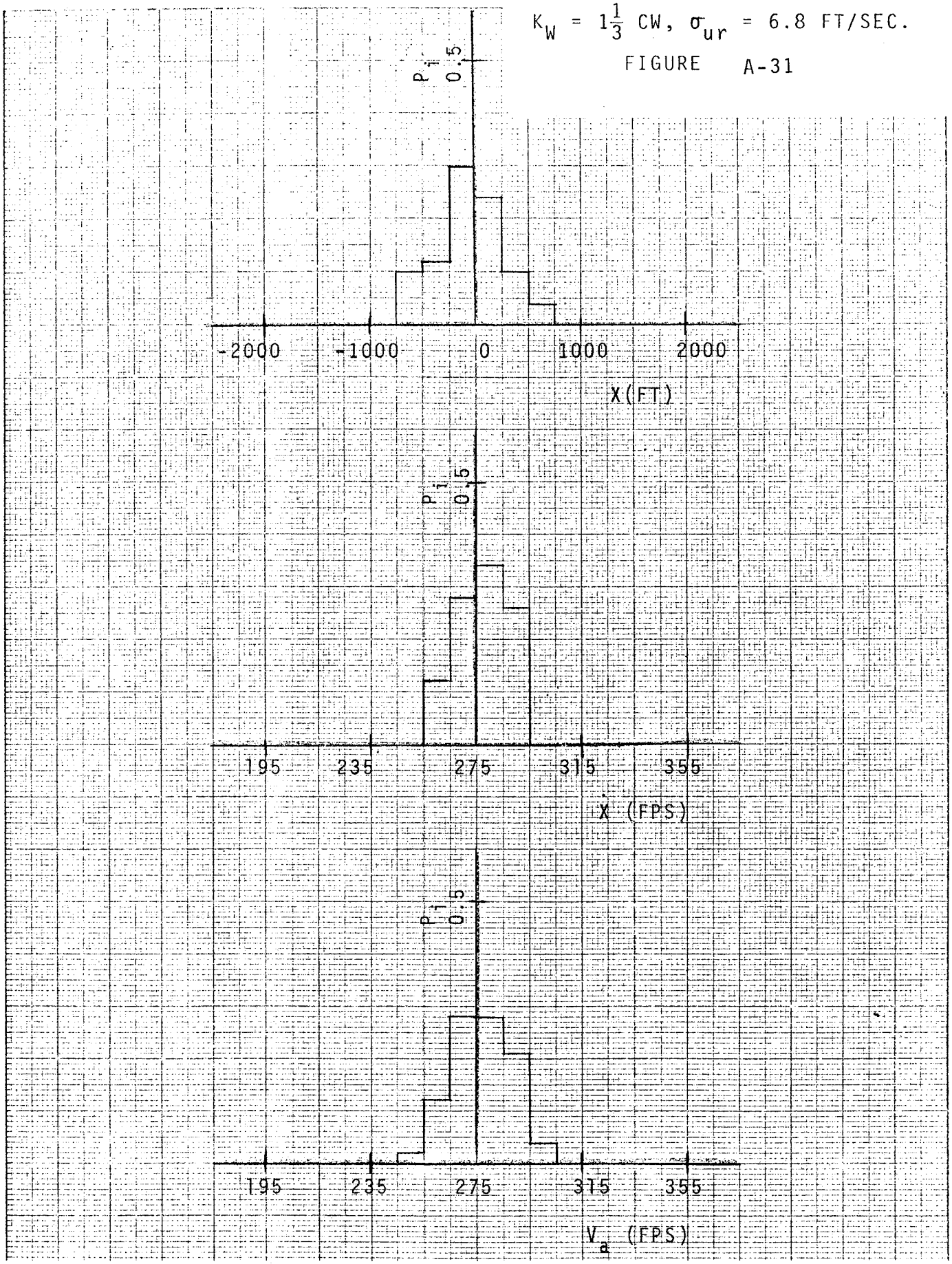

$K_W = 1\frac{1}{3}$ CW, σ_{ur} = 6.8 FT/SEC.

FIGURE A-32

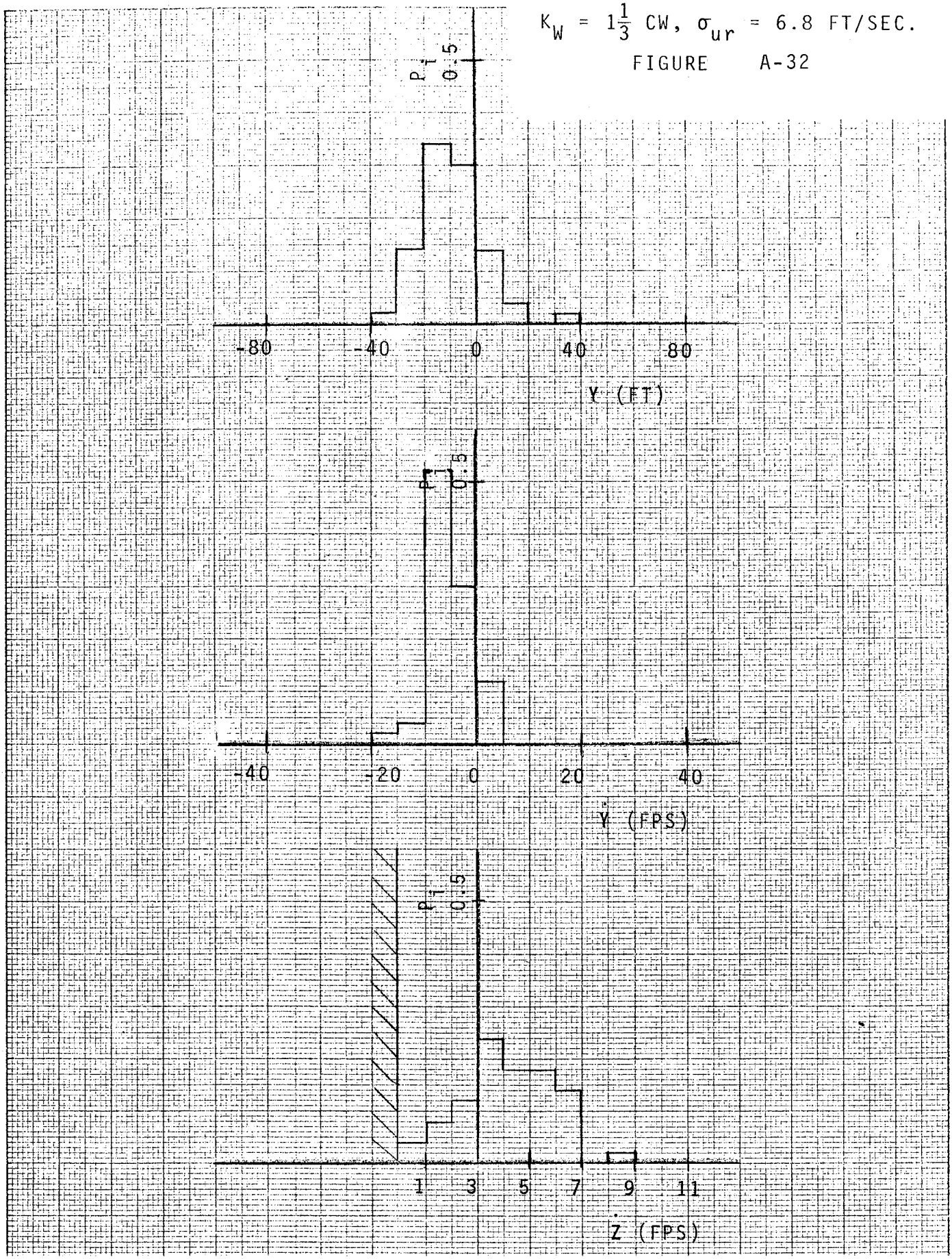

$K_W = 1\frac{1}{3}$ CW, σ_{ur} = 6.8 FT/SEC.

FIGURE A-33

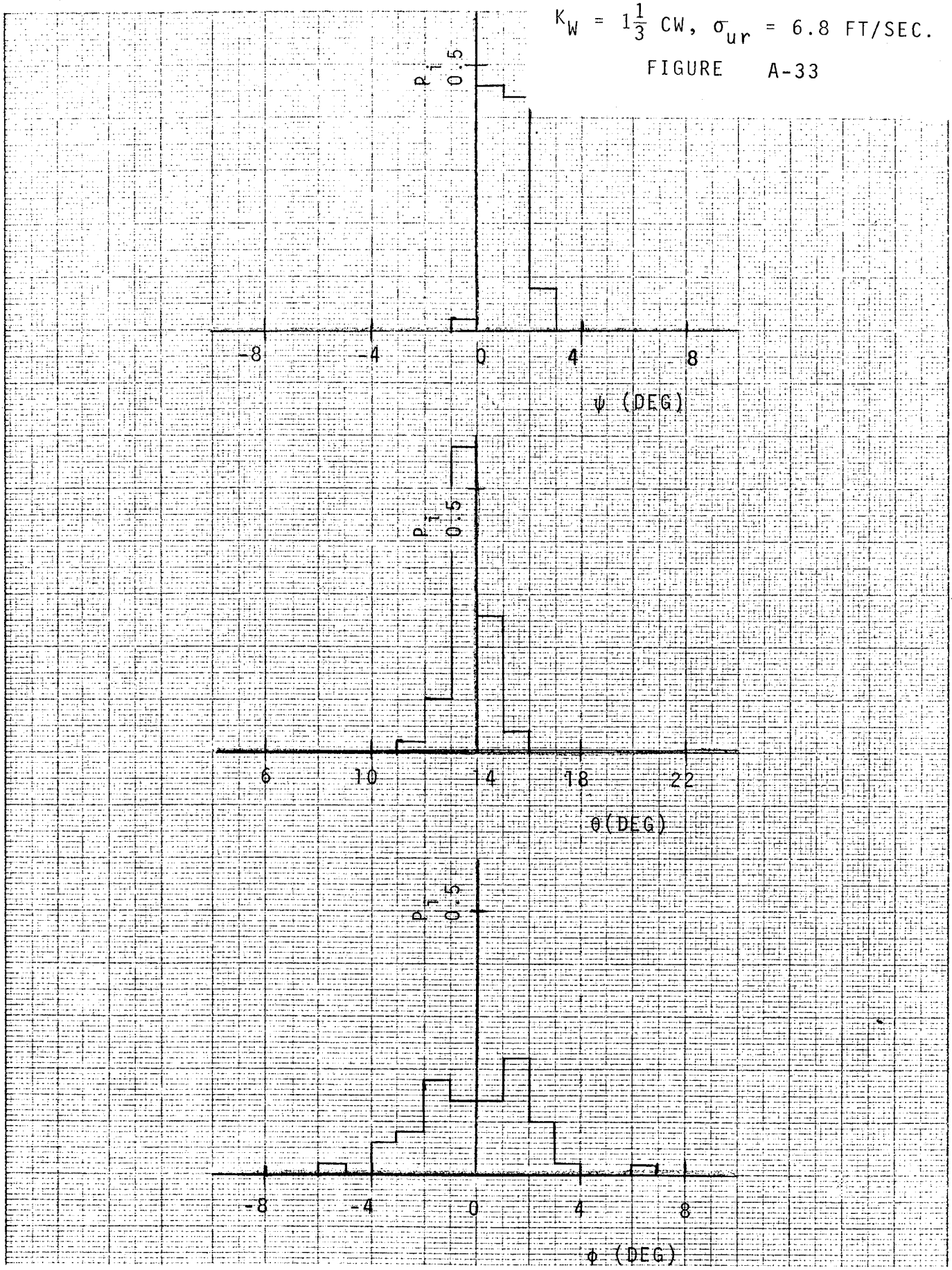

$K_W = 1\frac{1}{3}$ TW, $\sigma_{ur} = 6.8$ FT/SEC.

FIGURE A-34

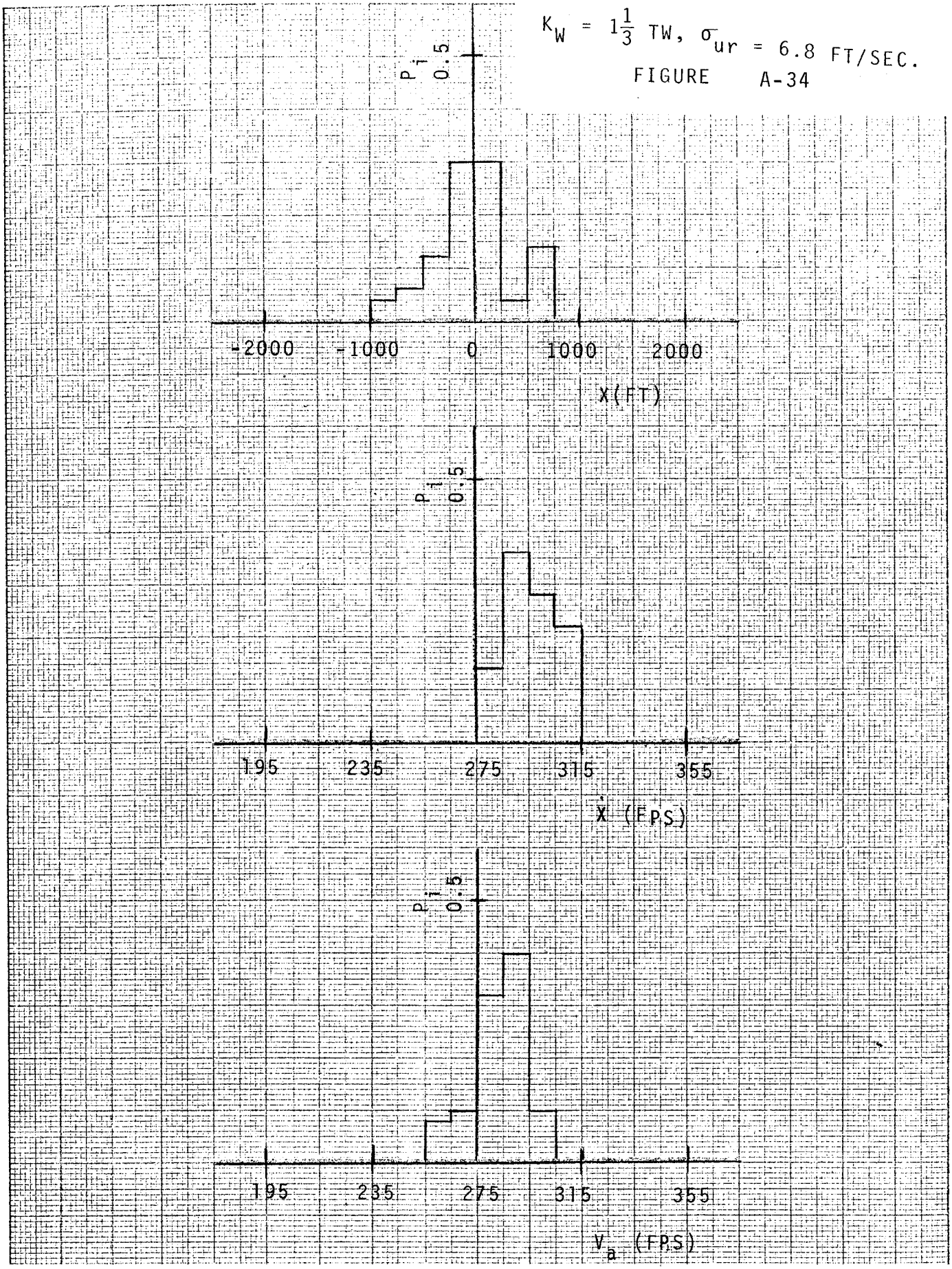

$K_W = 1\frac{1}{3}$ TW, σ_{ur} = 6.8 FT/SEC

FIGURE A-35

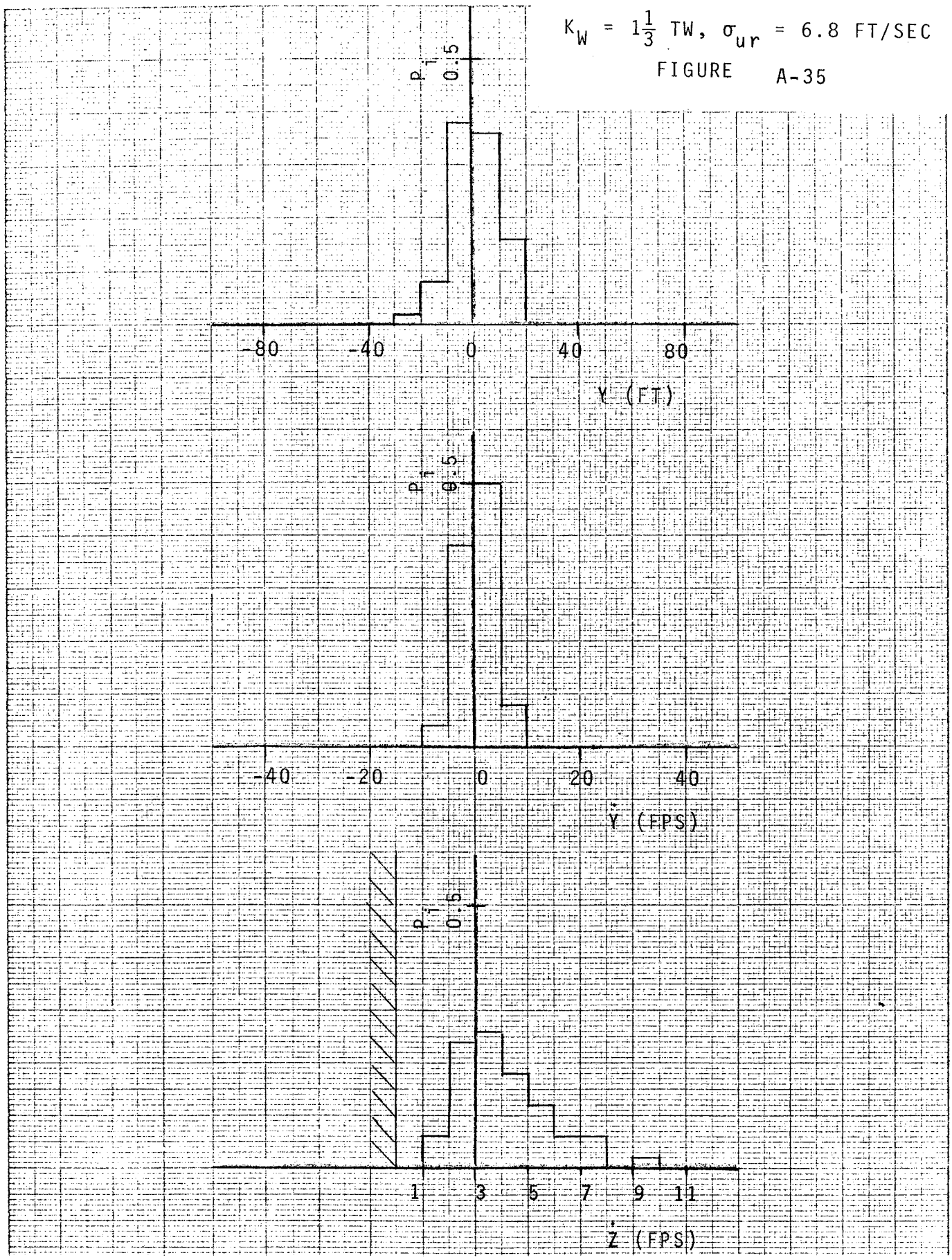

$K_W = 1\frac{1}{3}$ TW, σ_{ur} = 6.8 FT/SEC.

FIGURE A-36

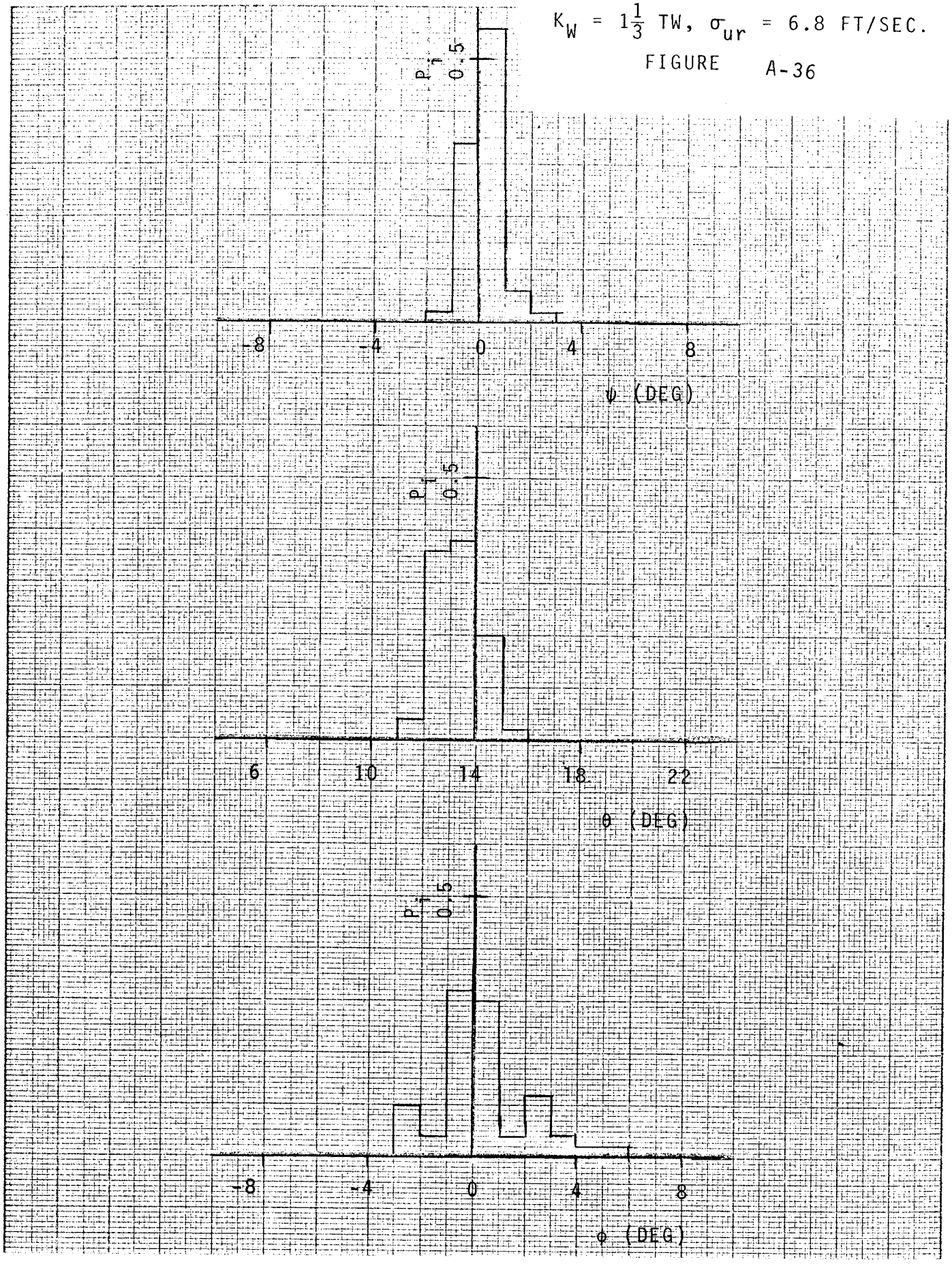

APPENDIX B

HISTOGRAMS OF RESULTS FOR MODIFIED SYSTEM

APPENDIX B

HISTOGRAMS OF RESULTS FOR MODIFIED SYSTEM

This appendix contains the histograms of 50 runs each for the SC117 Scanning Beam System and for the Precision Tracking Radar System. The system is the Modified System described in Section VIII.

These histograms are the results of the true Monte Carlo simulation tests. These are designated true Monte Carlo Runs since the wind magnitude (K_W), wind direction (ψ_W), and the standard deviation of the turbulence (σ_W) were randomly selected.

These histograms are discussed in Section VIII-E.

The figure numbers appropriate to the system and touchdown variable depicted are as follows:

Figure No.	System	TD Variables
B1	SC117 SBS	$X, \dot{X}, V_a$
B1(Cont.)	SC117 SBS	$Y, \dot{Y}, \dot{Z}$
B1(Cont.)	SC117 SBS	ψ, θ, ϕ
B2	PTR	$X, \dot{X}, V_a$
B2(Cont.)	PTR	$Y, \dot{Y}, \dot{Z}$
B2(Cont.)	PTR	ψ, θ, ϕ

The variables have the same meaning as those defined in Appendix A.

FIGURE B1 HISTOGRAMS FOR TRUE MONTE CARLO EVALUATION OF SC 117 SBS

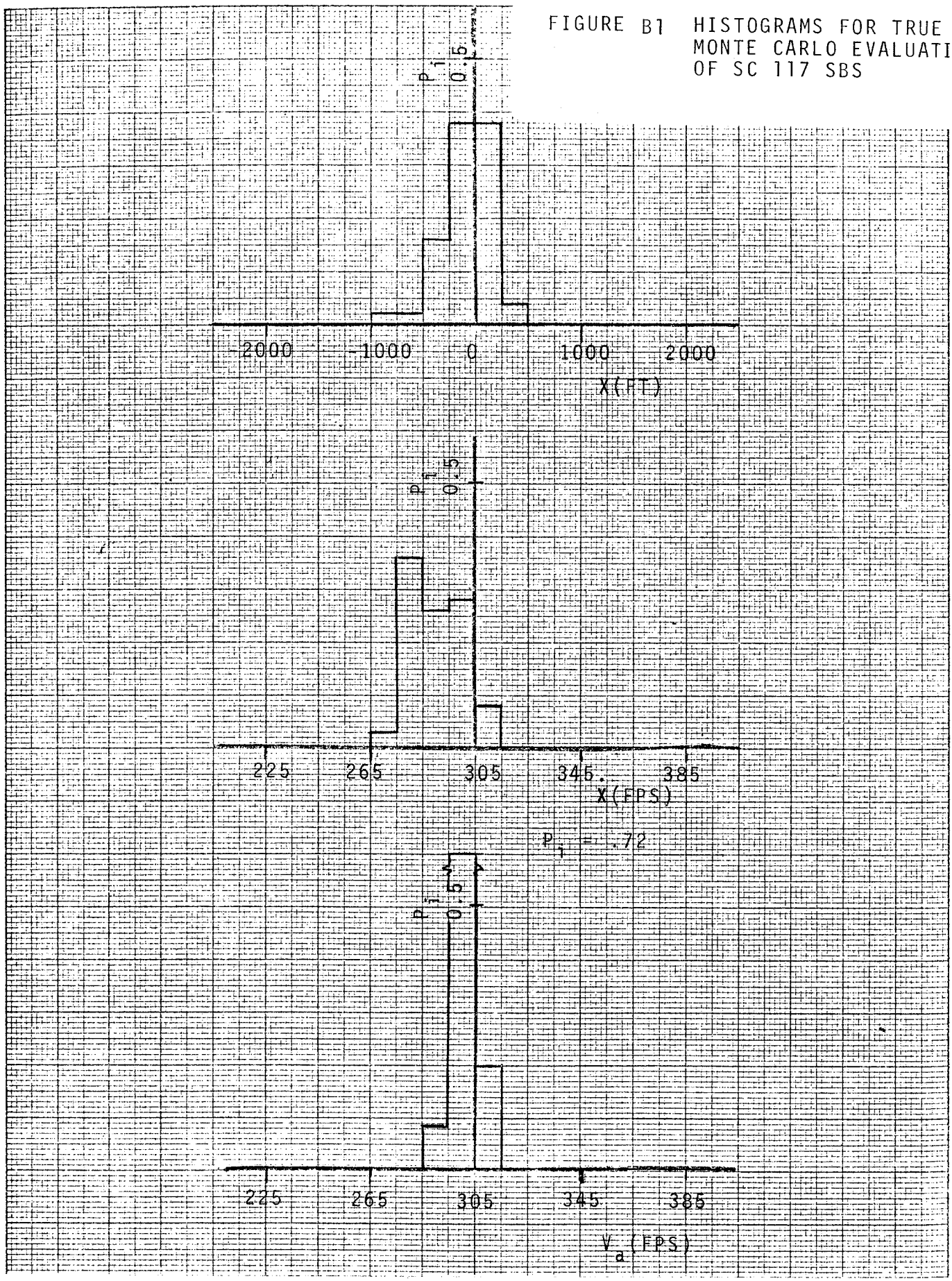

FIGURE B1 (CONTINUED)

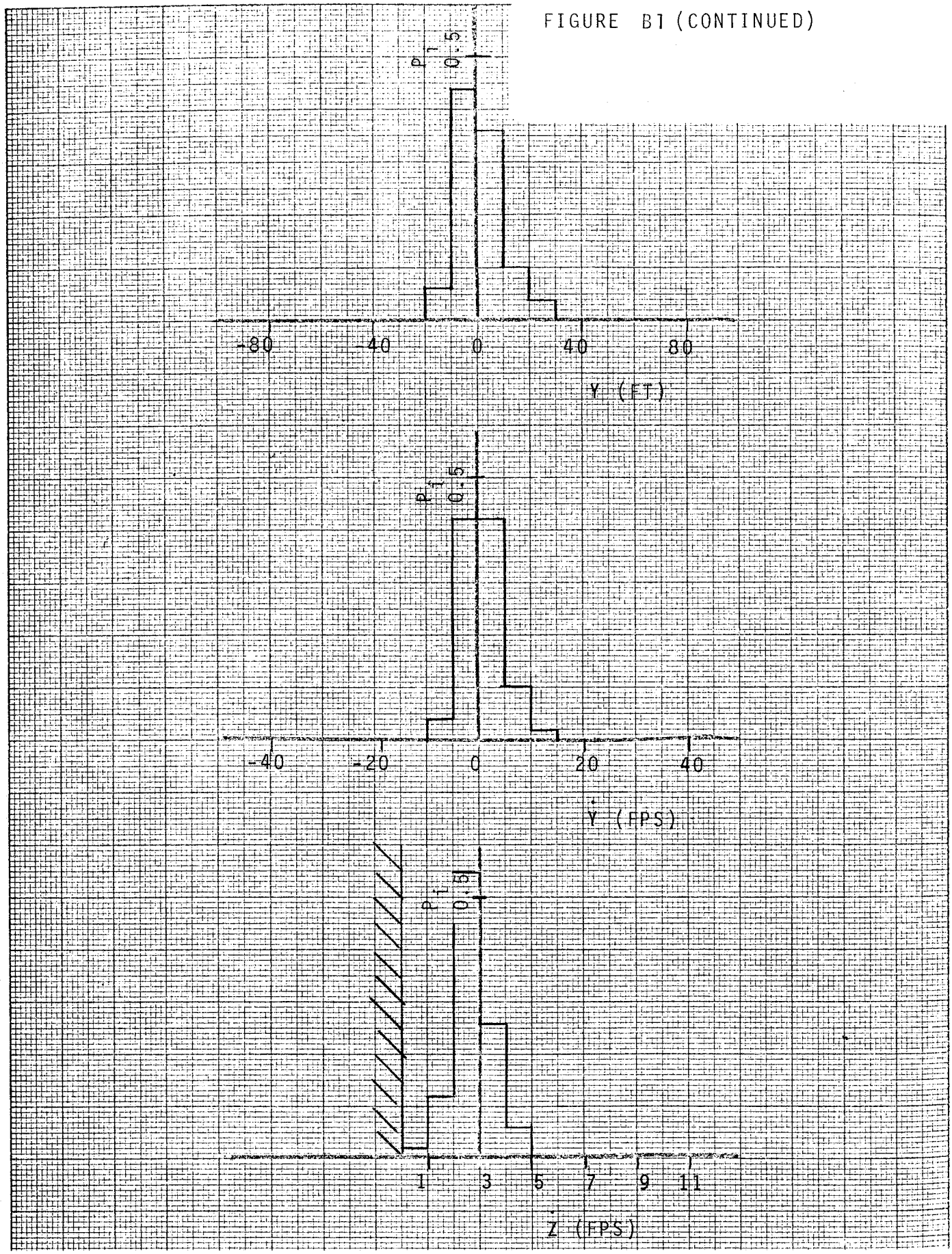

FIGURE B1 (CONTINUED

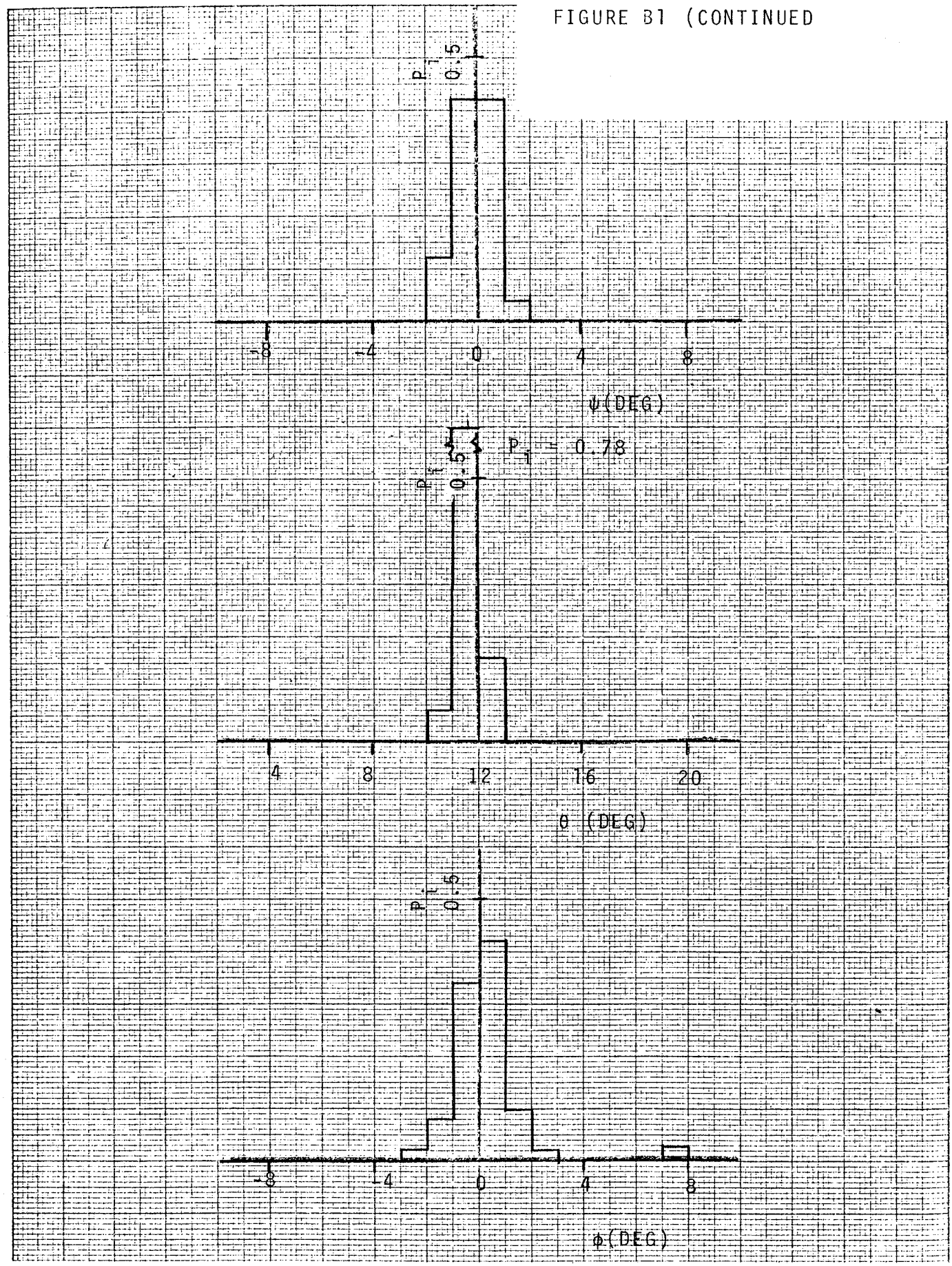

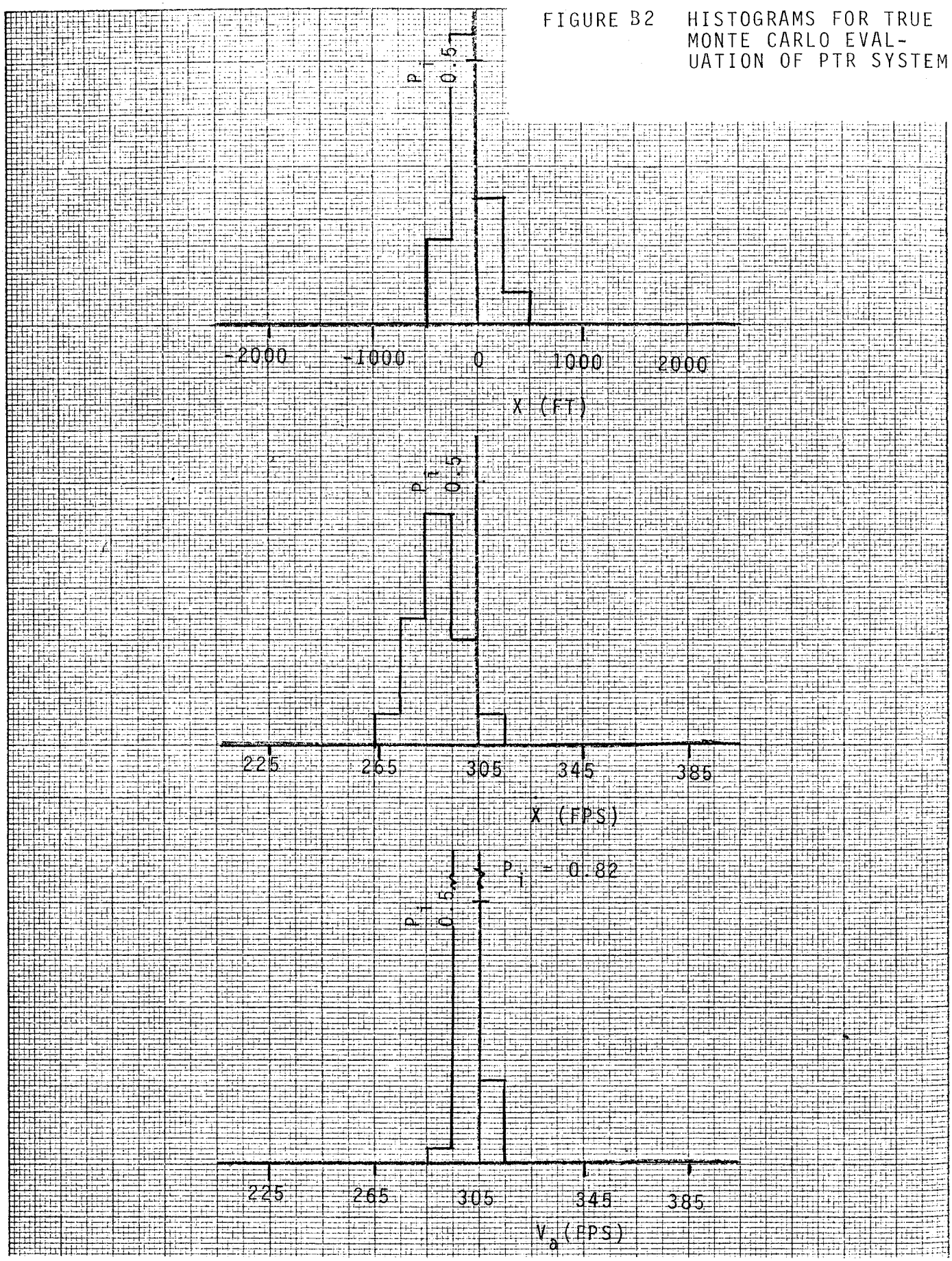

FIGURE B2 HISTOGRAMS FOR TRUE MONTE CARLO EVALUATION OF PTR SYSTEM

FIGURE B2 (CONTINUED)

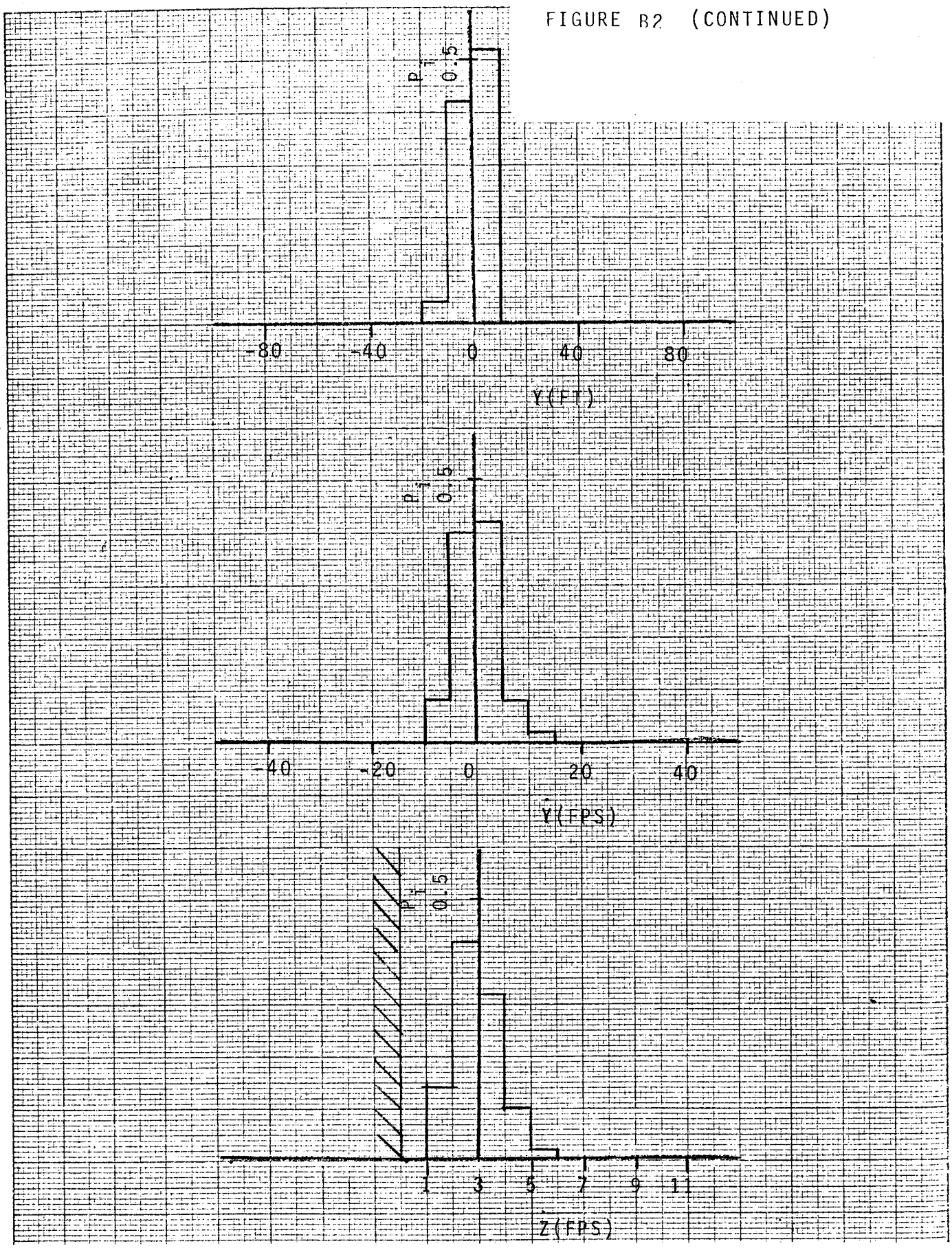

FIGURE B2 (CONTINUED)

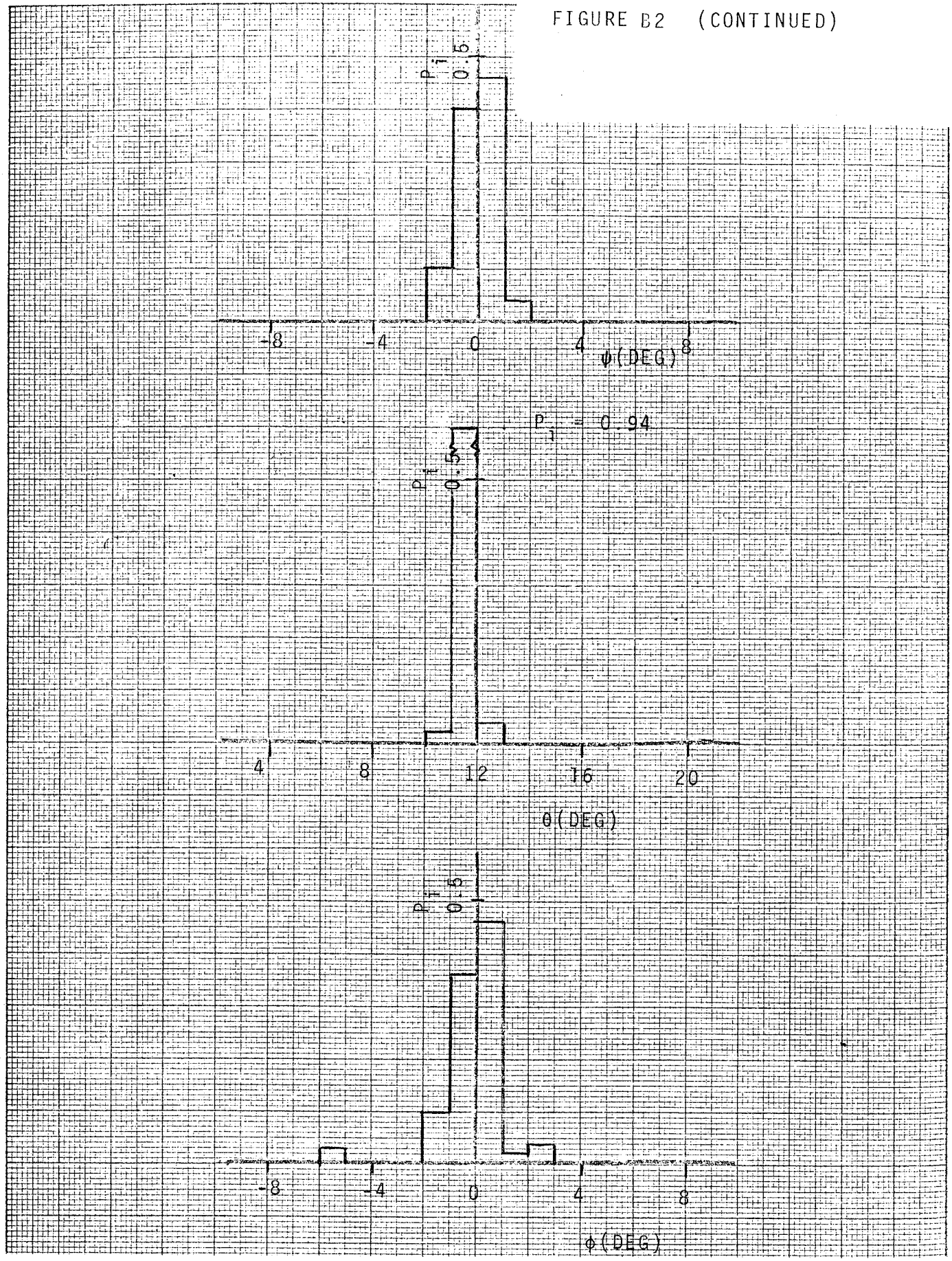

APPENDIX C

DATA BASE, MODELS AND CRITERIA

A. General.

This section describes the data, assumptions and models used in the simulation of the various tasks. This section also describes the criteria and specifications adopted as measures of performance. The order of presentation within this section is:

A. General

B. Vehicle

1. Physical Properties
2. Aerodynamics
3. Surface Actuator Models

C. Wind Model

D. Hardware Models

1. Precision Tracking Radar (TR)
2. Scanning Beam Systems (SBS)
3. Instrument Landing System (ILS)
4. Inertial Navigation System (INS)
5. Precision Ranging System (PRS)
6. Pitot Tube
7. Radar Altimeter

E. Initial State Errors and Initial State Estimation Errors

F. Performance Criteria

1. Touchdown Errors
2. Maneuver Constraints
3. Flight Control System Specifications

B. Vehicle.

1. Physical Properties.

Mass	6630 slugs
Reference Area	6084 ft^2
Lateral reference moment arm, $\bar{b}$	118.7 ft
Longitudinal reference moment arm, $\bar{c}$	68.4 ft
I_{xx}	3,348,000 slug-ft^2
I_{yy}	13,298,000 slug-ft^2
I_{zz}	14,426,000 slug-ft^2
I_{xz}	-53,000 slug-ft^2

2. Aerodynamics and Simulation.

Table C-1 defines the symbols used in the definition of the NADWO. Table C-2 lists the coefficient values used in this study for simulations of the vehicle. Table C-3 defines the sign convention.

Rigid body equations are used. The angular accelerations are computed in the body axis system as follows:

$$\dot{p} = \frac{I_{xz}}{I_{xx}} (\dot{r} + q\,p) + \frac{(I_{yy} - I_{zz})}{I_{xx}} r\,q + \Delta\dot{p}_a$$

$$\dot{q} = \frac{I_{xz}}{I_{yy}} (r^2 - p^2) + \frac{(I_{zz} - I_{xx})}{I_{yy}} r\,p + \Delta\dot{q}_a$$

$$\dot{r} = \frac{I_{xz}}{I_{zz}} (\dot{p} - r\,q) + \frac{(I_{xx} - I_{yy})}{I_{zz}} q\,p + \Delta\dot{r}_a$$

where: p is the body axis roll rate,

q is the body axis pitch rate, and

r is the body axis yaw rate

and where $\Delta\dot{p}_a$, $\Delta\dot{q}_a$, and $\Delta\dot{r}_a$ = components of angular acceleration due to aerodynamic forces.

The Euler rates equations for the conventional Euler angles in the sequence of yaw, pitch, and roll are:

$$\dot{\psi} = (r \cos \phi + q \sin \phi)/\cos \theta$$

$$\dot{\theta} = q \cos \phi - r \sin \phi$$

$$\dot{\phi} = p + \dot{\psi} \sin \theta$$

The translational accelerations due to forces are first computed in the body axis system. These are then converted to total accelerations in a runway inertial system as follows:

$$\begin{bmatrix} \ddot{X} \\ \ddot{Y} \\ \ddot{Z} \end{bmatrix} = \begin{bmatrix} C\psi C\theta & C\psi S\theta S\phi - S\psi C\phi & C\psi S\theta C\phi + S\psi S\phi \\ S\psi C\theta & S\psi S\theta S\phi + C\psi C\phi & S\psi S\theta C\phi - C\psi S\phi \\ -S\theta & C\theta S\phi & C\theta C\phi \end{bmatrix} \begin{bmatrix} \Delta\dot{u}_a \\ \Delta\dot{v}_a \\ \Delta\dot{w}_a \end{bmatrix} + \begin{bmatrix} 0 \\ 0 \\ 1 \end{bmatrix} g$$

where: $\Delta\dot{u}_a$, $\Delta\dot{v}_a$, $\Delta\dot{w}_a$ = components of translational body axis accelerations due to forces

g = gravity.

This deviates somewhat from the more standard procedure of computing total translational accelerations in the body axis system, integrating these to obtain body axis velocities and then converting to inertial velocities. The conversion is done at the acceleration level in this program because inertial accelerations are required in the simulation of the inertial navigation system.

The translational body axis accelerations components due to forces are computed from the aerodynamic and thrust terms as,

$$\dot{\Delta u} = \dot{\Delta u}_a + \frac{T \cos \theta_T}{m}$$

$$\dot{\Delta v} = \dot{\Delta v}_a$$

$$\dot{\Delta w} = \dot{\Delta w}_a - \frac{T \cos \theta_T}{m}$$

where: $\dot{\Delta u}_a$, $\dot{\Delta v}_a$, $\dot{\Delta w}_a$ = components of translational body axis accelerations due to aerodynamic forces.

The inertial acceleration due to gravity is computed as

$$g = g_{s\ell} \left(\frac{r_e}{r_e + h}\right)^2$$

where $g_{s\ell}$ is the gravitational constant at sea level, r_e is the earth's radius and h is the vehicle's altitude.

The total body axis acceleration components are computed by converting the stability axis terms to the body axis and summing these with the body axis terms as follows:

$$\Delta\dot{p}_a = \frac{1}{I_{xx}} (\Delta L_m + \Delta L_m^s \cos \alpha - \Delta N_m^s \sin \alpha)$$

$$\Delta\dot{q}_a = \frac{1}{I_{yy}} (\Delta M_m)$$

$$\Delta\dot{r}_a = \frac{1}{I_{zz}} (\Delta N_m + \Delta N_m^s \cos \alpha + \Delta L_m^s \sin \alpha)$$

$$\Delta\dot{u} = \frac{1}{m} (\Delta D + \Delta D^s \cos \alpha - \Delta L^s \sin \alpha)$$

$$\Delta\dot{v} = \frac{1}{m} (\Delta C)$$

$$\Delta\dot{w} = \frac{1}{m} (\Delta L + \Delta L^s \cos \alpha + \Delta D^s \sin \alpha).$$

where the superscript s indicates that the force or moment is computed from aerodynamic characteristics in the stability axis system.

The aerodynamic forces and moments which are included in the simulation program and the manner and coordinate system in which they are computed are as follows:

$$\Delta L^s_{m\beta} = Q_a S b C_{\ell\beta} \beta$$

$$\Delta L^s_{m\delta_a} = Q_a S b C_{\ell\delta_a} \delta_a$$

$$\Delta L^s_{m\delta_r} = Q_a S b C_{\ell\delta_r} \delta_r$$

$$\Delta L^s_{mp} = Q_a S b^2 C_{\ell p} p/(2V_a)$$

$$\Delta L^s_{mr} = Q_a S b^2 C_{\ell r} r/(2V_a)$$

$$\Delta M_{m\alpha} = Q_a S c C_m$$

$$\Delta M_{m\delta_e} = Q_a S c \Delta C_{m\delta_e}$$

$$\Delta M_{mq} = Q_a S c^2 C_{mq} q/(2V_a)$$

$$\Delta M_{m\dot{\alpha}} = Q_a S c^2 C_{m\dot{\alpha}} \dot{\alpha}/(2V_a)$$

$$\Delta M_{mge} = Q_a S c \Delta C_{mge}$$

$$\Delta N^s_{m\beta} = Q_a S b C_{n\beta} \beta$$

$$\Delta N^s_{m\delta_r} = Q_a S b C_{n\delta_r} \delta_r$$

$$\Delta N^s_{m\delta_a} = Q_a S b C_{n\delta_a} \delta_a$$

$$\Delta N^s_{mr} = Q_a S b^2 C_{nr} r/(2V_a)$$

$$\Delta N^s_{mp} = Q_a S b^2 C_{np} p/(2V_a)$$

$$\Delta D^s_{\alpha} = -Q_a S \Delta C_{Da}$$

$$\Delta D^s_{\delta_e} = -Q_a S \Delta C_{D\delta_e}$$

$$\Delta D_{ge} = -Q_a S \Delta C_{a\ ge}$$

$$\Delta D^s_{\ell g} = -Q_a S \Delta C^s_{D\ell g}$$

$$\Delta C_{\beta} = Q_a S C_{y\beta} \beta$$

$$\Delta C_{\delta r} = Q_a S C_{y\delta_r} \delta r$$

$$\Delta L^s_{\alpha} = -Q_a S \Delta C_{L\alpha}$$

$$\Delta L^s_{\delta e} = -Q_a S \Delta C_{L\delta_e}$$

$$\Delta L^s_{q} = -Q_a S c C_{Lq} q/(2V_a)$$

$$\Delta L^s_{\dot{a}} = -Q_a S c C_{L_{\dot{a}}} \dot{\alpha}/(2V_a)$$

$$\Delta L_{ge} = -Q_a S \Delta C_{n\ ge}$$

TABLE C-1

LIST OF AERO SYMBOLS

C_L	Untrimmed lift coefficient, $f(\alpha)$
C_D	Untrimmed drag coefficient, $f(\alpha)$
C_M	Pitching moment coefficient at zero elevon, $f(\alpha)$
$\Delta C_{L_{\delta_e}}$	Incremental lift coefficient due to elevon $f(\alpha, \delta_e)$
$\Delta C_{D_{\delta_e}}$	Incremental drag coefficient due to elevon $f(\alpha, \delta_e)$
$C_{M_{\delta_e}}$	Slope of pitching moment coefficient due to elevon, $f(\alpha, \delta_e)$
C_{L_q}	Lift damping derivative due to pitch rate, $f(\alpha)$
C_{M_q}	Pitch damping derivative due to pitch rate, $f(\alpha)$
$C_{L_{\dot{\alpha}}}$	Lift derivative due to angle of attack rate(plunge) $(\dot{\alpha})$, $f(\alpha)$
$C_{M_{\dot{\alpha}}}$	Pitch derivative due to angle of attack rate(plunge) $(\dot{\alpha})$, $f(\alpha)$
$\Delta C_{N_{ge}}$	Incremental lift coefficient due to ground effects, $f(\alpha, h)$
$\Delta C_{a_{ge}}$	Incremental drag coefficient due to ground effects, $f(\alpha, h)$
$\Delta C_{M_{ge}}$	Incremental pitching moment coefficient due to ground effects, $f(\alpha, h)$
$\Delta C_{L_{lg}}$	Incremental lift coefficient due to landing gear
$\Delta C_{D_{lg}}$	Incremental drag coefficient due to landing gear
$\Delta C_{M_{lg}}$	Incremental pitching moment coefficient due to landing gear
C_{Y_β}	Slope of sideforce coefficient due to sideslip, $f(\alpha)$
C_{ℓ_β}	Slope of rolling moment coefficient due to sideslip $f(\alpha)$
C_{N_β}	Slope of yawing moment coefficient due to sideslip, $f(\alpha)$
$C_{Y_{\delta_a}}$	Slope of sideforce coefficient due to aileron, $f(\alpha)$
$C_{\ell_{\delta_a}}$	Slope of rolling moment coefficient due to aileron, $f(\alpha)$
$C_{N_{\delta_a}}$	Slope of yawing moment coefficient due to aileron, $f(\alpha)$

TABLE C-1 (Continued)

$C_{Y_{\delta_r}}$	Slope of sideforce coefficient due to rudder, $f(\alpha)$
$C_{\ell_{\delta_r}}$	Slope of rolling moment coefficient due to rudder, $f(\alpha)$
$C_{N_{\delta_r}}$	Slope of yawing moment coefficient due to rudder, $f(\alpha)$
C_{ℓ_p}	Roll damping derivative to roll rate, $f(\alpha)$
C_{ℓ_r}	Roll damping derivative due to yaw rate, $f(\alpha)$
C_{N_p}	Yaw damping derivative due to roll rate, $f(\alpha)$
C_{N_r}	Yaw damping derivative due to yaw rate $f(\alpha)$

TABLE C-2

NADWO AERO DATA

EFFECT	ANGLE OF ATTACK			ELEVON											
COEFFICIENT	C_L	C_D	C_M	$\Delta C_{L_{\delta_e}}$						$\Delta C_{D_{\delta_e}}$					
AXIS SYSTEM	SA	SA	SA	SA						SA					
UNITS															
				δ_e=-40	-30	-20	-10	0	10	δ_e=-40	-30	-20	-10	0	10
α = 0	-0.05	0.015	0.014	-0.420	-0.400	-0.300	-0.150	0	0.150	0.076	0.059	0.034	0.007	0	0.007
5	0.15	0.020	-0.020	-0.435	-0.405	-0.295	-0.150	0	0.150	0.051	0.034	0.014	-0.002	0	0.020
10	0.35	0.037	-0.054	-0.450	-0.410	-0.285	-0.145	0	0.145	0.006	-0.009	-0.020	-0.020	0	0.031
15	0.54	0.070	-0.080	-0.465	-0.410	-0.275	-0.140	0	0.140	-0.034	-0.042	-0.045	-0.030	0	0.037
20	0.74	0.170	-0.103	-0.465	-0.400	-0.260	-0.130	0	0.130	-0.082	-0.086	-0.078	-0.044	0	0.043
25	0.91	0.370	-0.127	-0.465	-0.370	-0.240	-0.120	0	0.120	-0.128	-0.127	-0.103	-0.054	0	0.049
30	1.03	0.600	-0.141	-0.450	-0.330	-0.220	-0.110	0	0.110	-0.149	-0.142	-0.113	-0.063	0	0.051
35	1.08	0.750	-0.144	-0.370	-0.290	-0.190	-0.100	0	0.100	-0.163	-0.152	-0.121	-0.065	0	0.051

SA - Stability axes

TABLE C-2 (CONTINUED)

EFFECT	ELEVON (CONT.)						DAMPING		PLUNGE		GROUND EFFECTS							
COEFFICIENT	$C_{M_{\delta_e}} \times 10^2$						C_{L_q}	C_{M_q}	$C_{L_{\dot{\alpha}}}$	$C_{M_{\dot{\alpha}}}$	$\Delta C_{N_{ge}}$							
AXIS SYSTEM	SA						SA	SA	SA	SA	BA							
UNITS	-						1/rad	1/rad	1/rad	1/rad	-							
	δ_e=-40	-30	-20	-10	0	10					h = 0	11.86	23.72	35.58	47.44	71.16	94.88	≥118.6
α = 0	-.458	-.537	-.598	-.637	-.650	-.637	1.79	-1.30	3.05	0.415	0	0	0	0	0	0	0	0
5	-.458	-.537	-.598	-.637	-.650	-.637	1.79	-1.30	3.05	0.415	0.0240	0.0240	0.0162	0.0095	0.0062	0.0028	0.0013	0
10	-.458	-.537	-.598	-.637	-.650	-.637	1.79	-1.30	3.05	0.415	0.0481	0.0481	0.0325	0.0191	0.0124	0.0054	0.0025	0
15	-.451	-.529	-.589	-.628	-.640	-.628	2.06	-1.30	3.55	0.370	0.0722	0.0722	0.0488	0.0286	0.0186	0.0084	0.0038	0
20	-.444	-.521	-.580	-.618	-.630	-.618	2.20	-0.98	4.60	0.280	0.0965	0.0965	0.0651	0.0381	0.0248	0.0112	0.0051	0
25	-.423	-.496	-.552	-.588	-.600	-.588	2.16	-0.88	5.15	0.230	0.1203	0.1203	0.0815	0.0477	0.0310	0.0140	0.0064	0
30	-.402	-.471	-.525	-.558	-.570	-.558	2.08	-0.77	5.40	0.175	0.1444	0.1444	0.0976	0.0572	0.0372	0.0168	0.0076	0
35	-.374	-.439	-.487	-.519	-.530	-.519	1.90	-0.60	5.20	0.095	0.1683	0.1683	0.1137	0.0667	0.0434	0.0196	0.0089	0

SA - Stability Axes

BA - Body Axes

TABLE C-2 (CONTINUED)

EFFECT	GROUND EFFECTS (CONTINUED)															
COEFFICIENT	$\Delta C_{a_{ge}}$								$\Delta C_{M_{ge}} \times 10^2$							
AXIS SYSTEM	BA								BA							
UNITS	-								-							
	h = 0	11.86	23.72	35.58	47.44	71.16	94.88	118.6	h = 0	11.86	23.72	35.58	47.44	71.16	94.88	118.6
α = 0	0	0	0	0	0	0	0	0	0	0	0	0	0	0	0	0
5	0.0041	0.0041	0.0026	0.0017	0.0010	0.0005	0.0002	0	-0.38	-0.38	-0.24	-0.15	-0.10	-0.05	-0.02	0
10	0.0167	0.0167	0.0104	0.0067	0.0043	0.0020	0.0009	0	-0.77	-0.77	-0.48	-0.30	-0.20	-0.09	-0.04	0
15	0.0376	0.0376	0.0234	0.0150	0.0096	0.0044	0.0020	0	-1.16	-1.16	-0.72	-0.45	-0.30	-0.14	-0.06	0
20	0.0670	0.0670	0.0416	0.0267	0.0171	0.0078	0.0036	0	-1.55	-1.55	-0.96	-0.60	-0.40	-0.19	-0.08	0
25	0.1020	0.1020	0.0648	0.0415	0.0266	0.0123	0.0055	0	-1.94	-1.94	-1.20	-0.75	-0.50	-0.23	-0.10	0
30	0.1504	0.1504	0.0936	0.0600	0.0384	0.0176	0.0080	0	-2.32	-2.32	-1.44	-0.90	-0.60	-0.28	-0.12	0
35	0.2050	0.2050	0.1275	0.0815	0.0523	0.0240	0.0109	0	-2.71	-2.71	-1.68	-1.05	-0.70	-0.33	-0.14	0

BA - Body Axes

TABLE C-2 (CONTINUED)

EFFECT	LANDING GEAR			BETA			AILERON & RUDDER						DAMPING			
COEFFICIENT	$\Delta C_{L_{lg}}$	$\Delta C_{D_{lg}}$	$\Delta C_{M_{lg}}$	$C_{Y_{\beta_2}}$ X 10^2	$C_{L_{\beta_2}}$ X 10^2	$C_{N_{\beta_2}}$ X 10^2	$C_{Y_{\delta_a}}$	$C_{L_{\delta a_2}}$ X 10^2	$C_{N_{\delta a_2}}$ X 10^2	$C_{Y_{\delta r_2}}$ X 10^2	$C_{L_{\delta r_2}}$ X 10^2	$C_{N_{\delta r_2}}$ X 10^2	C_{L_p}	C_{L_r}	C_{N_p}	C_{N_r}
AXIS SYSTEM	SA	SA	BA	SA	SA	SA	SA	SA	SA	BA	SA	SA	SA	SA	SA	SA
UNITS	-	-	-	1/deg	1/deg	1/deg	1/deg	1/deg	1/deg	1/deg	1/deg	1/deg	1/rad	1/rad	1/rad	1/rad
α = 0	0	0.015	0	-0.70	-0.10	0.06	0	0.210	-0.040	0.47	0.15	-0.18	-0.130	0.375	0.03	-0.13
5	0	0.015	0	-0.75	-0.29	0.10	0	0.202	-0.046	0.46	0.14	-0.18	-0.135	0.373	-0.05	-0.12
10	0	0.015	0	-0.75	-0.37	0.09	0	0.195	-0.054	0.45	0.13	-0.18	-0.140	0.370	-0.12	-0.11
15	0	0.015	0	-0.75	-0.37	0.05	0	0.188	-0.065	0.40	0.10	-0.18	-0.155	0.352	-0.19	-0.14
20	0	0.015	0	-0.85	-0.28	0.01	0	0.180	-0.075	0.30	0.06	-0.17	-0.180	0.320	-0.26	-0.18
25	0	0.015	0	-1.25	-0.16	-0.08	0	0.168	-0.078	0.26	0.02	-0.15	-0.190	0.225	-0.33	-0.28
30	0	0.015	0	-1.70	-0.06	-0.31	0	0.144	-0.080	0.24	-0.01	-0.11	-0.200	0.175	-0.40	-0.37
35	0	0.015	0	-1.95	-0.04	-0.27	0	0.100	-0.081	0.31	-0.02	-0.10	-0.210	0.200	-0.42	-0.43

SA - Stability Axes

TABLE C-3

SIGN CONVENTION

AERODYNAMIC PARAMETER	SIGN CONVENTION
All lift coefficients	Positive for force upward
All drag coefficients	Positive for force aft
All sideforce coefficients	Positive for force to Pilot's right
All pitching moment coefficients	Positive for nose up moment
All rolling moment coefficients	Positive for right wing down moment
All yawing moment coefficients	Positive for nose right moment
Angle of attack	Positive for X body axis above velocity vector
Sideslip	Positive for X body axis left of velocity vector
Elevon	Positive for nose down moment
Aileron	Positive for right wind down moment
Rudder	Positive for nose left moment
Angular rates	Positive clockwise about respective axis, right hand rule
Altitude	Positive upward

3. Surface Actuator Models.

The control surface constraints used were:

a. Elevon

Single surface elevator and aileron

Range: $+15^{o}$ to -45^{o}

Max. Velocity: 20^{o}/sec (total of elevator plus aileron)

Aileron travel: $\pm 12.5^{o}$ differentially.

b. Rudders

$\pm 10^{o}$ at max. rate of 20^{o}/sec.

The transfer function of the elevon and rudder actuators, when in their linear range, was:

$$\frac{\delta_s}{\delta_{sc}} = \frac{1}{1 + \tau s}$$

where δ_s is the surface deflection,

δ_{sc} is the surface commanded deflection and

s is the Laplace operator

τ = 0.05 secs for the elevons and 0.033 for the rudders.

Since it is unrealistic to simply limit the output of the transfer function to simulate the surface and surface rate limits specified, the model shown in Figure C-1 was used. This model

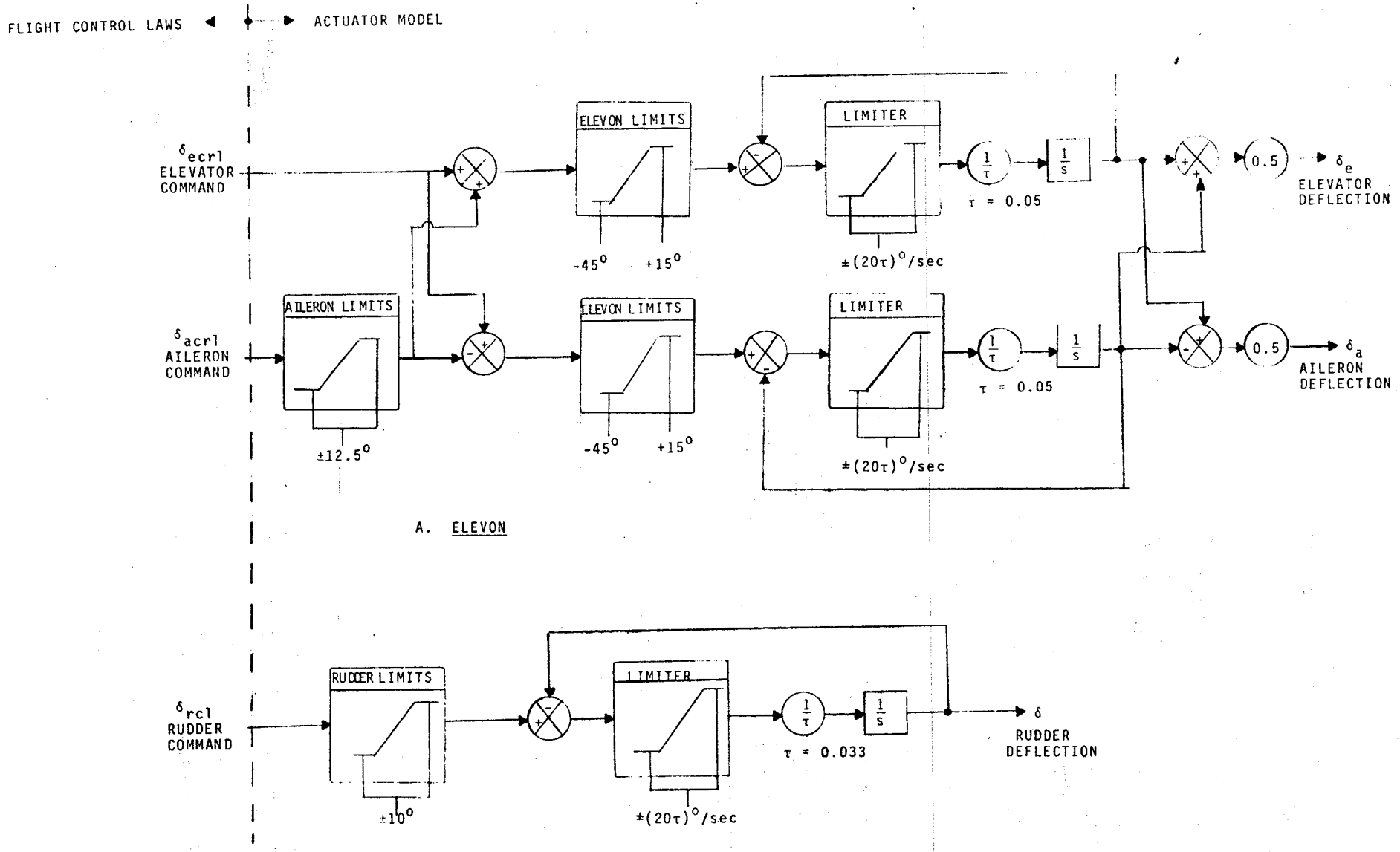

FIGURE C-1 ACTUATOR MODELS

simulates the inherent change in transfer function time constant during limiting which is not simulated by simpler models.

C. Wind Models.

1. Wind Shear.

The wind shears were defined by defining a wind velocity, V_W, as a function of altitude, h, and direction with respect to the runway, ψ_W. The mean wind, V_{MW}, was defined first and was described by:

$$V_{MW} = 0.69\ (6 + 3 \cos \psi_W + \cos^2 \psi_W)\ \log_{10}\ (6.5h)$$

where V_{MW} is expressed in knots and h in feet. $\psi_W = 0^o$ for headwinds (HW), $\psi_W = 90^o$ for crosswinds (CW) and $\psi_W = 180^o$ for tail winds (TW). The variation of the mean wind velocity with altitude and wind direction is illustrated below.

h(FEET)	V_{MW} (KNOTS)		
	$\psi_W = 0^\circ$	$\psi_W = 90^\circ$	$\psi_W = 180^\circ$
10	12.5	7.5	5.0
100	19.4	11.6	7.8
1000	26.3	15.8	10.5

The actual wind velocity, V_W, is formed from the mean wind velocity, V_{MW}, by

$$V_W = K_W V_{MW} \ ,$$

where K_W is a random number taken from a normal distribution with a mean and standard deviation given by

$$\overline{K_W} = 1 \qquad \text{(mean)}$$

$$\sigma_{K_W} = 1/3 \qquad \text{(standard deviation)}$$

The wind direction, ψ_W, is a random number taken from a normal distribution with a mean and standard deviation given by

$$\overline{\psi_W} = 0^o \qquad \text{(mean)}$$

$$\sigma_{\psi W} = \pi/3 \qquad \text{(standard deviation)}$$

For deterministic tests, K_W and ψ_W were selected constants as required by the particular test and specified in the description of test results. In Task II, deterministic tests to measure system sensitivity to rotating wind shears was made. In these tests, for HW rotation, $\psi_W = 0^o + 0.045^o(h_o - h)$; for CW rotation, $\psi_W = 90^o + 0.045^o(h_o - h)$; for TW rotation, $\psi_W = 180^o + 0.045^o(h_o - h)$ where h_o was the initial altitude and h the altitude.

2. Wind Gusts.

The wind gust model used was specified as follows. Independent gust magnitudes were selected for gust velocities along the X, Y and Z directions of a coordinate system defined by the X axis being rotated through the vehicle yaw attitude relative to the runway centerline, the Z axis being the local vertical and the Y axis being orthogonal to the X, Y axes. These magnitudes were selected from normally distributed random

numbers with zero means and standard deviations σ_X, σ_Y, σ_Z which are functions of altitude, h, and a number, σ_{ur}. σ_{ur} is selected from a Ragleigh distribution which is specified such that 6.8 ft/sec is exceeded 1% of the time. σ_{ur} is selected once per each simulated flight and varies only from flight to flight. The gust magnitudes selected from the σ_X, σ_Y, σ_Z distributions are selected for each computation cycle during each flight. The relationships between σ_X, σ_Y, σ_Z and h, σ_{ur} are given by

$$\sigma_X = \sigma_Y = \sigma_{ur} \quad , \qquad 0 < h \leq 100 \text{ ft.}$$

$$= \frac{\sigma_{ur}}{6.8} \left[-0.72 \log_{10} h + 8.24\right] , \quad 100 < h \leq 60{,}000 \text{ ft.}$$

$$\sigma_Z = \sigma_X \quad , \qquad h \geq 1750 \text{ ft.}$$

$$= 0.083\, h^{1/3}\, \sigma_X , \qquad 100 \leq h < 1750 \text{ ft.}$$

$$= 0.386\, \sigma_X \quad , \qquad h < 100 \text{ ft.}$$

The random gust magnitudes selected by the above procedure were processed through filters to obtain the correct spectrum. The filters for the X and Y gusts had transfer functions as follows (note that V = airspeed in feet per second):

$$G_X(s) = \frac{\sigma_X}{\sqrt{V}} \frac{33.4}{1 + \frac{1750}{V} s} , \qquad h \geq 1750 \text{ ft}$$

$$= \frac{\sigma_X}{\sqrt{V}} \frac{9.6\, h^{1/6}}{1 + \frac{145 h^{1/3}}{V} s} , \quad 100 \leq h < 1750 \text{ ft}$$

$$= \frac{\sigma_X}{\sqrt{V}} \frac{20.8}{1 + \frac{675}{V} s}, \qquad h < 100 \text{ ft}$$

$$G_Y(s) = \frac{\sigma_Y}{\sqrt{V}} \frac{1 + \frac{3020}{V} s}{\left[1 + \frac{1750}{V} s\right]^2}, \qquad h \geq 1750 \text{ ft}$$

$$= \frac{\sigma_Y}{\sqrt{V}} \frac{1 + \frac{252h^{1/3}}{V} s}{\left[1 + \frac{145h^{1/3}}{V} s\right]^2}, \qquad 100 \leq h < 1750 \text{ ft.}$$

$$= \frac{\sigma_Y}{\sqrt{V}} \frac{1 + \frac{1170}{V} s}{\left[1 + \frac{675}{V} s\right]^2}, \qquad h < 100 \text{ ft.}$$

The filter for the vertical gust was different in the region below 100 feet of altitude for the tests of Task II and Task III. The reason for this is that the model of vertical gusts being constant in both magnitude and frequency was considered unrealistic when approaching the ground. To account for the fact that large amplitude vertical gusts were not possible near the ground which was the assumption for Task II, the gust spectrum bandwidth was increased as the altitude decreased for Task III. This resulted in the same RMS value but lower amplitude density at every frequency. The vertical gust filters were:

$$G_Z(s) = \frac{\sigma_Z}{\sqrt{V}} (23.6) \frac{1 + \frac{3020}{V} s}{(1 + \frac{1750}{V} s)^2}, \qquad h \geq 1750 \text{ ft.}$$

$$= \frac{\sigma_Z}{\sqrt{V}} \sqrt{\frac{h}{\pi}} \frac{1 + \sqrt{3} \frac{h}{V} s}{(1 + \frac{h}{V} s)^2}, \qquad \begin{cases} \text{For Task II} \\ 100 \leq h < 1750 \text{ ft.} \\ \text{For Task III} \\ h < 100 \text{ ft.} \end{cases}$$

$$= \frac{\sigma_Z}{\sqrt{V}} \sqrt{\frac{100}{\pi}} \frac{1 + \sqrt{3} \frac{100}{V} s}{(1 + \frac{100}{V} s)^2}, \qquad \begin{cases} \text{For Task II} \\ h < 100 \text{ ft.} \end{cases}$$

D. Hardware Models

The hardware models were defined in terms of noise, bias and geometry. Noise was considered to be white noise and was taken from a normal distribution with zero mean and with the specified standard deviation. The noise figure was selected from the distribution during the course of each simulated flight. Bias was considered to be a fixed number for each simulated flight but was varied on a flight to flight basis. The bias was taken from a normal distribution with zero mean and with the specified standard deviation.

It is important to note that the most significant errors in tracking radar, scanning beam and conventional ILS systems are angular errors. This means that the touchdown errors may be biased by selection of the system's location. For example, if a one milliradian bias error exists in an angular measurement,

a ten foot error in the estimate of position at touchdown results when the measuring system is located 10,000 feet from the touchdown point. If the location is changed to 1,000 feet, the estimation of error is only 1 foot. The localizer beams of the conventional ILS and scanning beam system are particularly susceptible to the generation of large lateral errors due to their location at the stop end of the runway. A long runway results in a large error.

In order not to bias the results by means of unfavorable geometry, for Task II compromise locations were picked for the locations of the ground based systems.

For Task III which involved only the SC117 Scanning Beam system and the Precision Tracking Radar, the geometry was restored to most probable locations. Geometry is specified by giving the equipments (X,Y) coordinates with respect to the touchdown point as origin and the runway centerline as the X axis. The Y axis being perpendicular to the X axis and in the horizontal plane. The positive X direction is in the direction of flight.

The systems considered were:

1. Precision Tracking Radar (TR)

   a. Location: X_o = +2000 feet

      Y_o = + 200 feet

The location remainded fixed for both Task II and Task III.

b. Errors

Range Noise	8 feet RMS
Range Bias	1 foot RMS
Elevation Angle Noise	0.3 Milliradians RMS
Elevation Angle Bias	0.3 Milliradians RMS
Azimuth Angle Noise	0.3 Milliradians RMS
Azimuth Angle Bias	0.3 Milliradians RMS

2. Scanning Beam Systems (SBS)

a. Location for Task II

Axis of elevation beam

X_o = +2000 feet, Z_o = 0

Axis of azimuth beam

X_o = +2000 feet, Y_o = +200 feet

b. Location for Task III

Axis of elevation beam

X_o = +2000 feet, Z_o = 0 feet

Axis of azimuth beam

X_o = +8000 feet, Y_o = 0 feet

c. Errors for Task II

Range (DME) Noise	75 feet RMS
Range (DME) Bias	10 feet RMS
Elevation Angle Noise	0.61 Milliradians RMS
Elevation Angle Bias	0.87 Milliradians RMS
Azimuth Angle Noise	0.39 Milliradians RMS
Azimuth Angle Bias	0.63 Milliradians RMS

d. Errors for Task III

Range (DME) Noise	20 feet RMS
Range (DME) Bias	2 feet RMS
Elevation Angle Noise	0.61 Milliradians RMS
Elevation Angle Bias	0.87 Milliradians RMS
Azimuth Angle Noise	0.39 Milliradians RMS
Azimuth Angle Bias	0.63 Milliradians RMS

These numbers are representative of the performance specified for the SC117 Scanning Beam system.

3. Instrument Landing System (ILS)

a. Location of glide slope beam

X_o = -1330 feet

Y_o = 0 feet

b. Location of localizer beam (Configuration 1)

X_o = -1330 feet

Y_o = 0 feet

c. Location of localizer beam (Configuration 2)

X_o = +8000 feet

Y_o = 0 feet

d. Errors

Range (DME) Noise	75 feet RMS
Range (DME) Bias	10 feet RMS
Elevation Angle Noise	1.26 Milliradians RMS(See Note
Elevation Angle Bias	1.26 Milliradians RMS(See Note
Azimuth Angle Noise	1.4 Milliradians RMS
Azimuth Angle Bias	1.4 Milliradians RMS

NOTE: The elevation beam information was considered to be unreliable below 100 feet of altitude and was not used.

4. Inertial Navigation System (INS)

In each of the three axes, the errors were taken to be independent with the following characteristics:

Accelerometer Noise	0.0176 ft/sec^2 RMS
Accelerometer Bias	0.03 ft/sec^2 RMS(see Note)
Angular noise	0.267×10^{-5} rad/sec RMS
Angular drift bias	0.49×10^{-6} rad/sec RMS

NOTE: Accelerometer bias may be interpreted as an equivalent platform leveling error.

5. Precision Ranging System (PRS)

a. Location.

The assumption was made that the DME being interrogated is always located most favorably with respect to the coordinate being estimated. This is a most optimistic case and amounts to stating that the errors in the X, Y, Z coordinate measurements are equal to the range measurement error of the DME irrespective of geometry.

b. Errors (DME)

Noise	1.5 feet RMS
Bias	1.0 feet RMS

6. Pitot Tube

Based on data published for the Minneapolis-Honeywell Digital Air Data Computer HG280, the true airspeed measurement errors were modeled by white, gaussian noise passing through a single order lag filter with a 0.2 second time constant. The amplitude was 0.85 ft/sec RMS.

7. Radar Altimeter

Noise	2 feet RMS
Bias	1.5 feet RMS

E. Initial State Errors and Initial State Estimation Errors.

For Task III, it was necessary to develop a statistical model for errors in the state and errors in the estimate of the state at the initiation of primary flare.

The statistical model for vehicle state errors and the state estimation errors at start of primary flare were obtained by NASA/AMES from simulations of the flight regimes prior to the primary flare.

The guidance in effect in this region implies that the position errors and the estimation of position errors are not independent since guidance utilizes the estimated position. The velocity errors and estimation of velocity errors, however, are better modeled as being independent of each other since these errors both result in position errors which are corrected by the

position loop. The model, therefore, partially correlates the position errors and position estimation errors but treats the velocity and velocity estimation errors as dependent but not correlated.

In Task III, in the initial errors in the estimate of the state for each run were selected randomly from a zero mean, normal distribution with the following rms values.

Variable	RMS Value
σ_{x_s}	17 feet
σ_{y_s}	45 $(X_\psi/X_{\psi o})$ feet
σ_{z_s}	35 $(X_\theta/X_{\theta o})$ feet
$\sigma_{\dot{x}_s}$	1 ft/sec.
$\sigma_{\dot{y}_s}$	1.75 $(X_\psi/X_{\psi o})$ ft/sec
$\sigma_{\dot{z}_s}$	1 $(X_\theta/X_{\theta o})$ ft/sec

It can be seen that the rms values of the initial estimation errors in the Y and Z positions and velocities were made proportional to the range to the localizer, X_ψ, and glide slope, X_θ, beams respectively since these errors decrease with range for the constant angular error ground based systems considered. $X_{\psi o}$ and $X_{\theta o}$ are 20,800 (the nominal, no wind range) added to the X coordinate of the azimuth and elevation beam sources.

The initial guidance errors in Task III were randomly selected from a zero mean, normal distribution with the following rms values.

Variable	RMS Value
σ_{x_g}	67 feet
σ_{y_g}	6.7 feet
σ_{z_g}	0 feet
$\sigma_{\dot{x}_g}$	6.7 ft/sec.
$\sigma_{\dot{y}_g}$	1.7 ft/sec.
$\sigma_{\dot{z}_g}$	1.7 ft/sec.

Note that there is no guidance error in the z position since the predictive guidance system selected for study in Task III uses the Z coordinate as the independent variable at the start of the flareout.

Now, since it was assumed that the position errors were directly correlated with the initial errors in the estimate in state, the total position errors for each run were obtained by adding the guidance and state estimation errors as follows.

$$\Delta X_{ic} = \Delta X_s + \Delta X_g$$

$$\Delta Y_{ic} = \Delta Y_s + \Delta Y_g$$

$$\Delta Z_{ic} = \Delta Z_s + \Delta Z_g$$

where ΔX_s, etc. = random state estimation error with rms of σ_{X_S}, etc.

ΔX_g, etc. = random guidance error with rms of σ_{X_g}, etc.

However, since the total velocity errors were assumed to be dependent on the velocity state estimation errors but not correlate with them, the total velocity errors for each run were selected independently from a zero mean, normal distribution with the following rms values:

Variable	RMS Value
$\sigma_{\dot{x}_{ic}}$	$\sqrt{\sigma_{\dot{x}_s}^2 + \sigma_{\dot{x}_g}^2}$
$\sigma_{\dot{y}_{ic}}$	$\sqrt{\sigma_{\dot{y}_s}^2 + \sigma_{\dot{y}_g}^2}$
$\sigma_{\dot{z}_{ic}}$	$\sqrt{\sigma_{\dot{z}_s}^2 + \sigma_{\dot{z}_g}^2}$

F. Performance Criteria.

It was necessary to select criteria for allowable errors at touchdown, allowable maneuver constraints and, secondarily, autopilot criteria. The touchdown criteria and maneuver constraints are primary and the autopilot designed must satisfy these requirements. However, since the actual design procedure starts with the autopilot and then the guidance loop is closed around the autopilot-airframe, tentative autopilot criteria must be selected before the guidance loop is closed and the effect on the primary criteria can be fully assessed.

1. Touchdown Errors.

From FAA document AD695804, "An Evaluation of the C-141 Category 3 All-Weather Landing System", the performance goals selected for conditions at the touchdown point were:

a. longitudinal dispersion to be within ±500 feet of the mean for at least 95% of the landings.

b. lateral dispersion to be within ±25 feet of the centerline for at least 95% of the landings.

c. sink rate to lie between 1.5 and 5.5 feet/second for at least 95% of the landings with 3 feet/second being considered nominal.

d. lateral touchdown velocity to be less than 12 feet/second for at least 95% of the landings.

e. crab angle to be within $\pm 4^{o}$ of runway heading for at least 95% of the landings.

Not included in the reference document but adopted as an additional performance goal was the requirement that the roll attitude be less than 2.5^{o} for at least 95% of the landings.

2. Maneuver Constraints.

The maneuver constraints assumed for both the preliminary studies aimed at establishing the initial conditions and for the terminal landing study were:

a. g limit was assumed to be 3 g's.

b. q limit was assumed to be 400 lbs/ft^2.

c. landing gear must be lowered by the time the 100 foot altitude is reached.

d. landing gear may be lowered, but not retracted once lowered, at any time except as dictated by c above.

e. the maximum allowable pitch attitude at TD was assumed to be 21^{o}, (17^{o} for the Modified System of Section VIII).

f. for determination of initial conditions, the vehicle was assumed to be guided half way between the maximum L/D and the q limit in the flight phase prior to primary flare.

3. Flight Control System Specifications.

From MIL-C-18244A (WEP), "Control and Stabilization Systems: Automatic, Piloted Aircraft, General Specifications for", the criteria for acceptable autopilots for the landing configurations are:

a. the damping factor, ζ_θ, of the short period mode of the pitch oscillation shall be:

$$0.5 \leq \zeta_\theta \leq 1$$

b. the natural frequency, ω_θ, of the short period mode of the pitch oscillation shall be:

$$\omega_\theta \geq 0.75 + 3.1\ \zeta_\theta$$

c. the static gain, K, of the automatic flight control system defined as the ratio of elevator deflection to pitch altitude error shall be:

$$K \geq 2\ \left|\frac{C_{m_\alpha}}{C_{m_\delta}}\right|$$

where C_{m_α} is the pitch moment coefficient and C_{m_δ} is the control pitch moment coefficient.

d. the transfer function between bank command and bank angle, when fitted by a second order lag, shall exhibit a natural frequency ω_ϕ and damping factor, ζ_ϕ, within the limits:

$$0.6 \leq \zeta_\phi \leq 1.2$$

$$\omega_\phi \geq 0.46 + 1.46\zeta_\phi$$

G. Computation Rates Used in Simulation

The computation rates used in simulating the various subsystems are listed below.

1. 10 per second
   a. Guidance Laws
   b. Inertial Navigation System (translational data)
   c. Blending Algorithm
   d. Ground Measurement Systems (Radar, Scanning Beams, etc.)
2. 33 per second
   a. Flight Control System
   b. Inertial Navigation System (angular data)
3. 50 per second
   a. Vehicle Body Axis Angular Modes
   b. Vehicle Body Axis Translateral Modes
   c. Error Coefficients
   d. Wind Model
4. 100 per second
   a. Actuator Dynamics

APPENDIX D

DERIVATION OF PREDICTOR EQUATIONS

This section contains a derivation of the predictor equations that are used in the guidance system to predict the range and height required at the initiation of and during the terminal approach. In summary, the equations are derived for predicting the range and height traveled during each of the subphases (primary flare, glide with gear up, glide with gear down, and final flare) of the terminal trajectory. These ranges and heights are then summed to obtain the total predicted range and height traveled during the terminal approach. This is done by using the current vehicle velocity and sink rate as boundary conditions and first deriving the kinematic equations for the primary flare and final flare. In addition to height and range changes during these subphases, these equations determine the velocities of the vehicle at the end of the primary flare and the beginning of the final flare. These are the velocities at each end of the glide subphase and are then used to derive the equations for the glide phase. The details of this derivation are as follows:

The predicted time required for a constant vertical acceleration flare is,

$$\Delta t_f^p = \frac{(\dot{Z}^v - \dot{Z}_{ef}^p)}{\ddot{Z}_f}$$

$$= \frac{(\dot{Z}^v + V_{ef}^p \sin \gamma_g)}{\ddot{Z}_f}$$

where: V_{ef}^{p} = predicted velocity at end of flare

$\dot{Z}^{v}$ = current vehicle sink rate

$\ddot{Z}_{f}$ = desired vertical acceleration

γ_{g} = desired glide path angle

The predicted height at the end of flare is,

$$Z_{ef}^{p} = \int_{0}^{\Delta t_f^p}\int -\ddot{Z}_f \, dt^2$$

$$= \int_{0}^{\Delta t_f^p} -\ddot{Z}_f \, t \, dt + \dot{Z}^{v}$$

$$= -.5\ddot{Z}_f \, t^2 + \dot{Z}^{v} \, t \Big]_{0}^{\Delta t_f^p} + Z^{v}$$

$$= -.5\ddot{Z}_f \, (\Delta t_f^p)^2 + \dot{Z}^{v} \, \Delta t_f^p + Z^{v},$$

where: Z^{v} = current vehicle height.

The predicted velocity at the end of flare is,

$$V_{ef}^{p} = \int_{0}^{\Delta t_f^p} \dot{V} \, dt$$

$$= \int_{0}^{\Delta t_f^p} (-D/m - g \sin \gamma) \, dt,$$

where: D/m = drag acceleration

γ = flight path angle.

By substituting $D/m = (L/m)/(L/D)$ and $\sin \gamma = -\dot{Z}/V$ into the above equation, we obtain,

$$V_{ef}^{p} = \int_{0}^{\Delta t_f^p} \left[- \frac{(L/m)}{(L/D)} + g \frac{\dot{Z}}{V} \right] dt$$

where: (L/m) = lift acceleration

(L/D) = lift to drag ratio

V = velocity

By assuming,

$$(L/m) \cong \ddot{Z}_f + g$$

$$(L/D) \cong \text{constant} = (L/D)_{f\ avg}$$

$$V \cong \text{constant} = .5\ (V^{v} + V_{ef}^{p}),$$

and substituting these into the above equation, we obtain

$$V_{ef}^{p} = \int_{0}^{\Delta t_f^p} \left[- \frac{(\ddot{Z}_f + g)}{(L/D)_{f\ avg}} + \frac{g\ \dot{Z}}{.5\ (V^{v} + V_{ef}^{p})} \right] dt$$

Solving for $\dot{Z}$ gives,

$$\dot{Z} = \int - \ddot{Z}_f\ dt$$

$$= -\ddot{Z}_f\ t + \dot{Z}^{v}$$

Substituting this into the above equation and integrating gives,

$$V_{ef}^{p} = \int_{0}^{\Delta t_f^p} \left[- \frac{(\ddot{Z}_f + g)}{(L/D)_{f\ avg}} + \frac{g(\dot{Z}^{v} - \ddot{Z}_f\ t)}{.5\ (V^{v} + V_{ef}^{p})} \right] dt \quad .$$

$$= - \frac{(\ddot{Z}_f + g)\ t}{(L/D)_{f\ avg}} + \frac{g\ (\dot{Z}^v - .5\ \ddot{Z}_f\ t^2)}{.5\ (V^v + V^p_{ef})} \Bigg]_0^{\Delta t^p_f} + V^v$$

$$V^p_{ef} = V^v - \frac{(\ddot{Z}_f + g)\ \Delta t^p_f}{(L/D)_{f\ avg}} + \frac{g\ (\dot{Z}^v - .5\ddot{Z}_f\ \Delta t^p_f)\ \Delta t^p_f}{.5\ (V^v + V^p_{ef})}$$

The time required for an exponential final flare with a time constant, τ, is obtained from the following equation.

$$\dot{Z}_{td} = \dot{Z}^p_{eg}\ e^{-\Delta t^p_{ff}/\tau}$$

$$\Delta t^p_{ff} = \tau\ \ell n\ (\dot{Z}^p_{eg}/\dot{Z}_{td})$$

where: $\dot{Z}^p_{eg}$ = predicted sink rate at end of glide

$\dot{Z}_{td}$ = desired touchdown sink rate

The height lost during final flare is

$$\Delta Z^p_{ff} = \int_0^{\Delta t^p_{ff}} \dot{Z}\ dt$$

$$= \int_0^{\Delta t^p_{ff}} \dot{Z}^p_{eg}\ e^{-\ t/\tau}$$

$$= - \tau \dot{Z}^p_{eg}\ e^{-t/\tau} \Bigg]_0^{\Delta t^p_{ff}}$$

$$= - \tau \dot{Z}^p_{eg}\ e^{-\Delta t^p_{ff}/\tau} + \tau\ \dot{Z}^p_{eg}$$

$$\Delta Z^p_{ff} = \tau\ \dot{Z}^p_{eg}\ (1 - e^{-\Delta t^p_{ff}/\tau})$$

For a variable time constant of

$$\tau = \dot{Z}^p_{eg} / \ddot{Z}_{ff}$$

the height lost during final flare becomes

$$\Delta Z^p_{ff} = \frac{(\dot{Z}^p_{eg})^2}{\ddot{Z}_{ff}} \left[1 - e^{-\Delta t^p_{ff} / (\dot{Z}^p_{eg} / \ddot{Z}_{ff})} \right]$$

The velocity lost during final flare is

$$\Delta V = \int_0^{\Delta t^p_{ff}} \dot{V} \, dt$$

$$= \int_0^{\Delta t^p_{ff}} \left[-(D/m) - g \sin \gamma \right] dt$$

By substituting $(D/m) = (L/m)/(L/D)$, we obtain,

$$\Delta V = \int_0^{\Delta t^p_{ff}} \left[- \frac{(L/m)}{(L/D)} - g \sin \gamma \right] dt$$

By assuming,

$$(L/m) = g + \ddot{Z}_{ff}$$

$$(L/D) = \text{constant} = (L/D)_{ff\ avg}$$

$$\gamma = \text{constant} = .5 \, (\gamma_g + \gamma_{td}),$$

we obtain

$$\Delta V^p_{ff} = \int_0^{\Delta t^p_{ff}} \left[- \frac{(g + \ddot{Z}_{ff})}{(L/D)_{ff\ avg}} - g \sin \frac{(\gamma_g + \gamma_{td})}{2} \right] dt$$

$$= \left[\frac{-(g + \ddot{Z}_{ff})\, t}{(L/D)_{ff\ avg}} - g \sin \frac{(\gamma_g + \gamma_{td})\, t}{2} \right]_0^{\Delta t^p_{ff}}$$

$$= - \left[\frac{(g + \ddot{Z}_{ff})}{(L/D)_{ff\ avg}} + g \sin \frac{(\gamma_g + \gamma_{td})}{2} \right] \Delta t^p_{ff}$$

Assuming the touchdown velocity as a terminal boundary condition, the velocity at the end of glide is

$$V^p_{eg} = V_{td} - \Delta V^p_{ff}$$

If it is assumed that the landing gear is nominally lowered at an airspeed of $V_{a\ gd\ nom}$ during the glide phase, then the ground speed at which the gear is nominally lowered is

$$V_{gd\ nom} = V_{a\ gd\ nom} - \Delta V_w$$

where ΔV_w = average wind speed along velocity vector.

The predicted velocities available for glide with the landing gear up and down are then,

$$\Delta V^p_{g\ gu} = V^p_{ef} - V_{gd\ nom}$$

$$\Delta V^p_{g\ gd} = V_{gd\ nom} - V^p_{eg}$$

The predicted glide times with gear up and down are,

$$\Delta t_{g\ gu} = \frac{\Delta V_{g\ gu}}{\dot{V}_{g\ gu}} = \frac{\Delta V_{g\ gu}}{(D/m)_{g\ gu} + g \sin \gamma_g}$$

$$\Delta t_{g\ gd} = \frac{\Delta V_{g\ gd}}{\dot{V}_{g\ gd}} = \frac{\Delta V_{g\ gd}}{(D/m)_{g\ gd} + g \sin \gamma_g}$$

Again, by substituting $(D/m) = (L/m)/(L/D)$ and assuming

$$(L/m) = \text{constant} = g,$$

we obtain,

$$\Delta t_{g\ gu} = \frac{\Delta V_{g\ gu}}{g/(L/D)_{g\ gu} + g \sin \gamma_g}$$

$$\Delta t_{g\ gd} = \frac{\Delta V_{g\ gd}}{g/(L/D)_{g\ gd} + g \sin \gamma_g}$$

Since winds can cause the airspeeds at the end of primary flare and at the end of glide to vary significantly and since the total glide time for the NADWO is normally large as compared to the flare and final flare times, significant errors in the total prediction can develop if it is assumed that the lift to drag ratios during the gear up and gear down portions of the glide are constant. To avoid this, the average lift to drag ratios are computed as functions of the predicted airspeeds at the beginning of the gear up and at the end of the gear down segments of the glide.

$$(L/D)_{g\ gu} = f_1 (V^p_{a\ ef}, V_{a\ gd\ nom})$$

$$(L/D)_{g\ gd} = f_2 (V^p_{a\ gd\ nom}, V_{a\ eg})$$

where: $V^p_{a\ ef} = V^p_{ef} + \Delta V_w$

$V^p_{a\ eg} = V^p_{eg} + \Delta V_w$

Assuming an average velocity during each phase, the ranges traveled are,

$$\Delta X_f^p = (V^v \cos \gamma^v + V_{ef}^p \cos \gamma_g)\ \Delta t_f^p/2$$

$$\Delta X_g^p = (V_{ef}^p + V_{gd\ nom}) \cos \gamma_g\ \Delta t_{g\ gu}^p/2$$

$$= (V_{gd\ nom} + V_{eg}^p) \cos \gamma_g\ \Delta t_{g\ gd}/2$$

$$\Delta X_{ff}^p = (V_{eg}^p \cos \gamma_g + V_{td})\ \Delta t_{ff}^p/2$$

The height at the end of flareout is,

$$Z_{td}^p = Z_{ef}^p - \Delta X_g^p \sin \gamma_g + \Delta Z_{ff}^p$$

The predicted flareout initiation height for primary flare is therefore,

$$Z_{sf}^p = Z^v - Z_{td}^p$$

and the predicted flareout height for final flare is,

$$Z_{sff}^p = - \Delta Z_{ff}^p$$